

DOCTORAL DISSERTATION



NAZIOARTEKO
BIKAINASUN
CAMPUSA
CAMPUS DE
EXCELENCIA
INTERNACIONAL

Theoretical Study of Excited Triplet States of
Aromatic Molecules for Optoelectronic Applications
*Aplikazio Optoelektronikoetarako Molekula
Aromatikoen Egoera Kitzikatu Tripleteen Azterketa
Teorikoa*

MARIA ZUBIRIA ULACIA

Supervised by
Dr. Jon Mattin Matxain Beraza and Dr. David Casanova Casas

OCTOBER 2022

Theoretical Study of Excited Triplet States of
Aromatic Molecules for Optoelectronic
Applications *Aplikazio Optoelektronikoetarako*
Molekula Aromatikoen Egoera Kitzikatu
Tripleteen Azterketa Teorikoa

Dissertation presented in



NAZIOARTEKO
BIKAINTASUN
CAMPUSA
CAMPUS DE
EXCELENCIA
INTERNACIONAL



Submitted in fulfillment of the requirements of the

**DOCTORAL PROGRAMME IN THEORETICAL
CHEMISTRY AND COMPUTATIONAL
MODELLING**

Presented by

MARIA ZUBIRIA ULACIA

Supervised by

DR. JON MATTIN MATXAIN BERAZA

and

DR. DAVID CASANOVA CASAS

Euskal Herriko Unibertsitatea/Universidad del País Vasco & Donostia International
Physics Center

In DONOSTIA, OCTOBER 2022

Thesis Committee:

Dr. Fabrizia Negri

Dr. Enrique Ortí Guillén

Dr. Jose Javier López Pestaña

“Great dancers are not great because of their technique, they are great because of their passion.”

— Martha Graham

STATEMENT OF ORIGINALITY

Hereby I declare, that this dissertation is my original authorial work, which I have worked out by my own. All sources, references and literature used or excerpted during elaboration of this work are properly cited and listed in complete reference to the due source.

Maria Zubiria Ulacia
Donostia, October 2022

CONTENTS

Statement of Originality	v
Contents	vii
List of Figures	x
List of Tables	xiv
List of Publications	xix
1 INTRODUCTION	1
1.1 Organic Optoelectronics	2
1.2 The Triplet State in Organic Materials	4
1.3 Scope and Structure of the Thesis	9
2 THEORY AND METHODS	11
2.1 Foundations of Quantum Chemistry	12
2.2 Born-Oppenheimer Approximation	13
2.2.1 Electronic Schrödinger Equation	15
2.3 Wavefunction Methods	15
2.3.1 Hartree-Fock Method	16
2.3.2 Perturbation Theory	17
2.4 Density Functional Theory	19
2.4.1 Time-Independent Density Functional Theory	19
2.4.2 Time-Dependent Density Functional Theory	21
2.4.3 Constrained Density Functional Theory	24
2.5 Decomposition of Electronic States	25
2.5.1 Edmiston-Ruedenberg & Boys Method	27
2.5.2 Simple Diabatic Approach	28
2.5.3 Decomposition Based on the One-Electron Transition Density Matrix	30
3 TRIPLET EXCIMERS IN DIMERS OF SMALL AROMATIC MOLECULES	33
3.1 Introduction	34
3.2 Computational Methods	35
3.3 Results	35
3.3.1 Small Aromatic Molecules	35
3.3.2 Small Aromatic Dimers	40
3.3.3 Nature of Delocalized Triplets	48
3.4 Conclusions	54
4 THE MOLECULE OF PDI	55
4.1 Introduction	56
4.2 Methods	56
4.3 Molecular Structure	57

vii

4.4	Frontier Molecular Orbitals	60
4.5	Low-lying Excited States	61
4.6	Conclusions	65
5	PDI AGGREGATES: THE ROLE OF CT EXCITATIONS	67
5.1	Introduction	68
5.2	Computational Methods	68
5.3	Results	69
5.3.1	Crystal Structure	69
5.3.2	Intra- <i>vs.</i> inter-Column Interactions	71
5.3.3	Lowest Singlet and Triplet Excited States	73
5.3.4	Electronic Couplings	77
5.3.5	Triplet state localization	81
5.3.6	Triplet excitons and intermolecular distortions	82
5.4	Conclusions	85
6	PDI MODEL: TRIPLET EXCITONIC STATES CHARACTER DESCRIPTION IN DIMERS	87
6.1	Introduction	88
6.2	Computational Methods	89
6.3	Results	89
6.3.1	Low-lying Singlet Excited States	89
6.3.2	Adiabatic Excited States	90
6.3.3	LE/CT Interaction Energies	93
6.3.4	Symmetrized Diabatic States	94
6.3.5	Method Comparison	96
6.4	Conclusions	99
7	CONCLUDING REMARKS	101
7.1	Triplet Excimers in Small Aromatic Dimers	102
7.2	PDI Molecule, Aggregates and Models	103
7.2.1	PDI Molecule	103
7.2.2	PDI Aggregates	103
7.2.3	PDI Models	103
8	APLIKAZIO OPTOELEKTRONIKOETARAKO MOLEKULA AROMATIKOEN EGOERA KITZIKATU TRIPLETEEN AZTERKETA TEORIKOA	105
8.1	Sarrera	106
8.1.1	Optoelektronika Organikoa	106
8.1.2	Egoera Tripletea	108
8.1.3	Lanaren antolaketa eta helburua	113
8.2	Teoria eta Metodoak	114
8.2.1	Kimika Kuantikoaren Oinarriak	114
8.2.2	Born-Oppenheimer-en Hurbilketa	116
8.2.3	Uhin-Funtzio Metodoak	118
8.2.4	Dentsitate Funtzio Teoria	121

8.2.5	Egoera Elektronikoen Deskonposaketa	126
8.3	Dimero Aromatiko Txikien Eszimero Tripleteak	131
8.3.1	Sarrera	131
8.3.2	Metodologia	132
8.3.3	Monomeroak	133
8.3.4	Dimeroak	136
8.3.5	Ondorioak	145
8.4	PDI: molekula, agregatu eta modeloak	146
8.4.1	Sarrera	146
8.4.2	Metodologia	149
8.4.3	Molekula	150
8.4.4	Agregatuak	153
8.4.5	Modeloa	161
8.4.6	Ondorioak	168
8.5	Ondorio Nagusiak	170
A	DENSITY FUNCTIONAL APPROXIMATION	173
A.1	Local Density Approximation (LDA)	173
A.2	Generalized Gradient Approximation (GGA)	174
A.3	Meta-Generalized Gradient Approximation (mGGA)	174
A.4	Hybrid Functionals	175
B	LONG-RANGE CORRECTED DENSITY FUNCTIONAL THEORY	177
C	PDI MOLECULE	179
D	PDI AGGREGATE	181
D.1	<i>Intra-</i> and <i>inter-</i> column PDI Dimers	181
D.2	PDI Pentamer	183
D.3	Diabatic States of PDI Dimers	184
D.4	Triplet Excitons along intermolecular distortions	186
E	SINGLET EXCITON STATE RESULTS FOR THE DIABATIC PROCEDURE	193
F	SMALL AROMATIC EXCIMERS	195
F.1	Monomer Molecular Structure	195
F.2	Aromatic Dimers	196
F.2.1	Relative Energies	196
F.2.2	Intermediate Carbon-Carbon Distance	197
	BIBLIOGRAPHY	199

LIST OF FIGURES

Figure 1.1	Jablonski Diagram	4
Figure 1.2	Singlet Fission	6
Figure 1.3	Thermally Activated Delayed Fluorescence	7
Figure 1.4	Principle of triplet-triplet annihilation upconversion.	8
Figure 2.1	Ground and Excited State Potential Energy Surface	14
Figure 2.2	Simple schema for the characterization and diabaticization	28
Figure 2.3	TheoDORE: Electron-hole correlation picture	31
Figure 3.1	Excimers: studied systems	34
Figure 3.2	Benzene Triplet State distortion	36
Figure 3.3	Naphthalene and Anthracene structures: bond lengths	37
Figure 3.4	Benzene triplet: Elongated and Compressed	38
Figure 3.5	Jahn-Teller Distortion	39
Figure 3.6	HOMO and LUMO orbitals for the aromatic monomers	39
Figure 3.7	Spin density of the aromatic monomers	40
Figure 3.8	Covalent Dimers	43
Figure 3.9	MOs and Spin Densities of the Covalent Dimers	44
Figure 3.10	Localized Triplet Dimer	45
Figure 3.11	MOs and Spin Densities of the Localized Dimers	46
Figure 3.12	Delocalized Triplet Dimer	47
Figure 3.13	MOs and Spin Densities of the Delocalized Dimers	48
Figure 3.14	$T_{1_{adiabatic}}$ energies for each of the systems in the GS and T_1 geometries	49
Figure 3.15	Electron-Hole correlation plot: benzene	50
Figure 3.16	Electron-Hole correlation plot: naphthalene	51
Figure 3.17	Electron-Hole correlation plot: anthracene	52
Figure 4.1	PDI molecular derivatives studied in this work. 1 : bis(<i>n</i> -octyl)-2,5,8,11-tetraphenyl-PDI (R_1 : octyl; R_2 : phenyl); 2 : 2,5,8,11-tetraphenyl-PDI (R_1 : H; R_2 : phenyl); 3 : PDI (R_1 : H; R_2 : H).	56
Figure 4.2	PDI molecule: Structural parameters	57
Figure 4.3	PDI molecule: bond length analysis	59
Figure 4.4	Optimized PDI: Symmetry	60
Figure 4.5	(a) Atomic charge distribution(a.u.); (b) ground state dipole moment(Debye) for the PDI molecule in the crystal structure.	60
Figure 4.6	PDI molecule: frontier MO.	61
Figure 5.1	PDI crystal	70
Figure 5.2	PDI crystal: intermolecular distances	71

Figure 5.3	MO diagram for <i>intra</i> - and inter -column PDI dimers	72
Figure 5.4	Vertical Excitation Energies(CAM-B3LYP/6-31G(d)) for the number of PDI stacked molecules	74
Figure 5.5	PDI pentamer MOs	75
Figure 5.6	PDI trimer: spin density	81
Figure 5.7	Excitation energies of distorted(vertically) PDI trimer models	83
Figure 5.8	Excitation energies of distorted(horizontally) PDI trimer models	83
Figure 5.9	CT contributions and LE/CT coupling for the PDI eclipsed trimer	84
Figure 5.10	CT contributions and LE/CT coupling for the PDI eclipsed trimer	85
Figure 6.1	The PDI dimer used in this work. The excited states have been determined at the eclipsed configuration and along the longitudinal translation coordinate.	88
Figure 6.2	PDI dimer model: singlet diabats	90
Figure 6.3	PDI dimer model: triplets adiabatic states	90
Figure 6.4	CT Character for the adiabatic states.	91
Figure 6.5	Electron-hole correlation plots of the triplet excited states for two different PDI dimer configurations: eclipsed 0.00 Å and slip-stacked, 2.5 Å done at the TDA- ω B97XD/6-31G(d) level.	92
Figure 6.6	Comparison between the CT character obtained through the diabaticization procedure (SDA) (dot) and with the analysis of the transition density matrix (TDM)(cross)[91] for the selected triplet excited states.	93
Figure 6.7	Magnitude and modulation along the longitudinal translation coordinate of the $D_e \pm D_h$ terms for the interaction between CT/LE states of the dimer.	94
Figure 6.8	Adiabatic (dot) and symmetrized diabatic (cross) energies (a) A_g states (b) B_u for the PDI dimer computed at TDA- ω B97X-D/6-31G* level.	95
Figure 6.9	Comparison between excitation energies of the triplet excitation energies of the triplet states computed with TDA-CAM-B3LYP/6-31G(d)(cross) and TDA- ω B97XD/6-31G(d)(dot) along the longitudinal translation.	96
Figure 6.10	Comparison between CT character computed with TDA-CAM-B3LYP/6-31G(d)(cross) and TDA- ω B97XD/6-31G(d)(dot) along the longitudinal translation.	97
Figure 6.11	Interaction between CT and LE states computed at TDA-CAM-B3LYP(cross) and TDA- ω B97XD (dot) with 6-31G(d); for blue: A_g and purple: B_u states.	97

Figure 6.12	Comparison of symmetrized diabatic energy (top), CT character (middle) and interaction energy (bottom) for different diabaticization procedures: (i) specific MIOS, (ii) ER Method and (iii) Boys Method computed at ω B97XD/6-31G(d) level of theory.	98
Figure 8.1	Jablonski Diagrama	109
Figure 8.2	Singlet Fission	110
Figure 8.3	Termikoki Aktibatutako Fluoreszentzia Atzeratua	112
Figure 8.4	TTD GK printzipioa	113
Figure 8.5	Oinarrizko egoeraren eta egoera kitzikatuaren Gainazal Potentzial Energia	117
Figure 8.6	Simple schema for the characterization and diabaticization . .	128
Figure 8.7	TheoDORE: Elektroizulatu korrelazio irudia	131
Figure 8.8	Eszimeroak: Aztertutako egiturak	132
Figure 8.9	Jahn-Teller Distortsioa	134
Figure 8.10	Monomero aromatikoaren HOMO eta LUMO orbitalak	134
Figure 8.11	Monomero aromatikoaren spin dentsitatea	135
Figure 8.12	Dimero Kobalenteak	138
Figure 8.13	Dimero Kobalenteen MO eta spin dentsitateak	139
Figure 8.14	Tripletea Lokalizatua duten Dimeroak	140
Figure 8.15	Tripletea Lokalizatua duten Dimeroen MO eta Spin Dentsitateak	141
Figure 8.16	Tripletea Deslokalizatuta duten Dimeroak	142
Figure 8.17	Triplete Deslokalizatuta duten Dimeroen OM eta Spin Dentsitateak	143
Figure 8.18	Atal honetan aztertutako PDI deribatua. 1 : bis(<i>n</i> -octyl)-2,5,8,11-tetraphenyl-PDI (R ₁ : octyl; R ₂ : phenyl); 2 : 2,5,8,11-tetraphenyl-PDI (R ₁ : H; R ₂ : phenyl); 3 : PDI (R ₁ : H; R ₂ : H).	147
Figure 8.19	Atal honetan erabilitako PDI deribatua. Egoera kitzikatuak eklipsatuta den konfigurazioan aztertuta izan da eta luzeratako translazio koordinatuan.	148
Figure 8.20	PDI molekua: mukako OM.	151
Figure 8.21	PDI dimeroen zutabe barnetako eta zutabe arteko OM diagramak	154
Figure 8.22	Eszitazio energia bertikalak(CAM-B3LYP/6-31G(d)) multzokatutako PDI molekula batentzat	156
Figure 8.23	Distortsio bertikala jasaten duen PDI trimeroaren Energia Kitzikatuak	160
Figure 8.24	Distortsio horizontala jasaten duen PDI trimeroaren Energia Kitzikatuak	161
Figure 8.25	PDI dimero modelo: singlete diabatikoak	162
Figure 8.26	PDI dimero modelo: egoera triplete adiabaticoak	162
Figure 8.27	PDI dimero modelo: CT izaera	163

Figure 8.28	Elektroi-zulo korrelazio grafikoa egoera kitzikatu tripleterako PDI dimeroaren bi konformeroentzat: eklipsatua 0.00 Å eta distrotsionatua, 2.5 Å TDA- ω B97XD/6-31G(d) teoria mailan kalkulaturia.	164
Figure 8.29	CT izaeraren konparaketa diabatizazio prozedurarekin (puntu) eta trantsizio dentsitate matrizearekin (ixa)[91] aukaturako egoera kitzikatu tripleteentzat.	165
Figure 8.30	$D_e \pm D_h$ terminoen modulatioa translazio ardatz longitudinalanean KT/EL elkarrekintzetarako.	166
Figure 8.31	Energia adiabatiko (puntu) eta simetrizatutako diabatikoa (ixa) (a) A_g simetria eta (b) B_u simetriarako TDA- ω B97XD/6-31G* maila teorikoan kalkulaturia.	167
Figure 8.32	Energia diabatiko simetrikoren (goian), CT izaeraren (erdian) eta elkarrekintza energiearen (behean) konparaketa hiru diabatizazio prozedura desberdinetarako. (i) MIOS zehatz batzentako, (ii) ER eskema eta (iii) Boys eskema (TDA)- ω B97XD/6-31G* maila teorikoan kalkulaturia.	168
Figure D.1	Molecular orbital diagram of D2 computed at the TDA, CAM-B3LYP/6-31G(d) level.	181
Figure D.2	Molecular trimer of PDI 3 . Numbers indicate molecular labelling in Tables D.8-D.17.	186
Figure E.1	Energy profile (TDA- ω B97XD/6-31G(d)) of (dot) A_g adiabatic states and (cross) A_g LE and CT states for the PDI dimer along the longitudinal translation coordinate.	193
Figure F.1	MOs of the aromatic monomer systems.	195
Figure F.2	Structures corresponding to different intermediate carbon-carbon distance. (a) naphthalene distorted in the long axis, (b) naphthalene distorted in the short axis; (c) naphthalene distorted in the xy plane, (d) anthracene distorted in the long axis.	197

LIST OF TABLES

Table 3.1	Benzene Triplet State Distortion: bond distances and angles	36
Table 3.2	Energy difference (in eV) between the optimized ground and T_1 state computed at MP2/cc-pVTZ level of theory.	38
Table 3.3	T_1 vertical energies (eV) for each of the monomers computed with the cc-pVTZ basis set. CIS(D) and ω B97X-D orbital-to-orbital composition correspond to CIS and TDA transitions, respectively. H=HOMO; L=LUMO	40
Table 3.4	Intermolecular distances [d_{inter} (Å)], relative energies [E_{rel} (kcal/mol)], interaction energies [E_{int} (kcal/mol)] and binding energies [E_{bind} (kcal/mol)] for the most representative obtained minima for each of the systems. All computed at ω B97X-D/cc-pVTZ level of theory.	42
Table 3.5	Vertical T_1 energies (ΔE in eV) of benzene, naphthalene and anthracene eclipsed dimers computed with the TDA at the ω B97X-D/cc-pVDZ level. Transition composition obtained from TDA amplitudes. H = HOMO; L = LUMO.	49
Table 3.6	Composition of the T_1 adiabatic state in terms of LE and CT states computed at the ω B97X-D/cc-pVDZ level.	50
Table 3.7	Diabatic electronic energies (in eV) and the electronic couplings (in meV) obtained through the ER diabaticization of the eclipsed conformer of each system computed at the (TDA) ω B97X-D/cc-pVDZ level.	53
Table 4.1	PDI molecule: bonds, angles and dihedrals comparison.	58
Table 4.2	Typical bond distances	59
Table 4.3	MO energies for PDI 2 and PDI 3	61
Table 4.4	PDI molecule: Vertical Energies CAM-B3LYP/6-31G*	62
Table 4.5	PDI molecule: Vertical Energies B3LYP/6-31G*	64
Table 4.6	PDI molecule: Vertical Energies ω B97X/6-31G*	65
Table 5.1	PDI crystal characteristics	70
Table 5.2	Excitation Energies (TDDFT/TDA CAM-B3LYP/6-31G(d)) for <i>intra</i> - and <i>inter</i> -column PDI dimers	73
Table 5.3	PDI crystal: HOMO-LUMO gap vs. n	74
Table 5.4	Vertical Excitation Energies (CAM-B3LYP/6-31G* for the PDI pentamer	76
Table 5.5	Diabatic electronic energies and couplings	78
Table 5.6	PDI dimer: Diabatic contributions	80

Table 8.1	T ₁ monomero bakoitzaten energia bertikalak (eV) cc-pVTZ base multzoan kalkulaturu. ω B97X-D-ren kasuan orbitaletik orbitalerako konposizioak TDA trantsizioei dagokea. H=HOMO; L=LUMO	135
Table 8.2	Molekula arteko distantzia [d_{inter} (Å)], energia erlatiboak [E_{rel} (kcal/mol)], elkarrekintza energia [E_{int} (kcal/mol)] and lotura energies [E_{bind} (kcal/mol)] for the most representative obtained minima for each of the systems. All computed at ω B97XD/cc-pVTZ level of theory.	137
Table 8.3	T ₁ egoera adiabatikoaren izatera EL eta KT terminoetan adierazita ω B97XD/cc-pVDZ teoria mailan adierazita. . . .	143
Table 8.4	Energia diabatiko elektronikoa (in eV) eta akoplamenduak (in meV) ER diabatizazio eskema erabilia sistema bakoitzaren konformero eklipsatuentzat (TDA) ω B97X-D/cc-pVDZ teoria mailan kalkulaturu.	144
Table 8.5	PDI 2 eta PDI 3 OM energiak	151
Table 8.6	PDI molekula: Energia bertikalak CAM-B3LYP/6-31G*	152
Table 8.7	Kitzikapen energiak (TDDFT/TDA CAM-B3LYP/6-31G(d)) barne zutabe eta zutabe arteko PDI 2 rentzat	155
Table 8.8	PDI kristala: HOMO-LUMO tartea vs. n	156
Table 8.9	Energia Elektronikoa eta Akoplamendu Diabatikoak	158
Table 8.10	PDI dimeroa: Kontribuzio Diabatikoak	159
Table C.1	Vertical excitation energies (in eV) and oscillator strengths (in parenthesis) to the lowest singlet and triplet excited states computed at CAM-B3LYP/6-311+G(d) level for the PDI 2 . Orbital-to-orbital composition correspond to TDA transitions. H=HOMO; L=LUMO.	179
Table D.1	Excitation energies (in eV) and oscillator strengths (f) to the lowest singlet and triplet excited states of <i>inter</i> -column and <i>intra</i> - (D2) dimers computed at the TDA, CAM-B3LYP/6-31G(d) level.	182
Table D.2	Excitation energies (in eV) and oscillator strengths (f) to the lowest singlet and triplet excited states of <i>inter</i> -column and <i>intra</i> - (D2) dimers computed at the TDA, ω B97X-D/6-31G(d) level.	182
Table D.3	PDI pentamer: Vertical Energies B3LYP/6-31G(d)	183
Table D.4	PDI pentamer: Vertical Energies ω B97XD/6-31G(d)	183

Table D.5	Transition energies (in eV), oscillator strengths (in parenthesis), and diabatic contributions ω (in %) obtained through the ER diabatization for four excited singlet and triplet states of D1 and D2 dimers computed at the (TDA) CAM-B3LYP/6-31G(d) level. Diabatic states correspond to the ones mainly obtained as H,H-1 \rightarrow L,L+1 electronic promotions. $LE_A = A^*B$, $LE_B = AB^*$, $CT_{AB} = A^+B^-$, $CT_{BA} = A^-B^+$	184
Table D.6	Diabatic electronic energies (in eV) and electronic couplings obtained through the Boys diabatization of the four lowest excited singlets and triplet states of the PDI <i>intra</i> -dimers D1 (unit cell) computed at the (TDA) CAM-B3LYP/6-31G(d) level.	185
Table D.7	Transition energies (in eV), oscillator strengths (in parenthesis), and diabatic contributions ω (in %) obtained through the Boys diabatization for four excited singlet and triplet states of D1 dimer computed at the (TDA) CAM-B3LYP/6-31G(d) level. Diabatic states correspond to the ones mainly obtained as H,H-1 \rightarrow L,L+1 electronic promotions. $LE_A = A^*B$, $LE_B = AB^*$, $CT_{AB} = A^+B^-$, $CT_{BA} = A^-B^+$	185
Table D.8	Diabatic electronic energies (in eV) and electronic couplings (in meV) obtained through the ER diabatization of the seven lowest excited triplet states of the eclipsed trimer along the vertical distortion (3.7 Å) computed at the (TDA) CAM-B3LYP/6-31G(d) level. $LE_1 = 1^*23$, $LE_2 = 12^*3$, $LE_3 = 123^*$, $CT_{12} = 1^+2^-3$, $CT_{13} = 1^+23^-$, $CT_{21} = 1^-2^+3$, $CT_{31} = 1^-23^+$	186
Table D.9	Diabatic electronic energies (in eV) and electronic couplings (in meV) obtained through the ER diabatization of the seven lowest excited triplet states of the eclipsed trimer along the vertical distortion (4.0 Å) computed at the (TDA) CAM-B3LYP/6-31G(d) level. $LE_1 = 1^*23$, $LE_2 = 12^*3$, $LE_3 = 123^*$, $CT_{12} = 1^+2^-3$, $CT_{13} = 1^+23^-$, $CT_{21} = 1^-2^+3$, $CT_{31} = 1^-23^+$	187
Table D.10	Diabatic electronic energies (in eV) and electronic couplings (in meV) obtained through the ER diabatization of the seven lowest excited triplet states of the eclipsed trimer along the vertical distortion (4.2 Å) computed at the (TDA) CAM-B3LYP/6-31G(d) level. $LE_1 = 1^*23$, $LE_2 = 12^*3$, $LE_3 = 123^*$, $CT_{12} = 1^+2^-3$, $CT_{13} = 1^+23^-$, $CT_{21} = 1^-2^+3$, $CT_{31} = 1^-23^+$	187

Table D.11	Diabatic electronic energies (in eV) and electronic couplings (in meV) obtained through the ER diabatization of the seven lowest excited triplet states of the eclipsed trimer along the vertical distortion (4.8 Å) computed at the (TDA) CAM-B3LYP/6-31G(d) level. $LE_1 = 1^*23$, $LE_2 = 12^*3$, $LE_3 = 123^*$, $CT_{12} = 1^+2^-3$, $CT_{13} = 1^+23^-$, $CT_{21} = 1^-2^+3$, $CT_{31} = 1^-23^+$	188
Table D.12	Diabatic electronic energies (in eV) and electronic couplings (in meV) obtained through the ER diabatization of the seven lowest excited triplet states of the eclipsed trimer along the vertical distortion (5.3 Å) computed at the (TDA) CAM-B3LYP/6-31G(d) level. $LE_1 = 1^*23$, $LE_2 = 12^*3$, $LE_3 = 123^*$, $CT_{12} = 1^+2^-3$, $CT_{13} = 1^+23^-$, $CT_{21} = 1^-2^+3$, $CT_{31} = 1^-23^+$	188
Table D.13	Transition energies (in eV), oscillator strengths (in parenthesis), and diabatic contributions ω (in %) obtained through the ER diabatization for the lowest seven excited triplet states of the eclipsed trimer along the vertical distortion computed at the (TDA) CAM-B3LYP/6-31G(d) level. 3.7 Å displacement.	189
Table D.14	Transition energies (in eV), oscillator strengths (in parenthesis), and diabatic contributions ω (in %) obtained through the ER diabatization for the lowest seven excited triplet states of the eclipsed trimer along the vertical distortion computed at the (TDA) CAM-B3LYP/6-31G(d) level. 4.0 Å displacement.	189
Table D.15	Transition energies (in eV), oscillator strengths (in parenthesis), and diabatic contributions ω (in %) obtained through the ER diabatization for the lowest seven excited triplet states of the eclipsed trimer along the vertical distortion computed at the (TDA) CAM-B3LYP/6-31G(d) level. 4.2 Å displacement.	190
Table D.16	Transition energies (in eV), oscillator strengths (in parenthesis), and diabatic contributions ω (in %) obtained through the ER diabatization for the lowest seven excited triplet states of the eclipsed trimer along the vertical distortion computed at the (TDA) CAM-B3LYP/6-31G(d) level. 4.8 Å displacement.	190
Table D.17	Transition energies (in eV), oscillator strengths (in parenthesis), and diabatic contributions ω (in %) obtained through the ER diabatization for the lowest seven excited triplet states of the eclipsed trimer along the vertical distortion computed at the (TDA) CAM-B3LYP/6-31G(d) level. 5.3 Å displacement.	191

Table F.1	Intermolecular distances [d_{inter} (Å)], relative energies [E_{rel} (kcal/mol)], interaction energies [E_{int} (kcal/mol)] and binding energies [E_{bind} (kcal/mol)] for the most representative obtained minima for each of the systems. All computed at ω B97XD/cc-pVTZ level of theory.	196
-----------	---	-----

LIST OF PUBLICATIONS

PUBLICATION 1: Reference [1]

Y. Dai, M. Zubiria-Ulacia, D. Casanova and F. Negri
“*Impact of Charge-Resonance Excitations on CT-Mediated J-Type Aggregation in Singlet and Triplet Exciton States of Perylene Di-Imide Aggregates: A TDDFT Investigation*”,
in *Computation*, vol. 10, no. 2, 18, 2022, doi: 10.3390/computation10020018.

PUBLICATION 2: Reference [2]

S. Medina Rivero, J. Urieta-Mora, A. Molina-Ontoria, C. Martín-Fuentes, J. I. Urgel, M. Zubiria-Ulacia, V. Lloveras, D. Casanova, J. I. Martínez, J. Veciana, D. Écija, N. Martín, J. Casado
“*A Trapezoidal Octacyanoquinoid Acceptor Forms Solution and Surface Products by Antiparallel Shape Fitting with Conformational Dipole Momentum Switch*”,
in *Angewandte Chemie International Edition*, vol. 60, no. 33, pp. 17887-17892, 2021,
doi: 10.1002/anie.202104294.

PUBLICATION 3: Reference [3]

V. Kachwal, A. Srivastava, S. Thakar, M. Zubiria-Ulacia, D. Gautam, S. Majumder, V. K. P. Rao, D. Casanova, R. Chowdhury, N. Rath, S. Mukherjee, P. Alemany, I. R. Laskar
“*Engineering a light-driven cyanine based molecular rotor to enhance the sensitivity towards a viscous medium*”,
in *Mater. Adv.*, vol. 2, no. 14, pp. 4804-4813, 2021, doi: 10.1039/D1MA00277E.

PUBLICATION 4: Reference [4]

M. Zubiria-Ulacia, J. M. Matxain, D. Casanova
“*The role of CT excitations in PDI aggregates*”,
in *Phys. Chem. Chem. Phys.*, vol. 22, no. 28, pp. 15908-15918, 2020, doi:
10.1039/D0CP02344B.

PUBLICATION 5: Reference [5]

D. López-Carballera, M. Zubiria, D. Casanova, F. Ruipérez
“*Improvement of the electrochemical and singlet fission properties of anthraquinones
by modification of the diradical character*”,
in *Phys. Chem. Chem. Phys.*, vol. 21, no. 15, pp. 7941-7952, 2019, doi:
10.1039/C8CP07358A.

Chapter 1

INTRODUCTION

In this chapter the most important aspects of organic optoelectronics and materials; and the photophysical processes in triplet state are going to be introduced as well as the aim of this work.

1.1 ORGANIC OPTOELECTRONICS

Over the past 10 years, the field of organic optoelectronics has experienced a tremendous progress in both, the understanding of the fundamental physics of charge generation and transport and in the material design, fabrication, and processing methods. These reasons have made powerful the investigation in the area of optoelectronics. Being sun light a source of energy, optoelectronics is an area that studies and applies electronic systems and devices with the aim of detecting and controlling the source of light. For a better understanding, quantum mechanical effects should be taken into account, specially the interaction between fermions and light. In electronic materials, these effects are based under the presence of the electric field.

From the 90's to nowadays world's health is getting worse due to the increasing of the use of fossil fuels. To give a solution to these problem investigation about renewable energy has increased; and this has become one of the biggest challenge for the society. This means that the obtained energy must be clean and efficient as well as its use must be optimum and controlled. One solution to this problem can be solar energy. Although solar energy is abundant and free, the efficiency to get it, remains a challenge because all photovoltaic cells transmit photons with energies below the absorption threshold of the adsorbed material. This means a lot of energy is lost during the energy conversion [6].

Today's commercial photovoltaic industry is mainly lead by crystalline silicon and thin films, with efficiencies that reach 15-20% and 6-11% respectively [7]. To achieve greater efficiency, new technologies have been developed, such as dye-sensitized solar cells and organic photovoltaics [8]. The latter are quite attractive due to their easy handling. Furthermore, they have mechanical flexibility and a low fabrication cost.

In the mid-1980s Ching Tang and Steven van Slyke did a great demonstration of a low voltage and efficient thin film light emitting diode[9]. This diode has unique characteristics concerning high electroluminescent emission efficiency, low voltage drive and simplicity of fabrication. This demonstrates that the use of this kind of materials in optoelectronics could be viable[10]. Since this demonstration, researchers proved that organic thin films would be useful in some applications. Although they are relatively new in the market, their success is becoming bigger in the fields of *the organic light emitting device, or OLED* and, as mentioned before, organic solar cells.

Organic materials such as molecules, oligomers, polymers, aggregates and molecular solids have attracted the attention due to their huge potential and unique properties, such as their enormous chemical tunability. In molecular organic materials the charge transport property has been the most investigated until the present, because of their ability as hole and electron transporting materials. In general they are split into two groups: small molecules and polymers.

Small molecules are attractive because they are easy to purify and, also, because their ordered structures enable high charge carrier mobility. They have been also used as model systems for a variety of studies, such as exciton and charge carrier dynamics. On the other side, polymers give another advantage comparing to small

molecules. This advantage is focused in the facility of fabrication in a large-area device. Thanks to this easy design, synthesis and processing polymeric compounds have attracted the attention in device performance [11].

These polymeric compounds are introduced in solar cells with the use of electron donors (D) and electron acceptors (A). DA solar cells apply the photo induced electron transfer [12] to separate electrons from holes. This photo-induced electron transfer occurs from the excited state of the donor (lowest occupied molecular orbital, LUMO) to the LUMO of the acceptor. This acceptor must be a good electron acceptor with a strong electron affinity. After this charge separation, the electron and hole have to reach opposite electrodes, the cathode and the anode, respectively [13].

Organic semiconductors can have extremely high optical absorption coefficients. This offers the possibility to produce very thin solar cells. The electronic structure of this type of semiconductors is based on conjugated π -electrons. This means that the system might contain singly and doubly bonded carbons. Single bonds are known as σ -bonds, which are associated to localized electrons. Double bonds contain both bonds, the σ -bond and the π -bond. These π -electrons have more mobility than the σ -electrons. In other words, they can jump from site to site between carbon atoms due to the overlap between π orbital's along the configuration path[13].

The first systems analyzed in this work have been the molecular homodimers of benzene, naphthalene and anthracene, with special interest on the spin-triplet excimer state. Most of the studies on the benzene excimer have analysed structural aspects of [14], and have mainly focused on the singlet state [15]. Moving to the naphthalene, more information starts to appear. In this case, there is not only information about the geometry, but there is also information about the couplings that may appear regarding the geometry that the dimer can take [16]. In this work, we can see how the disposition of the molecules can be crucial for the π - π stacking, leading to a stronger coupling between states. Finally, for anthracene there is not as much information as for naphthalene, and most of the investigations are related to molecular dimerization and polymetization mechanisms [17]

The second part of the work is related with the study of the perylene-3,4:9,10-bis(dicarboximide) (PDI) molecule. PDI is a polycyclic aromatic chromophore [18] highly used in the dye industry. Nowadays, PDI is also studied as an advanced material with important applications in fluorescence [19] or organic semiconductor devices [20]. Although until some years ago the triplet state of PDI was only accessible via bimolecular sensitization [21], recent improvements have allowed to have a larger control of the triplet state formation [22]. In this way, the formation has been possible thanks to the covalent attachment of a stable radical to the chromophore. The interaction between linker and radical can be tuned to optimize the triplet state formation by the attachment position of the linker, its type or the nature of the radical. Eve though, there is not a protocol to design the chromophore radical yet [22].

The next section dicusses the different photophysical processes for the photo-generation and conversion of triplet states. For the generation of triplets *Intersystem*

Crossing(ISC) and *Singlet Fission*(SF) will be explained; and for the conversion *Phosphorescence*, *Thermally Activated Delayed Fluorescence*(TADF) and *Triplet-Triplet Annihilation*(TTA).

1.2 THE TRIPLET STATE IN ORGANIC MATERIALS

Before going in deep with the triplet state, it is important to analyze and understand the typical photophysical processes, see Figure 1.1. All the processes start with the absorption where an electron is excited from the ground state (S_0) to a higher energy level (blue line). At this point, there are different ways for the relaxation of the excited electron. The first one might be the vibrational relaxation (red curved line) [23]. Here, the excited electron gives vibrational energy to another electron in form of kinetic energy, being fast after absorbance and likely to occur. The excess of vibrational energy is then dissipated as heat by the internal conversion (IC) process (purple curved line) and the molecule relaxed to the ground vibrational level of the 1st excited state. At this point, the emission (pink line), a radiative process, takes place and the molecule arrives to its ground state.

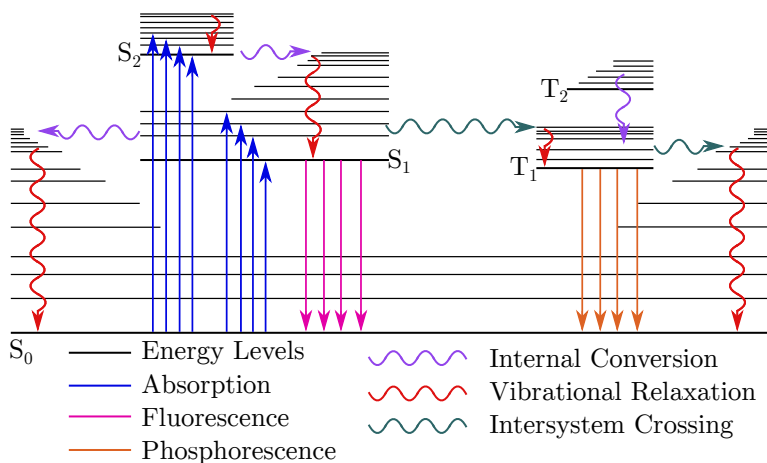


Figure 1.1: Radiative and non-radiative transitions described by the Jablonski diagram.

Organic molecules can be really interesting in order to increase the efficiency of solar cells. For that purpose, the analysis of the triplet state might be interesting. The reason of this interest is that the triplet state has a long lifetime allowing a longer diffusion for triplet excitons and thus a higher probability to reach a dissociation site. [24].

The properties of this triplet state show that the electron-hole pair is strongly bonded and therefore this requires strong acceptors for the dissociation. Moreover,

the emission from the triplet state is weak or forbidden (by spin-selection rules) which makes difficult their detection. All this allows the existence of photophysical processes related to charge transfer or high and low frequency photon conversion [25].

For the improvement of the experimental and technological results the optimization of the photophysical process is essential, but to obtain a resounding success the fundamental level of the process may be studied. Thus, the use of theoretical models can be crucial to understand the mechanisms used in the processes. Besides, the prediction of an optimum material for the optoelectronic technology is also important. This fundamental level can be understood as a generation and manipulation of the triplet state. For this there are two kinds of general processes: the photo-generation and the conversion of triplet excitons.

One way to generate this triplet state can be the *Intersystem Crossing* (ISC) (aquamarine curved line). This is mainly based in a radiationless process and occurs when a molecule is irradiated by UV-VIS light involving a change in the electronic spin [26][27]. ISC is created when a photon is absorbed. This absorption is followed by an internal conversion (IC), which is a transfer of population between states of the same spin multiplicity, until it arrives to the lowest singlet state. On this state, by ISC the photon arrives to the triplet manifold reaching the lowest triplet state [28]. When light is absorbed and creates S₁ state, the triplet state can become populated through ISC. This process can be written as [25],

$$k_{ISC} = \frac{2\pi}{\hbar} \langle {}^1\psi^0 | H_{SO} | {}^3\psi^0 \rangle [\text{FCWD}] \quad (1.1)$$

where ${}^1\psi^0$ and ${}^3\psi^0$ refer to the unperturbed singlet and triplet state wavefunctions. FCWD is the Franck-Condon Weighted Density of states; which means the ISC rate depends on two factors: the strength of the spin-orbit coupling and the vibrational overlap between the wavefunctions of the S₁ and the triplet state involved.

The ISC process has one big problem: the efficiency. Triplets generated via ISC generate a huge loss of energy in the conversion from the triplet to the singlet. Therefore, the design of new organic photosensitized materials can increase this efficiency. As an example new the material would have high capacity for aluminium absorption, minimum loss in energy and high ISC efficiency. These would represent huge progress in the area of organic optoelectronics. The group of Dr. Casanova have carried out numerous studies in the generation of those triplet states on the basis of ISC processes and their phosphorescence properties [29]–[33].

As an alternative, triplet states can be generated from the *Singlet Fission* (SF) mechanism. The singlet spin exciton splits in two triplet spin excitons [34] (Equation 1.3). As it is known in quantum chemistry, transitions between singlet and triplet state are forbidden because the spin multiplicity is not conserved. But on the case of SF, the process is spin symmetry allowed in the sense that the two generated triplets are coupled as an overall singlet [35].

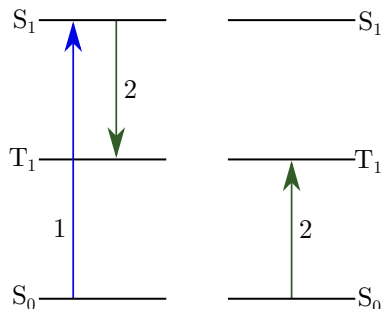


Figure 1.2: Singlet Fission: 1 The chromophore of the left undergoes an initial excitation to S_1 . 2 The excited chromophore shares its energy with the chromophore of the right, creating a T_1 state on each.

Thanks to this spin symmetry conservation SF processes are a fast. This phenomenon is a downconversion process of high-frequency photons into lower-energy excitations. Also it can be defined as the reverse reaction of the triplet-triplet annihilation [36], [37]. Often, SF process is described as the result of two consecutive steps where the initial excited state is assumed to be related to the lowest excited singlet of a monomeric chromophore (figure 1.2 eq 1.3).

$$S_1 \rightleftharpoons ({}^1TT) \rightleftharpoons T_1 + T_1 \quad (1.2)$$

$$(1.3)$$

The condition for this process to occur is that the S_1 state and the pair of triplets must be energetically close, fulfilling next condition: $E(S_1) > 2E(T_1)$. This process may increase organic solar cell efficiency because not only a singlet fission material could be able to absorb high-energy photons and but also because the chromophore is responsible of converting lower energy solar radiation into a single electron-hole pair per solar photon[38], [39]. So far, solar cells incorporating singlet fission materials have achieved external quantum efficiencies of up to 126% and internal quantum efficiencies close to 200%. Since 2011 the group of Dr. Casanova has involve in the study of the SF process [40], [41].

Moreover, there is a group of processes where the triplet exciton can be created by conversion. In most cases the energy of a pair of triplet excitations exceeds the energy of the first excited singlet state. With the encounter of two triplets with anti-parallel spin can generate a singlet excitation. These are the main processes where the conversion of the triplet state is important: the *Phosphorescence*, the *Thermally Activated Delayed Fluorescence*(TADF) and the *Triplet-Triplet Annihilation*(TTA).

Phosphorescence is the one of the most common process in the conversion of the triplet state. It is defined as a radiative transition between states of different electronic spin multiplicities. Most often, it is referred to the transition between the lowest triplet excited state and the ground singlet state [42]. The detection is

notoriously difficult [25]. This process can be induced by light absorption, electric current [43] and by a chemical reaction [44]. It has to be mentioned phosphorescence is very sensitive to molecular aggregation, temperature, and access of oxygen. The orange line of Figure 1.1 represents the phosphorescence process.

The lowest triplet state can be populated through the following sequence of photoprocesses: $S_0 \rightarrow S_n$ absorption. Via ISC, the the triplet state get populated and by IC the lowest triplet excited state gets populated leading a phosphorescence radiation.

This $T_1 \rightarrow S_0$ is spin forbidden which renders this process to be less intense compared with the spin-allowed fluorescence emission. However, in any real molecule there is always some degree of spin-orbit coupling present that renders the $T_1 \rightarrow S_0$ transition partially allowed being this the reason of the difficult detection.

Another way to convert triplet excitons is the *TADF*. On this process organic molecules have small singlet-triplet energy gaps. This allows the occupancy of states with a major energy level on the basis of the thermal energy. As it can be seen on Figure 1.3, TADF is an endothermic UC of the *Reverse Intersystem Crossing* (RISC) process from the T_1 to S_1 state. It can be thermally activated when the energy gap (ΔE_{ST}) is small and the lifetime of the T_1 is long enough [45]–[47]. RISC-UC is the result in emission with the exact spectral distribution. The triplet excitons involved in the thermal activated RISC process are cold excitons, these type of processes are the major type of excitons in common organic materials. In a TADF emitter, the conversion can be easily activated by the thermal motion of the molecule.

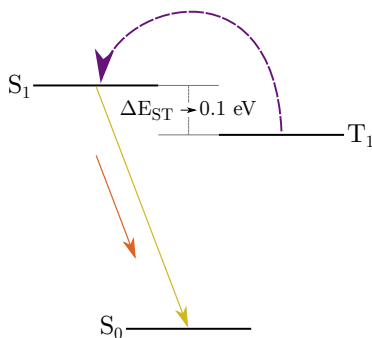


Figure 1.3: Thermally Activated Delayed Fluorescence process.

TADF can also be explained by the next equation:



Although there have been found quite successful materials to perform TADF, such as metal-organic complexes, pure organic TADF materials are more promising. Their structure can be easily modified. As TADF process involves triplet excitons, the

fluorescence of this kind of materials shows a sensitive response to temperature and external mechanical force. This makes them good materials for sensor applications.

For an efficient TADF material, the key is in the thermally activated RISC, where the rate constant can be expressed in a Boltzmann distribution relation:

$$k_{\text{RISC}} \propto \exp\left(\frac{\Delta E_{\text{ST}}}{k_{\text{B}}T}\right) \quad (1.5)$$

where k_{B} is the Boltzmann constant and T is the temperature[48].

TTA is a special case of *upconversion* (UC) photons. Their conversion from IR to Vis represents one of the best alternatives to the improvement of the photovoltaic cells and the photo-catalytic production of the hydrogen starting from water. But actually, the typical components are not able to transform photons to low frequencies. This represents a huge limitation for the use of TTA in solar cells.

The main requirement for the upconversion by TTA is a bimolecular system. This consists of an emitter molecule suffering efficient TTA and a sensitizer molecule that serves to absorb the incident light creating triplet excitations. These are fed into the emitter manifold. This process is based on the anti-Stokes delayed fluorescence. It was first reported by Parker and Hatchard in the 60s [49], [50].

Figure 1.4 represents the TTA-UC process. On the first step it can be seen how the sensitizer absorbs photons with low energy. This is followed by ISC to the lowest triplet state. Guaranteeing a fast triplet-triplet energy transfer (TET) the energy is stored in the lowest triplet state of the emitter molecules. Then, both emitters interact and triplet-triplet annihilation happens (TTA, step 4). The excited emitter is in the S_1 state. In a rapid way and at higher energy that the initially absorbed fluorescence happens.

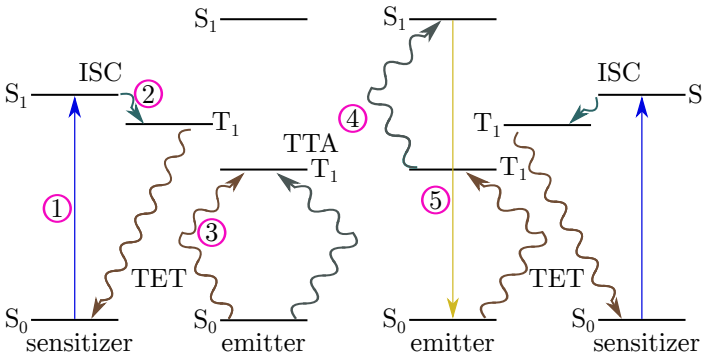
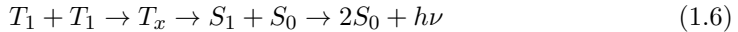


Figure 1.4: Principle of triplet-triplet annihilation upconversion.

TTA also can be seen as the next equation[48]:



where T_1 , S_1 and S_0 stand for the lowest triplet excited state, the lowest excited singlet state and the ground state, respectively.

TTA-UC shows-off a strong oscillator strength of singlet-singlet transitions to absorb and emit the light. The intermediate energy storage is facilitated by long-lived T_1 triplet states. The TTA-UC is an incoherent process, and the energy storage in the triplet states allows the efficient operation under low-light conditions. But there are some requirements which have to be fulfilled in order to have TTA-UC: on the one hand, the *sensitizer* must be a species with strong absorption in the desired region with high intersystem crossing yield. Its triplet lifetime must be long ($>10 \mu\text{s}$) and the singlet-triplet gap might be small. On the other hand, the *emitter specie* must have a triplet with a long lifetime ($>100 \mu\text{s}$), a singlet state below twice the energy of the first triplet and a high fluorescence quantum yield [51].

1.3 SCOPE AND STRUCTURE OF THE THESIS

In this thesis, several molecular systems have been studied from a computational point of view. Moreover, the following work also gives information about the theoretical procedures for the characterization of the excited states. With this in mind, the whole manuscript is divided in three main blocks.

The first of these makes reference to the basic concepts of Quantum Chemistry (QC). Here, a small overview about the most important methods employed for the calculation of electronic states is presented. Additionally, the most significant methods for the analysis of excited states, such as, states diabatization or the decomposition of the transition density matrix (TDM), are introduced. Thanks to these tools, one is able to gather detailed physical insight about the nature of excited states.

After the general overview of optoelectronics and the most important aspects of the QC, the results of the manuscript are presented. This is divided into two main blocks. The first is a basic study of small aromatic systems: benzene, naphthalene and anthracene dimers. The main challenge of this part of the work is to try to identify triplet excimeric states. For this, a variety dimers will be designed in order to find structures with no bond formation and delocalized spin density. Moreover, the main structural and electronic properties of each of the conformers and the type of interaction are going to be studied. In the final part of this section, the nature of the excited lowest triplet state is going to be analyzed with the aim to see the properties of the excimeric state.

The second part of the results belongs entirely to the perylene-3,4:9,10-bis(dicarboximide) (PDI) molecule. As a starting point, the most important characteristics of the molecule are studied, such as, the molecular structure, the frontier molecular orbitals (MOs) or the low-lying excited states. This study will reveal important

information for further investigations, as the aggregates of PDI or the behaviour of a dimer translating one of the monomers in the longitudinal axis.

In the case of the aggregates, the terms of local excitations (LE) and charge transfer (CT) states are used to characterize the excited states. The role of the inter-chromophore CT states is also rationalized for the lowest singlet and triplet states in terms of exciton couplings and diabatic contributions. In the singlet state, the transition is described by the relation between electron and hole couplings. Even if the triplet excitons present strong superexchange interactions, the energy gap between LE and CT states is much larger than in the singlet state, which decreases the LE/CT mixing.

The properties mentioned above can be tuned by distorting the system. This modulation might cause some changes in the properties of the excited states. In this case, a general diabaticization procedure has been used. Here, excited states are expressed in the diabatic basis, which coincide with LE and CT states. Thanks to this approach, energy profiles, CT characters and most important couplings could be studied.

Chapter 2

THEORY AND METHODS

This chapter is dedicated to introduce and describe the theoretical foundations and details of the methods employed during the thesis. One of the main goals of quantum chemistry is to find solutions of the time-dependent or time-independent Schrödinger equations for molecular systems, and to provide computational estimates of their properties. In practice, the exact solution of the Schrödinger equation of real systems is not affordable, and approximations are required in order to describe ground and excited electronic states, their energies, and properties.

2.1 FOUNDATIONS OF QUANTUM CHEMISTRY

The existence of atoms and smaller particles were demonstrated experimentally during the end of the XIXth century and beginning of the XXth. Unfortunately, the classical laws of electromagnetism were not able to explain the stability of such systems. Hence, a novel physical framework had to be developed to explain these new experimental evidences. The development of quantum mechanics has its origins in the beginning of the last century[52]–[54], having an enormous impact on the understanding of the microscopic world. Bohr and Sommerfeld were the first proposing a model which explained the stability of the simplest atom, Hydrogen. According to their model, the Hydrogen atom could be defined as a negatively charged electron moving around a positively charged nucleus in several allowed orbits with fixed energies. These electrons, based on Plank’s radiation theory, could only jump from one orbit to another by absorbing or emitting a certain quantity of radiation, corresponding to their energy difference. This idea was further expanded to multielectron atoms and molecules by Schrödinger and Heisenberg, among others. Nowadays, it can be said that quantum mechanics allows to understand the behaviour of matter in a microscopic scale.

According to quantum mechanics, all the information of a given quantum system can be obtained through its wave-function, that is, solving the Schrödinger equation [55]. This is a differential equation in space and time which depends on the mass and charge of the particles. The time-dependent form of this equation can be written as,

$$-i\hbar\frac{\delta}{\delta t}\Psi(\mathbf{r}, \mathbf{R}, t) = \hat{H}(\mathbf{r}, \mathbf{R})\Psi(\mathbf{r}, \mathbf{R}t) \quad (2.1)$$

where the Hamiltonian operator, \hat{H} , is the energy operator of the system containing all the interactions occurring in the studied system and \hbar is the reduced Planck constant. For stationary systems, the time-dependent Schrödinger equation is derived to the time-independent Schrödinger equation, which is written as

$$\hat{H}(\mathbf{r}, \mathbf{R})\Psi(\mathbf{r}, \mathbf{R}) = E\Psi(\mathbf{r}, \mathbf{R}) \quad (2.2)$$

where E is the energy of the system described by the Hamiltonian operator (\hat{H}), and the wavefunction (Ψ) is its associated eigenfunction, respectively. The Ψ depends on the position of all the nuclei and electrons containing all the information about the system but it can only be solved for one-electron systems.

For a system with N electrons and M nuclei the Hamiltonian is defined by the following terms: the kinetic energies of the nuclei (\hat{T}_n) and electrons (\hat{T}_e), the electron-nucleus interaction (\hat{V}_{ne}) and the repulsion between nuclei (\hat{V}_{nn}) and electrons (\hat{V}_{ee}). Therefore, the molecular Hamiltonian can be expressed as,

$$\hat{H} = \hat{T}_e(\mathbf{r}) + \hat{T}_n(\mathbf{R}) + \hat{V}_{ee}(\mathbf{r}, \mathbf{r}) + \hat{V}_{nn}(\mathbf{R}, \mathbf{R}) + \hat{V}_{ne}(\mathbf{r}; \mathbf{R}) \quad (2.3)$$

In atomic units ($\hbar = 1$, $e = 1$, $m_e = 1$, $a_0 = 1$) the different terms in equation 2.3 are defined as,

$$\hat{T}_e(\mathbf{r}) = - \sum_{i=1}^N \frac{\nabla_i^2}{2} \quad (2.4)$$

$$\hat{T}_n(\mathbf{R}) = - \sum_{A=1}^M \frac{\nabla_A^2}{2m_A} \quad (2.5)$$

$$\hat{V}_{ee}(\mathbf{r}, \mathbf{r}) = \sum_{i>j}^N \frac{1}{|\vec{r}_i - \vec{r}_j|} \quad (2.6)$$

$$\hat{V}_{nn}(\mathbf{R}, \mathbf{R}) = \sum_{A>B}^M \frac{Z_A Z_B}{|\vec{R}_A - \vec{R}_B|} \quad (2.7)$$

$$\hat{V}_{ne}(\mathbf{r}; \mathbf{R}) = - \sum_{i=1}^N \sum_{A=1}^M \frac{Z_A}{|\vec{r}_i - \vec{R}_A|} \quad (2.8)$$

2.2 BORN-OPPENHEIMER APPROXIMATION

Hence, to overcome the three-body problem in the application of equation 2.2 to molecules, approximations are mandatory. One of the most typical approximation in quantum chemistry is the so called Born-Oppenheimer approximation [56], based on the fact that the nuclei are much heavier than the electrons. The masses of the proton and neutron are about 1800 times larger than the electron mass. As a result, electrons motion is several orders of magnitude faster than the motion of the nuclei. Therefore, electrons are assumed to respond instantaneously with respect to the nuclei, thus, they can be considered to move in the mean field generated by electrons. As a consequence, the Schrödinger equation can be split in two related equations: the electronic and the nuclear equations. For the electronic equation, the nuclear kinetic term (\hat{T}_n) is neglected, the nuclear repulsion term (\hat{V}_{nn}) is constant and the interaction between nuclei and electrons (\hat{V}_{ne}) is parametrically dependent on the coordinates of the fixed nuclei. As a result, the electronic Schrödinger equation does not treat nuclear motion and the electronic part of the equation can be solved,

$$\hat{H}_e(\mathbf{r}; \mathbf{R})\psi_e(\mathbf{r}; \mathbf{R}) = E_e(\mathbf{R})\psi_e(\mathbf{r}; \mathbf{R}) \quad (2.9)$$

$$\hat{H}_e = \hat{T}_e(\mathbf{r}) + \hat{V}_{ee}(\mathbf{r}, \mathbf{r}) + \hat{V}_{nn}(\mathbf{r}, \mathbf{r}) + \hat{V}_{ne}(\mathbf{r}; \mathbf{R}) \quad (2.10)$$

where the electronic wavefunction is $\psi_e(\mathbf{r}; \mathbf{R})$. Once the electron motion has been described, one might focus on the nuclear one.

Having in mind the assumptions done to formulate the electronic motion, the nuclear one can be written. On this way, adding the electronic energy (E_e) to the

nuclear repulsion (\hat{V}_{nn}) a *Potential Energy Surface*(PES), $U(R)$, is provided for the nuclei and the nuclear Schrödinger equation can be written like,

$$(\hat{T}_n + U(\mathbf{R}))\psi_n(\mathbf{R}) = E_{tot}\psi_n(\mathbf{R}) \quad (2.11)$$

For the system under study this PES represents the most important quantity to obtain information about the vibrational levels, equilibrium geometries and chemical reactivity.

In Figure 2.1 the PES for the ground and excited system of a diatomic molecule is described. This is obtained by solving the electronic equation at different fixed nuclear positions. This PES is then used as a potential for the nuclear motion in the Schrödinger nuclear equation. Similar to the ground state, the PES can also be obtained for excited states (Figure 2.1). When the molecule absorbs an exact quantity of energy ($h\nu$), one or more electrons get excited. Then, the electronic state suffers a change creating an excited state, which is higher in energy comparing to that of the ground state. Applying the Schrödinger equation to this excited state, the PES for the excited state is calculated. As it can be observed on Figure 2.1, the difference of both electronic states is calculated with the vertical excitation.

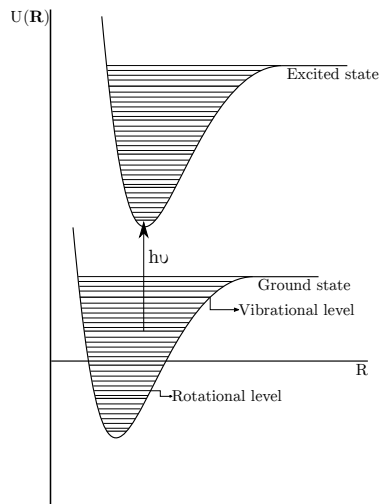


Figure 2.1: Potential Energy Surface (PES) of the ground state and the first excited state; represented with respect to the nucleus coordinate.

Summarizing, in the Born-Oppenheimer approach, the electron and nuclei movement are decoupled in order to simplify the molecular Schrödinger equation. In this way, electronic and nuclear equations are obtained. Unfortunately, solving both equations require of further approximations.

2.2.1 Electronic Schrödinger Equation

ab initio methods enable to compute a solution for the electronic Schrödinger equation as long as the nuclei position is fixed and the total number of electrons in the system is known. With this, it is possible to calculate the electronic energy and wavefunction, always within the Born-Oppenheimer Approximation. Using appropriate operators chemical properties, such as, electron density or dipolar moments can be obtained through the wavefunction. As explained above, solving the electronic Schrödinger equation is a problem and so some approximations are needed. These approximations are classified mainly into two different groups: (i) those in which the many-electron wavefunction(Ψ) is used and (ii) the one focused on the electron density ($\rho(r)$). In the following sections the most important aspects of each of the methods are going to be explained.

Nevertheless, before going in deep it is important to understand the basis of the quantum chemistry, the molecular orbital(MO). The MO is used to localize the probable areas where the electron can be found in a given region of space. The electronic structure calculations are based on the orbital approximation and the molecular orbitals expression as a linear combination of atomic orbitals (MO-LCAO),

$$\phi_i(r) = \sum_{\mu} c_{\mu i} \phi_{\mu}(r) \quad (2.12)$$

where $c_{\mu i}$ is the expansion coefficient of the atomic orbital ϕ_{μ} in the molecular orbital ϕ_i .

The key point to determine the accuracy of a calculation is the selection of the atomic orbitals, also known as basis set, used to build the MOs.

To solve this Schrödinger equation there are different approaches. These are (i) wavefunction based methods, (ii) Density Functional Theory (iii) Quantum Monte Carlo. The next sections will be focused of the first two as these are the ones used in all the work.

2.3 WAVEFUNCTION METHODS

One way of solving the electronic Schrödinger equation is by the so called wavefunction methods. These methods are divided into the Hartree-Fock (HF) and post-HF methods.

2.3.1 Hartree-Fock Method

The Hartree-Fock approximation [57] is the simplest wavefunction method and analogue to the MO approximation. The model Hamiltonian, \hat{H} , also known as the Fock operator, \hat{F} , represents a model of N non-interacting electrons,

$$\hat{F} = \sum_i (\hat{h}_i) + \hat{J}_i + \hat{K}_i = \sum_i (\hat{h}_i + \hat{g}_i) \quad (2.13)$$

where \hat{g}_i encompasses the Coulomb (\hat{J}_i) and exchange (\hat{K}_i) operators.

$$\hat{J}_i \psi_j(1) = \int \psi_j^*(2) \frac{1}{r_{12}} \psi_j(2) dx_2 \psi_i(1) \quad (2.14)$$

$$\hat{K}_i \psi_j(1) = \int \psi_j^*(2) \frac{1}{r_{12}} \psi_i(2) dx_2 \psi_j(1) \quad (2.15)$$

\hat{J}_i is the one-electron Coulomb operator which defines the repulsion resulting from electron j and \hat{K}_i is the one-electron exchange operator. ψ_i is the one-electron wavefunction of the i^{th} electron, ψ_j represents the one-electron wavefunction of the j^{th} electron and $\frac{1}{r_{12}}$ is the separation between electron 1 and electron 2.

By preserving the antisymmetry and applying the variational principle, a single *Slaeter determinant* (Equation 2.16) is optimized,

$$\psi(\mathbf{1}, \mathbf{2}, \dots, \mathbf{N}) = (N!)^{-\frac{1}{2}} \begin{vmatrix} \phi_i(\mathbf{1}) & \phi_j(\mathbf{1}) & \cdots & \phi_N(\mathbf{1}) \\ \phi_i(\mathbf{2}) & \phi_j(\mathbf{2}) & \cdots & \phi_N(\mathbf{2}) \\ \vdots & \vdots & \ddots & \vdots \\ \phi_i(\mathbf{N}) & \phi_j(\mathbf{N}) & \cdots & \phi_N(\mathbf{N}) \end{vmatrix} \quad (2.16)$$

where $(N!)^{-\frac{1}{2}}$ is a normalization factor and N are the electrons which are occupying the N spin orbitals $(\phi_i, \phi_j, \dots, \phi_N)$. Even if the HF method is exact for the hydrogen atom, it cannot provide a full description for atoms which go beyond the hydrogen because both Ψ and \hat{H} are approximations. Consequently, it does not have electron correlation. Nevertheless, this method can calculate the 99% of the total electronic energy. However, it fails when applied to chemical reactions unless electron correlation is included by using post-HF methods.

Since electron motions are not completely independent HF cannot describe the electron correlation and so a solution to this can be the introduction of the electron correlation $E_{(corr)}$ concept. As it was defined by Löwdin, the $E_{(corr)}$ is the energy difference between the exact energy (E_{exact}) and its HF value (E_{HF}) for a given complete basis set,

$$E_{corr} = E_{exact} - E_{HF} \quad (2.17)$$

where E_{exact} refers to the exact nonrelativistic energy of the system and E_{HF} is the HF energy. As HF is able to provide most of the total energy, it is the reference for post-HF methods. These methods are also wavefunction based methods but in comparison to HF they are more accurate being able to go beyond the Slater determinant and include electron correlation.

Different post-HF approaches have been developed, such as, Configuration Interaction (CI), full and truncated, and Perturbation Theory. In this thesis, Perturbation Theory has been used as the post-HF method which is going to be explained in the next section.

2.3.2 Perturbation Theory

As mentioned above, the HF method suffers some problems when trying to reproduce some chemical problem. To overcome with this situation electron correlation (Equation 2.17 is needed. One of the theories to beat the problem is the Møller-Plesset Perturbation Theory (MP). To a better understanding of the MP method, the Rayleigh-Schrödinger Perturbation Theory [58] should be explained. In this way, one may say that the perturbational methods express the Hamiltonian, \hat{H} as the sum of an unperturbed Hamiltonian, \hat{H}_0 and the perturbation operator, \hat{V} ,

$$\hat{H} = \hat{H}^{(0)} + \lambda\hat{V} \quad (2.18)$$

where λ is a parameter which controls the perturbation. The solutions for the Schrödinger equation in the non-degenerate and unperturbed case are defined like

$$\hat{H}^{(0)}|\Psi_i^{(0)}\rangle = E_i^{(0)}|\Psi_i^{(0)}\rangle \quad (2.19)$$

$$\hat{H}|\Psi_i\rangle = E_i|\Psi_i\rangle \quad (2.20)$$

being i the subindex that indicated the electronic state. Taking Equation 2.18 and developing Equation 2.20 in the Taylor's expansion:

$$|\Psi_n\rangle = |\Psi_i^{(0)}\rangle + \lambda|\Psi_i^{(1)}\rangle + \lambda^2|\Psi_i^{(2)}\rangle + \dots \quad (2.21)$$

$$E_n = E_i^{(0)} + \lambda E_i^{(1)} + \lambda^2 E_i^{(2)} + \dots \quad (2.22)$$

where, in this case, i indicates the order of the approximation. To simplify the derivation, one assumes that the eigenstates of \hat{H}_0 are normalized,

$$\langle\Psi_i^0|\Psi_i^0\rangle = 1 \quad (2.23)$$

so the following conditions is imposed:

$$\langle\Psi_i^0|\Psi_i\rangle = 1 \quad (2.24)$$

Substituting Equation 2.21 and Equation 2.22 in the Schrödinger equation,

$$(\hat{H}^0 + \lambda \hat{V})(|\Psi_i^{(0)}\rangle + \lambda |\Psi_i^{(1)}\rangle + \lambda^2 |\Psi_i^{(2)}\rangle + \dots) =$$

$$(E_i^{(0)} + \lambda E_i^{(1)} + \lambda^2 E_i^{(2)} + \dots)(\Psi_i^{(0)} + \lambda \Psi_i^{(1)} + \lambda^2 \Psi_i^{(2)} + \dots) \quad (2.25)$$

and identifying the terms with the same power of λ :

$$\hat{H}^0 |\Psi_i^{(0)}\rangle = E_i^{(0)} |\Psi_i^{(0)}\rangle \quad (2.26)$$

$$\hat{V} |\Psi_i^{(0)}\rangle + \hat{H}^0 |\Psi_i^{(1)}\rangle = E_i^{(1)} |\Psi_i^{(0)}\rangle + E_i^{(0)} |\Psi_i^{(1)}\rangle \quad (2.27)$$

$$\hat{H} |\Psi_i^{(2)}\rangle + \hat{V} |\Psi_i^{(1)}\rangle = E_i^{(2)} |\Psi_i^{(0)}\rangle + E_i^{(1)} |\Psi_i^{(1)}\rangle + E_i^{(0)} |\Psi_i^{(2)}\rangle \quad (2.28)$$

To get the expressions for the 0^{th} , 1^{st} , 2^{nd} and n^{th} order energies is necessary to multiply the Equations 2.26, 2.27 and 2.28 by $\langle \Psi_n^{(0)} |$, and so

$$E_i^{(0)} = \langle \Psi_i^{(0)} | \hat{H}_0 | \Psi_i^{(0)} \rangle \quad (2.29)$$

$$E_i^{(1)} = \langle \Psi_i^{(0)} | \hat{V} | \Psi_i^{(0)} \rangle \quad (2.30)$$

$$E_i^{(2)} = \langle \Psi_i^{(0)} | \hat{V} | \Psi_i^{(1)} \rangle \quad (2.31)$$

The Møller-Plesset Perturbation Theory (MP) is a special case of the above theory. Then a small perturbation, \hat{V} , also known as the correlation potential is added

$$\hat{V} = \hat{H} - \hat{F} \quad (2.32)$$

As the wavefunction $\Psi_0^{(0)}$ is an eigenfunction of \hat{F} , the corresponding eigenvalue, $E_0^{(0)}$ is

$$E_0^{(0)} = \langle \Psi_0^{(0)} | \hat{F} | \Psi_0^{(0)} \rangle = \sum_a^N \varepsilon_a \quad (2.33)$$

where a corresponds to the occupied orbitals. Similarly, any other Slater determinant built from the HF wavefunction and substituting the occupied molecular orbitals by the unoccupied ones, is also an eigenfunction of \hat{F} . Concerning Equation 2.30 it can be demonstrated that the first order correction (MP1) delivers in the HF energy. Hence, the first contribution to the correlation energy comes from the second order term

$$E_0^{(2)} = \langle \Psi_0^{(0)} | \hat{V} | \Psi_0^{(0)} \rangle = - \sum_{k \neq 0} \frac{|\langle \Psi_0^{(0)} | \hat{V} | \Psi_k^{(1)} \rangle|^2}{E_k^{(0)} - E_0^{(0)}} \quad (2.34)$$

As the Brillouin's theorem[59] says, singly-excited determinants do not interact with the HF wavefunction, so only the doubly-excited determinants contribute to Equation 2.34. When speaking about spin orbitals, the MP2 energy is given by

$$E_0^{(2)} = E_{MP2} = \frac{1}{4} \sum_{occ}^N \sum_{virt}^V \frac{|\langle occ || virt \rangle|^2}{\varepsilon_{occ} - \varepsilon_{virt}} \quad (2.35)$$

where N is the number of electrons and V the number of spin orbitals that have been used to generate the doubly-excited determinants.

2.4 DENSITY FUNCTIONAL THEORY

Density Functional Theory is nowadays one of the most popular method for the electronic structure calculations because the total electron density is computed without the request of a wavefunction. This includes electron correlation which has less computational cost than post-HF methods.

2.4.1 Time-Independent Density Functional Theory

In the 1st theorem of Hohenberg and Kohn [60], they proved the determination of the electronic properties of a system with a non-degenerate ground state, which are unequivocally determined by the electron density $\rho(\mathbf{r})$. Therefore, the electronic ground state energy is a functional of $\rho(\mathbf{r})$, and it is defined as:

$$E_0[\rho] = T[\rho] + E_{ee}[\rho] + V_{ext}[\rho] \quad (2.36)$$

where the dependence of the density with the electronic coordinates (\mathbf{r}) has been omitted, and $T[\rho]$ is the kinetic energy functional, $E_{ee}[\rho]$ is the electron-electron repulsion and V_{ext} is the external potential. In molecular systems the *external potential* is the electron-nuclear attraction, so the equation (2.36) can be written as:

$$E_0[\rho] = T[\rho] + E_{ee}[\rho] + E_{en}[\rho] \quad (2.37)$$

where $E_{en}[\rho]$ is system dependent, whereas $T[\rho]$ and $E_{ee}[\rho]$ are universally defined. These independent terms are gathered in the so-called Hohenberg-Kohn functional, $F_{HK}[\rho]$:

$$F_{HK}[\rho] = T[\rho] + E_{ee}[\rho] \quad (2.38)$$

Even if this 1st theorem establishes that in principle the ground state density $\rho(\mathbf{r})$ is enough to obtain the properties of interest, it does not say anything about how to find this density. At this point, the 2nd Hohenberg-Kohn theorem becomes

important. It points out that knowing the ground state electron density, it is possible to calculate all ground state electronic properties once the appropriate functional dependencies are established. These functionals apply the variational principle for the energy functional. And so, the ground state density can be searched knowing the exact form of the $E[\rho]$.

2.4.1.1 The Kohn-Sham Equation

However, since the exact form of the functional is unknown, Kohn and Sham [61], using a non-interacting reference system, developed an approach to determine the electronic density in the ground state. They showed that the exact ground state electronic energy, E_0 , of an N -electron molecule with a ground state electron density ρ is given by,

$$E_0 = -\frac{1}{2} \sum_{i=1}^N \langle \psi_i(1) | \nabla_i^2 | \psi_i(1) \rangle + \int v(r) \rho(1) d\vec{r}_1 + \frac{1}{2} \iint \frac{\rho(1)\rho(2)}{r_{12}} d\vec{r}_1 d\vec{r}_2 + E_{xc}[\rho] \quad (2.39)$$

where v is the external potential due to the presence of the nuclei, θ_i are the KS orbitals, and the $E_{xc}[\rho]$ is the exchange-correlation energy. In this scheme, the exact ground state ρ can be built from the KS orbitals according to,

$$\rho = \sum_{i=1}^N |\theta_i|^2 \quad (2.40)$$

and the KS orbitals are the one-electron eigenfunctions of the KS Fock operator:

$$\hat{F}_{KS}(1)\theta_i(1) = \epsilon_i\theta_i(1) \quad (2.41)$$

where \hat{F}_{KS} is the Kohn-Sham operator, defined like,

$$\hat{F}_{KS} = -\frac{1}{2}\nabla_1^2 + v(1) + \sum_{j=1}^n \hat{J}_j(1) + V_{xc}(1) \quad (2.42)$$

where \hat{J} is the Coulomb operator and V_{xc} is the exchange-correlation potential, which handles the effects of both the exchange and electron correlation. Except for the exchange operators which are replaced by V_{xc} , \hat{F}_{KS} is similar to the Fock operator in HF equations.

Since exchange correlation functional depends of the electron density, KS equations need to be solved self-consistently through an iterative procedure. The starting point is a guess density where the \hat{F}_{KS} is built and the set of equations are solved. This process is repeated until convergence is achieved.

Even though, the physical significance of the Kohn-Sham orbitals is still under debate [62]. For some authors the significance of these kind of orbitals is that they allow the exact ρ being calculated from equation (2.39). In the same way, the Kohn-Sham orbital energies should not be confused with molecular orbital energies. However, other authors associate to the KS orbitals a similar physical meaning as the HF canonical orbitals because they based on the fact that the exact Kohn-Sham orbital energy for the HOMO is just the negative ionization potential [62], [63], being analogous to the HF equations. Besides, some publications show the results obtained from molecular orbitals using KS are quiet similar to those obtained from standard MO-LCAO [62], [64] methods.

The Kohn-Sham formalism is still exact for the uniform electron gas but E_{xc} and v_{ex} are unknown. To solve this problem, practical approximations are done, which are known as Density Functional Approximations (DFAs). The first of these is the so-called Local Density Approximation (LDA) [65], where each volume element with local density $\rho(\vec{r})$ is considered to be a homogeneous electron gas. As the density variance in molecular systems is not slow, this approximation is not really accurate. Thus, more sophisticated functionals taking into account the inhomogeneous character of the electron density are advisable, as those also depending on the density gradient ($\nabla\rho(r)$). This approximations is known as Generalized Gradient Approximation (GGA) and it has shown to improve upon LDA functionals for most chemical applications [66]. Including the Laplacian of the density, $\nabla^2 \rho(r)$, more improvements can be done. This functionals are known as meta-GGA [67].

Furthermore, some fractions of Hartree-Fock exchange can be included into the functionals, calling them Hybrid Functionals [68], where the exchange part comes from Hartree-Fock and the correlation part from DFT. The amount of HF exchange depends on local properties of each particular system. Nevertheless, these type of functionals present some failures when speaking about valence orbital energies, electronic excitation spectra or van der Waals bonds. To overcome with this problems, long-range corrected functionals are the most convenient. Here, the long-range correction supplements the long-range exchange effect in exchange functionals when the Hartree-Fock exchange integral is replaced with the long-range parte of the exchange functionals. Thanks to this long-range correction, the self-interaction error is reduced [69]. You will find a more detailed explanation in Appendix A.

Finally, for the case of large systems some approaches are recommended because the density functionals do not describe correctly the long-range dispersion interactions [70]. Appendix B has a more detailed information about long-range corrected functionals.

2.4.2 Time-Dependent Density Functional Theory

DFT has emerged as a powerful method to compute potential energy surfaces of the ground state, but the use of this theory is still developing for the excited electronic

states [71]. Within the DFT framework, electronic excitations can be explored with Time-Dependent Density Functional Theory (TD-DFT) [72]–[74]. Molecular TD-DFT excited state energies are commonly determined through a response formalism applied on the KS ground state density, and avoiding the direct computation for electronic excited states. In this way, vertical excitations are singly-excited with respect to the ground state, giving a success to the method. This gives to the method a good success. Time dependent means a dependence in time of the electrons when the *fixed* nuclear framework is subject to a periodic radiation field.

2.4.2.1 Runge-Gross Theorem

When any N-electron system is attached to a time-dependent potential, all physical observables are uniquely determined in two cases if the time-dependent density and the state of the system at any time are known [75]. The Runge-Gross theorem proves that molecular systems where their densities $\rho(\mathbf{r},t)$ in response of an external scalar potential $\nu(\mathbf{r},t)$ will always differ. This theorem is analogue to that of the first of Hohenberg-Kohn.

From this theorem, the time-dependent external potential, which is associated to a certain time-dependent density, $\rho(\mathbf{r},t)$, is unique until a purely time-dependent function $c(t)$. This determines the total time-dependent wavefunction, being unique up to a time-dependent phase factor $\alpha(t)$,

$$\Psi(t) = e^{-i\alpha(t)}\tilde{\Psi}[\rho](t) \quad (2.43)$$

2.4.2.2 Time-Dependent Kohn-Sham Equations

Regarding the second Hohenberg-Kohn theorem, it has been seen that the variational minimization of the ground state ends in the Kohn-Sham orbitals. On the other hand, there is not a variational principle for the total energy in the time-dependent framework of DFT. Even though, it exists an analogous quantity to that of the ground state, known as quantum mechanical action A ,

$$A = \int_{t_0}^{t_1} \left\langle \Psi(t) \left| i \frac{\partial}{\partial t} - \hat{H} \right| \Psi(t) \right\rangle dt \quad (2.44)$$

which in fact can be expressed in terms of the density as there is a unique mapping between the density and wavefunction, *e.g.* $A[\rho(\mathbf{r},t)]$.

$$A[\rho(\mathbf{r},t)] = \int_{t_0}^{t_1} \left\langle \Psi[\rho](t) \left| i \frac{\partial}{\partial t} - \hat{H} \right| \Psi[\rho](t) \right\rangle dt \quad (2.45)$$

In the time-dependent framework the density must be the one that makes the action stationary

$$\frac{\partial A[\rho]}{\partial \rho(\mathbf{r}, t)} = 0 \quad (2.46)$$

where $A[\rho]$ can be written as,

$$A[\rho] = B[\rho] - \int_{t_0}^{t_1} \int \nu(\mathbf{r}, t) \rho(\mathbf{r}, t) d\mathbf{r} dt \quad (2.47)$$

being $B[\rho]$ independent from the external potential. Within the assumption of the existence of a potential, for an independent particle system $\nu_{eff}(\mathbf{r}, t)$ the time-dependent Kohn-Sham equations are derived. The orbitals of the system $\psi(r, t)$ $\psi(r, t)$ carries the charge density $\rho(\mathbf{r}, t)$ of the real interacting system,

$$\rho(\mathbf{r}, t) = \sum_i f_i |\psi_i(\mathbf{r}, t)|^2 \quad (2.48)$$

where f_i makes reference to the orbital occupation numbers. For the expression of $B[\rho]$ one must consider that $\nu_{eff}(r, t)$ exists,

$$B[\rho] = \int_{t_0}^{t_1} \left\langle \Psi[\rho](t) \left| i \frac{\partial}{\partial t} - \hat{H} t \right| \Psi[\rho](t) \right\rangle dt - \frac{1}{2} \int_{t_0}^{t_1} \int \int \frac{\rho(\mathbf{r}_1, t) \rho(\mathbf{r}_2, t)}{|\mathbf{r}_1 - \mathbf{r}_2|} - A_{XC}[\rho] \quad (2.49)$$

$A_{XC}[\rho]$ represents the exchange-correlation functional and its role is analogous to that of the exchange-correlation energy in DFT. And so, the time-dependent Kohn-Sham equation can be written like,

$$\left[-\frac{1}{2} \nabla^2 + \nu_{eff}(\mathbf{r}, t) \right] \psi_i(\mathbf{r}, t) = i \frac{\partial}{\partial t} \psi_i(\mathbf{r}, t) \quad (2.50)$$

and $\nu_{eff}(\mathbf{r}, t)$ is defined like,

$$\nu_{eff}(\mathbf{r}, t) = \nu(\mathbf{r}, t) + \int \frac{\rho(\mathbf{r}_1, t)}{|\mathbf{r}_1 - \mathbf{r}'|} d\mathbf{r}' + \nu_{XC}(\mathbf{r}, t) \quad (2.51)$$

Even if $A_{XC}[\rho]$ is unknown, it can be expressed in the limit of a slowly varying external potential,

$$A_{XC} = \int_{t_0}^{t_1} E_{XC}[\rho(t)] dt \quad (2.52)$$

being E_{XC} the time-independent exchange correlation functional. This is an assumption called the adiabatic approximation and is local in time becoming standard in TDDFT. Within the adiabatic approximation,

$$\nu_{XC}(\mathbf{r}, t) = \frac{\partial A_{XC}[\rho]}{\partial \rho(\mathbf{r}, t)} \approx \frac{\partial E_{XC}[\rho]}{\partial \rho_t(\mathbf{r})} = \nu_{XC}(\mathbf{r}, t) = \nu_{XC}[\rho(r)_{\rho=\rho(t)}] \quad (2.53)$$

where ν_{XC} is just the exchange-correlation potential of DFT evaluated with the density at a certain time t . If the LDA functional is inserted, the Adiabatic Local Density Approximation (ALDA) will be obtained and this assumes that the exchange-correlation potential at \mathbf{r} and t will be equal to the of the homogeneous electron gas.

2.4.2.3 Linear Response Theory

When the potential is weak, a good strategy could be to use the linear response TDDFT(LR-TDDFT) in order to obtain the excitation energies. With this, the time-dependent Kohn-Sham equation will be solved in a perturbative way up to the first order.

Regarding the formulation, in LR-TDDFT the excitation energies (ω) and amplitudes are obtained from the non-Hermitian eigenvalue equation, also known as Casidas's equation of Random-Phase Approximation(RPA) [73],

$$\begin{bmatrix} \mathbf{A} & \mathbf{B} \\ \mathbf{B}^* & \mathbf{A}^* \end{bmatrix} \begin{bmatrix} \mathbf{X} \\ \mathbf{Y} \end{bmatrix} = \omega \begin{bmatrix} \mathbf{1} & \mathbf{0} \\ \mathbf{0} & -\mathbf{1} \end{bmatrix} \begin{bmatrix} \mathbf{X} \\ \mathbf{Y} \end{bmatrix} \quad (2.54)$$

where each of the matrix elements depend on the exchange-correlation functional, and are defined in the following way,

$$\mathbf{A}_{ia,jb} = \delta_{ij}\delta_{ab}(\varepsilon_a - \varepsilon_i) + (ia|jb) - C_{HF}(ij|ab) + (1 - c_{HF})(ia|f_{xc}|jb) \quad (2.55)$$

$$\mathbf{B}_{ia,jb} = (ia|jb) - c_{HF}(ib|aj) + (1 - c_{HF})(ia|f_{xc}|jb) \quad (2.56)$$

where ε correspond to orbital energies and a and b make reference to occupied and virtual orbitals, respectively. For the \mathbf{A} matrix, the first term is the energy difference between i and the second term correspond to the antisymmetrized two electron integrals being the same for the first term of the \mathbf{B} .

2.4.3 Constrained Density Functional Theory

The Constrained Density Functional Theory (C-DFT) is useful tool to compute densities as well as Kohn-Sham wavefunctions for two or more than two diabatic-like states which are used to build the CI matrix. Directly it can construct charge- and

spin-localized states and give a direct measure for the inner-sphere reorganization energy [76].

The significance of C-DFT is ephemeral due to the improvement in functional approximation of ab-initio techniques. C-DFT not only offers a partial workaround to some of the detrimental effects, but also it provides a rout to obtain the diabatic electronic states, up to the charge-transfer excited state by using Kohn-Sham equations.

In order to use this method, C-DFT has been redefined so that the constrains are written in terms of the charge and spin on arbitrary molecular fragments.

2.5 DECOMPOSITION OF ELECTRONIC STATES

The diabaticization of electronic states refers to the transformation of adiabatic states into a new representation, i.e., the diabatic basis. In this procedure, potential energy surfaces and states get coupled due to the smoothness of the electronic Hamiltonian and the insignificance of the nuclear momentum.

As explained in section 2.2, the Born-Oppenheimer approximation decouples the motion of the electrons from the nuclei in molecular systems. This leads to the concept of adiabatic electronic states and potential energy surfaces. These adiabatic states (and their corresponding energies) are calculated by fixing the nuclear positions. The potential is created by the electrons in a single electronic adiabatic state; this is the place where nuclei move. Moreover, the Born-Oppenheimer approximation is only valid when electronic states are energetically well separated. So the atomic motion of molecules is governed by a single unique PES. This approximation breaks down when more than one PES are close enough in energy. In such a case, electronic states can become strongly coupled by the nuclear momentum operator. These type of nonadiabatic transitions are quite common in processes as photo-dissociation and reactions of electronically excited species [77].

When electronic and nuclear motions are divided, the Born-Oppenheimer Approximation conduces to electronic adiabatic states and potential energy surfaces [78]. However, the nuclear momentum vector couplings in the adiabatic representation [79] can vary at conical intersections. The adiabatic representation can lead to geometric phase effects, which carries inconveniences in computation. Alternatively, one can use the diabatic state basis, for which nuclear momentum vectors vanish. Strictly, diabatic states cannot be obtained from a finite number of adiabatic states[80].

To construct these diabatic states, two approaches might be used. The first one is the dynamical approach [81], [82]. This involves a a great transformation of the nuclear momentum couplings where the best scenario would be to have these couplings totally transformed. Nevertheless, in regions which are far from the conical intersection or there is a small energy gap between adiabatic states, it is no necessary to expect that the nonremovable part of the coupling is smaller than the

removable part of it [83]; thereby the dynamical approach is arbitrary. Nonetheless, a standard approach could be a transformation of the removable part around the conical intersection.

The second strategy to obtain diabatic states is based on the measure of the smoothness of diabatic states as functions of nuclear coordinates. A possible explanation for such a quote might be based in a generalized Born-Oppenheimer analysis of the order of the removable and nonremovable dynamical couplings [83].

The quality of diabatic states based on the smoothness of the electronic states is dictated by several criteria: (i) the resulting diabatic states must be unique for each nuclear geometry; (ii) the diabatization must be carried out in terms of adiabatic wavefunctions to take advantage of the variational principle; and (iii) the smoothness of the diabatic states must be a result from their orbital and configurational uniformity as functions of nuclear coordinates. Using ‘diabatic prototypes’, the smoothness of the diabatic states can be measured because each of the diabatic characters can be specified and this contributes to the states.

A possible alternative is the ‘initial state’ being a good diabatic state at some particular geometry. Furthermore, it can be good to update this state along nuclear coordinates in order to build diabatic states in other geometries. To obtain the greatest diabatic state, diabatic prototypes are defined using adiabatic wavefunctions.

In order to find global diabatic states there is a conflict between both criteria to define the one-electron molecular orbitals which are used to construct multielectron configuration state functions (CSFs). On the one hand, due to the invariance of atomic orbitals, those localized on individual atoms are preferred when there is a geometry change. On the other hand, there is a difficulty on identifying the essential character of the excited state because atomic localized orbitals lead to slow convergence of the configuration interaction (CI) expansion. Apart from atomic orbitals, there are also natural orbitals, which lead to a rapid convergence and help to identify the diabatic states.

This diabatization scheme can be based on configurational uniformity. This diabatic prototypes are defined as dominant CSFs of adiabatic states expressed by CI-based wavefunctions. Nevertheless, prototypes can be obtained from any molecule. A difficult situation to construct these diabatic states is when the system has multiple reaction pathways, because each pathway has its own diabatic prototype.

In order to obtain these diabatic states based on the configurational uniformity concept, the first thing is to consider N adiabatic states $\psi_{n=1\dots k\dots N}$ and diabatic states $\phi_{n=1\dots k\dots N}$. Also, it has to be assumed all wavefunctions are real and that they are transformed into each other by an orthogonal matrix T_{nk} , called the adiabatic/diabatic transformation matrix. This matrix is defined like

$$\phi_k = \sum_{n=1}^N \psi_n T_{nk}, \quad (2.57)$$

where, by definition, diabatic states ϕ_k should be smooth and slowly varying with changes in the nuclear coordinates.

In this work two types of diabaticization techniques have been used: the one implemented in Q-Chem package and the other is a procedure which has been developed at the Universita di Bologna in the group of Prof. Negri. For those implemented in Q-chem, two different models have been used: (i) Edmiston-Ruedenberg(ER) localization [84] (ii) Boys localization [85], where in both procedures the diabatic states are constructed as linear combinations of adiabatic states.

2.5.1 Edmiston-Ruedenberg & Boys Method

When there are multiple charge or electronic excitation centers, the diabatic states might be constructed using Edmiston-Ruedenberg or Boys localization methods. For this, the diabatic states $\{|\Xi_I\rangle\}$ are constructed as linear combinations of the adiabatic states $\{|\Phi_J\rangle\}$ with a general rotation matrix whose size is $N_{state} \times N_{state}$,

$$|\Xi_I\rangle = \sum_{J=1}^{N_{states}} |\Phi_J\rangle U_{ji} \quad I = 1 \dots N_{states}. \quad (2.58)$$

In analogy to orbital localization [84], in Boys diabaticization a maximization of the charge separation between diabatic state centers is done

$$f_{Boys}(\mathbf{U}) = f_{Boys}(\{|\Xi_I\rangle\}) = \sum_{I,J=1}^{N_{states}} |\langle \Xi_I | \vec{\mu} | \Xi_I \rangle - \langle \Xi_J | \vec{\mu} | \Xi_J \rangle|^2, \quad (2.59)$$

where $\vec{\mu}$ represents the dipole operator. On the other hand, the ER diabaticization maximizes the self-interaction energy:

$$f_{ER}(\mathbf{U}) = f_{ER}(\{|\Xi_I\rangle\}) = \sum_{I=1}^{N_{states}} \int d\vec{R}_1 \int d\vec{R}_2 \frac{\langle \Xi_I | \hat{\rho}(\vec{R}_2) | \Xi_I \rangle \langle \Xi_I | \hat{\rho}(\vec{R}_1) | \Xi_I \rangle}{|\vec{R}_1 - \vec{R}_2|^2} \quad (2.60)$$

being $\hat{\rho}(\vec{R})$ the density operator at \vec{R} position,

$$\hat{\rho}(\vec{R}) = \sum_j \delta(\vec{R} - \vec{r}^{(j)}) \quad (2.61)$$

and $\vec{r}^{(j)}$ representing the j^{th} electron position.

In each of the methods different assumptions are done for the system with some fictitious external potential. In the case of Boys-localized diabaticization, a fictitious field which is linear in space is assumed, whereas assuming a fictitious potential energy responding linearly to the charge density of the system ER-localized diabaticization is obtained.

2.5.2 Simple Diabatic Approach

This procedure [86] has been developed in order to obtain diabatic energies. For this, first adiabatic states are computed via QC calculations and then, different linear combinations in order to obtain the diabatic state energies.

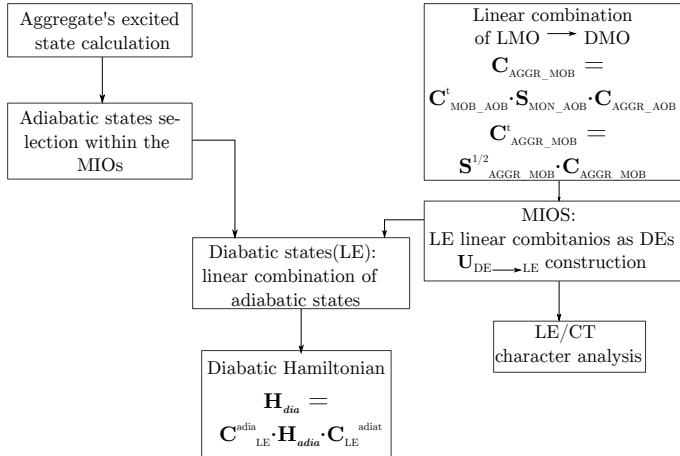


Figure 2.2: Simple schema for the characterization and diabaticization

When speaking about TDDFT calculations, the exciton wavefunction is described by single excitation. For the character analysis and diabaticization next facts are considered:

- Focus the attention in the Minimal Orbital Space (MIOS)
- Number of excitations. For an aggregate with n molecules the number will be n^2
- The selection of the adiabatic states
 - the wavefunction is dominated by some of the n^2 excitations

Moreover, the Hamiltonian's matrix dimension is n^2 and the diabatic LE basis of the aggregate encompasses the FE states (localized on each monomer) and CT states, where both of the molecules are involved .

To describe the protocol developed for the state character analysis, the first step is to express the Delocalized Molecular Orbitals (DMO) as linear combinations of the Localized Molecular orbitals (LMO) applying the projection operator as it has been done in some other works [87], [88]:

$$|\psi_{MON_i}\rangle\langle\psi_{MON_i}|\psi_{AGGR_j}\rangle = C_{i,j}^{AGGR_{MOB}}|\psi_{MON_i}\rangle, \quad (2.62)$$

where $|\psi_{MON_i}\rangle$ are the MOs corresponding to the isolated monomers in the atomic orbital basis (AOB) and $|\psi_{AGGR_j}\rangle$ are those of the aggregate. Moving to matrix formulation, $\mathbf{C}_{MON_{AOB}}$ matrix column vectors are formed with $|\psi_{MON_i}\rangle$. This matrix will be a block diagonal matrix which will contain the MO coefficients in the AOB from each monomer and where the off diagonal blocks are going to be zero. Something similar happens with $|\psi_{AGGR_j}\rangle$ and its following matrix.

$C_{i,j}^{AGGR_{MOB}}$ coefficients in the monomer orbital basis (MOB) define the linear combinations of DMOs in terms of LMOs. For a given j orbital aggregate, these coefficients forms the columns of the $\mathbf{C}_{AGGR_{MOB}}$ matrix, which are obtained as

$$\mathbf{C}_{AGGR_{MOB}} = \mathbf{C}_{MON_{AOB}}^t \cdot \mathbf{S}_{MON_{AOB}} \cdot \mathbf{C}_{AGGR_{AOB}}, \quad (2.63)$$

where $\mathbf{S}_{MON_{AOB}}$ is the overlap matrix of the monomers in the AOB and \mathbf{t} indicates the transpose.

As the monomer orbitals belong to different monomers, the MOB overlap matrix needs to be orthogonalized using the Löwdin's symmetric transformation [89]. The overlap matrix $\mathbf{S}_{AGGR_{MOB}}$ between the LMOs is calculated using the monomer orbitals MO's and the overlap of the aggregate orbitals in the aggregate configuration $\mathbf{S}_{AGGR_{AOB}}$,

$$\mathbf{S}_{AGGR_{MOB}} = \mathbf{C}_{MON_{AOB}}^t \cdot \mathbf{S}_{AGGR_{AOB}} \cdot \mathbf{C}_{MOB_{AOB}} \quad (2.64)$$

After applying the Löwdin's orthogonalization, the matrix $\mathbf{C}_{AGGR_{MOB}}^L$ is obtained as,

$$\mathbf{C}_{AGGR_{MOB}}^L = \mathbf{S}_{AGGR_{MOB}}^{-\frac{1}{2}} \cdot \mathbf{C}_{AGGR_{MOB}} \quad (2.65)$$

Even if the dimension of $\mathbf{C}_{AGGR_{MOB}}^L$ corresponds to the full dimension of the MOB, the occupied DMOs are mainly determined by the occupied LMOs, where both belong to the MIOS. The same happens to the unoccupied MOs. Therefore, only the submatrices extracted from $\mathbf{C}_{AGGR_{MOB}}^L$ and that belong to the MIOS are going to be useful in the following steps.

After expressing DMOs as linear combinations of LMOs which belong to the MIOS, generic delocalized excitations (DE) ($i_{occ} \rightarrow j_{empty}$) of DMOs can be expanded in terms of LEs between LMOs. The coefficients of this kind of expansions are given by,

$$U_{k \rightarrow l, i \rightarrow j}^{DE \rightarrow LE} = \text{MIOS}(occ)_{k,i}^{AGGR_{MOB,L}} \cdot \text{MIOS}(unocc)_{l,j}^{AGGR_{MOB,L}} \quad (2.66)$$

where $\text{MIOS}(occ)_{k,i}^{AGGR_{MOB,L}}$ and $\text{MIOS}(unocc)_{l,j}^{AGGR_{MOB,L}}$ are the orthogonalized expansion coefficients of the aggregate's occupied and empty orbitals, respectively, in the MOB. The elements obtained through Equation 2.66 for a unitary matrix $\mathbf{U}_{DE \rightarrow LE}$ whose columns describe each DE excitations in terms of LE excitations.

Once the description of DEs as linear combinations of LEs within the MIOS has been done, it is time to calculate and select the excited adiabatic states. The n^2 exciton states subset originated from the MIOS is selected from the full set of computed eigenstates, which are Gram-Schmidt orthogonalized [90]. These eigenstates are used to form the columns of the \mathbf{C}_{DE}^{adia} matrix and the excitation energies (n^2) form the diagonal \mathbf{H}_{adia} matrix.

To express the adiabatic states as linear combinations of LEs, it is good to know that the CT/FE nature of each adiabatic state is obtained by the following matrix multiplication,

$$\mathbf{C}_{LE}^{adia} = \mathbf{U}_{DE \rightarrow LE} \cdot \mathbf{C}_{DE}^{adia} \quad (2.67)$$

Finally, to obtain the matrix representation of the Hamiltonian in the diabatic LE basis, \mathbf{H}_{dia} , the following matrix transformation is used,

$$\mathbf{H}_{dia} = \mathbf{C}_{LE}^{adia} \cdot \mathbf{H}_{adia} \cdot \mathbf{C}_{LE}^{adia^t} \quad (2.68)$$

2.5.3 Decomposition Based on the One-Electron Transition Density Matrix

Thanks to the power that has achieved the excited-state electronic structure theory [91], computations on large molecular systems are possible. The reason for this is that there has been an increasing in the computational power, as well as, a development of new electronic structure methods [92]–[95]. As nowadays it is possible to perform excited-state calculations in large molecular systems, the analysis of these computations might be challenging due to the amount of produced data. Therefore, huge effort has been devoted to develop new methods to analyze the electronic structure computations and make them reproducible. These methods enclose visualization techniques [96], [97], while quantitative descriptors have been used to measure charge transfer (CT) [98]–[100], double excitation character [101], [102], and entanglement [103].

Using a fragment-based analysis scheme, TheoDORE provides a set of tools to go beyond the MO picture. In this way, we can characterize the CT character of excited states in donor-acceptor systems [104] or transition metal complexes can be assigned with an excited-state character [105]. The method used in this work is the "Fragment-based excited-state analysis within a correlated electron-hole picture", which is represented in Figure 2.3.

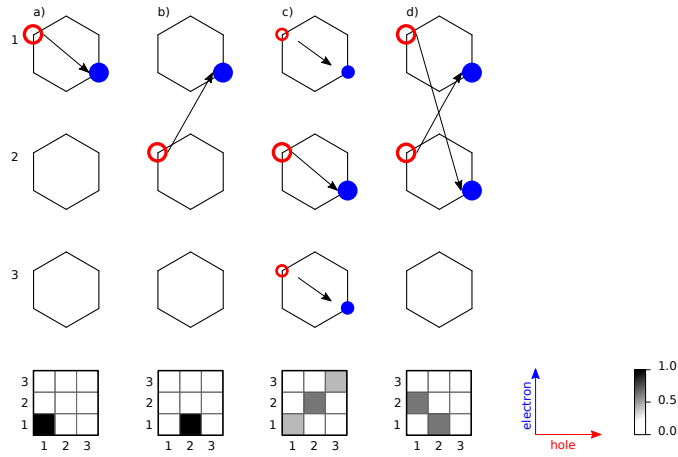


Figure 2.3: Types of excited states a) local excitation on fragment 1 b) charge transfer from 2 to 1 c) delocalized Frenkel states and d) charge resonance states. Bottom squares represent the analysis using the electron-hole correlation plots.

The main idea of this analysis is the fragmentation of the system, as it is represented on Figure 2.3. In this case, the system is divided into 3 different fragments: 1, 2 and 3 and so the representation will be done over them. The first scenario that appears is a localized excitation, Figure 2.3 a. Furthermore, we can obtain a charge transfer, when the electron is transferred from one fragment to the other, 2.3 b. Figure 2.3 c represents a dominant contribution located on the 2^{nd} fragment and followed by two smaller LE excitons; this is known as a Frenkel Exciton. this can be followed by smaller contributions and they are known as Frenkel excitations. Finally, Figure 2.3 d shows a a charge resonance state, in other words, a linear combination of CT states which go in opposite directions.

Chapter 3

TRIPLET EXCIMERS IN DIMERS OF SMALL AROMATIC MOLECULES

This chapter investigates possible triplet states and their properties in molecular dimers of small aromatic molecules. At first, molecular and electronic structures, and the excited state of the monomers will be explored. Secondly, we study the properties of different dimer conformers.

3.1 INTRODUCTION

It is well known that interactions between aromatic systems can notably modify excited state properties [106]. A remarkable example of that is the formation of excimers. In 1996 and reviewed in 2021, the International Union of Pure and Applied Chemistry (IUPAC) defined the excimer [107] as an electronically excited dimeric complex formed by one ground and one excited molecular entity, which decays immediately after deexcitation because it does not exist in the ground state. In principle, excimers might present either singlet or triplet spin multiplicity upon the nature of the excited monomeric species (M^*). Excimer formation can be expressed in a form of a photophysical reaction (equation 3.1) with ${}^{1,3}M^*$ and 1M as the reactant species. The importance of this formation is related with the photoelectronic properties in species with large π -systems [16].



Even if previous research has been directed in the analysis of the singlet states, there are some others where they point naphthalene dimer as a promising system for obtaining the triplet excimeric state [16], [106]. For singlet excimeric states, it has been seen that the system is bounded by exciton and charge resonance, whereas for the triplet state the main contribution is the LE/CT coupling. Moreover, in other systems, as the PDI aggregates (Chapter 5), it has been seen how the CT excitations can play an important role [4]. Following this, a series of aromatic systems have been designed taking as reference benzene, naphthalene and anthracene molecules.

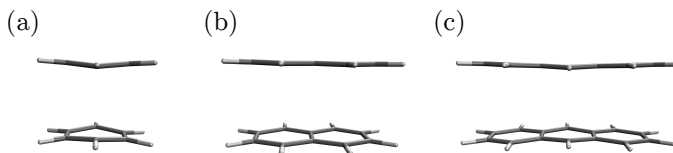


Figure 3.1: Molecular dimers of aromatic hydrocarbons studied in this Chapter. a) benzene dimer; b) naphthalene dimer; c) anthracene dimer.

In this chapter, we focus on the study of low energy triplet states in dimers of small aromatic molecules: benzene, naphthalene and anthracene (Figure 3.1). In particular, we are interested in the formation of triplet excimers, in which strong interaction between monomers is expected. This interaction is expected to stabilize the system, lowering the energy of the triplet state in the dimer. In order to characterize the nature of triplet states, we will mainly focus on two different aspects: (i) spatial distribution of the two unpaired electrons, and (ii) energy stabilization with respect to the monomeric triplet. The former, determined for instance by the representation of the spin density, can be used as a necessary condition of triplet excimer formation, as in the excimer the two unpaired electrons should be delocalized over the two

monomers. Moreover, since excimers involve strong orbital interaction between the two molecules, we might expect important stabilization with respect to T_1 of the monomer. Moreover, we will characterize intermolecular electronic couplings in terms of local excitations (LE) and charge transfer (CT) states.

3.2 COMPUTATIONAL METHODS

Molecular structures of benzene, naphthalene and anthracene have been optimized in vacuum by means of MP2 and DFT, using the long-range corrected functional ω B97X-D [108] combined with the cc-pVTZ basis set. Molecular geometries obtained at the two different levels do not present significant differences.

Vertical transition energies to the lowest singlet and triplet state have been obtained with the second order perturbation correction of the configuration interaction approach, CIS(D) [109], as well as with TDDFT. TDDFT calculations were done with and without TDA [110]. Q-Chem package [111] has been used to carry out all electronic structure calculations of this chapter.

Geometry optimizations and vertical excitation energies for the different conformers of molecular dimers has been also performed by means of DFT using the ω B97X-D functional. One of the problems of this level of theory has been the computational time. To alleviate it, the cc-pVDZ basis set has been used for the computational study of the dimers, as the results only present small variations with respect to calculations with the larger cc-pVTZ basis.

Diabatization of the electronic transitions computed within the TDA was performed with the ER localization scheme [84]. To obtain the diabatic energies and couplings the diagonal and off-diagonal matrix elements of the diabatic Hamiltonian have been used, respectively. Due to symmetry reasons, diabaticization of spin triplet excited states of benzene conformers have been done considering 32 adiabatic states. For conformers of naphthalene and anthracene, however, diabaticization of spin triplet excited states have been computed considering 16 adiabatic states, derived from electronic promotions from HOMO- n to LUMO+ n ($n = 0, 3$). To complete the information of the diabatic states, the one transition density matrix [91] has been analyzed in order to further characterize electronic excitations by means of electron-hole correlation plots.

3.3 RESULTS

3.3.1 Small Aromatic Molecules

In this section the three aromatic molecules (benzene, naphthalene and anthracene) will be analyzed and characterized in terms of the molecular and electronic structure for the ground and low-lying excited states. The aim of this research is to get a deep understanding of the triplet state properties in these molecules.

3.3.1.1 Molecular Structures

The molecular structure of the benzene ground state molecule holds a D_{6h} symmetry, optimized at the MP2 and DFT level, in agreement with previous works [112]. All carbon-carbon bond distances ($d(\text{C-C})$) are about 1.394 Å with C-C-C bond angles of 120° . Molecular optimization on the triplet PES identifies two minima. In both cases the molecular symmetry reduces to the D_{2h} point group, corresponding to elongated and compressed distorted forms, respectively (Figure 3.2).

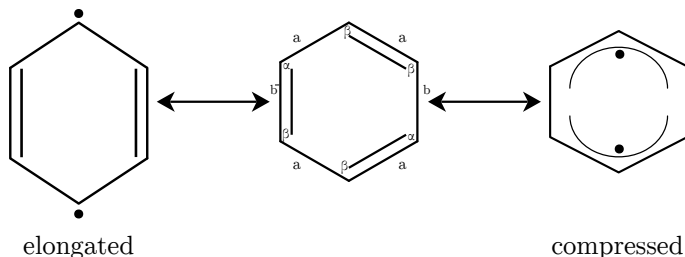


Figure 3.2: Elongated (left) and compressed (right) distorted triplet state minima of benzene. a , b , α and β indicated structural parameters in Table 3.1.

The main structural optimized parameters defining the elongated and compressed triplet state forms are shown in Table 3.1.

Table 3.1: Optimized C-C bond distances a and b (in Å), and α and β C-C-C bond angles ($^\circ$) for the elongated and compressed forms of the triplet benzene compared to the ground state (S_0) counterparts.

	S_0	T_1 -elongated	T_1 -compressed
a	1.394	1.467	1.375
b	1.394	1.348	1.510
α	120.0	119.0	121.0
β	120.0	120.5	119.5

Comparing these values to those of the ground state geometry, it can be seen that structural changes do not only correspond to the increase and decrease of bond lengths, but they also suggest a change in the hybridization of the carbon atoms. The distorted conformers show how both, the elongated and compressed structures, suffer significant changes. This means that they depart from the typical sp^2 hybridization towards a sp^3 hybridization. For instance, the largest C-C bond distance in the T_1 -compressed conformer elongates up to 1.51 Å. On the other hand, C-C-C bond angles remain very close to 120° .

Naphthalene and anthracene triplet state structures preserve the D_{2h} symmetry of the ground state singlet, but with notable changes in the optimized bond distances (Figure 3.3).

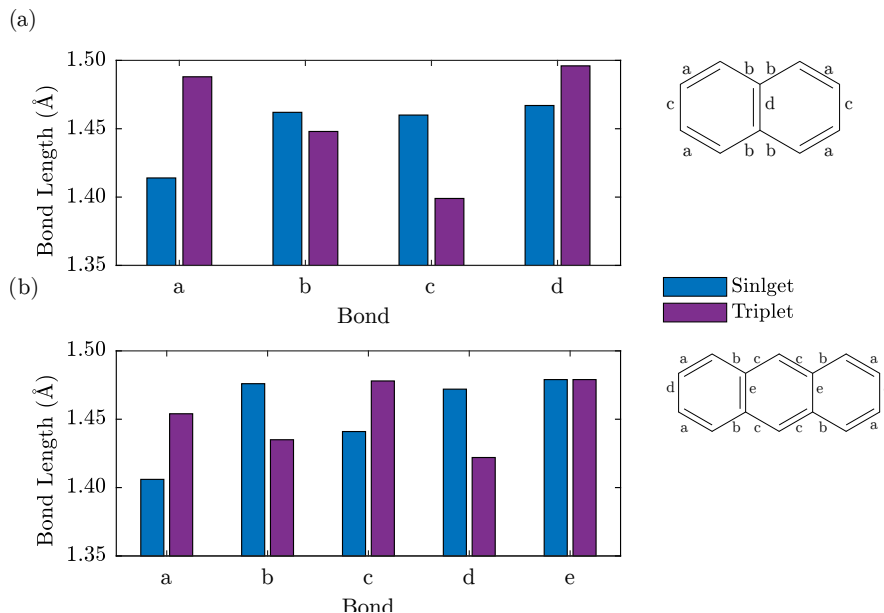


Figure 3.3: Optimized bond lengths of (a) naphthalene and (b) anthracene in their ground (singlet) and triplet states.

In naphthalene, all triplet state C-C bond distances are notably modified with respect to the ground state singlet. The biggest difference can be appreciated on the zig-zag edge bond *a*. Due to this elongation, side by side bonds become smaller as well as the one that unifies both rings. On the other hand, the anthracene molecule does not show as drastic changes as in naphthalene. Even if analogous bonds suffer the same distortions, the same does not happen to the centre bonds which share each of the rings. Here, in both states, the bond distance in singlet and triplet states remains the same.

Another feature to be mentioned is the relative stability in the benzene conformers, see Figure 3.4. Here it can be seen that one of them, the compressed form, is more stable than the elongated but with a small energy gap. This means that this conformational change can happen at room temperature. The molecular structure in naphthalene and anthracene prevents the presents of multiple low-energy triplet conformers.

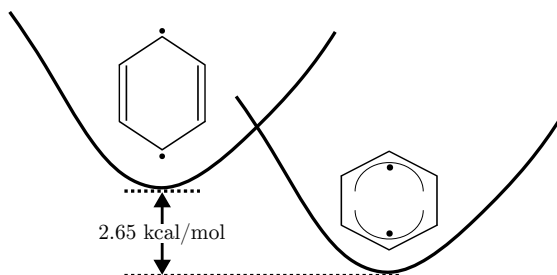


Figure 3.4: Relative energy between the compressed and elongated conformers of the benzene triplet molecule computed at MP2/cc-pVTZ level of theory.

Along the benzene, naphthalene and anthracene series, the increase of the conjugation length reduces the HOMO-LUMO gap, resulting in a systematic decrease of the computed singlet-triplet adiabatic energy differences (Table 3.2).

Table 3.2: Energy difference (in eV) between the optimized ground and T_1 state computed at MP2/cc-pVTZ level of theory.

Benzene	Naphthalene	Anthracene
4.410	3.642	2.470

3.3.1.2 *Electronic Structure*

To fully understand the behaviour of the triplet state in the desired systems, it is important to characterize its electronic structure. Before going in deep with this analysis, it is important to see why benzene suffers the mentioned distortions. It is already known that benzene is quite a special system, with a high symmetry (D_{6h}) resulting in the degeneration of MOs and electronic states. In the ground state, frontier π -orbitals of benzene are doubly degenerated, with HOMO and HOMO-1 fully occupied, and LUMO and LUMO+1 completely empty (Figure 3.5). But in the triplet state these two sets of MOs hold three and one electron, respectively. The fractional occupancy of degenerate orbitals triggers Jahn-Teller distortions [113], breaking the molecular symmetry and the orbital degeneracy. This is the reason why the benzene triplet structure shows a D_{2h} symmetry in the elongated and compressed forms. Naphthalene and anthracene molecules hold lower symmetry (D_{2h}), with no MO degeneracy in the ground-state and so they do not suffer from a Jahn-Teller distortion in the triplet state.

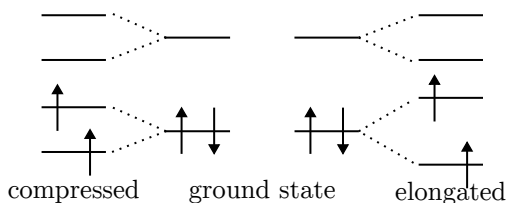
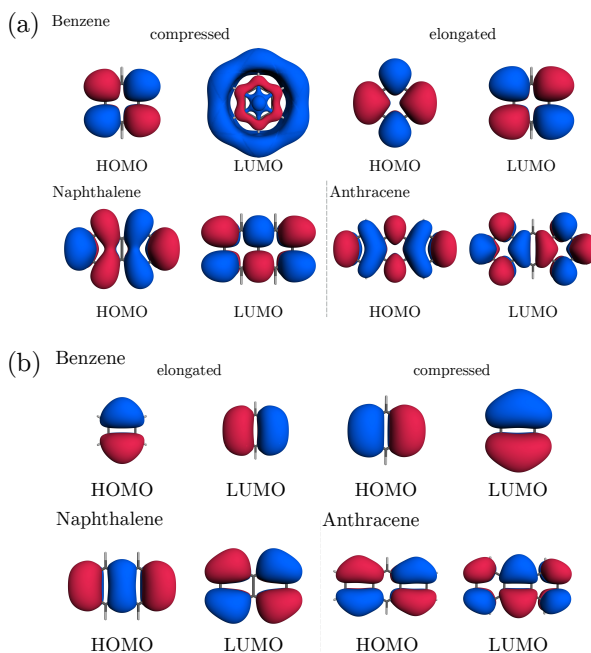


Figure 3.5: Jahn-Teller distortion suffered by the triplet benzene.

Frontier spin-orbitals (α and β) for the triplet state of the three aromatic molecules in general resemble those of the ground state, mostly corresponding to delocalized π -orbitals (Figure 3.6). In order to describe the spatial distribution of the

Figure 3.6: (a) and (b) correspond to the α and β , respectively, MOs for each of the systems.

two additional α -electrons, we make use of the spin density representations (Figure 3.7). Triplet state spin density of the three systems largely delocalize over the entire molecules. Spin density distributions in the two Jahn-Teller forms of benzene are qualitatively different. The compressed conformation shows a larger delocalization with respect to that of the elongated one. In naphthalene and anthracene, although the density is delocalized over the entire molecule, the unpaired electrons mainly lie on the zig-zag molecular edges.

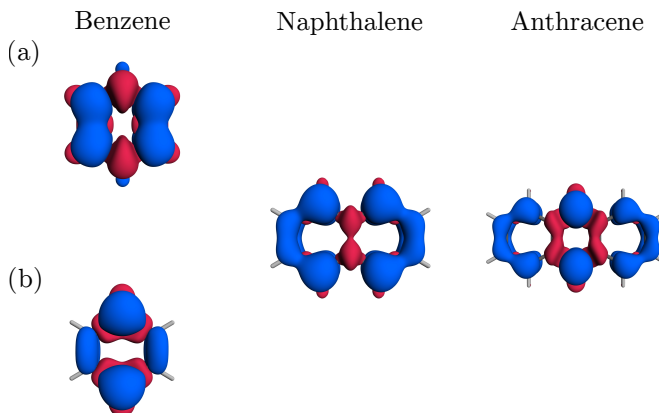


Figure 3.7: Spin densities of the studied monomers. (a) and (b) correspond to the compressed and elongated, respectively, triplet structures of the benzene.

3.3.1.3 *Low-lying states at the Franck-Condon region*

To complete the analysis of the triplet state in the three aromatic molecules, we analyze the lowest electronic excitations, i.e., T_1 and S_1 , at the ground state geometry (Table 3.3).

Table 3.3: T_1 vertical energies (eV) for each of the monomers computed with the cc-pVTZ basis set. CIS(D) and ω B97X-D orbital-to-orbital composition correspond to CIS and TDA transitions, respectively. H=HOMO; L=LUMO

method		benzene	naphthalene	anthracene
CIS(D)		4.470	3.846	2.553
	Composition	43% H-L+1	71% H-L	78% H-L
ω B97X-D		4.313	3.226	2.309
	Composition	48% H-L+1	89% H-L	91% H-L

Electronic transition from the ground state to the lowest triplet and singlet excited states involve mainly the HOMO \rightarrow LUMO transition. Like for the adiabatic triplet energies (Table 3.2), vertical excitation energy to T_1 (and S_1) decreases with the molecular size, in accordance with the reduction of the HOMO-LUMO gap.

3.3.2 Small Aromatic Dimers

In this section, we aim to find an excimeric states with spin-triplet multiplicity. For that, one has to be conscious about the structure of the system. An important

characteristic of these species is that the intermolecular interaction takes place through space (not through bond). As there might be quite a lot of possible structures to find this specific state, some initial pre-optimized structures have been considered in the search. Concretely, we have explored co-planar eclipsed conformers and different distortions along the x and y axes. In the following sections, we present the results for the most relevant structures, and while the rest of the structures are discussed in Appendix F.

The results obtained in the characterization of monomers have shown that that the ω B97X-D long-range corrected functional provides similar results to MP2 and CIS(D) calculations. Hence, taking into account the size of the systems and the computational cost, the analysis for these dimers has been done within DFT/TDDFT. Regarding the basis set, optimizations have been performed with the cc-pVTZ basis. In order to further decrease the computational load, we have also considered the cc-pVDZ basis set. As the results did not vary significantly between the two basis sets, the decomposition of the electronic states has been carried out by the smaller one (cc-pVDZ).

3.3.2.1 *Relative Stability*

The first step has been to analyze each optimization and see which kind of conformers were obtained. Analysis of the local minima on the PES of the triplet state of the dimer indicates that all structures can be classified into three different groups regarding to the intermolecular distance. Table 3.4 shows the most relevant information about the different conformers obtained for each of the systems. The basis set superposition error (BSSE) of interaction and binding energies has been corrected with the counterpoise method. For this, the following general nomenclature has been used,

$$E_{geometry}^{basis}(geometry) \quad (3.2)$$

and so, the corresponding interaction and binding energies are computed using the following equations,

$$E_{int}^{CP} = E_{AB}^{AB}(AB) - E_{AB}^{AB}(A) - E_{AB}^{AB}(B) \quad (3.3)$$

$$E_b^{CP} = E^{CP}(AB) - E_A^A(A) - E_B^B(B) \quad (3.4)$$

$$E^{CP}(AB) = E_{AB}^{AB}(AB) + \delta_{AB}^{BSSE} \quad (3.5)$$

$$\delta_{AB}^{BSSE} = E_{AB}^A(A) + E_{AB}^B(B) - E_{AB}^{AB}(A) - E_{AB}^{AB}(B) \quad (3.6)$$

where $E_{AB}^{AB}(AB)$ corresponds to the energy of the system in the basis and geometry of the dimer. $E_{AB}^{AB}(A)$ or $E_{AB}^{AB}(B)$ corresponds to the corrected energies of each monomer in the system. $E_{AB}^A(A)$ or $E_{AB}^B(B)$ is referred to the energies of each monomer in the dimer and $E_A^A(A)$ or $E_B^B(B)$ concerns the energies of the monomer itself. For the

triplet state, one of the energies corresponds to the singlet state monomer and the other to the triplet state.

Table 3.4: Intermolecular distances [d_{inter} (Å)], relative energies [E_{rel} (kcal/mol)], interaction energies [E_{int} (kcal/mol)] and binding energies [E_{bind} (kcal/mol)] for the most representative obtained minima for each of the systems. All computed at ω B97X-D/cc-pVTZ level of theory.

Distortion	d_{inter}	E_{rel}	E_{int}	E_{bind}
Benzene				
intermediate	2.733	26.770	-6.722	3.976
long	3.536	18.610	-3.920	-4.311
short	1.588	0.000	-64.834	-22.832
Naphthalene				
intermediate	3.134	16.928	-6.920	-0.032
long	3.558	9.162	-6.931	-6.855
short	1.605	0.000	-63.743	-15.782
Anthracene				
intermediate	3.102	19.708	-10.594	-4.448
long	3.587	12.707	-10.502	-10.378
short	1.606	0.000	-74.633	-22.866

Taking into account that all conformers were built like co-planar structures, regarding the relative energy for each of the systems one realizes that those distorted in the short axis have converged to lower energy than the other two distortions. This can also be reinforced by regarding to the intermolecular distance. For this particular case, the distance gets so short that makes one think in the creation of a bond between both monomers.

Comparing this values with those of the singlet state, it can be said that it does not matter which distortion is selected as the intermolecular distance remains almost the same, all of them are above 3.4 Å. Moreover, the energy difference between each conformer is small. On the other hand, more differences could be found for the interaction and binding energies. On this case, the structure of each of the monomers in the dimer do not vary drastically and so the energies are very similar. All this information can be found in Appendix F (Table F.1).

3.3.2.2 *Systems with Short Carbon-Carbon Distance*

As mentioned before, the first set of structures correspond to those with the shortest distance between the two monomers. These structures have been obtained through the initial distortion in the short axis and the minima on the triplet PES converge

to the formation of a σ bond between the two molecules. Related to these results, it is known that dimerization in acenes might be activated thermally or via light absorption [114]. Figure 3.8 shows the optimized structures triplet state covalent dimers of benzene, naphthalene and anthracene, with the bond length of the new σ bond indicated.

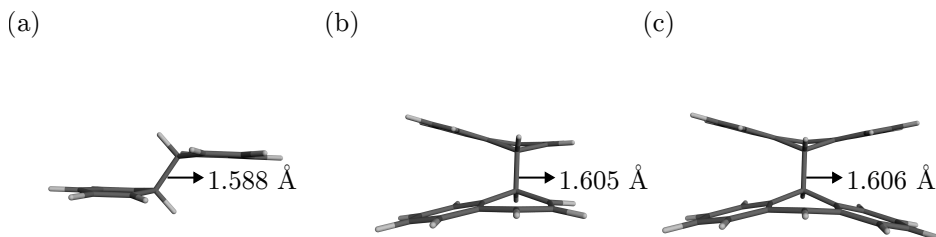


Figure 3.8: Covalent structures for the benzene, naphthalene and anthracene triplet dimers obtained at the ω B97X-D/cc-pVTZ level of theory.

Furthermore, the creation of the bond has generated changes in the monomeric C-C distances ($d(\text{C-C})$). The bonds which are near the intermonomeric σ -linkage, have suffered a distortion. Concretely, they appear elongated, moving from the typical sp^2 hybridization with a bond distance of 1.394 Å to 1.50 Å corresponding to a sp^3 hybridization.

Another key factor to label this type of structures as covalent dimers are the MOs and the representation of the spin density. As Figure 3.9 shows, the most representative aspect of these type of triplet state dimers is the formation of a σ -bonding orbital between the two monomers, in agreement with the short C-C distances indicated in Figure 3.8. On the other hand, the spin density corresponding to the two unpaired α -electrons delocalizes over the entire system. Although these dimers can be of great interest for instance in radical induced polymerization reactions [114], [115], they are not the focus of the present study, and we do not investigate them any further.

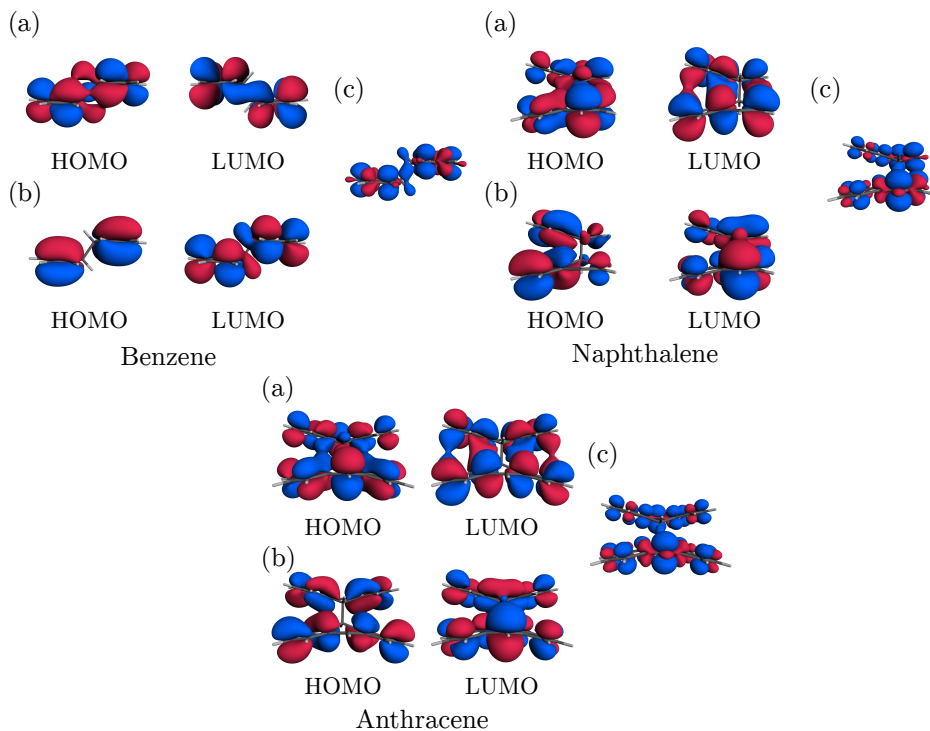


Figure 3.9: Molecular orbitals and spin densities of benzene, naphthalene and anthracene covalent dimers, where (a) are the α orbitals, (b) are the β ones and (c) shows the spin density computed at ω B97X-D/cc-pVTZ

3.3.2.3 Systems with π - π Stacking Carbon-Carbon Distance

Apart from the bonded dimers, there are some other local minima which do not show a covalent bond, Figure 3.10. These structures have been obtained through the distortion in the long axis. Comparing to the previous case, now the monomers remain flat, meaning that there are no sp^3 carbon atoms. Regarding their intermolecular distance, it can be seen that it belongs to the typical π - π stacking distance. In these dimers, individual molecular structures are very close to the S_0 and T_1 minima of the monomers, respectively. Hence, we identify them as localized triplet dimers. The overall symmetry of this type of dimers is C_1 (no symmetry elements), since the two monomers are not equivalent.



Figure 3.10: Localized triplet dimers of benzene, naphthalene and anthracene optimized at the ω B97X-D/cc-pVTZ level of theory.

As Figure 3.11 shows, and as predicted by our structural analysis, the non-equivalency of the two monomers in this type of triplet state conformers can be related to a localized triplet state. In particular, the α HOMO and the β LUMO are mostly localized on the molecule with a T_1 -like geometry. As a result, the triplet state spin density is strongly localized on this monomer (Figure 3.11c). Therefore, we might conclude that the localized triplet dimers correspond to the spin-triplet state, analogous to the ground state singlet, in which molecules aggregate through weak Van der Waals intermolecular interactions. Therefore, these are also not good candidates for the study of triplet state excimers in PAHs.

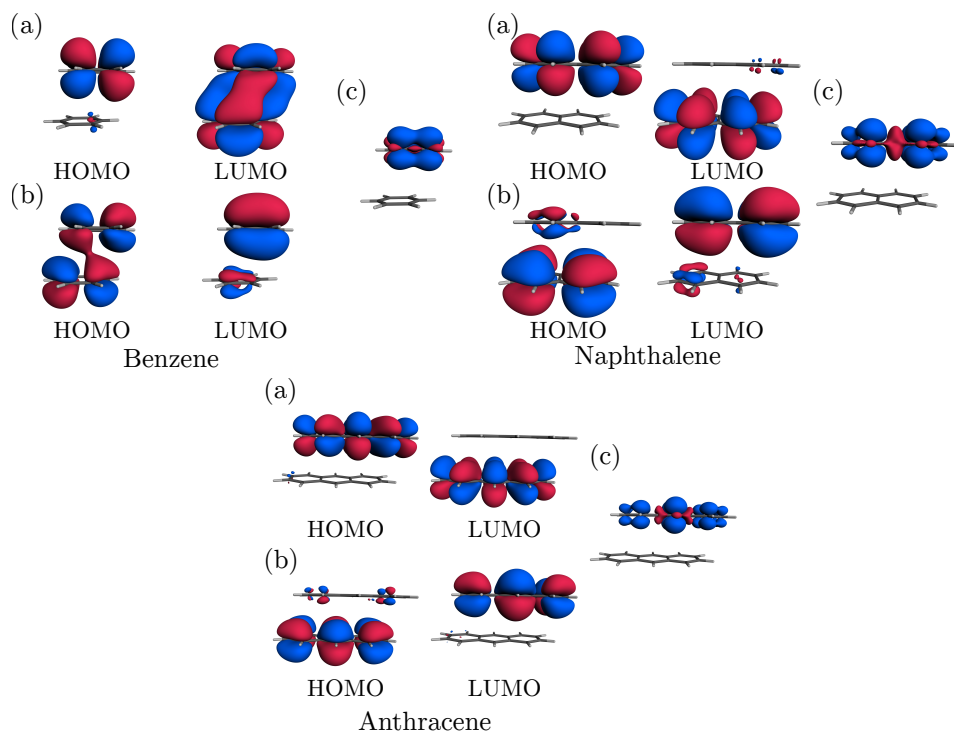


Figure 3.11: Molecular orbitals and spin densities of benzene, naphthalene and anthracene localized triplet dimers, where (a) are the α orbitals, (b) are the β ones and (c) shows the spin density computed at ω B97X-D/cc-pVTZ.

3.3.2.4 Systems with Intermediate Carbon-Carbon Distance

The last type of structures which also show a minima on the PES exhibit intermediate carbon-carbon distances between monomers. Figure 3.12 corresponds to the lowest energy stacked structures (more structures can be found in Appendix F). On the one hand, as Figure 3.12 shows, the separation between monomers is notably shorter than the typical π - π stacking distance (Figure 3.10), but they are not as short as in the covalent dimers (Figure 3.8). This distances correspond to 2.733 Å 3.134 Å and 3.102 Å, for benzene, naphthalene and anthracene, respectively. Moreover, it is worth mentioning that some of these structures present non-planar monomers, with different bending degrees, i.e., in benzene. This system has a stronger interaction between the two monomers than the naphthalene and anthracene, which can be related to the smaller intermolecular distance.

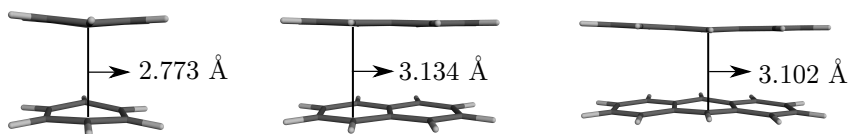


Figure 3.12: Structures of delocalized triplet states in benzene, naphthalene and anthracene dimers optimized with ω B97X-D/cc-pVTZ level of theory.

Interestingly, the two molecules in these dimers are equivalent and, contrary to the other type of triplet dimers, have a high symmetry. Consequently, we label them as delocalized triplet dimers. All the structures present stacked conformations and, although the monomers are non-planar, they all hold a global D_{2h} symmetry. Locally, benzene, naphthalene and anthracene monomers show C_{2v} .

The highly symmetric dimers with intermediate C-C distances are the most promising triplet state excimer candidates. As shown in Figure 3.13, eclipsed conformers of benzene, naphthalene and anthracene hold α and β MOs and spin densities completely delocalized over the whole molecular dimer. Spin distribution presents some differences depending on the number of aromatic rings. In particular, benzene and anthracene show a larger spin density in the central region of each of the monomers.

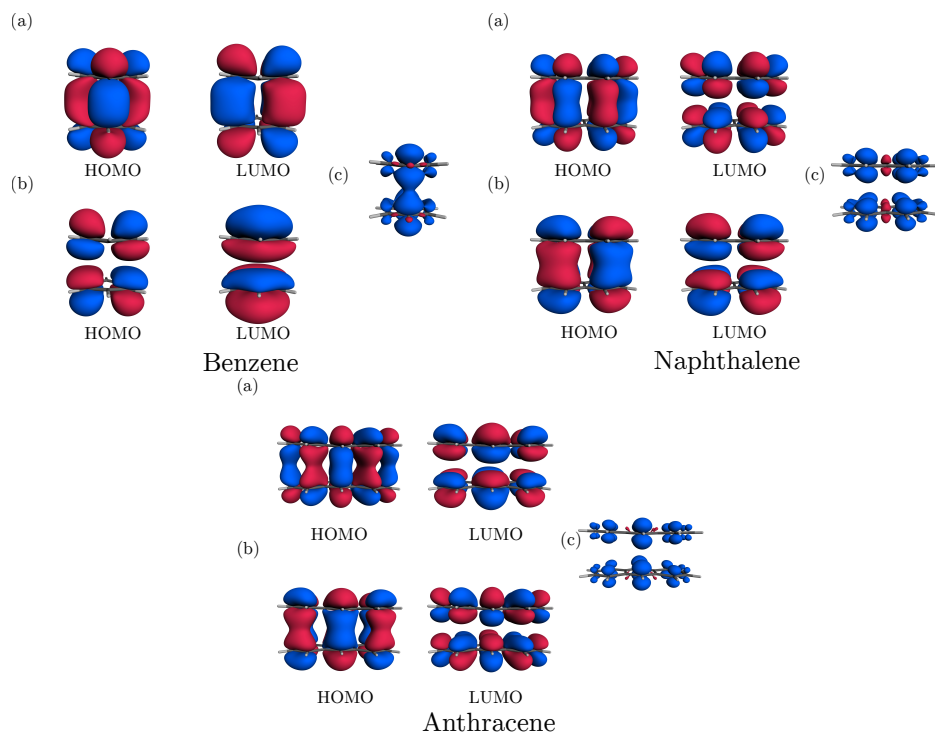


Figure 3.13: Molecular spin orbitals and spin densities of benzene, naphthalene and anthracene delocalized triplet dimers, where (a) are the α orbitals, (b) are the β ones and (c) shows the spin density computed at ω B97X-D/cc-pVTZ.

3.3.3 Nature of Delocalized Triplets

Before going in deep in the analysis of the nature of the excited states it can be important to see what happens in the T_1 state when moving from the monomer to the eclipsed dimer. Figure 3.14 shows the change in the triplet state excitation energy in the triplet state geometry. T_1 vertical energies of the monomer and dimer at the ground state geometry barely change (blue vs. orange bars). However, at the T_1 geometries there is an important reduction of the singlet-triplet gap, highlighting the impact of structural relaxation induced by intermolecular interactions at the triplet state.

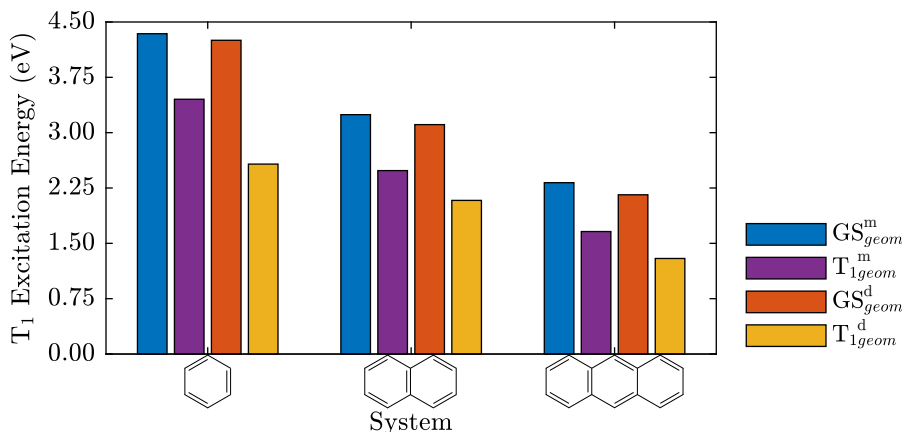


Figure 3.14: T_1 energies (ω B97X-D/cc-pVDZ) for the studied systems. Blue and purple bars correspond to the T_1 vertical energies of the monomers at the ground state (GS) and T_1 geometries, respectively; orange and yellow bars refer to the T_1 vertical energies of the dimers at the GS and T_1 geometries, respectively.

Vertical T_1 energies at triplet optimized geometries of the dimers are also shown in Table 3.5.

Table 3.5: Vertical T_1 energies (ΔE in eV) of benzene, naphthalene and anthracene eclipsed dimers computed with the TDA at the ω B97X-D/cc-pVDZ level. Transition composition obtained from TDA amplitudes. H = HOMO; L = LUMO.

dimer	ΔE	Composition
Benzene	2.574	91 % H-L
Naphthalene	2.082	86 % H-L
Anthracene	1.296	86 % H-L

In order to describe the nature of the triplet states in the eclipsed dimers, we evaluate their CT character through the decomposition of T_1 with a ER diabatisation scheme. Table 3.6 shows that the adiabatic triplet state in the eclipsed dimers corresponds to a mixing of LE and CT terms. The LE state is dominant in all systems, with contributions above 70 %.

Table 3.6: Composition of the T_1 adiabatic state in terms of LE and CT states computed at the ω B97X-D/cc-pVDZ level.

dimer	ω_{LE}	ω_{CT}
Benzene	73	27
Naphthalene	87	13
Anthracene	88	12

To further complete these analysis, the one-electron transition density matrix has been decomposed with the help of electron-hole correlation plots [91]. In this representation the LE contributions appear in the anti-diagonal, whereas CT contributions are placed in the main diagonal. The left part of following pictures represents the analyzed adiabatic state. In the middle, we show the nature of LE and CT terms contributing to the adiabatic state. Finally, the plots on the right contain a finer decomposition of the transition density matrix by considering different molecular fragments.

Figure 3.15 shows the decomposition of T_1 in the benzene dimer. The electron-hole correlation plot of the adiabatic state indicates larger contribution of the LE states (anti-diagonal squares are darker), in agreement with the ER decomposition (Table 3.6). Diabatic LE and CT states appear as no mixing, indicating the success of the diabaticization. Finally, on the right side of the figure it can be seen which group of atoms are involved in the LE and CT states. The lowest LE transition mainly takes place between atoms in different fragments. The CT contributions are localized in the central region of the dimer (blue rectangle in Figure 3.15). One needs to bear in mind that in central region the carbon atoms between both monomers show the shortest carbon-carbon distance.

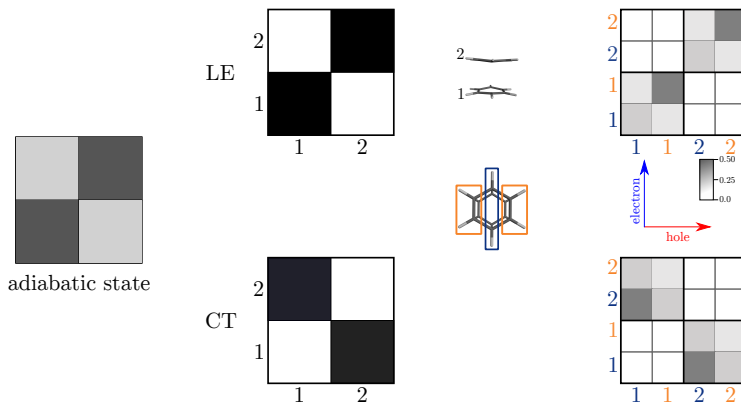
Figure 3.15: Electron-Hole correlation plots of adiabatic and the LE and CT triplet diabatic states for the eclipsed conformer of the benzene dimer computed at ω B97X-D/cc-pVDZ level.

Figure 3.16 exhibits the analysis of the eclipsed triplet in the naphthalene dimer. Just like for the benzene dimer, the representation of the adiabatic state shows that there is a mixing between the LE and CT. LE has a bigger weight as the anti-diagonal squares are darker than the main diagonal ones. This is in agreement with the results obtained in Table 3.6. The generated diabatic states have a rather pure character (no mixing). The last section of the picture shows the naphthalene system divided in three different groups. The first corresponds to the bond that unifies both rings (blue), the second makes reference to the group of atoms which are far from each other (orange) and finally the group which is outside the molecule (green). In the case of the LE state, the biggest contribution comes from the carbon atoms with the shortest C-C intermolecular distance (orange rectangle), with a small contribution from the carbons at the edge (green rectangle). The CT state shows similar contributions.

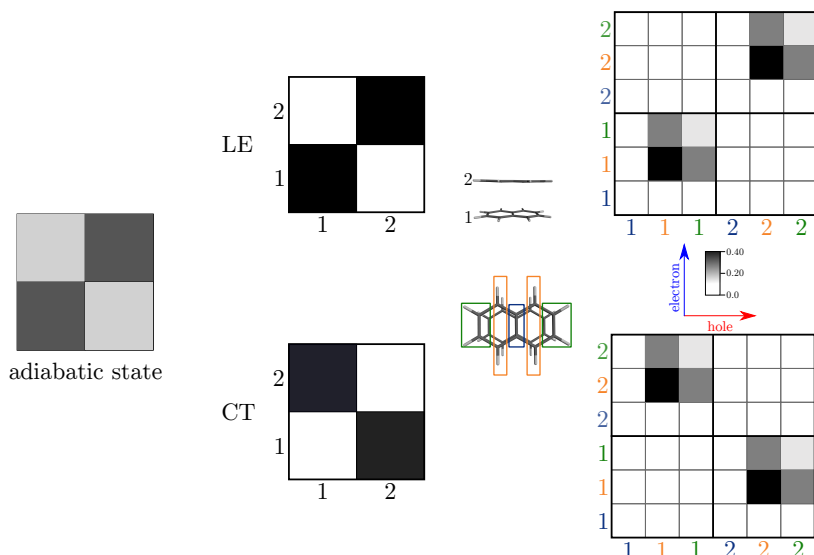


Figure 3.16: Electron-Hole correlation plots of the adiabatic and LE and CT triplet diabatic states for the eclipsed conformer of the naphthalene dimer computed at ω B97X-D/cc-pVDZ level.

Finally, in Figure 3.17 we analyse the one-electron transition density matrix for the anthracene dimer. Here, again, is repeated the predominance of the LE state as it is seen in Table 3.6. As in previous cases, the diabatic states show a pristine physical character. For the analysis of the diabatic states, the anthracene has been divided into four different groups as it is shown in Figure 3.17. Here it is seen that LE states are mainly localized in the non-centered rings, green and yellow areas, whereas CT contributions are mainly localized in the of atoms at the center of each ring.

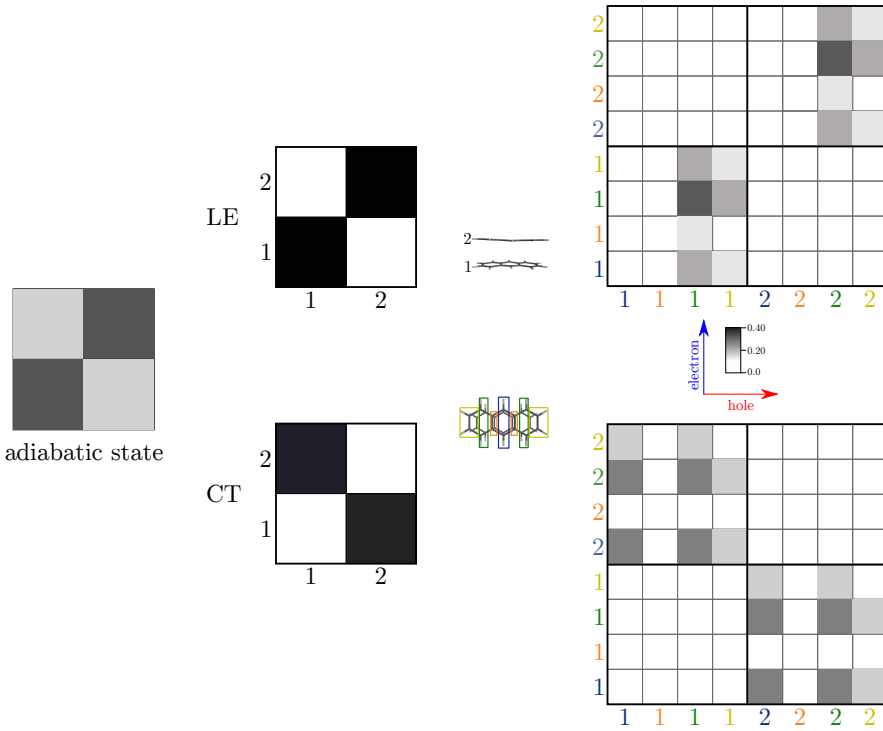


Figure 3.17: Electron-Hole correlation plots of the adiabatic and LE and CT triplet diabatic states for the eclipsed conformer of the anthracene dimer computed at ω B97X-D/cc-pVDZ level.

In addition to the state decomposition, the diabaticization procedure (see section 2.5) also allow to represent the electronic Hamiltonian in the diabatic state basis, that is, the diabatic Hamiltonian. In the case of a molecular homodimers with 2 LE and 2 CT terms, the diabatic Hamiltonian takes the form:

$$\begin{pmatrix} E_{LE} & V_{DC} & V_e & V_h \\ V_{DC} & E_{LE} & V_h & V_e \\ V_e & V_h & E_{CT} & V_{CT} \\ V_h & V_e & V_{CT} & E_{CT} \end{pmatrix} \quad (3.7)$$

where E_{LE} and E_{CT} correspond to LE and CT state energies, respectively; and V_{DC} and V_{CT} are the couplings between the two LE and two CT states, respectively. V_e and V_h are the electron and hole couplings related to the LE/CT interactions,

$$V_e = \langle \text{LE}_A | \hat{H} | \text{CT}_{AB} \rangle = \langle \text{LE}_B | \hat{H} | \text{CT}_{BA} \rangle \quad (3.8)$$

$$V_h = \langle \text{LE}_A | \hat{H} | \text{CT}_{BA} \rangle = \langle \text{LE}_B | \hat{H} | \text{CT}_{AB} \rangle \quad (3.9)$$

As indicated above, in the diabaticization of the triplet manifold in benzene, naphthalene and anthracene dimers we have considered a larger space. The reason for this selection can be related with the orbital-to-orbital contributions for the T_1 state of the monomers. In the case of the benzene, due to its degeneracy, 32 adiabatic states have been selected and so, the diabatic Hamiltonian is a 32×32 matrix. On the other hand, for naphthalene and anthracene 16 adiabatic states have been selected, ending up with a 16×16 matrix.

The diabaticization within the spin-triplet manifold for each of the systems results in pairs of degenerated LE and CT states, respectively. Even if more than 4 states have been selected to perform the diabaticization, the selection of the diabatic states the following criteria has been done in the following way, (i) Selection of the lowest LE and CT states in energy, (ii) From those states, select the ones which have a major contribution in the adiabatic state. The results of the diabaticization are shown on Table 3.7.

Table 3.7: Diabatic electronic energies (in eV) and the electronic couplings (in meV) obtained through the ER diabaticization of the eclipsed conformer of each system computed at the (TDA) ω B97X-D/cc-pVDZ level.

dimer	$E(^3\text{LE})$	$E(^3\text{CT})$	$\Delta E_{(LE-T_1)}$	$\Delta E_{(CT-LE)}$	V_e	V_h
Benzene	4.120	6.082	1.546	1.982	771	827
Naphthalene	3.621	4.772	1.539	1.158	544	541
Anthracene	2.680	3.641	1.385	0.961	320	335

Benzene shows diabatic states at 4.120 eV (LE) and 6.082 eV (CT). We note that these energies are quite high compared with the T_1 adiabatic energy (1.546 eV). Moreover, the difference in energy between both diabatic states is 1.982 eV. The most interesting information comes from the electron and hole couplings. The coupling corresponding to the electron is about 771 meV and the one related to the hole is 827 meV. These are rather large values, indicating that the interaction between the LE and CT states in T_1 is strong. In the naphthalene dimer we can see that the LE is at 6.217 eV and the CT at 4.772 eV. The LE state is 1.539 eV above the T_1 and the difference between diabatic states is 1.158 eV. Regarding the couplings, these have decreased considerably with respect to those of the benzene, 544 meV (V_e) and 541 V_h , but still they remain quite large, i.e., strong interaction between LE and CT states. Finally, the anthracene dimer shows 2.680 eV for the LE state and 3.641 eV for the CT state. In this case, T_1 and LE are closer in energy (1.385 eV apart) and the diabatic states are much closer than for the other two systems (0.961 eV). Probably the most drastic difference can be observed in the diabatic couplings, with in the order of 300 meV.

Overall, these results allows us to conclude that these eclipsed conformers of benzene, naphthalene and anthracene might form an excimeric state. Firstly, the

symmetric delocalization of the spin density is in agreement with a triplet excimeric state. Moreover, after the decomposition of the electronic states in diabatic contributions, it has been seen that even if the major contribution to the adiabatic state corresponds to LE, the CT state contribution is not negligible. Besides, this can be empathized with the interaction between this two diabatic states, V_e and V_h . Even if these values decrease while the system size, they remain high for the three studied dimers.

3.4 CONCLUSIONS

In conclusion, we have explored the possible formation of spin-triplet excimers in dimers of benzene, naphthalene and anthracene. After the optimization of the different considered conformers, three types of structures have been obtained. The first of these correspond to covalently bonded dimers, which are the most stable ones due to the bond formation. In these dimers, the shortest carbon-carbon distance is no longer than 1.61 Å. Their MOs as well as the spin density are delocalized over the entire system. These conformers have been discarded for further analysis because their structure is incompatible with the through-space interaction present in excimers. The second group of structures correspond to π - π stacking dimers, with intermolecular distances around 3.50-3.60 Å. One characteristic of these conformers is the localization of MOs and spin density on one of the monomers. These dimers are formed by dispersion interactions with no bond formation. As the triplet state is localized on one of the molecules, these dimers can be seen as a combination of the S_0 and T_1 structures. For this reason, this group of structures cannot be associated with excimers, and have not been used for further analysis. Finally, we have found some structures with intermediate intermolecular carbon-carbon distances, between 2.77 and 3.11 Å. Moreover, MOs and spin densities are symmetrically delocalized over the whole dimer. Therefore, they can be good candidates to hold excimeric states. In order to see if the excimer is formed in those structures of intermediate distance, the nature of the electronic excited states have been analyzed in depth. For that, the first step has been to see if the CT state contributes to the adiabatic T_1 state. Our results indicate that this contribution is not negligible, as this value is higher than 10 % for the three systems. Finally, representation of the electronic Hamiltonian in the LE and CT state basis has allowed to identify the LE/CT coupling to be the strongest interaction in the T_1 state. All these results makes us to conclude that the eclipsed dimers of benzene, naphthalene and anthracene can be classified as (triplet) excimers.

Chapter 4

THE MOLECULE OF PDI

In this chapter some properties of the Perylene-3,4:9,10-bis(dicarboximide) (PDI) will be discussed. Mainly, the analysis of the most representative properties such as the electronic structure and the ground and electronic excited states will be to be discussed.

4.1 INTRODUCTION

Perylene-3,4:9,10-bis(dicarboximide) or known as PDI have been widely studied as industrial colorants [116]. Moreover, they have been quite attractive due to their potential in applications related to optoelectronic devices, such as photovoltaic cells [8], [117]–[123], light-emitting diodes [124]–[126], transistor applications, [127], [128] or molecular wires [129], [130]. It has also been used as biochemical applications, [131], [132] or as materials for singlet exciton fission [133]–[135]. Besides, PDIs have been used as building blocks to construct artificial photosynthetic systems. This PDI and its derivatives (Figure 4.1) are one of the most versatile and attractive family of dyes, which have been largely employed in photophysical applications [127], [130], [136]–[138]. Concretely, PDIs are excellent molecular candidates for organic optoelectronics due to their nearly ideal properties, such as intense absorption capability, strong π -stacking interactions, high fluorescence quantum yield, and excellent thermal and photochemical stability due to its structural rigidity.

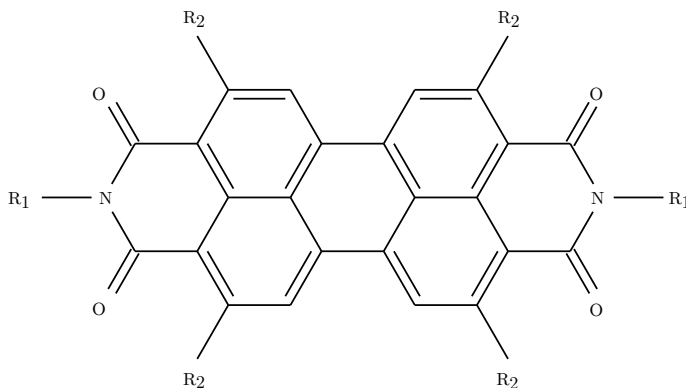


Figure 4.1: PDI molecular derivatives studied in this work. **1**: bis(*n*-octyl)-2,5,8,11-tetraphenyl-PDI (R_1 : octyl; R_2 : phenyl); **2**: 2,5,8,11-tetraphenyl-PDI (R_1 : H; R_2 : phenyl); **3**: PDI (R_1 : H; R_2 : H).

The present study performs a detailed characterization of the electronic structure properties of PDI with special interest on the bis(*n*-octyl)-2,5,8,11-tetraphenyl-PDI derivative (Figure 4.1).

4.2 METHODS

Molecular structures of PDI derivatives were optimized in vacuum by means of DFT, using the Coulomb-attenuating B3LYP (CAM-B3LYP) functional [139] and with the 6-31G(d) basis set. Optimized geometries were confirmed as energy minima on the potential energy surface through frequency analysis within the harmonic vibration approximation. All structures showed positive force constants.

Vertical excitation energies and transition properties to the lowest singlet and triplet excited states were obtained with the (linear response) TDDFT. Calculations were done with and without the TDA,[110] with the same exchange-correlation functional and basis set as in ground state calculations. Excitation energies and oscillator strengths computed with the 6-311+G(d) larger basis set (Table C.1) show rather small differences. This choice of the CAM-B3LYP functional has been motivated by its ability to properly describe electronic transitions with weak electron/hole overlaps, such as in CT excitations.

All electronic structure calculations discussed in this chapter were carried out with the Q-Chem package.[111]

In this section the molecular and electronic structure for the ground and low-lying excited states of the PDI molecule will be analyzed and characterized. For this, we discuss structural parameters, characterize frontier orbitals, and explore the dependence of excitation energies and transition properties with the employed exchange-correlation functional.

4.3 MOLECULAR STRUCTURE

As commented in section 4.1, the PDI molecular structure is rather rigid, planar and highly symmetric. In the following, the structural characteristics of the PDI molecule will be analysed in terms of bond lengths, angles and symmetry properties. The

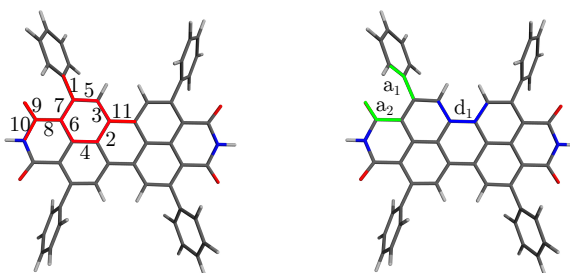


Figure 4.2: Analysed bond distances, angles and dihedrals in the optimized and crystal structures.

molecular structure of PDI in the crystal exhibits a nearly planar core with extended alkyl chains (R_1 , Figure 4.1) and lateral phenyl substituents (R_2) largely twisted out of the main molecular plane[133]. Molecular geometries of the PDI molecule **2**, *i.e.*, replacing alkyl chains by hydrogen atoms, optimized at the DFT level with different energy functionals result in a C_1 geometry with a slightly non-planar core, which overall are very close to the experimental one (Figure 4.2 and Table 4.1) and in good agreement with MP2 calculations[140].

In the bonds where heteroatoms are present, like nitrogen or oxygen, optimized and crystal bond lengths also are similar. The same happens for angles and dihedrals. Optimized and crystal structures have a_1 is around 120° . This can be understood like the rotation of the phenyl to overcome the steric hindrance. The molecular core exhibits a non-zero torsion ($d_1 \sim 6.3^\circ$), triggering a symmetry loss with respect to the planar conformation ($D_{2h} \rightarrow C_1$).

Table 4.1: Optimized and crystal structure bond lengths (\AA), angles ($^\circ$) and dihedral ($^\circ$) of the PDI molecule. See Figure 4.2 for labelling. Crystal bond lengths are given by the mean value of analogue bonds.

param.	Crystal			Optimized		
	1	2	3	1	2	3
C···C(1)	1.505	1.491	1.083			
C···C(2)	1.422	1.422	1.427			
C···C(3)	1.384	1.377	1.385			
C···C(4)	1.410	1.422	1.420			
C···C(5)	1.432	1.407	1.398			
C···C(6)	1.419	1.429	1.415			
C···C(7)	1.384	1.388	1.373			
C···C(8)	1.513	1.485	1.481			
C···O(9)	1.210	1.212	1.212			
C···N(10)	1.401	1.384	1.388			
C···C(11)	1.473	1.475	1.473			
a_1	123.5	121.0	-			
a_2	119.7	125.4	123.8			
d_1	5.5	6.3	0.0			

Table 4.2 shows the values of the following standard bond lengths: C···C, C···N and C···O. These are the most characteristic bond types of an aromatic system. C···C(1 and 8) belongs to the Csp^2-Csp^3 bond type. Although in both structures values do not vary to much, it can be seen there is a greater difference with the standard bond lengths, around 1.50 \AA for the structures and 1.53 \AA for the standard length.

Table 4.2: Standard bond lengths [141], [142].

Bond		Value
C...C	Csp^3-Csp^3	1.53 Å
	$Csp^2=Csp^3$	1.52 Å
	$Csp^2=Csp^2$	1.32 Å
	$Csp^2=Csp^2$ (aromatic)	1.38 Å
C...N	Csp^3-Nsp^2 (cyclic amide)	1.45 Å
C...O	$Csp^2=O$	1.24 Å

Focusing on the $Csp^2=Csp^2$ aromatic bond type, it can be seen that all the other C...C bond distances are close to the standard bond length for aromatic bonds (1.38 Å) [141]. This comes in agreement with the aromaticity of the system. And this is the reason why there is not any pure $Csp^2=Csp^2$ bond type.

Amide's (Csp^3-Nsp^2) standard bond length is 1.45 Å. In the analysed structures (C...N(10)) the values are smaller; 1.38 Å for the optimized and 1.40 Å for the crystal structure. In the case of the carbonyl ($Csp^2=O$) group, with a standard value of 1.24 Å the values of the analysed structures (C...O(9)) are smaller, 1.21 Å for each structure.

Figure 4.3 shows a summary of the comparison between C...C bonds. Here, it can be seen in a clear way there is not presence of $Csp^2=Csp^2$.

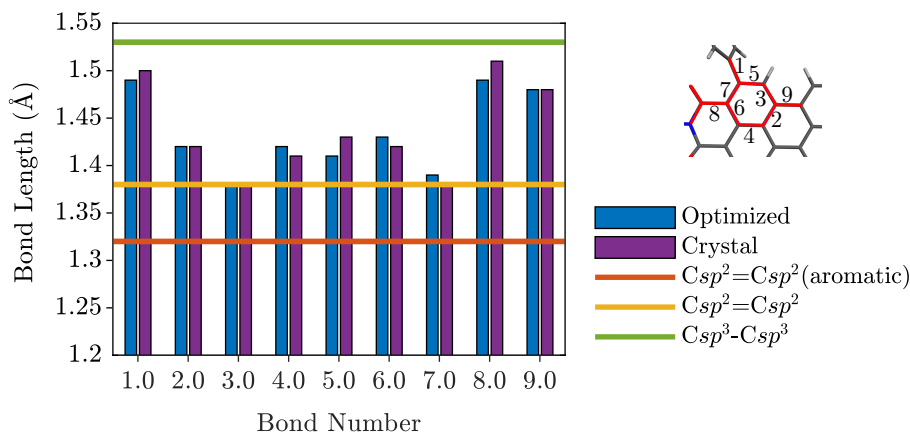


Figure 4.3: Analysed bond distances, angles and dihedrals in the optimized and crystal structures.

On the other hand, the optimized structure of **3** ($R_1 = H$, $R_2 = H$) is perfectly planar, holding D_{2h} symmetry (Figure 4.4), indicating the ability of R_2 substitution to disrupt the PDI core and ruling out packing effects as the origin of non-planarity.

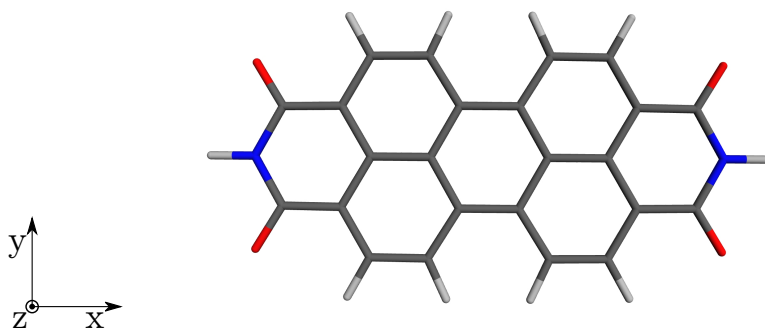


Figure 4.4: Structural representation of optimized PDI moiety at the CAM-B3LYP/6-31G* level.

The presence of heteroatoms, i.e., N and O, induces the polarization of bonds and generates a distribution of partial atomic charges (Figure 4.5).

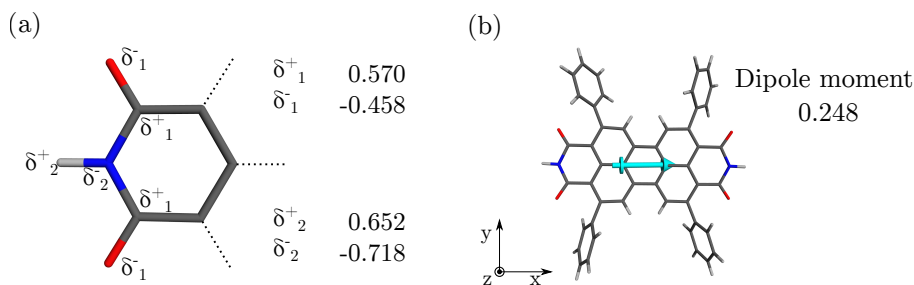


Figure 4.5: (a) Atomic charge distribution(a.u.); (b) ground state dipole moment(Debye) for the PDI molecule in the crystal structure.

It is also worth noticing that the molecular symmetry loss induced by the peripheral phenyl groups (optimized and crystal **1** and **2** structures) induce a non-zero (small) permanent dipole moment (0.248 Debye), obviously vanishing in the D_{2h} geometry (model **3**).

4.4 FRONTIER MOLECULAR ORBITALS

To fully understand the photophysical properties of the studied system, it is important to characterize its electronic structure. In particular, the characteristics of the energy levels at the frontier between occupied and virtual orbital space is of special interest, since it controls the nature of the low-lying electronic transitions.

The two frontier molecular orbitals of **2**, that is the HOMO and the LUMO, correspond to π -orbitals largely delocalized over the main molecular plane, with spurious electron density on the phenyl substituents (Figure 4.6), and with small

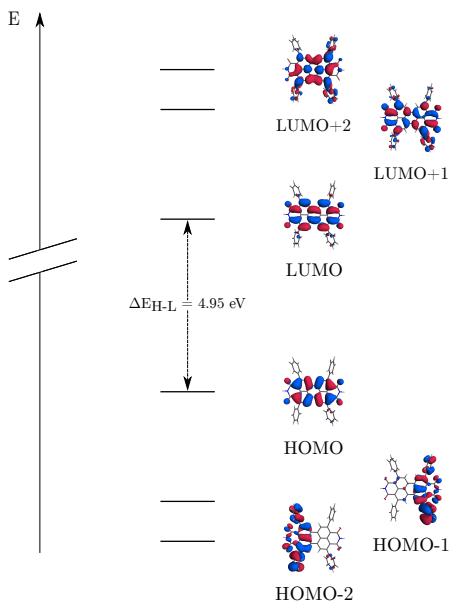


Figure 4.6: Frontier molecular orbitals computed for the PDI crystal molecule obtained at the CAM-B3LYP/6-31G* level.

modification of HOMO and LUMO π -energies related to symmetry loss (Table 4.3). Beyond the HOMO-LUMO orbital space, energetically lower (higher) occupied (unoccupied) molecular π -orbitals of the PDI backbone mix with molecular orbitals of the lateral phenyls.

Table 4.3: MO energies (in Hartrees) for PDI **2** and the optimized PDI **3** computed at CAM-B3LYP/6-31G(d) level.

	HOMO-1	HOMO	LUMO	LUMO+1
PDI 2	-0.281	-0.262	-0.080	-0.023
PDI 3	-0.329	-0.266	-0.093	-0.026

4.5 LOW-LYING EXCITED STATES

Once the ground state has been analysed in detail, the excited states of the PDI molecule are characterized. For that, the lowest spin singlet and triplet excited states have been computed by means of TDDFT. These calculations have been performed with three different exchange-correlation functionals, B3LYP, CAM-B3LYP and

ω B97X. Table 4.4 contains computational results for the low-lying excited states: excitation energies, oscillator strengths and electronic contributions.

Table 4.4: Vertical excitation energies (in eV) and oscillator strengths (in parenthesis) to the lowest singlet and triplet excited states computed at CAM-B3LYP/6-31G(d) level for the PDI **2**. Orbital-to-orbital composition correspond to TDA transitions. H=HOMO; L=LUMO.

State	TDDFT	TDA	Composition
S ₁	3.01(0.720)	3.19(0.986)	95 % H→L
S ₂	3.42(0.047)	3.47(0.057)	75 % H-1→L
S ₃	3.58(0.234)	3.61(0.232)	72 % H-2→L
S ₄	3.88(0.010)	3.91(0.015)	57 % H-3→L
S ₅	3.94(0.006)	3.97(0.010)	41 % H-9→L
T ₁	1.46	1.93	88% H→L
T ₂	2.67	2.95	31% H-2→L,24% H→L+1
T ₃	2.92	3.05	32% H-1→L,10% H→L+1
T ₄	3.05	3.14	55% H-2→L
T ₅	3.11	3.34	40% H→L+3

Vertical transition energies to the lowest-lying singlet and triplet states of **2** involve the HOMO→LUMO transition (Table 4.4). Excitation to the S₁ state is optically allowed, with a transition dipole moment on the molecular plane and oriented along the long molecular axis. The computed transition energy (3.01 eV) is in rather good agreement with other TDDFT calculations,[140] although blue shifted with respect to the absorption peak in toluene solution (2.34 eV). [143] The next two excited singlets, i.e., S₂ and S₃, are computed at ~0.3-0.5 eV above S₁. They mainly correspond to electronic promotions from the HOMO-1 and HOMO-2 to the LUMO. Inspection of the involved occupied orbital indicates some intramolecular CT character in both states, with sizeable participation of the π -electrons at the side phenyls. Although the aim is not to represent accurate experimental energies, some data has been checked from the work of Zimmerman et al. [40]. In this work, the absorption energy for S₁ is 2.36 eV and for S₂ 2.68 eV. On the other hand, checking the computational results of Table 4.4 and Table 4.6, one can see that there is an extra state between the two experimental values. The reason for this, is that the computed S₂ state has an oscillator strength near to 0, making it difficult to detect within the experiment.

The (HOMO→LUMO) lowest triplet state (T₁) lies rather below with respect to the first excited singlet, ~1.25 eV at the TDA. The large T₁/S₁ energy difference stems from a sizeable HOMO/LUMO spatial overlap resulting in a strong exchange interaction between the two frontier orbitals. T₁ is energetically

well-separated from the rest of the triplet manifold, with T₂-T₄ states computed more than 1 eV above it.

Another interesting point would be to analyze the impact of TDA [110] in the computed states. It is already known that this approximation reduces the computational cost which this leads to the underestimation of the relative intensities with respect to TDDFT. Despite, its use in the triplet state might be a good option. The reason for this is that TDA recovers the correct state order [144] as well as it resolves the triplet instability problem. Moreover, the transition moments do not satisfy the Thomas-Reiche-Kuhn sum rule [145]–[147]. In the case of interacting electron systems, this rule allows a direct calculation of collective frequencies in a long wavelength limit. Computed singlet-to-singlet energies with TDA follow the same trend as full TDDFT, with TDA gaps being slightly larger (by 0.2-0.3 eV). TDDFT vs. TDA differences are sensibly larger for the triplet states, in particular for T₁, $E_{\text{TDA}}(\text{T}_1) - E_{\text{TDDFT}}(\text{T}_1) = 0.47$ eV. Importantly, TDDFT and TDA states hold almost identical electronic structure character, indicating that in this case TDA might be a reasonable approximation in order to perform, at the very least, semi-quantitative characterization of electronic transitions in PDI systems.

Finally, a comparison between different energy functionals containing different amounts of Hartree-Fock exchange has been done.

Table 4.5 represents the energies computed with the different functionals as well as TDA and TD-DFT energies. Analysing B3LYP functional it can be said that there is a big difference between the energies of B3LYP and the two long range corrected functionals (Table 4.4, Table 4.6). Furthermore, regarding values of the oscillator strength, it can be seen that they present rather different distributions amongst low-lying excited singlets. It is known that B3LYP underestimates charge transfer states.

Table 4.5: Vertical excitation energies (in eV) and oscillator strengths (in parenthesis) to the lowest singlet and triplet excited states computed at B3LYP/6-31G(d) level for the PDI **2**. Orbital-to-orbital composition correspond to TDA transitions. H=HOMO; L=LUMO.

State	TDDFT	TDA	Composition
S ₁	2.60(0.275)	2.63(0.440)	93% H-1→L
S ₂	2.63(0.314)	2.72(0.083)	94% H-2→L
S ₃	2.71(0.079)	2.79(0.733)	90% H→L
S ₄	2.92(0.032)	2.93(0.088)	90% H-3→L
S ₅	3.02(0.041)	3.02(0.075)	92% H-4→L
T ₁	1.57	1.75	95% H→L
T ₂	2.40	2.42	92% H-1→-L
T ₃	2.51	2.53	91% H-2→-L
T ₄	2.63	2.69	67% H-3→-L
T ₅	2.86	2.88	60% H-4→-L

On the other hand, Table 5.4 shows the low-lying singlet and triplet excited states computed with the ω B97X functional. In contrast with Table 4.5 and in agreement with Table 4.4 the order of the singlet states remains the same. This means that S₁ for the long-range corrected functionals has the highest oscillator strength and the orbital-to-orbital composition corresponds to the HOMO→LUMO transition. Whereas for the B3LYP functional a switching of states is appreciated.

Table 4.6: Vertical excitation energies (in eV) and oscillator strengths (in parenthesis) to the lowest singlet and triplet excited states computed at ω B97X/6-31G(d) level for the PDI **2**. Orbital-to-orbital composition correspond to TDA transitions. H=HOMO; L=LUMO.

State	TDDFT	TDA	Composition
S ₁	3.21(0.785)	3.40(1.035)	92% H→L
S ₂	3.74(0.042)	3.82(0.050)	57% H→1-L
S ₃	3.90(0.289)	3.97(0.296)	54% H→2-L
S ₄	4.20(0.003)	4.23(0.005)	39% H→9-L
S ₅	4.26(0.011)	4.31(0.028)	45% H→10-L
T ₁	1.42	2.06	83% H→L
T ₂	2.68	3.08	33% H→L+2
T ₃	3.06	3.26	43% H→1-L
T ₄	3.17	3.35	37% H→2-L
T ₅	3.23	3.46	30% H→L+4

Comparing values obtained with CAM-B3LYP and ω B97X, it can be observed that both functionals produce the same HOMO-to-LUMO transition, with a similar non-zero oscillator strength. The difference in energy can be related to the different amount of HF exchange. The exchange interaction at the long-range for CAM-B3LYP is 65 % [148], whereas for ω B97X is 100%. This is the reason why ω B97X gives higher transition energies than CAM-B3LYP. Moreover, the other biggest difference between the analyzed functionals is the character of the S₁ state. As it was explained before, long-range corrected functionals give a HOMO→LUMO transition whereas the hybrid one is HOMO-1→LUMO transition. Taking into account Figure 4.6 we can see that the character of the states changes completely depending on the selected functional. While B3LYP shows an internal CT character, both long-range corrected functionals show a transition between totally delocalized MOs.

4.6 CONCLUSIONS

In conclusion, the low-lying electronic states of the PDI molecule have been characterized. The obtained computational results rationalize the photophysical properties of PDI and the effects resulting from intermolecular interactions, which are substantially distinct within the singlet and triplet state manifolds.

The four lateral phenyl rings in the PDI derivative **1** induce a (small) loss of planarity to the PDI backbone, slightly tuning single-particle energies around the Fermi level, even if the HOMO and LUMO are located almost exclusively on the PDI core. Alkyl chain substitution at the nitrogen atoms has barely any effect on

the properties of valence electrons. On the other hand, R₁ and R₂ substitutions play a major role in the aggregation of PDI molecules, largely limiting side interactions.

Chapter 5

PDI AGGREGATES: THE ROLE OF CT EXCITATIONS

In this chapter the molecular PDI aggregate will be analyzed. This investigation aim to compute excited states, characterize their electronic nature and describe their optoelectronic properties.

5.1 INTRODUCTION

While low-lying singlet excitations of PDI have been largely investigated [143], [149]–[153], there is less information about the triplet states. Despite that the triplet manifold is not initially accessible through photo-excitation, recent studies have identified spin triplets as the photophysical product states upon exciton decay processes in PDI dimers[154] and in the crystal.[133] Triplet excitons in organic compounds are typically optically transparent or weakly active at most, and present several advantages with respect to excited singlets, they exhibit longer-lifetimes that might result in longer diffusion lengths and higher probability to reach interfaces and electron-hole dissociation sites, which can facilitate their manipulation and make them suitable in optoelectronic applications [155]–[160].

In this chapter we aim to unravel the electronic structure intricacies of the singlet and triplet manifold in the crystal and in molecular aggregates by means of a variety of quantum chemistry calculations. The aim is to characterize the low-lying excited states in terms of LE, CT states and intermolecular electronic couplings. Although the nature of the singlet excitations of PDI aggregates in terms of LE and CT contributions has been investigated by several authors [149], [150], [152], the role of CT states in the triplet manifold remains largely unknown.

5.2 COMPUTATIONAL METHODS

Recently, Walter et al.[151] determined the suitability of CAM-B3LYP in the computation of electronic excitations of perylene dimers, while ω B97X-D[108] seems to provide better results in perylene bisimide dimers. Comparison of the performance of CAM-B3LYP, B3LYP, ω B97X and ω B97X-D exchange-correlation functionals in the characterization of singlet and triplet excitations in the monomer and dimer of **2** can be found in appendix A. Importantly, CAM-B3LYP and ω B97X-D provide very similar results for the studied PDI dimers (Tables D.1 and D.2). Unless indicated, discussed excitation energies and transition properties presented in the manuscript have been obtained for the structure of molecules and oligomers, e.g., dimers and trimers, in the crystal of **1**,[133] and by replacing the *n*-octyl chains by hydrogen atoms with N-H bond distance of 1.012 Å (PDI **2**).

Diabatization of electronic transitions computed within the TDA was performed by means of the ER localization scheme.[161] Diabatic energies and electronic couplings were obtained as the diagonal and off-diagonal matrix elements of the diabatic Hamiltonian, respectively. Diabatization of spin singlet and triplet excited states of molecular dimers of **2** have been done considering the four adiabatic states (mainly) corresponding to electronic promotions from the two highest occupied molecular orbitals (HOMO and HOMO-1) to the two lowest unoccupied molecular orbitals (LUMO and LUMO+1). Diabatization of triplet excited states of molecular trimers of **3** have been done with seven adiabatic states. Increasing the number

of adiabatic states barely modifies the characterization of the lowest singlets and triplets in terms of diabatic states. Diabatic state energies and couplings obtained with the Boys localization scheme[162] are nearly identical to ER values (Tables 5.5, 5.6 and D.5-D.7). Direct calculation of CT states and (spin) localized triplets in PDI dimers and trimers has been done with the C-DFT method[76] by restricting the local charge or spin on different monomers, respectively.

Parameters employed to obtain excitation energies and oscillator strengths in PDI oligomers through the dipole-dipole classical interaction model were: $|\mathbf{R}| = 15.95 \text{ \AA}$, $\theta = 42.5^\circ$ for the *inter*-column interaction, and $|\mathbf{R}| = 4.80 \text{ \AA}$, $\theta = 47.0^\circ$ and $|\mathbf{R}| = 5.00 \text{ \AA}$, $\theta = 44.6^\circ$ for the *intra*-column dimers within the unit cell and between cells, respectively.

5.3 RESULTS

The aim of this chapter is to describe the properties of low-lying excited states in PDI aggregates. In order to capture the electronic structure intricacies emerging from intermolecular interactions, a cluster approach is used, in which oligomeric structures with variable number of molecules are taken from the tetraphenyl PDI crystal. The obtained results derived from ground and excited state calculations will contribute to understand the nature of electronic states in aggregates of **1** in general and in particular of its crystal structure.

5.3.1 Crystal Structure

The crystal structure of PDI **1** is represented in Figure 5.1 [133]. PDI molecules are arranged in slip-stacked columns with an interplanar separation of $\sim 3.5 \text{ \AA}$ and two π -stacked molecules in the unit cell. Molecular columns are spatially well-separated to each other to accommodate for the alkyl chains and side phenyl groups. The crystal packing is formed by different columns of stacked PDI molecules.

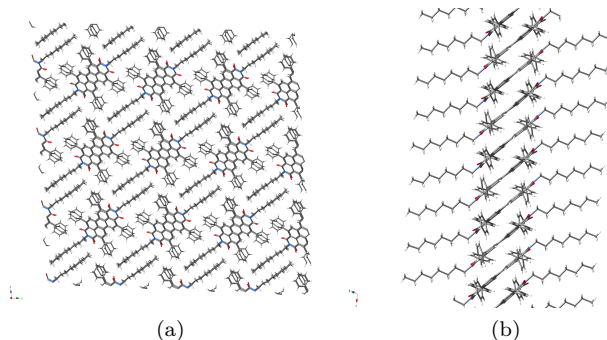


Figure 5.1: Figure (a) and (b) shows the disposition of the molecules in the PDI crystal structure.

Structural parameters regarding the length and the angles of the unit cell can be found in Table 5.1. The three dimensional PDI crystal structure belongs to the triclinic lattice and exhibits a P_{-1} space group symmetry.

Table 5.1: Lattice parameters, cell lengths (in Å) and angles (in degrees), of the PDI crystal unit cell [133].

length		angle	
a	9.87	α	93.6
b	15.53	β	99.2
c	16.39	γ	106.0

Figure 5.2 represents the intermolecular distances of the PDI molecule. This representation has been done with three molecules of PDI because distances change every three molecules. Intermolecular distances between molecular planes are d_c and d_d , 3.61 Å and 4.05 Å respectively. These distance values suggest the presence of π - π stacking interactions since these are within the range of reported values [163]–[165].

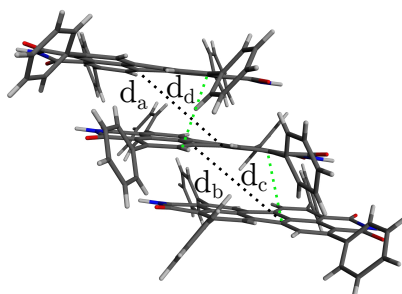


Figure 5.2: Part of the PDI crystal showing intermolecular distances: $d_a=4.74$ Å; $d_b=5.15$ Å; $d_c=3.61$ Å; $d_d=4.05$ Å. These distances have been measured directly from the crystal structure.

5.3.2 Intra- vs. inter-Column Interactions

First, a preliminary exploration has been performed to evaluate the relative magnitude of intermolecular interactions within a molecular crystal column and between adjacent columns. To that end, three different molecular dimers from the crystal structure were considered, i.e., the two distinct *intra*-column dimers, constituted by the two molecules within the unit cell (**D1** dimer) and between different cells (**D2** dimer), and the *inter*-column dimer with the shortest spatial separation. All dimers hold nearly co-planar PDI cores with a stacked conformation in the *intra*-column dimers, while in the *inter*-column dimer the two molecules nearly lie on the same plane in a diagonal disposition separated by lateral phenyl rings.

Molecular orbitals of the *intra/inter* systems exhibit rather different profiles. The four frontier orbitals computed for the *inter*-dimer are localized on either one of the two monomers, with rather small HOMO/HOMO-1 and LUMO/LUMO+1 energy gaps (Figure 5.3, right). On the other hand, molecular orbitals of the *intra*-column dimers are delocalized over the two molecules and show considerably larger energy splittings (Figure 5.3, left). These results point towards strong and weak intermolecular interactions for the *intra*- and *inter*-column dimers, respectively.

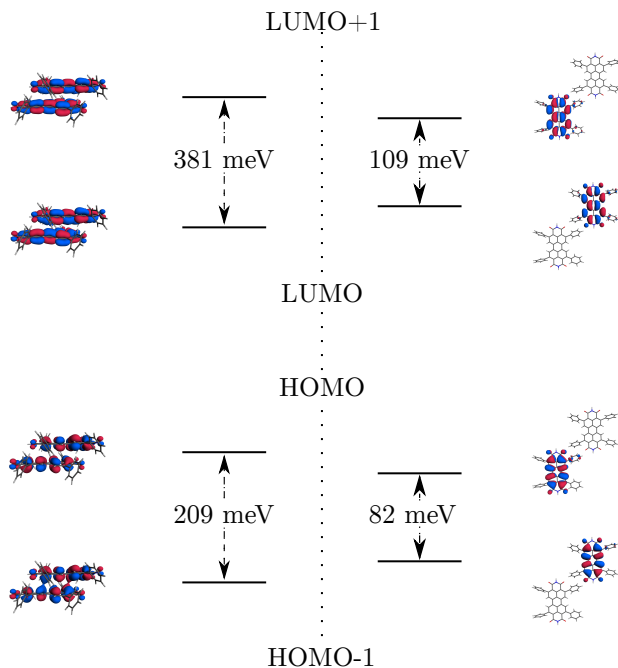


Figure 5.3: Molecular orbital (MO) diagrams of PDI dimers between molecules within the same column (unit cell *intra*-column dimer **D1**, left) and molecules for adjacent columns (*inter*-column dimer, right) computed at the TDA, CAM-B3LYP/6-31G(d) level. Representation of MOs for **D2** dimer can be found in Figure D.1.

Energy difference between S_1 and S_2 states of molecular homodimers can be used as approximation of twice the electronic coupling between the lowest excited singlets localized on each monomer. Low-lying transitions computed for the different dimers can be found in Table 5.2. The computed S_1/S_2 energy gap is much larger in the *intra*-column dimers than for the *inter*-dimer, indicating stronger excitonic coupling in the former. It is worth noting that, while in *inter*-dimer TDDFT excitation energies and oscillator strengths for the two lowest singlets are in good agreement with the classical dipole-dipole model (equation 5.1) for a J-aggregate [166], larger discrepancies appear for the slip-stacked dimers. The classical dipole-dipole interaction model predicts J-aggregation for the *intra*-dimers, with $J_{Coul}^{dd} = -182$ meV (**D1**) and -212 meV (**D2**), but, while CAM-B3LYP results also indicate bright and dark S_1 and S_2 states in dimer **D1**, the lowest excited singlet in **D2** corresponds to a dipole-forbidden transition. Moreover, in the two *intra*-column dimers, electronic structure calculations locate both excited singlets (S_1 and S_2) being red shifted with respect to the lowest transition in the monomer (3.19 eV).

Table 5.2: Excitation energies (in eV) and oscillator strengths (in parenthesis) to the lowest singlet excited states (S_1 and S_2) of *intra*-column (**D1** and **D2**) and *inter*-column dimers computed at the TDDFT/TDA CAM-B3LYP/6-31G(d) level (TDA), and with the dipole-dipole classical interaction between monomeric transitions (dip-dip).

method	S_1	S_2
<i>intra</i> -column D1		
TDA	2.95 (1.009)	3.04 (0.000)
dip-dip	3.01 (1.863)	3.37 (0.000)
<i>intra</i> -column D2		
TDA	3.04 (0.000)	3.12 (1.121)
dip-dip	2.98 (1.844)	3.40 (0.000)
<i>inter</i> -column		
TDA	3.17 (2.042)	3.19 (0.021)
dip-dip	3.18 (1.970)	3.20 (0.000)

These results suggest that excitonic couplings between stacked PDI molecules cannot be simply derived from the direct coupling of local excitations, such as in the classical dipole-dipole interaction model,

$$J_{Coul}^{dd} = \frac{|\boldsymbol{\mu}|^2(1 - 3\cos^2\theta)}{4\pi\epsilon_0|\mathbf{R}|^3} \quad (5.1)$$

where $\boldsymbol{\mu}$ is the molecular transition dipole moment, \mathbf{R} is the distance vector connecting the two transition dipoles, and θ the angle between $\boldsymbol{\mu}$ and \mathbf{R} vectors. Computed couplings indicate that aggregation induced effects are dominated by the coupling of co-planar slip-stacked PDI molecules, while the interaction between molecules in different columns play a much lesser role. Therefore, the study will be followed by considering clusters of stacked molecules within a crystal column.

5.3.3 Lowest Singlet and Triplet Excited States

To systematically explore the extent of the aggregation induced effects in the electronic excited states of PDI, a comparison has been done between excitation energies of the lowest singlet and triplet states for clusters of different sizes, i.e., with different number of stacked PDI molecules (Figure 5.4). The excitation energy to both states decrease with the number of PDI molecules, and seem to reach a plateau around 5-6 molecules for the singlet and at smaller clusters (2-3 molecules) for T_1 . The energy stabilization of S_1 (311 meV), computed as the difference between excitation energy of the sextamer and the monomer, is considerably larger than for

T_1 (59 meV). Not surprisingly, the major decrease in T_1 and S_1 excitation energies occur from the monomer to the dimer and trimer, indicating that first neighbor interactions are the most important ones.

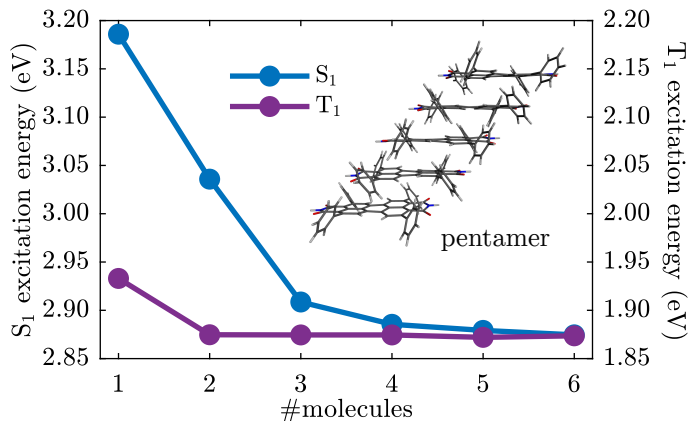


Figure 5.4: Vertical excitation energies (in eV) to the lowest singlet (blue, left axis) and triplet (purple, right axis) as a function of the number of PDI stacked molecules computed with the CAM-B3LYP/6-31G(d) level with the TDA. Inset: slip-stacked pentamer of PDI **2**.

This results can be related to the systematic HOMO-LUMO gap reduction with the number of stacked molecules shown in Table 5.3. It can be appreciated how the energy decreases while the number of stacked PDI molecules increases. Moreover, the main decrease in energy happens between 1 and 2 (0.19 eV) and 2 and 3 (0.22 eV) stacked molecules in the PDI crystal. Beyond 4 stacked PDI molecules the computed gap barely changes.

Table 5.3: Energy difference(ΔE_{HL}) between the HOMO and LUMO orbitals, in eV. Calculations done at CAM-B3LYP/6-31G* level.

1	2	3	4	5	6
4.95	4.76	4.54	4.54	4.49	4.49

Next, the case with five stacked chromophores has been considered as a representative model to describe the photophysical properties of PDI (**1**) aggregates, since in the pentamer S_1 and T_1 computed energies have converged, i.e., there are almost no changes in S_1 and T_1 energies between stacked pentamer and hexamer crystal aggregates. Moreover, in stacked oligomers with an odd number of molecules, local excitations on the central monomer more closely preserve the symmetry of the individual molecule, facilitating molecule/oligomer comparisons. Molecular orbitals

of the pentamer are largely delocalized and differently stabilized upon $\pi - \pi$ intermolecular interactions (Figure 5.5). The HOMO-LUMO gap is considerably reduced with respect to the monomer (Figure 4.6), in agreement with the smaller vertical excitation energies to S_1 and T_1 .

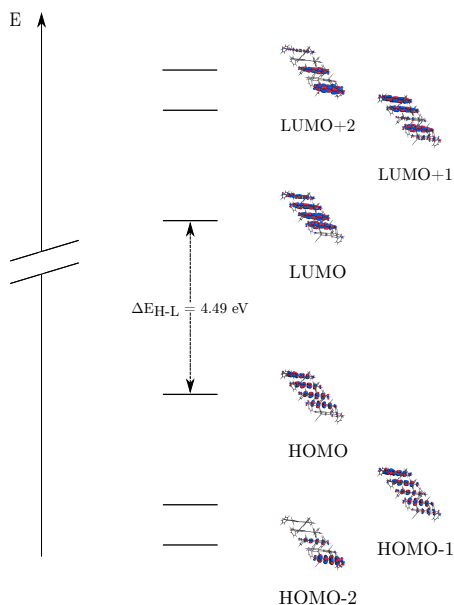


Figure 5.5: Frontier molecular orbitals and their energy diagram for the stacked pentamer of PDI derivative **2** computed at CAM-B3LYP/6-31G(d) level.

Table 5.4 lists excitation energies, oscillator strengths and electronic contributions for the PDI pentamer’s low-lying excited states. The five lowest singlets are computed with a fairly narrow energy window below the energy of the monomer, and show a distribution of oscillator strengths ranging from nearly zero to the most active (HOMO-to-LUMO) transition, resembling the lowest singlet transition of **D1** (Table 5.2). These states are obtained as the configuration interaction of several orbital transitions and exhibit important spatial delocalization. Like in the **D1** and **D2** dimers, CAM-B3LYP results for the singlet-singlet transitions are qualitatively different with respect to the state distribution around S_1 of the monomer obtained with the classical excitonic model of local excitations interacting through J_{Coul}^{dd} (equation 5.1). The lowest-energy end of the triplet manifold shows even larger degeneracy, with computed energies within a small energy range around the T_1 energy of the monomer (1.93 eV).

Table 5.4: Vertical excitation energies (in eV), oscillator strengths (in parenthesis) and main electronic composition for the lowest excited singlet and triplet states of the PDI stacked pentamer computed at the (TDA) CAM-B3LYP/6-31G(d) level, and by the classical dipole-dipole interaction (dip-dip). H = HOMO; L = LUMO.

state	dip-dip	TDA	composition
S ₁	2.85 (4.091)	2.88 (0.153)	39% H-1→L
S ₂	2.99 (0.000)	2.91 (1.303)	49% H→L
S ₃	3.19 (0.335)	2.97 (0.191)	20% H-4→L
S ₄	3.39 (0.000)	3.02 (0.084)	19% H-3→L
S ₅	3.53 (0.026)	3.07 (0.628)	30% H-2→L+2
T ₁	1.93	1.87	34% H→L
T ₂	1.93	1.88	28% H-1→L
T ₃	1.93	1.93	42% H-2→L+1
T ₄	1.93	1.95	22% H-3→L
T ₅	1.93	1.96	23% H-4→L

The S₁ state shows an excitation energy of 2.88 eV with an oscillator strength of 0.15. The composition of this excitation does not correspond to the HOMO-LUMO promotion, 39 % HOMO(-1)-LUMO. This case exemplifies that not always the lowest excited state can be described with the two frontier orbitals, in particular, in systems with degeneracies (or near degeneracy) between HOMOs and/or LUMOs. S₂ is the brightest excitation as indicates its larger oscillator strength (1.30). Like for S₁ state, there are several orbital-orbital terms contributing to the transition, but in this case, the HOMO-LUMO electron promotion appears with a contribution of 49 %. The other three excited states are close in energy and the oscillator strengths are not very high. Taking into account their composition, it can be seen that different orbitals contribute in these transitions. Orbital composition of these states suggest that the low-lying singlet excitations are delocalized over several molecules. This is quite significant for bright states. It is worth noticing that, for the two brightest states, S₂ and S₅, the transition dipole moment goes in the direction of the long molecular axis, the *x* axis, like for the S₁ transition in the PDI molecule.

The T₁ transition is computed at 1.87 eV and is built as two main contributions: HOMO-LUMO and HOMO(-1)-LUMO. T₂ is very close to T₁ in energy (0.03 eV above) and HOMO-LUMO and HOMO(-1)-LUMO(+1) being the main contributions with very similar amplitudes. The other three spin triplet excitations are close in energy.

Comparing this values with those obtained for the isolated PDI crystal monomer, it can be said that the energy window of the 5 states, singlet and triplet, is quite different. For the isolated crystal monomer, the difference of the singlet states is 0.78 eV and for the triplet 1.41 eV. For the crystal pentamer, the singlets are in a

range of 0.19 eV and the triplets 0.09 eV. This small energy window can be seen as a combination of each lowest-lying monomer's transition, S_1 and T_1 . Apart from this, the calculations for the isolated molecule of the crystal indicate that S_2 and S_3 states have partial CT character. This cannot be appreciated in the PDI crystal pentamer because the computed low-lying transitions are obtained as electronic promotions between occupied and virtual orbitals that are combinations of the HOMO and LUMO, that is the lowest excited singlet and triplet states in the PDI pentamer mainly emerge from the molecular S_1 and T_1 excitations.

As additional calculations, the comparison between different exchange correlation functionals, B3LYP, CAM-B3LYP and ω B97X, has been done. Results obtained with these functionals can be found in Appendix C. In the aggregate, things are not as clear as in the PDI crystal monomer; not only because the excitation energy arises increasing the HF exchange, but also due to the unclear trend of the oscillator strengths.

5.3.4 Electronic Couplings

In order to further characterize electronic transitions in PDI aggregates and understand in more detail the nature of the electronic interactions governing the properties beyond the classical approximation (Kasha's model), the aim is to decompose the computed (adiabatic) singlet and triplet excitations in terms of diabatic states, i.e., electronic transitions with well defined character. To that aim, the ER diabatization scheme is used to express the lowest excited singlet and triplet states in the **D1** and **D2** dimers in terms of LE and CT. In the following, the phase of the LE and CT singlet diabats is assigned according to the conventional exciton model based on translational symmetry of the transition dipole moment [167], [168]. The sign of the couplings between (dark) triplet states is assigned in comparison to the singlet-singlet values.

Electronic couplings between diabatic states can be classified upon the nature of the interacting terms [169], as the coupling of two LE, or direct coupling (V_{DC}), which can be approximated by J_{Coul}^{dd} for large interchromophore distance; the interaction of LE and CT states as electron (V_e) and hole (V_h) couplings (commonly expressed as the electron and hole transfer integrals); [170] and the interaction between the two CT states (V_{CT}):

$$V_{DC} = \langle LE_A | \hat{H} | LE_B \rangle \quad (5.2)$$

$$V_e = \langle LE_A | \hat{H} | CT_{AB} \rangle = \langle LE_B | \hat{H} | CT_{BA} \rangle \quad (5.3)$$

$$V_h = \langle LE_A | \hat{H} | CT_{BA} \rangle = \langle LE_B | \hat{H} | CT_{AB} \rangle \quad (5.4)$$

$$V_{CT} = \langle CT_{AB} | \hat{H} | CT_{BA} \rangle \quad (5.5)$$

where $LE_A = A^*B$, $LE_B = AB^*$, $CT_{AB} = A^+B^-$, $CT_{BA} = A^-B^+$, and A and B correspond to the two monomers in the dimer. In the perturbative limit, the energy

of the two lowest excited singlet states, symmetric (+) and antisymmetric (−) with respect to transnational symmetry, can be expressed as the sum of the LE energy, the self-energy Δ_{CT} , and the direct (V_{DC}) and LE/CT (J_{CT}) couplings [168]:

$$E_{\pm} = E_{LE} + \Delta_{CT} \pm V_{DC} \pm J_{CT} \quad (5.6)$$

$$\Delta_{CT} = -\frac{V_e^2 + V_h^2}{E_{CT} - E_{LE}} \quad (5.7)$$

$$J_{CT} = -\frac{2V_e V_h}{E_{CT} - E_{LE}}. \quad (5.8)$$

Hence, the relative magnitude and sign of V_{DC} , V_e and V_h , and the LE/CT energy gap determine the nature of the lowest exciton, i.e., optically bright (+) or dark (−), eventually resulting in J- or H-aggregation [170]. If $V_{DC} < 0$ ($V_{DC} > 0$) the symmetric (antisymmetric) solution is stabilized inducing J-aggregation (H-aggregation). On the other hand, in-phase V_e and V_h ($V_e V_h > 0$) couplings promote J-aggregation (independently of their individual signs), while out-of-phase couplings induce H-aggregates. The overall photophysical properties of the aggregate arise from the competition between LE/LE and LE/CT interactions [171]. The V_{DC} coupling dominates for long-range interactions, but at short inter-chromophore distances molecular orbitals overlap and V_e and V_h couplings (superexchange) [168] can become important, and might overcome LE/LE.

Diabatization within the spin-singlet manifold of the two *intra*-column dimers results in two pairs of degenerated states with LE and CT character, respectively. LE obtained energies, 3.16 eV (**D1**) and 3.14 eV (**D2**), are very close to the energy of the monomer (Table 5.5). Interestingly, CT states are only 0.11-0.13 eV above the LE energy and, although the LE/CT energy gap is method dependent [151], [152], the relatively low energy of CT diabats has been confirmed by charge C-DFT calculations imposing the cation-anion configuration (A^+B^-) in the dimer.

Table 5.5: Diabatic electronic energies (in eV) and electronic couplings (equations 5.2-5.5, in meV) obtained through the ER diabatization of the four lowest excited singlets and triplet states of the PDI *intra*-dimers **D1** (unit cell) and **D2** (between cells) computed at the (TDA) CAM-B3LYP/6-31G(d) level.

dimer	$E(^1LE)$	$E(^1CT)$	V_{DC}	V_e	V_h	V_{CT}
D1	3.16	3.27	106	-176	-134	-2
D2	3.14	3.27	97	-92	-40	-13
dimer	$E(^3LE)$	$E(^3CT)$	V_{DC}	V_e	V_h	V_{CT}
D1	1.95	3.25	-1	-182	-143	-2
D2	1.94	3.28	1	-123	-54	-3

The charge-constrained CT is computed at 3.33 (**D1**) eV and 3.48 (**D2**) eV with respect to the ground state, rather close to the CT energies obtained through diabaticization.

Excitonic coupling between the two local (singlet) excitations in both dimers is positive ($V_{DC} > 0$), and slightly larger for **D1**, favoring the anti-parallel configuration of (local) transition dipole moments. This result is in complete contradiction with the point dipole interaction approach, which has to be completely disregarded to model slip-stacked PDI aggregates. On the other hand, the computed V_{DC} values are in very good quantitative agreement with the Coulombic coupling obtained by Oleson et al. [149] derived from atomic transition charge densities.[172], [173]

$^1\text{LE}/^1\text{CT}$ couplings are rather strong, in particular for **D1**. Although the interplanar separation is equal in both dimers (3.5 Å), the transverse slip is larger between molecules of different unit cells (**D2**) by 0.3 Å, substantially decreasing orbital overlap between the two monomers. In both π -stacked dimers the magnitude of V_e is at least 40 meV larger than V_h , inline with the much larger orbital splitting between LUMO/LUMO+1 (381 meV in **D1** and 190 meV in **D2**) than for the HOMO/HOMO-1 pair (299 meV in **D1** and 109 meV in **D2**), and in good agreement with hole and electron transfer integrals[149] computed using the polarization-including procedure.[174] Importantly, the two V_e and V_h couplings are in-phase (J-aggregation). Competition between direct coupling and superexchange ultimately results in J-aggregation in **D1**, for which the LE/CT couplings are much stronger, and in H-aggregation in **D2** (Table 5.2).

The excitonic couplings between the two localized triplets are two orders of magnitude smaller than in the spin singlet space since ^3LE is optically dark. This different behavior can be rationalized by approximating the V_{DC} within the HOMO/LUMO model for interacting chromophores with orthogonal orbitals:

$$V_{DC}^{S=0} \approx 2(h_A l_A | h_B l_B) - (h_A h_B | l_A l_B) \quad (5.9)$$

$$V_{DC}^{S=1} \approx -(h_A h_B | l_A l_B), \quad (5.10)$$

where h_X and l_X are the HOMO and LUMO of monomer $X = A, B$, and $(pq|rs)$ is a two electron integral in chemists' notation. The J -like first integral in equation 5.9 is expected to dominate V_{DC} in the singlet, since it involves the overlap of orbitals in the same monomer. This contribution vanishes for triplet states (equation 5.10), where only the K -like term remains, resulting in much weaker direct coupling. On the other hand, the LE/CT couplings can be estimated as the hole and electron transfer integrals independently of the spin,

$$V_h^{S=0,1} \approx t_h \equiv -\langle h_A | \hat{H} | h_B \rangle \quad (5.11)$$

$$V_e^{S=0,1} \approx t_e \equiv \langle l_A | \hat{H} | l_B \rangle, \quad (5.12)$$

which explains the rather similar LE/CT couplings computed for singlets and triplets in each dimer. Like in the singlet case, the couplings between ^3CT diabats are rather

small, since they correspond to integrals involving the orbital overlap between different molecules:

$$V_{CT}^{S=0} \approx 2(h_A l_B | h_B l_A) - (h_A h_B | l_A l_B) \quad (5.13)$$

$$V_{CT}^{S=1} \approx -(h_A h_B | l_A l_B). \quad (5.14)$$

Table 5.6: Transition energies (in eV), oscillator strengths (in parenthesis), and diabatic contributions ω (in %) obtained through the ER diabaticization for the two lowest excited singlet and triplet states of **D1** and **D2** dimers computed at the (TDA) CAM-B3LYP/6-31G(d) level. $\omega(\text{LE}) = \omega(\text{LE}_A) + \omega(\text{LE}_B)$, $\omega(\text{CT}) = \omega(\text{CT}_{AB}) + \omega(\text{CT}_{BA})$.

state	ΔE (f)	$\omega(\text{LE})$	$\omega(\text{CT})$
D1 dimer			
S _{1,+}	2.96 (1.009)	50	50
S _{2,-}	3.04 (0.000)	96	4
T _{1,+}	1.87	94	6
T _{2,-}	1.95	100	0
D2 dimer			
S _{1,-}	3.04 (0.000)	96	4
S _{2,+}	3.12 (1.123)	52	48
T _{1,+}	1.92	98	2
T _{2,-}	1.94	100	0

Table 5.6 shows the decomposition of electronic singlet and triplet transitions in terms of diabatic contributions for the two *intra*-column dimers. In the **D1** dimer, superexchange overcomes the direct coupling and the lowest (adiabatic) excited singlet is obtained as the symmetric combination of LE and CT. The LE/CT mixing is remarkable, with CT contributions amounting to 50% of the transition. On the contrary, the anti-symmetric singlet (vanishing transition dipole moment) is almost entirely obtained as local excitations (CT contributions $\sim 4\%$). The composition of the two lowest singlets in **D2** are almost identical to the unit cell dimer, but with the inverse state ordering. This rather different behaviour of symmetric and anti-symmetric solutions can be rationalized by considering the coupling of Frenkel excitons (FE, equation 5.15) to charge resonances (CR, equation 5.16). FE can only mix with CR with the same symmetry (equation 5.18), and the FE/CR interaction is dictated by the relative sign and magnitude of electron and hole couplings (equation 5.17). In **D1** and **D2**, V_e and V_h have the same sign and similar magnitudes, resulting in strong (symmetric) and weak (anti-symmetric) interactions.

$$|\text{FE}_{\pm}\rangle = \frac{1}{\sqrt{2}}(|\text{LE}_A\rangle \pm |\text{LE}_B\rangle) \quad (5.15)$$

$$|\text{CR}_{\pm}\rangle = \frac{1}{\sqrt{2}}(|\text{CT}_{AB}\rangle \pm |\text{CT}_{BA}\rangle) \quad (5.16)$$

$$\langle \text{FE}_{\pm} | \hat{H} | \text{CR}_{\pm} \rangle = V_e \pm V_h \quad (5.17)$$

$$\langle \text{FE}_{\pm} | \hat{H} | \text{CR}_{\mp} \rangle = 0 \quad (5.18)$$

Despite the strong V_e and V_h couplings in the triplet state (Table 5.5), CT terms barely mix into the lowest-lying triplets, even for the symmetric states (CT contributions $\sim 6\%$). This result can be understood by evaluating the energy contribution to the excitation energy resulting from superexchange (J_{CT} , equation 5.8). CT energy is almost the same for the spin singlet and triplet, but ${}^3E_{LE} \ll {}^1E_{LE}$. As a consequence, J_{CT} is an order of magnitude smaller in the spin triplet state than in the singlet.

5.3.5 Triplet state localization

The above results quantify the energetic stabilization of the T_1 state upon molecular stacking (Figure 5.4), which is considerably weaker than for the singlet excitation, and with nearly no involvement of CT states due to the large energy gap between ${}^3\text{LE}$ and ${}^3\text{CT}$. These results are inline with a strongly bonded hole/electron pair spatially restricted to one molecule. The localization of the triplet state is confirmed by the spin density distribution computed for the trimer of slip-stacked PDIs, which appears to be almost completely confined within the central monomer as shown in Figure 5.6, and with the sum of all atomic spin density values of the central monomer obtained by the Mulliken population analysis equal to 1.97 (~ 2 electrons).

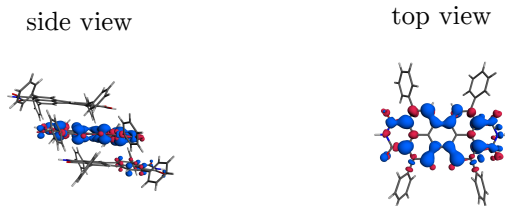


Figure 5.6: Spin density of the T_1 state for the slip-stacked PDI trimer computed at the CAM-B3LYP/6-31G(d) level.

But, on the other hand, the spatial representation of the spin density does not inform about the localization/delocalization tendency or strength, that is the energy

required to localize the triplet state. Therefore, here we define the triplet *state localization energy* as the energetic cost to force the two unpaired electrons to be (completely) located on one monomer:

$$\Delta E_{SL}(T_1) = E_L(T_1) - E(T_1) \quad (5.19)$$

where $\Delta E_{SL}(T_1)$ is the triplet state localization energy, and $E_L(T_1)$ and $E(T_1)$ are the energies of the localized and free (with no spatial restrictions) triplets, respectively. Calculation of the localized triplet state have been performed with the C-DFT approach and applied to the dimer and trimer slip-stacked PDIs from the crystal structure of **1**. Localization energy is computed as 25 and 14 meV for the **D1** and **D2** dimers, respectively. The small energy cost to constrain the triplet state in one monomer is an indication of the strong localization character of the lowest triplet. Moreover, the computed values are in very good agreement with half of the adiabatic energy gaps between the two lowest triplets in **D1** and **D2**, 38 and 11 meV respectively, relating the spin localization energy with triplet exciton coupling.

5.3.6 Triplet excitons and intermolecular distortions

So far it has been characterized in great detail the low-lying excitations in PDI aggregates. But all these results have been obtained with a static approach, i.e., by taking molecular and oligomeric coordinates from the crystal structure of **1**. Therefore, these results, although can be a good indication of the behavior of molecular aggregates in general, they focus on the slip-stacked aggregation mode and do not account for alternative aggregation motives. Additionally, even for the case of co-facial molecular arrangements, we cannot discard the role of structural distortions tuning interstate energies and electronic couplings, and eventually playing an important role in the photophysics of PDI aggregates, as it has been noted by several theoretical investigations.[150]–[152] Hence, this section investigates how intermolecular distortions might modify the excited state distribution and their properties. To that aim, a coplanar trimer of the unsubstituted (D_{2h} symmetric) PDI derivative **3** is considered.

Computation of the triplet energies along the vertical distortion of the eclipsed trimer indicates a reduction of the triplet excitation energy for intermolecular separations smaller than 4.5 Å (Figure 5.7), in particular for the lowest triplet. For separations bigger than 4.5 Å it can be seen that the vertical energy reaches a convergence. This convergence is near to the T_1 energy of the monomer, so it can be concluded that from 4.5 Å on, each of the monomer behaves as a independent monomer.

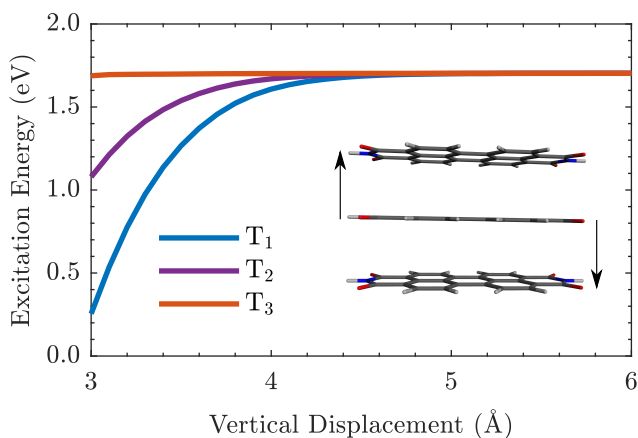


Figure 5.7: Vertical excitation energies to T_1 - T_3 states (in eV) for PDI **3** eclipsed trimer along the vertical distortion.

Translational displacements also influence triplet energies, with totally or partially eclipsed and alternate conformations reducing and increasing the S_0/T_1 energy gap, (Figure 5.8). When the distortion is on the eclipsed configuration, the T_1 energy decreases while the energy increases when the distortion is on the alternate form. Once the trimers are distorted enough, a convergence in energy can be observed. These results suggest the potential involvement of breathing and in-plane vibrations to the triplet exciton redshift experimentally observed upon aggregation,[133] by tuning the $\pi - \pi$ interactions.

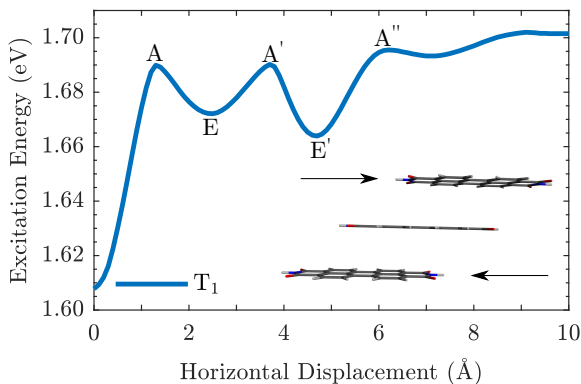


Figure 5.8: Vertical excitation energies (in eV) to T_1 along the horizontal (antiparallel) distortion for PDI **3** trimer with vertical separation of 4 Å. A and E labels indicate eclipsed and alternate configurations with $E = 0.0$ Å, $A = 1.3$ Å, $E' = 2.5$ Å, $A' = 3.7$ Å, $E'' = 4.7$ Å and $A'' = 6.2$ Å displacements.

Characterization of T_1 in terms of diabatic states along the D_{2h} distortion pinpoints the role of CT configurations in the electronic structure of the lowest triplet (Figures 5.9 and 5.10). Shorter molecular distance stabilize CT contributions, which become energetically closer to the LE triplet energy, and facilitate spatial overlap of frontier orbitals. As a result, the CT mixing in the $S_0 \rightarrow T_1$ transition increases up to 14% at 3.7 Å of intermolecular separation, while the energy difference between CT and LE triplet diabats decreases. Simultaneously, the average LE/CT coupling, defined as

$$V_{average}^{LE/CT} = \frac{1}{N_c} \sqrt{\sum_{ij} |\langle LE_i | \hat{H} | CT_j \rangle|^2}, \quad (5.20)$$

where i and j indices run over the three LE and four CT states respectively, and N_c is the total number of couplings ($N_c = 12$), increases as the molecules become closer to each other. Detailed analysis of T_1 at different intermolecular separations can be found in Appendix D.4.

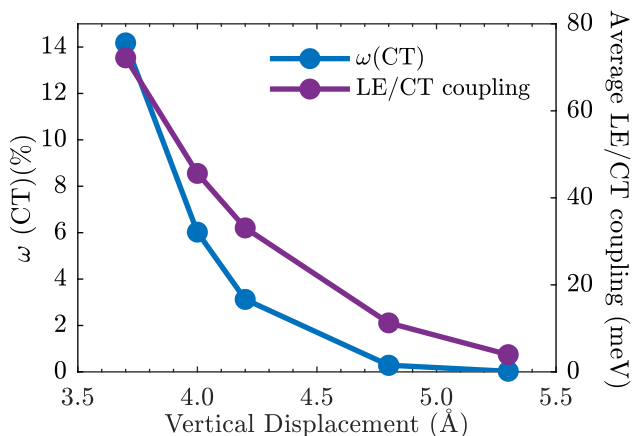


Figure 5.9: CT contributions $\omega(\text{CT})$ (blue, in %) and average LE/CT coupling for the T_1 of PDI **3** eclipsed trimer along the vertical distortion.

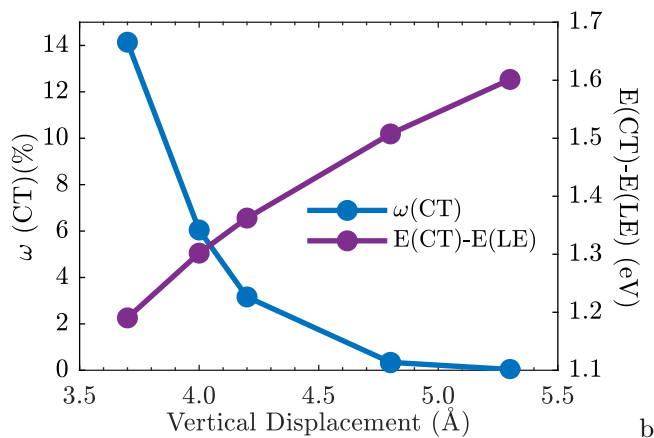


Figure 5.10: CT contributions $\omega(\text{CT})$ (blue, in %) and energy difference for the T_1 of PDI **3** eclipsed trimer along the vertical distortion.

5.4 CONCLUSIONS

In conclusion, R_1 and R_2 substitutions play a major role in the aggregation of PDI molecules, largely limiting side interactions. Such effect is clearly manifested in the crystal structure of **1**, organized in well-separated slip-stacked molecular columns, with strong electronic intra-column interactions and weakly interacting inter-column contacts. Such feature allows to predict that $\pi - \pi$ interactions dominate the (opto)electronic properties of **1** in the crystal and in molecular aggregates in general.

Electronic transitions to the lowest singlet and triplet states in **1** correspond to HOMO \rightarrow LUMO single electron promotions, where lateral phenyl rings do not have any contribution. The lowest excited singlet is largely stabilized upon aggregation. Such effect cannot be only explained by excitonic coupling of the localized singlets, and emerges from molecular orbital overlap, the low energy gap between LE and CT diabats, and the competition between LE/LE and strong LE/CT couplings. The mixing of CT terms in the transition to the lowest excited states in molecular dimers is remarkable (as high as 50% of the transition), invalidating the use of perturbative approaches to characterize tetraphenyl PDI aggregates, and π -stacked PDI molecules in general.

Relaxation of the triplet state through $\pi - \pi$ interactions is much softer than in the singlet. Molecular aggregates of PDI show strongly bounded hole/electron pairs in the triplet state, resulting in the localization of the two unpaired electrons on one molecule. The impact of CT configurations is much weaker in the triplet state. Interestingly, superexchange interaction in the triplet is as strong as in the singlet, but the large gap between ^3LE and ^3CT hinders its role. This conclusion is

particularly important in the design of molecular dimers, oligomers or aggregates with triplet states with strong CT character.

The strong LE character of the triplet can be relaxed, to some extent, by molecular distortions able to increase intermolecular $\pi - \pi$ interactions and stabilize the charge separation energy.

Chapter 6

PDI MODEL: TRIPLET EXCITONIC STATES CHARACTER DESCRIPTION IN DIMERS

This chapter discusses the properties of triplet states in co-planar PDI dimers. The performed analysis relies on TDDFT calculations, and in the decomposition of electronic transitions in terms of diabatic states, i.e., local excitations (LE) and charge transfer (CT) excitations. The obtained results show the interchange between H/J-aggregation character of the lowest triplet and singlet states for small longitudinal shifts.

6.1 INTRODUCTION

As seen in subsection 5.3.6 the distortion on the PDI trimer can be an interesting aspect to analyze. To be more precise, it can be important to understand the nature of the triplet states. This is the reason why when the aggregates' are constituted by equivalent chromophores symmetrically arranged, (Figure 6.1) a symmetry-adapted (SA) superposition of LE states, Frenkel excitons (FE), are formed with the intermolecular interactions that mix the LE states. Something similar happens for the ionic states, that form delocalized charge resonance (CR) states [175]–[177]. In this case, the PDI aggregate takes C_{2h} symmetry point group as the intermolecular displacements along the longitudinal displacement are considered. As a result, the most relevant π - π^* excited states belong to the A_g and B_u representations. Since only *ungerade* (u) states are accessible through dipole-allowed transitions, state symmetry can be employed to identify H- and J- aggregation modes.

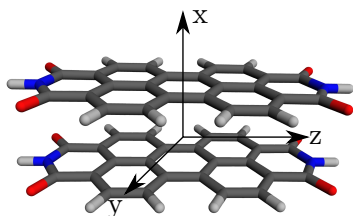


Figure 6.1: The PDI dimer used in this work. The excited states have been determined at the eclipsed configuration and along the longitudinal translation coordinate.

In the following section, the attention has been focused on three main objectives related with the analysis of excited states in terms of LE and CT contributions in PDI dimers. First, a validation of the diabaticization procedure has been done, [86], for singlet and triplet states and compare it with an analysis of the transition density matrix [91]. Then, the triplet state LE/CT modulation has been done. We explore how the translation coordinate triggers the lowest-lying state symmetry (A_g/B_u) switch, related to the H-/J- character alternation as it has been previously shown for singlets [86], [167], [171]. Moreover, excited state energies and character have been compared with two different exchange-correlation functionals: ω B97X-D and CAM-B3LYP. Finally, the simple diabaticization approach used has been compared with the ER and Boys localization methods.

6.2 COMPUTATIONAL METHODS

The method employed to analyze and characterize the nature of the triplet excited states has been fully described on section 2.5.2. In comparison to the previous chapter, on this case the PDI-monomer structure is the same one as it has been used in previous PDI aggregates investigations, optimized at the BLYP-D/TZV(P) level of theory [178] and fixing the intermolecular distance at 3.4 Å, which has been the same as in previous works [86], [152]. The excited states calculations have been performed for the eclipsed conformer and for 0.5 Å displacements up to 8 Å along the longitudinal translation coordinate.

The excitation energies have been determined with TDDFT using the Tamm-Dancoff approximation (TDA) [110], using CAM-B3LYP[148] and ω B97X-D [108] functionals and the 6-31G* basis set. The reason for the use of ω B97X-D is that it provides reliable description of the CT character in singlet excitons of PDI dimers [151]. All QC calculations have been done with Gaussian 16 [179]. Finally, the CT characters have been described with the SDA approach and by analysing transition density matrices with the TheoDORÉ program [91].

6.3 RESULTS

In this section an extent analysis of the PDI dimer will be done. The brief description of the singlet states will help to understand what can happen on the triplet state. In this state, the modulation of the triplet state will be carried out as well as their couplings. Finally, the results will be compared with two long-range corrected functionals and three different approaches for the computation of the diabatic states.

6.3.1 Low-lying Singlet Excited States

Before going in deep in the analysis of the triplet states, it might be useful to understand how the singlet states behave. In previous investigations of excitation energy profiles and CT character of PDI aggregates, it has been observed that the computed states are strong mixtures of two diabatic states. Nevertheless, the weight of the different contributions depends strongly on the energy difference between FE and CT diabatic states, as well as on their couplings [86], [151], [152]. Due to this, the CT character of the lowest singlet states has a dependence on the selected functional. For this analysis, TDA-computed states have been computed instead of the full TDDFT linear response. As a result, it has been seen that even if the adiabatic energies are similar for the TDDFT with and without the TDA approximation, the LE and CT states show a different profile, where the B_{2u} states suffer a crossing 6.2 that it is not seen for the full TDDFT results.

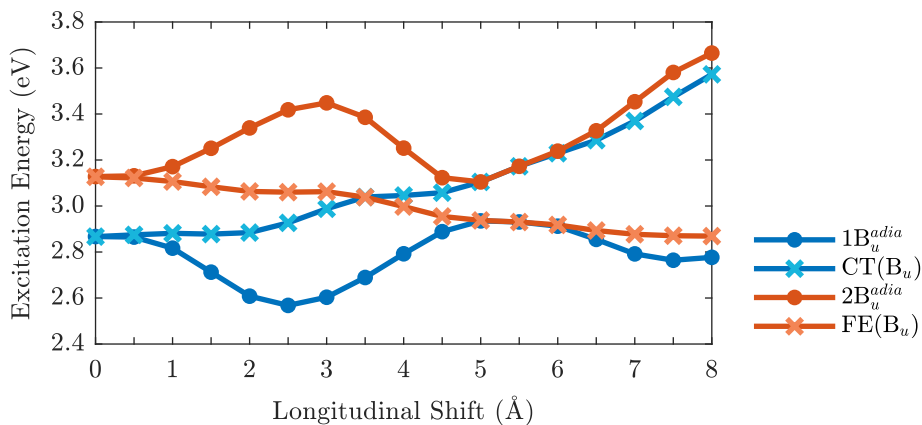


Figure 6.2: Excitation energy profiles (TDA- ω B97XD/6-31G(d)) of B_u adiabatic (dot) singlet excitation states and B_u FE and CT states (cross). For large interactions, adiabatic and diabatic states differ from each other.

6.3.2 Adiabatic Excited States

For the case of the triplet states, the analysis has been done only at the TDA level due to the relevant contribution from de-excitations that contains the full TDDFT linear response. With this, the energy profiles for the longitudinal shifting have been plotted, as it is shown on Figure 6.3. Here, it can be seen how the state energies oscillate, leading to switching in the state order.

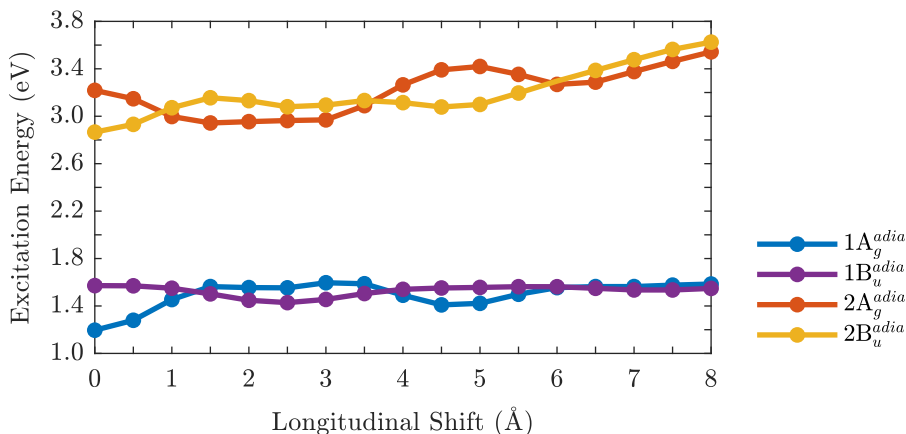


Figure 6.3: Computed adiabatic excitation energy profiles for the PDI Dimer at TDA- ω B97X-D/6-31G* level

Even if it is a big energy difference between the lowest and highest excited states, it can be said that they follow almost the same pattern. Along the displacement there several state crossings, in agreement with the pattern followed by singlet states.

Moreover, regarding the CT character (Figure 6.4), two main ideas appear. The first of these is that the the two lowest triplet states show almost a pure LE character. Whereas, the highest ones are mainly CT, and this comes in agreement with some other works, [4].

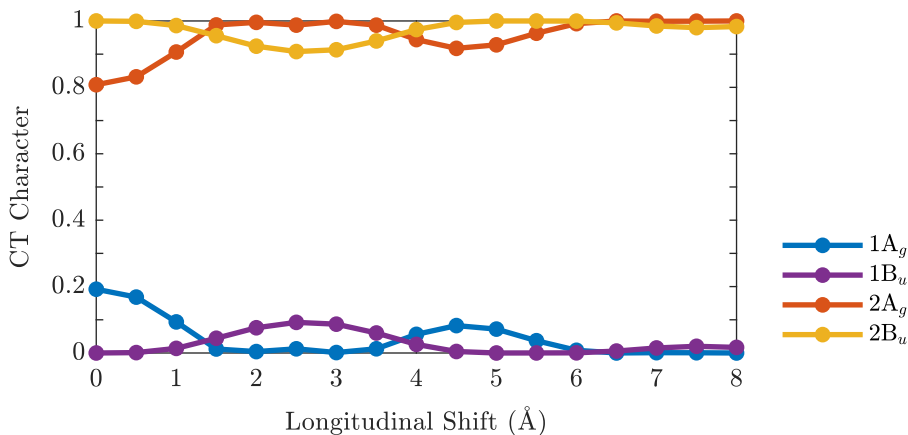


Figure 6.4: CT Character for the adiabatic states.

Another way to explore the CT character is by plotting the electron-hole correlation using the TheoDOR Toolbox[91]. This program allows to visualize the nature of the excited states. For this, the system must be considered in fragments, that is, one fragment for each molecule. For the understanding of Figure 6.5, it has to be mentioned that when the coloured squares are in the main off-diagonal, the plot represents a LE; and in the other way round, if the coloured ones are those of the main diagonal a CT state is represented.

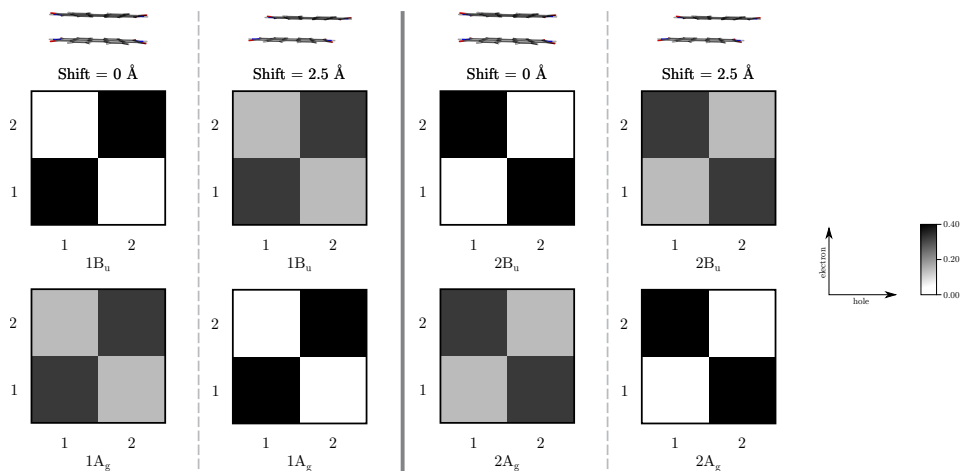


Figure 6.5: Electron-hole correlation plots of the triplet excited states for two different PDI dimer configurations: eclipsed 0.00 Å and slip-stacked, 2.5 Å done at the TDA- ω B97XD/6-31G(d) level.

This representation stands out the results of Figure 6.4. Focusing on the eclipsed conformation, it is clearly seen that the $1B_u$ and $2B_u$ are LE and CT pure states, respectively, as characterized by electron-hole correlation plots, whereas the $1A_g$ and $2A_g$ states are mainly LE and CT with a little of state mixing, represented by the light grey. For the 2.5 Å longitudinal shifting the same pattern can be followed but with some differences. On this case, the pure LE and CT states correspond to the $1B_u$ and $2B_u$ states respectively; while the B_u states show small mixing.

In addition to the TheoDORE electron-hole correlation plots, this program also allows to extract the CT character of the excitation, Figure 6.6. A good agreement can be seen for both methods in the case of the lowest states, whereas for higher ones this agreement is broken. The reason for this is that for some intermolecular configurations the selected π - π^* states are spread over more than one computed excited state. The diabaticization procedure gives well defined CT character because the selected π - π^* exciton states are not projected in the entire exciton state and moreover they are renormalized. In contrast, TheoDORE gives the CT character of the selected π - π^* states in the entire space of the computed exciton states; that is why both plots do not coincide for higher excited states.

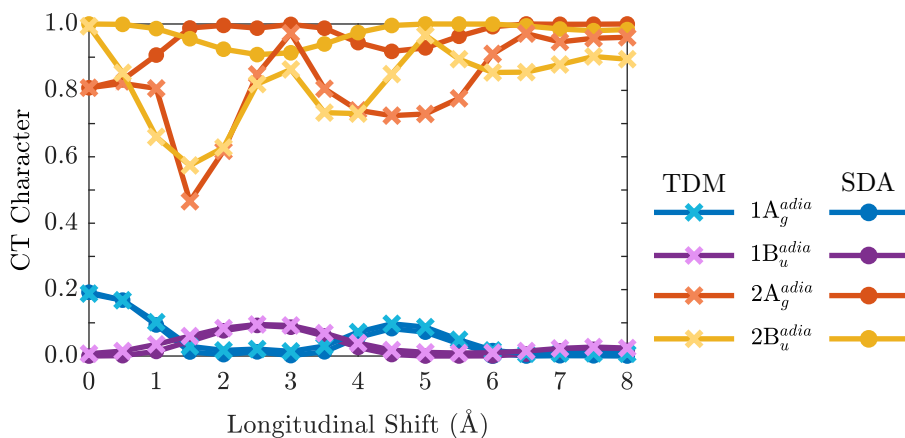


Figure 6.6: Comparison between the CT character obtained through the diabatisation procedure (SDA) (dot) and with the analysis of the transition density matrix (TDM)(cross)[91] for the selected triplet excited states.

6.3.3 LE/CT Interaction Energies

State order switching is easily rationalized by the oscillating trend of the interactions between the CT and LE states. This interactions, [4], [86], [152], [169], are given by the combinations of the D_e and D_h transfer integrals, Figure 6.7. Here, it is clearly seen an oscillation of the CT/LE interaction. This determines an interchange between the lowest states described by the A_g and B_u symmetry. To be more exact, this happens in a range of 2-3 Å, where the interaction between LE and CT is almost negligible for the A_g symmetry. This oscillation also helps to understand the switching of Figure 6.3. This is because when the interaction between LE and CT of B_u states is on its maximum pushes the $1B_u$ state below $1A_g$, doing a simile with the switching character from H- to J-type.

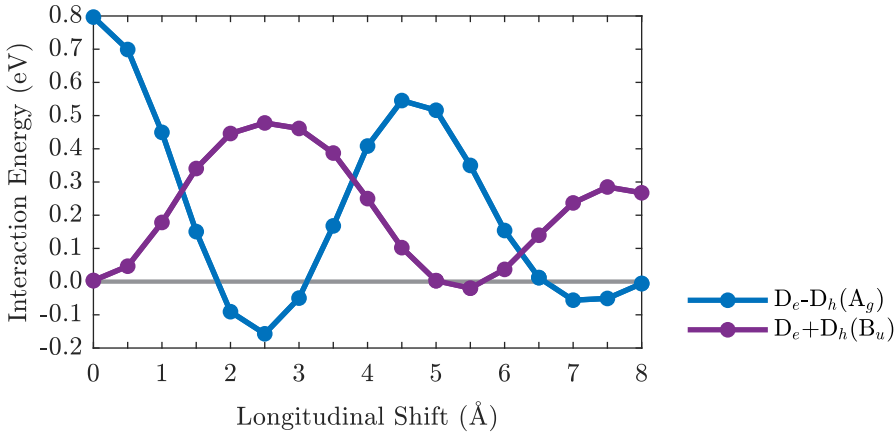


Figure 6.7: Magnitude and modulation along the longitudinal translation coordinate of the $D_e \pm D_h$ terms for the interaction between CT/LE states of the dimer.

With these results it is possible to suggest that thanks to the modulation of intermolecular organization in molecular aggregates the radiative and nonradiative decays from the lowest triplet exciton states, which is related to the nature and symmetry of the lowest energy state. The whole concept can be used for systems presenting dimerization-induced triplet state populations[180].

6.3.4 Symmetrized Diabatic States

For this particular system the symmetry-adapted Hamiltonian can be used due to the high symmetry of the system. In this case, each of the symmetries, A_g and B_u have been treated in two different graphs to have a better understanding about the situation.

The major difference, for A_g symmetry, between the singlet (Appendix E) and triplet states (Figure 6.8) is the energy difference between the 1st and 2nd states. It is known that in the case of the singlet states[4], the interaction between the diabatic states is larger than for the triplet states. Even though, this low LE/CT mixing is enough to modulate the triplet excitation energies allowing to have a switching between the A_g and B_u states.

For the A_g symmetries it can be seen that for small translations, 0.0\AA - 1.5\AA there is a decoupling between the adiabatic and the symmetrized diabatic states, whereas this is not the case for the B_u symmetry. This is directly related to Figure 6.7. When the D_e-D_h curve is on its maximum the adiabatic and symmetrized diabatic energies decouple. Just on this point D_e+D_h is on its minimum, so the adiabatic and symmetrized diabatic energies are coupled. In this range of shifting, the decoupling that corresponds to the B_u symmetry is smaller and this might be justified with the

smaller interaction energy value; 80 meV for the A_g symmetry and 50 meV for the B_u symmetry.

For bigger translations, the symmetrized diabatic and adiabatic energies tend to couple because the LE/CT interaction energy decreases on its respective maximum curves.

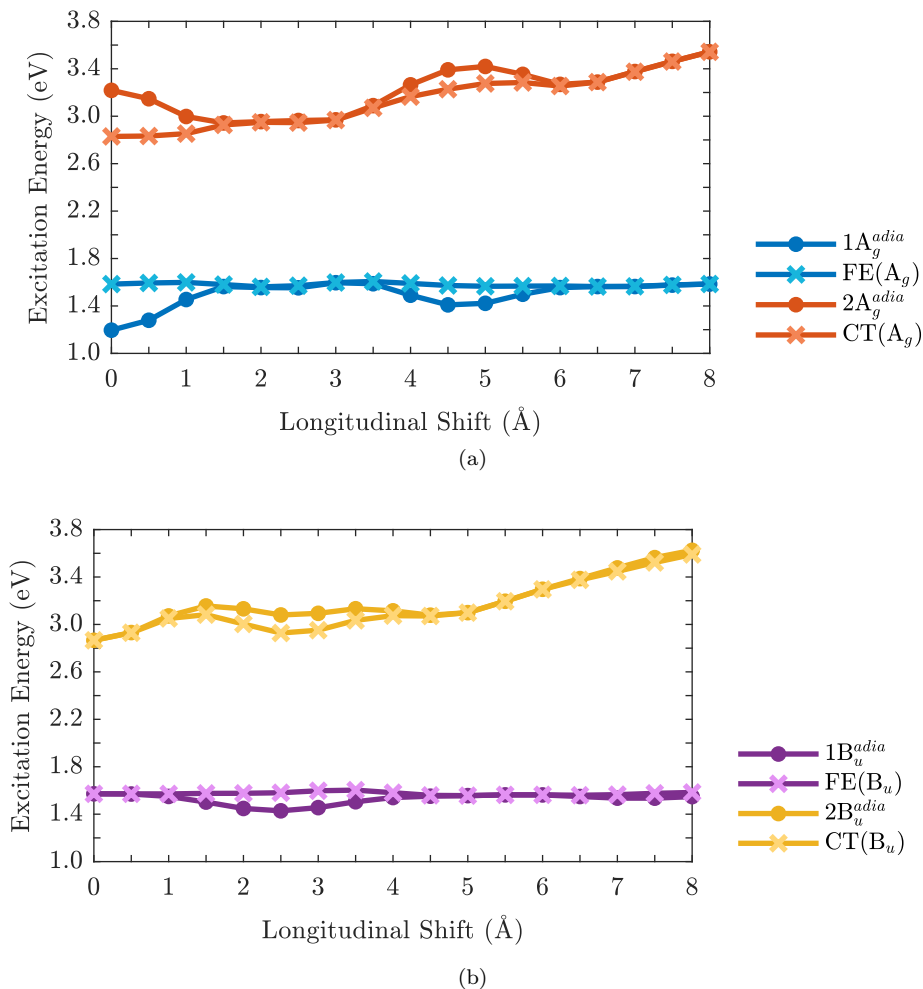


Figure 6.8: Adiabatic (dot) and symmetrized diabatic (cross) energies (a) A_g states (b) B_u for the PDI dimer computed at TDA- ω B97X-D/6-31G* level.

6.3.5 Method Comparison

To finish the study of PDI model dimers, the influence of two different long-range corrected hybrid functionals, ω B97X-D and CAM-B3LYP, and the difference between different diabatic methods/procedures have been analyzed.

In some works has been remarked that for singlet excitons [86], [152] the selection of the functional is crucial for the proper characterization of LE and CT states. But for the case of the triplet exciton states, it has been seen that there are few differences. Figures 6.9 and 6.10 show this comparison with two different long-range functionals. Focusing the attention in the lowest states, it is seen that both methods do not give very different results; this difference is never larger than 10 meV. For higher energies, two main differences appear. The first of these is located from 0.0 Å to 3.0 Å where the energy difference is higher for the $2A_g$ state than for the $2B_u$ one, 20 meV and 13 meV respectively. Nevertheless, for higher displacements, the energy difference increases equally, 30 meV, for both states. This increasing in energy is related to the CT character of the states.

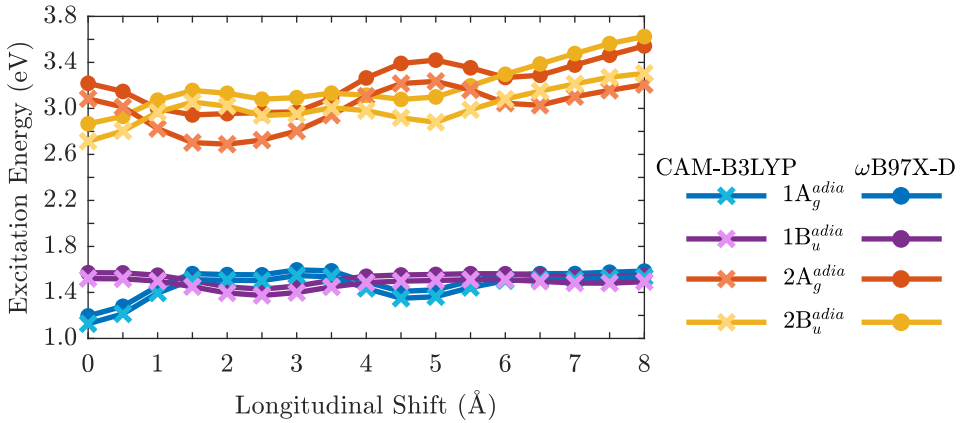


Figure 6.9: Comparison between excitation energies of the triplet excitation energies of the triplet states computed with TDA-CAM-B3LYP/6-31G(d)(cross) and TDA- ω B97XD/6-31G(d)(dot) along the longitudinal translation.

If we compare both, the lower energy of the CT states computed with CAM-B3LYP and their CT character with those computed with the ω B97XD functional it can be said that the CT character of the lowest states is slightly larger at the TDA-CAM-B3LYP level. This is not a surprising feature because it has been seen that there is a little discrepancy between the CAM-B3LYP and ω B97XD functionals when computing singlet excited states [152].

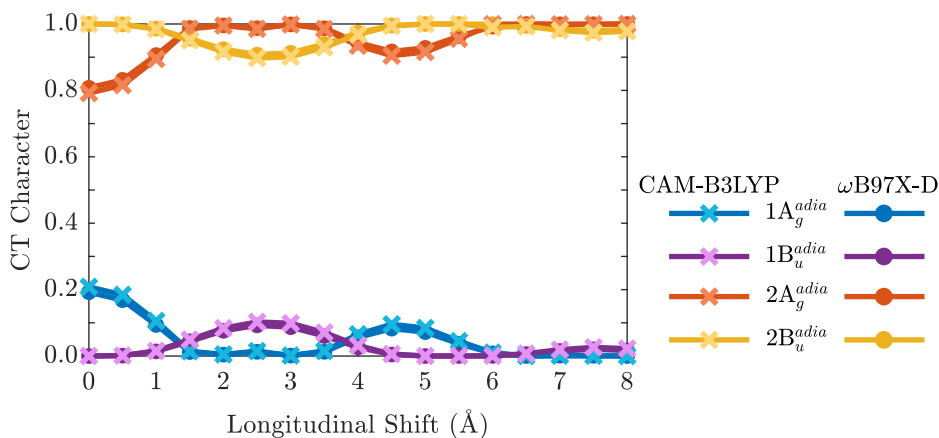


Figure 6.10: Comparison between CT character computed with TDA-CAM-B3LYP/6-31G(d)(cross) and TDA- ω B97XD/6-31G(d)(dot) along the longitudinal translation.

Even though, it has been interesting to analyze the CT/LE interaction (Figure 6.11) because there is not any functional dependence obtaining practically the same values for TDA-CAM-B3LYP and TDA- ω B97XD. Even if the use of other long-range corrected hybrid functionals may provide similar results to those obtained here, what it is not recommended is the use of nonhybrid or hybrid functionals because they tend to underestimate the CT states [181]. The reason for this is that at the distance we are working on, 3.4\AA , a right long-range behaviour through the HF exchange is needed.

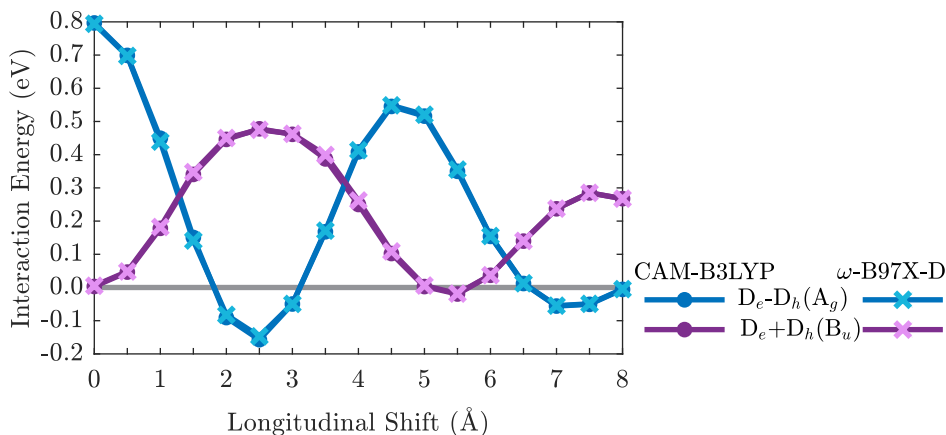


Figure 6.11: Interaction between CT and LE states computed at TDA-CAM-B3LYP(cross) and TDA- ω B97XD (dot) with 6-31G(d); for blue: A_g and purple: B_u states.

As it has been explained in subsection 2.5.2, the method used to obtain the diabatic states were based in some simplified space, called MIOS. Nevertheless, it is known that there are some other diabaticization methods where the whole space is taking into account. For this comparison ER and Boys methods have been the selected ones. Figure 6.12 shows a small comparison between some diabaticization methods.

1: Simple Diabatization Approach; 2: ER Method; 3: Boys Method

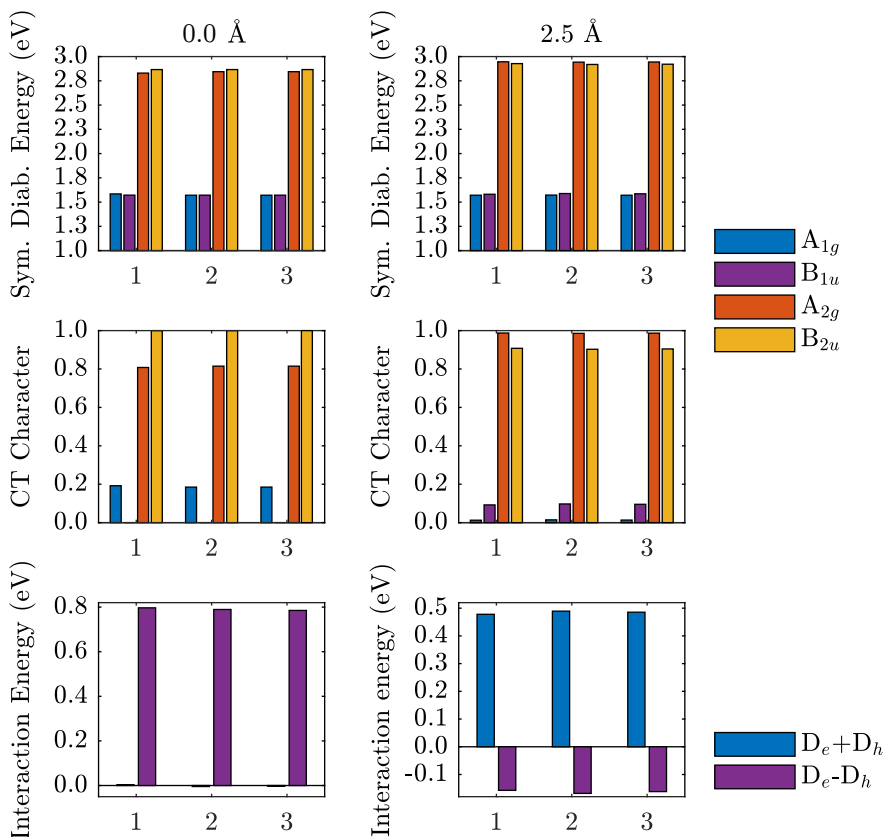


Figure 6.12: Comparison of symmetrized diabatic energy (top), CT character (middle) and interaction energy (bottom) for different diabatization procedures: (i) specific MIOS, (ii) ER Method and (iii) Boys Method computed at ω B97XD/6-31G(d) level of theory.

For the eclipsed and 2.5 Å shifted conformers it can be seen how all three methods show almost identical values. As the excitations of this system are very well known described with the last two HOMOs and first two LUMOs, the developed diabaticization procedure can describe perfectly the diabatic energies.

6.4 CONCLUSIONS

As the main conclusion of this chapter, it has to be pointed out that the modulation of the triplet excitation states of PDI aggregates have been analyzed at the TDDFT level, paying attention to the intramolecular displacement along the longitudinal translation coordinate.

It has been seen how the triplet excited states can be defined in terms of the interactions between the LE and CT diabatic states. Even if the triplet excitations are dark states, it has been seen a kind of CT-mediated J-aggregation-like mechanism for small longitudinal displacements, similar to those of the singlet states.

To finish, the results from two long-range corrected hybrid functionals have been compared. The most significant conclusion is that the magnitude and modulation of the LE/CT interactions are almost independent on the selected functional. With this, the selection of the functional is not so important to define the CT contributions in the low-lying triplet excitation energies because the energy difference between the LE and CT states is big enough. Moreover, when the diabatic states have been compared with SDA and ER/Boys methods, it has been seen that for this particular system there is not any significant difference.

Chapter 7

CONCLUDING REMARKS

This chapter gathers all the important ideas mentioned in the whole manuscript.

In this thesis, the triplet excited state of different aromatic systems have been studied. For this, the manuscript has been divided into two main blocks. The first of them makes a basic analysis of the triplet state in some aromatic model systems; i.e. different dimer conformers of benzene, naphthalene and anthracene. The aim of this has been to analyze the nature of these triplet states in general, and to see if there is any excimeric state in those systems in particular. The second part deals with the PDI derivatives, aggregates and molecules. This analyzes and characterizes in detail the PDI molecule and a certain derivative of it, which has been called as PDI **2**.

To characterize the excited states there are different approaches and the one used in this work has been the decomposition of the electronic states. For this, it is important to have a good understanding of the studied monomer because it gives relevant information about the behaviour of the dimers. After the monomers analysis, we go beyond the dimers and try to characterize each excited state in terms of Local Excitons (LE) and Charge Transfer (CT) states.

7.1 TRIPLET EXCIMERS IN SMALL AROMATIC DIMERS

In the first part we investigated the triplet excimeric states in small aromatic dimers mentioned above. For that, the first step has been to understand the behaviour of the triplet state in the corresponding monomers. The most important aspect of this section has been to analyze the spin density. The reason for this is that its delocalization confirms that the triplet state is delocalized over the molecule and so the same can happen in the dimer conformers.

In order to find the excimeric state, a group of conformers have been designed by distorting one of the monomers in the long and short axis as well as considering the eclipsed conformer. All these distortions have shown a minima in the PES and three different type of conformers have been obtained: (i) covalent dimers, (ii) triplet localized dimers and (iii) triplet delocalized dimers. The first of these show a bond formation with delocalized MOs and spin density. The second show typical π - π stacking carbon-carbon distance and localized MOs and spin density. The last group corresponds to an intermediate carbon-carbon distance between monomers. With no bond formation and delocalized MOs and spin density. To define an excimeric state two main conditions should be fulfilled: (i) both monomers must interact through the space, no bond formation, and (ii) the triplet state should correspond to the whole system, delocalized spin density. Due to these reasons those conformers with intermediate carbon-carbon distance, the third group of structures, are the best candidates to continue with the research.

Apart from the spin delocalization it is also important the analysis of the triplet excited states. Regarding the composition of the T_1 adiabatic state it has been seen that the participation of the CT is not negligible as in all the systems its weight is

above the 10 %. The same result has been obtained in a qualitative and quantitative way.

In the picture of the one-electron density matrix decomposition, we have seen that the mixture that the T_1 shows can be perfectly decomposed in well defined pure LE and CT states. Moreover, we have been able to see which are the group of atoms that take part in each of the diabatic states. An important property of the triplet state in these dimers is the strong interaction between the LE and CT states, in agreement with the important CT contribution in the adiabatic state. After this analysis, we can conclude that the eclipsed conformers of benzene, naphthalene and anthracene can be identified as triplet state excimers.

7.2 PDI MOLECULE, AGGREGATES AND MODELS

7.2.1 PDI Molecule

In the study of the PDI molecule we have seen that in the analysis of the electronic structure the most representative MOs showed an internal CT character. The reason for this is that HOMO-2 and HOMO-1 have MOs localized in one site of the molecule, whereas, HOMO, LUMO+1 and LUMO+2 are delocalized over the entire molecule. The electronic excited states have been computed with different DFT functionals. In this case, B3LYP has been rejected because it underestimates the energy of the CT states. This is why further analysis has been done with CAM-B3LYP.

7.2.2 PDI Aggregates

In the study of PDI aggregates we first characterize the electronic transitions to the lowest singlet and triplet states, corresponding to HOMO→LUMO transitions. Both states get stabilized while the size of the aggregate. Apart from the excitonic coupling of localized singlets, the stabilization can also be explained with the MO overlap, the low energy gap between LE and CT states and the competition between LE/LE and strong LE/CT couplings. In the triplet state π - π interactions are not as strong as in the singlet state. The hole/electron pairs are strongly bounded and so the impact of the CT is weaker.

7.2.3 PDI Models

Molecular distortions are able to increase the intermolecular π - π interactions and stabilize the charge separation energy. This can be confirmed in the second part which corresponds to the PDI **3** model. One of the most surprising result is that even

if triplet excitons are dark states, the CT-mediated J-aggregation-like mechanism can be appreciated.

Another thing to be mentioned is the method used to decompose the adiabatic states in terms of LE and CT states. Up to this moment, the decomposition was done through the ER method, but here the Simple Adiabatic Approach (SDA) has been used. This method is based on the MIOS (Minimal Orbital Space). The last section of this work shows that both methods give almost the same results, at least for the studied system.

Overall, we have seen that the triplet states may play a very important role in the properties of different promising organic molecules in the field of optoelectronics. In these cases, the analyzed systems show good interaction between LE and CT states, which can have promising applications. Moreover, we have seen that the tools used to analyze the triplet state in all the systems are extremely useful in the analysis of the triplet state.

Chapter 8

APLIKAZIO OPTOELEKTRONIKOETARAKO MOLEKULA AROMATIKOEN EGOERA KITZIKATU TRIPLETEEN AZTERKETA TEORIKOA

Azken atal honetan lan guztian zehar aztertutakoaren laburpen bat egingo da. Optoelektronikati hasiz eta kimika kuantikoaren oinarriak aipatuz. Ondoren, bi bloke nagusi aztertuko dia, biek ala biek, optoelektronika dutelarik ardatz. Amaitzeko guztiaren lortutako emaitzen laburpen bat egingo da ikertutako emaitza esanguratsuenak azalduz.

8.1 SARRERA

8.1.1 Optoelektronika Organikoa

Azken 10 urteetan, optoelektronika organikoaren alorrak aurrerapen handia izan du, bai kargak sortzeko eta garraiatzeko oinarritzeko fisikaren ulermenean baita materialen diseinuan, fabrikazioan eta prozesatzeko metodoetan ere. Arrazoi horiek bultzatu dute optoelektronikaren inguruko ikerketa. Eguzki-argia energia-iturri denez, optoelektronika sistema eta gailu elektronikoak aztertzen eta aplikatzen dituen eremua da, argi-iturria detektatzeko eta kontrolatzeko helburuarekin. Hobeto ulertzeko, efektu mekaniko kuantikoak hartu behar dira kontuan, batez ere fermioien eta argiaren arteko elkarrekintza. Material elektronikoetan, efektu horiek eremu elektrikoaren presentzian oinarritzen dira.

90eko hamarkadatik gaur egun arte, munduaren osasuna okerrera doa, erregai fosilen erabilera gero eta handiagoa delako. Arazoi honi irtenbide bat emateko asmoz energia berriztagarriei buruzko ikerketa areagotu egin da, gizartearen erronka handienetako bat bihurtuz. Horrek esan nahi du lortutako energia garbia eta eraginkorra izan behar dela, baita erabilera optimoa eta kontrolatua ere. Arazo honen konponbideetako bat *eguzki energia* izan daiteke. Eguzki-energia ugaria eta librea bada ere, energia hori lortzeko eraginkortasuna erronka bat da oraindik, zelula fotovoltaiko guztiek fotoiak igortzen dituztelako energia erabiliz, material adsorbanatuaren xurgapen-mugatik behera. Horrek esan nahi du energia asko galtzen dela energia bihurtzean [6].

Gaur egungo industria fotovoltaiko komertziala silizio kristalinoak eta film meheek gidatzen dute batez ere, eta eraginkortasunak % 15-20 eta % 6-11 bitartekoak dira, hurrenez hurren [7]. Eraginkortasun handiagoa lortzeko, silizio kristalinoa eta film meheak kanpoan geratu dira, eta, teknologia berri batzuk garatu dira, hala nola tindaketarekin sentsibilizatutako eguzki-zelulak eta fotovoltaiko organikoak [8]. Azken hauek oso erakargarriak dira erraz erabiltzen direlako. Gainera, malgutasun mekanikoa dute eta oso merkea da fabrikatzea.

1980ko hamarkadaren erdialdean, Ching Tangek eta Steven van Slykek tentsio baxuko eta argi mehe eraginkorreko erakustaldi handi bat egin zuten argia igortzen zuen diodo batekin [9]. Diodo honek ezaugarri bereziak ditu emisio elektroluminiszentean eraginkortasun handiari, behe-tentsioko bulkadari eta fabrikazioaren sinpletasunari dagokienez. Horrek erakusten du optoelektronikan material mota honen erabilera bideragarria izan litekeela [10]. Frogapen honetatik, ikertzaileek ikusi zuten film mehe organikoak erabilgarriak izango zirela zenbait aplikaziotan. Merkaturan berriak diren arren, haien arrakasta gero eta handiagoa da alderdi hauetan: *argi organikoa igortzen duen gailua, edo OLED* eta lehen aipatu bezala eguzki-zelula organikoak.

Erakarpen hori haien egitura kimikoa aldatzeko gaitasunari esker sortu da. Gaitasun hori dela eta, propietate materialak zuzenean film mehean sar daitezke.

Material organikoek, hala nola molekulek, oligomeroek, polimeroek, agregatuek eta solido molekularrek, atentzioa eman dute beren propietate potentzial eta berezi handiengatik. Material organiko molekularretan, kargak garraiatzeko jabetza izan da orain arte gehien ikertu dena, materialak garraiatzeko elektroik eta zulo gisa duten gaitasunagatik. Oro har, bi taldetan banatzen dira: molekula txikiak eta polimeroak.

Molekula txikiak erakargarriak dira garbitzeko errazak direlako eta, gainera, haien egitura ordenatuek karga handiko garraiolarien mobilitateak ahalbidetzen dituzte. Eredu gisa ere erabili izan dira hainbat azterketatarako, hala nola kargatzeko eta kargatzeko dinamiketarako. Beste aldean, polimeroek beste abantaila bat ematen dute molekula txikiarekin alderatuz. Abantaila hau azalera handiko gailu batean fabrikatzeko instalazioan zentratzen da. Diseinu erraz horri esker, sintesiak eta prozesatzeko konposatu polimerikoek arreta jarri dute gailuaren errendimenduan [11].

Konposatu polimeriko hauek eguzki-zeluletan erabiltzen dira, elektroik-emaileen (ingelesez, D) eta elektroik-hartzaileen (ingelesez, A) erabilerarekin. DA eguzki-zelulek fotoinduzitutako elektroik-transferentzia aplikatzen dute [12] elektroikak zuloetatik bereizteko. Fotoindukzio honek elektroien transferentzia eragiten du emailearen egoera kitzikatutik (bajuen okupatutako orbital molekularra, ingelesez HOMO) hartzailearen HOMOrara. Hartzaile honek elektroikak jasotzeko gaitasuna izateaz gain elektroik afinitate handikoa izan behar da. Karga banaketa honen ondoren, elektroikak eta zuloak aurrez aurre dauden elektrodoetara iritsi behar dute, katodoa eta anodoa, hurrenez hurren [13].

Erdieroale organikoek xurgapen optikoko koefiziente oso handiak izan ditzakete. Honek eguzki-zelula oso meheak ekoizteko aukera eskaintzen du. Erdieroaleen egitura elektronikoa π -elektroietan oinarritzen da. Horrek esan nahi du sistema karbono lotura bakun eta bikoitzen arteko txandakatze batez egina dagoela. Lotura sinpleak σ bezala ezagutzen dira eta elektroik lokalizatuei lotuta daude. Lotura bikoitzek bi loturak dituzte: σ lotura eta π lotura. π -elektroik horiek mugikortasun handiagoa dute σ -elektroiekin alderatuz; hau da, karbono-atomoen artean leku batetik bestera salto egin dezakete, π orbitalen arteko gainjartzearen ondorioz [13] konfigurazio-bidean.

Lan honetan aztertu diren lehen sistemak bentzenoa, naftalenoa eta antrazenoa izan dira. Bentzenoaren kasuan, ikerketa gehienak geometriaren erlaxazioaren analisiaren eta spin estatuaren mendekotasunaren bidetik joan dira [14] edo azterketa nagusia [15] singletean zentratu da. Naftalenoa mugituz, informazio gehiago agertzen hasten da. Kasu honetan, geometriari buruzko informazioaz ez ezik, dimeroak har dezakeen geometriari buruz ager daitezkeen akoplamenduei buruzko informazioa ere badago [16]. Lan honetan ikus dezakegu molekulen jarrera erabakigarria izan daitekeela pilatzeko. Horrek estatuen arteko lotura hobetzen du. Azkenik, antrazenoaren kasurako ez dago horrenbesteko informaziorik egoera tripleteari dagokionez. Naftalenoari gertatzen zaion bezala, ikerketa gehienak polimerizazioarekin dute zerikusia [17].

Lanaren bigarren zatian, hautatutako molekula organikoa Perylene-3,4: 9,10-bis (dikarboximida) molekula (PDI) izan da. PDI kromoforo aromatiko poliziklikoa

da [18]. Nahiz eta gaur egun tinta-industrian asko erabili, gehiago aztertzen da fluorezsentzian aplikazio garrantzitsua duten material aurreratu gisa [19] edo gailu erdieroale organiko [20] bezala. Duela urte batzuk PDIaren egoera tripletea sentibilizazio bimolekularraren bidez soilik lor daitekeen arren, gaur egun hobekuntza batzuk egin dira eta egoera triplete horren eraketa kontrolatu ahal izan da [22]. Horrela, formazioa posible izan da erradikal baten atxikimendu kobalenteari esker. Linkerraren atxikipen-posizioa, mota edo erradikala aldatzen bada linkerraren eta erradikalaren arteko elkarrekintza doitu daiteke egoera tripletea optimizatzeko. Hala ere, ez dago protokolorik kromoforo erradikala kentzeko.

Ezaugarri elektronikoko horiek prozesu fotofisikoak dira. Hurrengo atalean, egoera tripletearen fotogenerazioari eta bihurtetari buruzko informazioa emango da. Tripletearen generazioa ahalbidetzen duten prozesuak honakoak dira: *Sistemen Arteko Gurutzaketa* (ingelesez, ISC) eta *Singletearen Fisioa* (SF) eta konbertsioan aldiz honakoak: *Fosforeszentzia*, *Termikoki Aktibatutako Fluorezsentzia Atzeratua* (ingelesez, TADF) eta *Triplete Triplete Desegitea* (ingelesez, TTA).

8.1.2 Egoera Tripletea

Tripletearen egoeran sakondu aurretik, garrantzitsua da prozesu fotofisiko tipikoak aztertzea eta ulertzea (8.1 Irudia). Prozesu guztiak fotoi baten xurgapenarekin hasten dira, non elektroi bat oinarri egoeratik (S_0) energia maila handiago batera (lerro urdina) kitzikatzen den. Une honetan, elektroi kitzikatua erlaxatzeko modu ezberdinak daude. Lehena bibrazio-erlaxazioa izan daiteke (lerro kurbatu gorria) [23]. Hemen, elektroi kitzikatuak energia bibrazionala ematen dio beste elektroi bati energia zinetikoaren forman. Absortzioa azkarra izanik hau da orokorrean gertatzen dena. Energia bibrazionalaren soberakina bero gisa desegiten da barne-bihurketa (ingelesez, IC) prozesuaren bidez (lerro kurbatu morea) eta molekula 1.go egoera kitzikatuaren maila bibrazionalera erlaxatzen da. Puntu honetan, emisioa gertatzen da (lerro arrosa), erradiazio prozesu bat izanik, eta molekula bere lurrera iristen da.

Molekula organikoak interesgarriak izan daitezke eguzki-zelulen eraginkortasuna handitzeko. Horretarako, interesgarria izan daiteke egoera tripletearen analisisa. Interes honen arrazoia zera da, egoera tripleteak bizitza luzea duela eta ondorioz hedapen luzeagoa ahalbidetzen duela. Honi esker, probabilitate handiagoa dago disoziazio gune batera iristeko [24].

Egoera hirukoitz honen propietateek erakusten dute elektroi-zulo bikotea oso lotua dagoela eta, beraz, hau disoziatzeko elektroi hartzaile sendoak behar direla. Gainera, egoera tripletetik datorren emisioa debekaturik dago (spin aukeraketa arauengatik), eta horrek zaildu egiten du horien detekzioa. Horrek guztiak kargen transferentziarekin edo frekuentzia altu eta baxuko fotoi bihurtetarekin zerikusia duten prozesu fotofisikoak izatea ahalbidetzen du [25].

Emaitza esperimental eta teknologikoak hobetzeko, ezinbestekoa da prozesu fotofisikoaren optimizazioa, baina arrakasta borobila lortzeko prozesuaren funtsezko

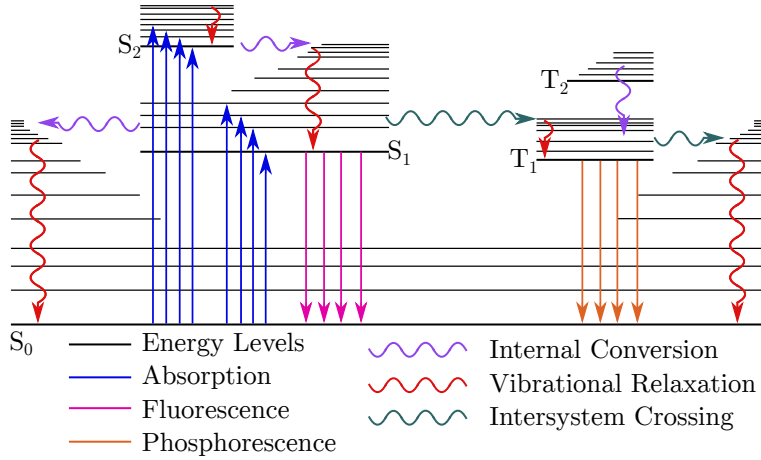


Figure 8.1: Jablonski diagramak deskribatutako trantsizio erradiatibo eta ez-erradiatiboak.

maila azter daiteke. Horrela, eredu teorikoak erabiltzea beharrezkoa izan daiteke prozesuetan erabiltzen diren mekanismoak ulertzeko. Gainera, teknologia optoelektronikorako material optimoa iragartzea ere garrantzitsua da. Oinarrizko maila hau tripletearen generazio eta manipulazio gisa uler daiteke. Horretarako, bi prozesu orokor mota daude: foto-generazioa eta tripletearen konbertsioa.

Egoera hirukoitz hau sortzeko moduetako bat *Sistemen Arteko Gurutzaketa* (ISC)(akuamarina lerro kurbatua) izan daiteke. Hau erradiaziorik gabeko prozesu batean oinarritzen da batez ere, eta molekula bat UV-VIS argiak irradiatzen duenean ematen da, spin [26], [27] aldaketa gertatuz. ISC fotoi bat xurgatzen denean sortzen da. Xurgapen horren ondoren barne-konbertsioa (IC) gertatzen da, hau da, spin anizkoitasun berdina duten populazioaren transferentzia. Eta azkenik energetikoki egoera kitzikatu singlete baxuenera iristen da. Egoera honetan, ISC bidez, fotoia hainbat tripleteetara iristen da, azkenik, energetikoki baxuena den egoera tripletean amaitzako [28]. Argia xurgatzen denean eta S_1 egoera sortzen denean, egoera tripletea ISC-ri esker populatu daiteke. Prozesu hau [25] honela idatz daiteke,

$$k_{ISC} = \frac{2\pi}{\hbar} \langle {}^1\psi^0 | H_{S0} | {}^3\psi^0 \rangle [\text{FCDP}] \quad (8.1)$$

non ${}^1\psi^0$ eta ${}^3\psi^0$ perturbaziorik gabek ouhin-funtzio singlete eta tripleteak diren, hurrenez hurren. FCWD estatuen Franck-Condon Dentsitate Ponderatua da. HONek esan nahi du, ISC tasa bi faktoreren mende dagoela: spin-orbita akoplamenduaren indarra eta bertan inplikaturatko S_1 egoera tripletearen arteko gainjartze bibrazionala.

ISC prozesuak arazo handi bat du: eraginkortasuna. ISC bidez sortutako tripleteek energia galera handia sortzen dute triplete-singlete konbertsioan. Beraz, fotosentifikatutako material organiko berrien diseinuak eraginkortasun hori areagotu dezake.

Adibide berri gisa, materialak ahalmen handia izango luke argia xurgatzeko, energia minimoa galtzeko eta ISC eraginkortasun handia izateko. Optoelektronika organikoan aurrerapen handia izango litzateke. Casanova doktorearen taldeak ikerketa ugari egin ditu hiru estatu horien belaunaldian ISC prozesuei eta haien fosforeszentzia propietateei buruz [29]–[33].

Alternatiba gisa, egoera tripleteak *Singletearen Fisioa*-ren (SF) mekanismoaren bitartez sor daitezke. Eszitoi singletea bi eszitoi tripleteetan banatzen da [34] (8.3 ekuazioa). Kimika kuantikoan ezaguna den bezala, singletaren eta tripletearen arteko trantsizioak debekatuta daude, spin anizkoitasuna ez delako kontserbatzen. Baina SFren kasuan, prozesua spin baimendua da, sortzen diren bi tripleteak singlete orokor gisa elkartzen baitira [35].

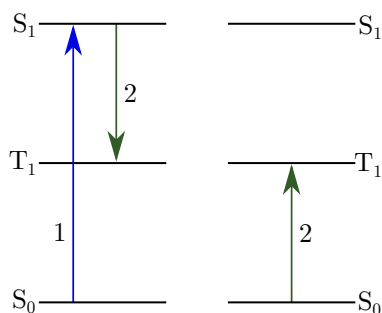


Figure 8.2: Singletearen Fisioa: 1 Ezkerreko kromoforoak S₁-erako kitzikapena jasaten du. 2 Kitzikatutako kromoforoak eskuineko kromoarekin partekatzen du energia, eta T₁-ko estatu bat sortzen du bakoitzaren gainean.

Spin simetria kontserbazioari esker, SF prozesuak azkarrak dira. Fenomeno hau maiztasun altuko fotoiak energia gutxiagoko eszitazioan bihurtzeko prozesua da. Hau Triplete Triplete Desegitea [36], [37]-ren alderantzizko erreakzio bezala ere defini daiteke. Askotan, SF prozesua elkarren segidako bi urratsen emaitza bezala deskribatzen da, non hasierako egoera kitzikatua kromoforo monomeriko baten kantete kitzikatuenarekin erlazionatuta dagoela suposatzen den (8.2 irudia eta 8.3 ekuazioa).

$$S_1 \rightleftharpoons ({}^1TT) \rightleftharpoons T_1 + T_1 \quad (8.2)$$

$$(8.3)$$

Prozesu hau gertatzeko baldintza S₁-eko estatuak eta triplete pareak energetikoki hurbil egon behar dutela, hurrengo baldintza betez: $E(S_1) > 2E(T_1)$. Prozesu honek eguzki-zelula organikoaren eraginkortasuna handitu dezake, singlete fisioko material batek energia altuko fotoiak xurgatu ditzakeelako. Gainera, kromoforoa energia gutxiagoko eguzki-erradiazioa eguzki-fotoi bakoitzeko elektroizulo bakar bat bihurtzearen arduraduna delako. Orain arte, singlete fisio materialak barne zituzten eguzki-zelulek kanpo-eraginkortasun kuantikoak lortu dituzte, % 126 artekoak, eta

barne-eraginkortasun kuantikoak, % 200 ingurukoak. 2011z geroztik, Casanova doktorearen taldeak SF prozesuaren ikerketan parte hartu du [40], [41].

Gainera, prozesu multzo bat dago non tripletea konbertsioz eman daitekeen. Kasu gehienetan, eszitazio triplete pare baten energiak lehen singlete-egoera kitzikatua-aren energia gainditzen du. Spin antiparaleloa duten bi tripleteen topaketarekin, kitzikapen singlete bat sor daiteke. Honela, hauek dira egoera tripletearen bihurteta burutzen duten prozesu nagusiak: *Fosforeszentzia*, *Termikoki Aktibatutako Fluoreszentzia Atzeratua* (TADF) eta *Triplete Triplete Desegitea* (TTA).

Fosforeszentzia da egoera tripletearen informazioa lortzeko metodarik ohikoena. Spin elektronikoko ugari dituzten egoeren arteko trantsizio erradiatiboa da. Gehienetan, eszitazio triplete baxuenaren eta oinarri egoeraren arteko transizioan gertatzen da [42]. Detektatzea oso zaila da [25]. Prozesu hau eragin daiteke argi xurgapenarekin, korrante elektrikoarekin [43] eta erreazio kimiko baten bitartez [44]. Fosforeszentzia oso sentikorra da agregazio molekularrarekiko, tenperaturarekiko eta oxigenoaren sarbidearekiko. 8.1 irudiko lerro larankak fosforeszentzia prozesua adierazten du.

$S_0 \rightarrow S_n$ absortzioaren bidez, egoera triplete baxuena bete daiteke. ISC-ren bidez, tripletea populatu egiten da, eta IC-ren bidez, tripleterik baxuena populatzen da fosforeszentzia erradiazio bat bideratuz.

$T_1 \rightarrow S_0$ hau debekatuta dago, eta horrek prozesu hau intentsitate txikiagokoa bihurtzen du espinak onartutako fluoresentzia emisioarekin alderatuta. Hala ere, edozein molekula errealetan beti dago $T_1 \rightarrow S_0$ transizio bihurtzen duen espin-orbita baten akoplamendu mailaren bat. Hau da detektatze zailaren arrazoa.

Tripleteak eraldatzeko beste modu bat *TADF* da. Prozesu honetan molekula organikoek energia-hutsune txikiak dituzte. Horrela, energia termikoan oinarritutako energia-maila handiko egoerak okupatzen dira. 8.3 irudian ikus daitekeenez, *TADF Sistemen Arteko Gurutzaketa Alderantzikatua* (ingelesez, RISC) prozesuaren goi konbertsioa (ingelesez, UC) endotermiko bat da, T_1 -etik S_1 -rea. Termikoki aktiba daiteke energia-arrakala txikia denean (δ_{EST}) eta T_1 -en bizitza osoa nahikoa luzea denean [45]–[47]. RISC-UC, espektro banaketa zehatza duen emisioaren emaitza da. Aktibatutako RISC prozesu termikoan parte hartzen duten tripleteak eszitazio hotzak dira. Prozesu mota hauek material organiko komunetan eszitazio mota nagusienak dira. TADF igorgailu batean, konbertsioa erraz aktiba daiteke molekularren mugimendu termikoaren bidez. TADF ondorengo ekuazioaren bitartez ere adierazi daiteke,



TADF egiteko nahiko material arrakastatsuak aurkitu diren arren, hala nola, konplexu organiko metalikoak, TADF soilik dituzten material organikoak oparagoak dira. Erraz alda daiteke haien egitura. TADF prozesuak eszitazio tripleten beharra duenez, material hauen fluoresentziak oso erantzun sentikorra dauka tenperatura eta kanpo indar mekanikoarekiko. Horrek material onak bihurtzen ditu sentsoarek aplikatzeko.

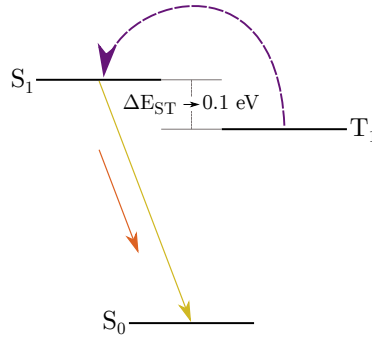


Figure 8.3: Termikoki Aktibatutako Fluoreszentzia Atzeratuaren prozesua.

TADF material eraginkor batentzat, gakoa termikoki aktibatutako RISC-ean dago, non tasaren konstantea Boltzmannen banaketa erlazio batean adieraz daitekeen:

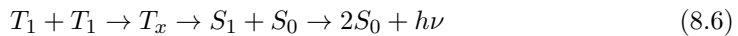
$$k_{\text{RISC}} \propto \exp\left(\frac{\Delta E_{\text{ST}}}{k_{\text{B}}T}\right) \quad (8.5)$$

k_{B} Boltzmann-en konstantea eta T temperatura izanik [48].

TTA UC fotoien kasu berezi bat da. IR-tik VIS-erako konbertsioa zelula fotovoltaikoen hobekuntzaren eta uretatik abiatuta hidrogenoaren ekoizpen fotokatalitikoaren alternatiba onenetako bat da. Baina gaur egun, osagai tipikoak ez dira gai fotoiak frekuentzia baxuetara bihurtzeko. Hau muga handia da eguzki-zeluletan TTA erabiltzeko.

TTA bidezko UC gertatzeko baldintza nagusia sistema bimolekular bat da. Hau TTA eraginkorra jasaten duen molekula igorle batek eta argi intzidentea xurgatzeko balio duen molekula sensibilizatzaile batek osatzen dute. Hauek igorlean elikatzen dira. Prozesu hau Stocken aurkako fluoreszentzia atzeratuan oinarritzen da. Parker eta Hatchardek 60ko hamarkadan eman zuten horren berri [49], [50].

8.4 irudiak TTA-UC prozesua adierazten du. Lehen urratsean ikus daiteke nola sensibilizatzaileak energia gutxiko fotoiak xurgatzen dituen. Horren ondoren, SHG-ak egoera triplete baxuenera garraiatze du. Triplete-triplete energia transferentzia azkarra (ingelesez, TET) bermatuz, molekula igorleen egoera triplete baxuenean biltegitratzen da energia. Orduan, bi igorleek elkarrengatik dute eta Triplete-Triplete Deuseztapena gertatzen da (TTA, 4. urratsa). Igorlea S_1 n dago. Azkar eta energia handiagoarekin, hasieran xurgatutako fluoreszentzia gertatzen da. TTA hurrengo ekuazio gisa ere ikus daiteke [48]:



non T_1 , S_1 eta S_0 egoera triplete baxuena, egoera singlete baxuena eta oinarri egoera, hurrenez hurren, diren.

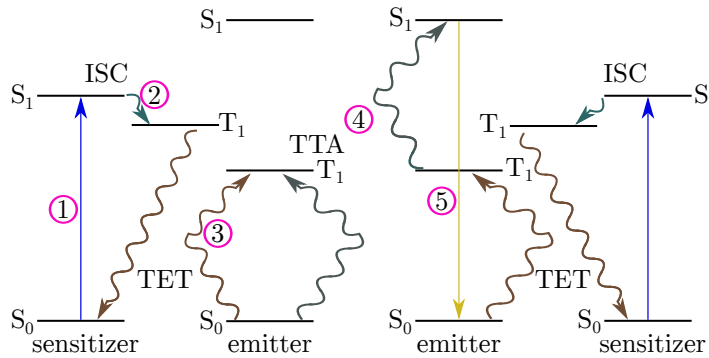


Figure 8.4: Triplet Triplet Deuseztatzearen Goi KONpertsio Printzioa.

Argia absorbatu eta emititzeko, singlete-singlete trantsizioetan oszilatzailearen sendodatura oso nabaria da TTA-UC-an. Energiaren bitarteko biltegitratzea T_1 -eko tripleteen bidez errazten da. TTA-UC prozesu inkoherentea da, eta energia-biltegitratzeak argi gutxiko baldintzetan funtzionatzen uzten du. Baina badira TTA-UC izateko bete behar diren baldintza batzuk: alde batetik, *sentsibilizatzailea* xurgapen handiko espeziea izan behar du sistema arteko gurutzaketa handiko eskualdean. Tripletearen bizitzak luzea izan behar du ($>10 \mu\text{s}$) eta singlete-triplete tartea txikia izan daiteke. Beste alde batetik, *espezie igorlearen* tripletearen bizitzak altua izan behar du ($>100 \mu\text{s}$), singlete egoera bat lehen tripletearen energiaren bikoitza baino txikiagoa eta fluoreszentzia handiko errendimendu kuantikoa [51].

8.1.3 Lanaren antolaketa eta helburua

Tesi honetan bi sistema nagusi aztertu dira ikuspegi konputazionaletik. Horretaz gain, hurrengo lanak egoera kitzikatuen karakterizaziorako prozedura teorikoei buruzko informazioa ere ematen du. Hori kontuan hartuta, lan idatzi osoa hiru bloke nagusitan banatuta dago.

Lehenengoak Kimika Kuantikoaren (ingelesez, QC), oinarriko kontzeptuei egiten die erreferentzia. Hemen metodo garrantzitsuenei buruzko ikuspegi orokor txiki bat egiten da. Puntu berean, egoera eszitatatuak aztertzeko metodo esanguratsuenak sakontzen dira, hala nola trantsizio-dentsitatearen matrizearen (ingelesez, TDM) deskonposizioaren diabatizazioa. Tresna horiei esker, egoera eszitatuei zentzu fisikoa emateko gai gara.

Optoelektronikaren ikuspegi orokorra eta QC alderdirik garrantzitsuenak ikusi ondoren, lanaren emaitzak aurkeztuko dira. Hau bi bloke nagusitan banatuko da. Lehenengo sistema aromatiko txikien oinarriko azterketa da, bentzenoa, naftalenoa eta antrazenoa. Lanaren zati honen erronka nagusia da egoera eximeriko hirukoitz bat aurkitzea. Horretarako, dimero batzuk diseinatuko dira loturarik gabeko egiturak eta spin-dentsitate deslokalizatua aurkitzeko. Gainera, konformamero bakoitzaren

ezaugarri estruktural eta elektroniko nagusiak eta elkarrekintza mota desberdinak aztertuko dira. Azken zatian, egoera triplete baxuenaren izaera aztertuko da, egoera eximerikoaren ezaugarriak ikusteko.

Emaitzen bigarren zatia Perylene-3,4: 9,10-bis (PDI) molekula, agregatu eta deribatuei dagokie. Abiapuntu gisa, molekularen ezaugarri garrantzitsuenak aztertzen dira, hala nola, egitura molekularra, mugako orbital molekularrak (OM) edo egoera kitzikatu baxuak. Ikerketa honek informazio garrantzitsua emango du ikerketa gehiago egiteko, adibidez, PDI agregatuak edo ardatz longitudinalean distortsionatutako dimeroaren portaera aztertuko dira.

Agregatuen kasuan, eszitazio lokalen (ingelesez, LE) eta kargen transferentzia egoeren (ingelesez, CT) terminoak erabiltzen dira kitzikatutako egoerak ezaugarritzeko. Barne kromoforoen CTko estatuen zeregina ere arrazionalizatu egiten da singlete eta triplete egoerarik baxuenetarako, akoplamendu eta ekarpen diabatikoei dagokienez. Singlete egoeran, trantsizioa elektroien eta zuloen arteko akoplamenduen erlazioak deskribatzen da. Nahiz eta tripleteek elkarreragin handiak izan, LE eta CT egoeren arteko energia-tartea oso handiagoa da, eta horrek LE/CT nahastea gutxitzen du.

Aipatutako propietateak sistema distortsionatuz alda daitezke. Modulazio honek zenbait aldaketa eragin ditzake egoera kitzikatuen propietateetan. Kasu honetan, diabatizazio-prozedura orokor bat erabili da. Hemen, kitzikatutako estatuak LE eta CT estatuekin bat datozen termino diabatikoak adierazten dituzte. Ikuspegi horri esker, profil energetikoak, kargen transferentziaren ezaugarriak eta akoplamendu garrantzitsuenak azter daitezke.

8.2 TEORIA ETA METODOAK

8.2.1 Kimika Kuantikoaren Oinarriak

XIX. mende amaieraren eta XX.aren hasieraren artean atomo eta partikula txikien existentzia frogatu zen modu esperimentalean. Hala ere, elektromagnetismoaren oinarritzko legeak ez ziren gai sistema horien egonkortasuna azaltzeko. Arazo hori aurre egiteko, mekanika kuantikoaren garapena [52]–[54] behar beharrezkoa izan zen. Honi esker, mundu mikroskopikoaren nondik norakoak ulertzeko modua bazen. Bohr eta Sommerfeld izan ziren lehenak atomorik sinpleenaren egonkortasuna azaltzeko modelo bat proposatu zutenak. Atomo hori, hidrogenoa zen. Modelo honen arabera, Hidrogeno atomoa negatiboki kargatutako elektroï bat bezala definitu zitekeen. Eta hau, modu positiboan kargatutako nukleo baten inguruan zebilen bueltaka energia zehatz bat zuten orbiten inguruan. Plank-en erradiazio teorian oinarrituta, elektroï hauek orbita batetik bestela salto egin zezaketen, energia zehatz bat absorbatu edo eminitzen bazuten. Aurkikuntza hau oinarritzat hartuz, Schrödinger eta Heisenberg-ek sistema multielektroniko eta molekulentzako garatu zuten teoria. Esan daiteke, gaur egun mekanika kuantikoari esker uler daitekeela mundu mikroskopikoa.

Mekanika kuantikoarekin bat eginik, sistema kuantikoaren informazio guztia bere uhin-funtziotik lor daiteke, hau da, Schrödinger-en ekuazioa ebatziz [55]. Denbora eta espazioa oinarritzat dituen ekuazio diferentziala da Schrödinger-en ekuazioa. Honek, partikulen masa eta kargaren dependentzia du. Denborarekiko menpekotasuna duen ekuazioa honela idatzi daiteke,

$$-i\hbar \frac{\delta}{\delta t} \Psi(\mathbf{r}, \mathbf{R}, t) = \hat{H}(\mathbf{r}, \mathbf{R}) \Psi(\mathbf{r}, \mathbf{R}, t) \quad (8.7)$$

non operadore Hamiltondarra, \hat{H} , sistemaren energia operadorea den. Honek sistemako elkarrekintza guztien informazioa du. Bestalde, \hbar Planck-en konstante murriztua da. Sistema geldikorren ekuazioa, 8.7 ekuazioa, denborarekiko independentea den ekuazioan bilakatzen da,

$$\hat{H}(\mathbf{r}, \mathbf{R}) \Psi(\mathbf{r}, \mathbf{R}) = E \Psi(\mathbf{r}, \mathbf{R}) \quad (8.8)$$

non E sistemaren energia den operadore Hamiltondarrak, \hat{H} , definitzen duena eta uhin-funtzioa, Ψ , Hamiltondarrari atxikitutako funtzio propioa den. Ψ -k nukleo guztien posizioaren eta informazio guztia pilotzen duten elektroien menpekotasuna du. Dena den, 8.7 Ekuazioa elektro bakarreko sistemetzako soilik ebatzi daiteke.

N elektro eta M nukleo dituen sistema batentzat, Hamiltondarra honako terminoekin definitzen da: nukleoaren, \hat{T}_n , eta elektroaren, \hat{T}_e , energia zinetikoa, nukleo-elektroi elkarrekintza, \hat{V}_{ne} eta nukleoaren, \hat{V}_{nn} , eta elektroaren, \hat{V}_{ee} , arteko aldarapena. Honekin, Hamiltondar molekularra honela idatzi daiteke,

$$\hat{H} = \hat{T}_e(\mathbf{r}) + \hat{T}_n(\mathbf{R}) + \hat{V}_{ee}(\mathbf{r}, \mathbf{r}) + \hat{V}_{nn}(\mathbf{R}, \mathbf{R}) + \hat{V}_{ne}(\mathbf{r}; \mathbf{R}) \quad (8.9)$$

Unitate atomikoetan ($\hbar = 1$, $e = 1$, $m_e = 1$, $a_0 = 1$), 8.9 Ekuazioaren terminoak honela defini daitezke,

$$\hat{T}_e(\mathbf{r}) = - \sum_{i=1}^N \frac{\nabla_i^2}{2} \quad (8.10)$$

$$\hat{T}_n(\mathbf{R}) = - \sum_{A=1}^M \frac{\nabla_A^2}{2m_A} \quad (8.11)$$

$$\hat{V}_{ee}(\mathbf{r}, \mathbf{r}) = \sum_{i>j}^N \frac{1}{|\vec{r}_i - \vec{r}_j|} \quad (8.12)$$

$$\hat{V}_{nn}(\mathbf{R}, \mathbf{R}) = \sum_{A>B}^M \frac{Z_A Z_B}{|\vec{R}_A - \vec{R}_B|} \quad (8.13)$$

$$\hat{V}_{ne}(\mathbf{r}; \mathbf{R}) = - \sum_{i=1}^N \sum_{A=1}^M \frac{Z_A}{|\vec{r}_i - \vec{R}_A|} \quad (8.14)$$

8.2.2 Born-Oppenheimer-en Hurbilketa

8.8 Ekuazioaren arazoei aurre egin ahal izateko, hainbat hurbilketa beharrezkoak dira. Kimika Kuantikoan ohikoena den hurbilketa Born-Oppenheimer-en hurbilketa [56] da. Honen oinarria nukleo eta elektroien arteko pisu diferentzia da. Protoi eta neutroien masak 1800 aldiz handiagoak dira elektroienak baino. Ondorioz, elektroien mugimendua hainbat aldiz azkarragoa da. Beraz, onartu daiteke elektroiek erantzuna berehalakoa dela nukleoekin alderatuz gero. Honela, ulertu daiteke nukleoak elektroiek sortutako eremuan mugitzen direla. Honi esker, Schrödinger-en ekuazioa elkarrekin erlazionatuta dauden bi ekuazioetan bana daiteke: ekuazio elektronikoa eta nuklearra. Ekuazio elektronikoa, nukleoaren termino zinetikoa, \hat{T}_n , alde batera uzten da, aldarapen nuklearra, \hat{V}_{nn} , konstante manentzen da eta nukleo/elektroi elkarrekintza, \hat{V}_{ne} , parametro moduan tratatzen da. Parametro hau zehaztutako nukleoaren koordinatuetan oinarritzen da. Honi esker, Schrödingerren ekuazio elektronikoa ez du mugimendu nuklearra kontutan hartzen eta ondorioz zati elektronikoa ebatzi daiteke,

$$\hat{H}_e(\mathbf{r}; \mathbf{R})\psi_e(\mathbf{r}; \mathbf{R}) = E_e(\mathbf{R})\psi_e(\mathbf{r}; \mathbf{R}) \quad (8.15)$$

$$\hat{H}_e = \hat{T}_e(\mathbf{r}) + \hat{V}_{ee}(\mathbf{r}, \mathbf{r}) + \hat{V}_{nn}(\mathbf{r}, \mathbf{r}) + \hat{V}_{ne}(\mathbf{r}; \mathbf{R}) \quad (8.16)$$

non uhin-funtzio elektronikoa $\psi_e(\mathbf{r}; \mathbf{R})$ den. Behin uhin-funtzio elektronikoa deskribatuta, nuklearra aztertu daiteke. Honela, energia elektronikoa, E_e , elkarrekintza nuklearrari, \hat{V}_{nn} , gehitzen bazaio, *Gainazal Potentzial Energia* (ingelesez, PES), $U(R)$, definitzen da. Honekin Schrödinger-en ekuazio nuklearra idatzi daiteke,

$$(\hat{T}_n + U(\mathbf{R}))\psi_n(\mathbf{R}) = E_{tot}\psi_n(\mathbf{R}) \quad (8.17)$$

Aztergai den sistematentzat, PES-ak biltzen du informaziorik baliotsuena maila bibrazional, geometria optimo eta errektibotasun kimikoari dagokionean.

8.5 Irudiak molekula diatomiko baten oinarritzko egoera eta egoera kitzikatuari dagozkion PES-a deskribatzen du. Hau, nukleoaren koordinatuak finkatuz ekuazio elektronikoa ebatzita lortzen da. Egoera kitzikatuaren kasuan, molekulak energia, $h\nu$, kantitate zehatz bat absorbatzen duenean elektroi bat edo gehiago egoera kitzikatura pasatzen dira; egoera hau PES-a baino energia handiagokoa izanik. Bi egoeren arteko energia diferentzia eszitazio bertikalaren bitartez kalkulatu da.

Laburbilduz, Born-Oppenheimer-en hurbilketan, elektroi eta nukleoaren mugimenduak desakoplatu egiten dira Schrödingerren ekuazio molekularra sinplifikatzeko asmoz. Honela, ekuazio elektronikoa eta nuklearrak lor daitezke. Hala ere, zoritxarrez, bi ekuazioak ebatzi ahal izateko hurbilketa gehiago behar dira

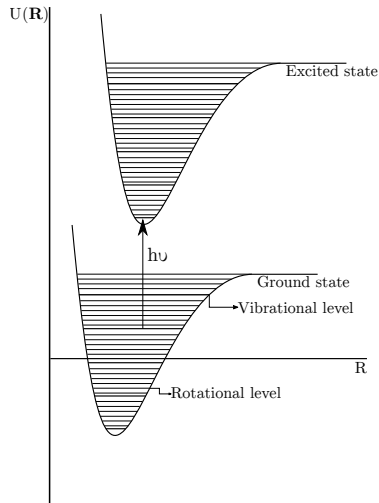


Figure 8.5: Oinarritzko egoeraren eta egoera kitzikatuaren Gainazal Ponenzial Energia (PES); nukleoaren koordinatuarekiko errepresentatuta.

8.2.2.1 Schrödingerren Ekuazio Elektronikoa

ab initio metodoari esker Schrödingerren ekuazio elektronikoa ebazteko aukera badago beti ere nukleoaren posizioa finkatuta badago eta sistemaren elektroi kopurua ezaguna bada. Hori esker, energia eta uhin-funtzio elektronikoa kalkulatu daitezke Born-Oppenheimer-en Hurbilketa erabilita. Operadore egokiak erabiliz propietate kimikoak, hala nola, elektroi dentsitatea edo momentu dipolarra, lor daitezke uhin-funtzioaz baliatuz. Lehen aipatu bezala, Schrödingerren ekuazioa ebazteko arazoak daudenez, hainbat hurbilketa erabili behar dira; eta hauek, orokorrean, bi talde desberdinetan sailkatzen dira: (i) elektroi-anitzeko uhin-funtzioa (Ψ) oinarri dutenak eta (ii) elektroi dentsitatea ($\rho(r)$) ardatz dutenak. Ondorengo azpiataletan, metodo bakoitzaren propietate garrantzitsuenak aipatuko dira.

Metodo bakoitza sakondu aurretik, garrantzitsua da kimika kuantikoaren oinarria ongi ulertzea. Oinarri hau Orbital Molekularren (ingelesez, MO) nondik norakoak ulertzean datza. MO hauek elektroiaren posizioaren eremu probableak definitzen ditu. Egitura elektronikoen kalkulua orbitalen hurbilketan oinarritzen dira eta MO-ren espresioak orbital atomikoen konbinazio linear gisa (ingelesez, MO-LCAO),

$$\phi_i(r) = \sum_{\mu} c_{\mu i} \phi_{\mu}(r) \quad (8.18)$$

non $c_{\mu i}$, ϕ_{μ} orbital atomikoen espantzio koefizientea den ϕ_i orbital molekularrean.

Kalkuluaren zehaztasuna determinatzeko, oso garrantzitsua da orbital atomikoen aukeraketa. Hau, base-multzo bezala da ezaguna eta OM-ak eraikitze erabiltzen da.

8.2.3 Uhin-Funtzio Metodoak

Schrödinger-en ekuazio elektronikoak ebazteko moduetako bat uhin-funtzio metodoak erabiltzea da. Metodo hauek Hartree-Fock (HF) eta post-HF metodoetan sailkatzen dira.

8.2.3.1 Hartree-Fock Method

Hartree-Fock (HF) hurbilketa [57] uhin-funtzio metodorik sinpleena da eta MO hurbilketaren analogoa. Hamiltondar modeloa, \hat{H} , Fock operadore, \hat{F} , ezaguna, elkarrekintzarik gabeko N elektroien modeloa adierazten du,

$$\hat{F} = \sum_i (\hat{h}_i) + \hat{J}_i + \hat{K}_i = \sum_i (\hat{h}_i + \hat{g}_i) \quad (8.19)$$

non \hat{g}_i -k Coulomb, eta trukaketa, \hat{K}_i operadoreak barne dituen,

$$\hat{J}_i \psi_j(1) = \int \psi_j^*(2) \frac{1}{r_{12}} \psi_j(2) dx_2 \psi_i(1) \quad (8.20)$$

$$\hat{K}_i \psi_j(1) = \int \psi_j^*(2) \frac{1}{r_{12}} \psi_i(2) dx_2 \psi_j(1) \quad (8.21)$$

\hat{J}_i elektroi bakarreko Coulomb-en operadorea da eta j elektroietik datorren aldarapena definitzen du. \hat{K}_i elektroi-bakarreko trukaketa operadorea da. ψ_i i elektroien elektroi-bakarreko uhin-funtzioa da; ψ_j j , elektroien elektroi-bakarreko uhin-funtzioa adierazten du eta $\frac{1}{r_{12}}$ 1 elektroien eta 2 elektroien arteko distantzia da.

Antisimetria zainduz eta printzipio bariatzionala ezarriz, *Slaeter-en Determinante* bakarria optimizatzen da,

$$\psi(\mathbf{1}, \mathbf{2}, \dots, N) = (N!)^{-\frac{1}{2}} \begin{vmatrix} \phi_i(\mathbf{1}) & \phi_j(\mathbf{1}) & \cdots & \phi_N(\mathbf{1}) \\ \phi_i(\mathbf{2}) & \phi_j(\mathbf{2}) & \cdots & \phi_N(\mathbf{2}) \\ \vdots & \vdots & \ddots & \vdots \\ \phi_i(\mathbf{N}) & \phi_j(\mathbf{N}) & \cdots & \phi_N(\mathbf{N}) \end{vmatrix} \quad (8.22)$$

non $(N!)^{-\frac{1}{2}}$ normalizazio faktorea den eta N elektroiak. Hauek N spin orbitalak ($\phi_i, \phi_j, \dots, \phi_N$) okupatzen dituzte. HF metodoa hidrogeno atomoarentzako zehatza den arren, ezin ditu hidrogenotik haratago dauden molekula deskribatu Ψ eta \hat{H} hurbilketak direlako eta ondorioz ez dauka elektroien korrelaziorik. Dena den, metodo honek energia elektroniko totalaren %99a kalkula dezake. Nahiz eta erreazio kimikoetan porrot egin post-HF metodoak erabilia elektroien korrelazioa gehitu daiteke ta arazoa konpondu.

Elektroien mugimenduak ez direnez erabat independenteak HF-ek ezin du elektroien korrelazioa deskribatu. Hau hobetzeko kontzeptu berri bat gehitzen da, elektroien

korrelazioa, $E_{(corr)}$. Löwdin-ek definitu zuen bezala, $E_{(corr)}$ energia zehatzaren, E_{exact} , eta HF energiaren, E_{HF} arteko diferentzia da base multzo osoan,

$$E_{corr} = E_{exact} - E_{HF} \quad (8.23)$$

non E_{exact} sistemaren energia ez-relatibistikoari egiten dion erreferentzia eta E_{HF} HF energia den. HF gai denez energia totalaren zati haundi bat deskribatzekoa, post-HF metodoentzako erreferentzia gisa erabiltzen da. Hauer uhin-funtzio metodoetan oinarritzen dira baita ere baina HF alderatuz gero zehatzagoak dira. Gainera, Slaeter-en determinazteaz haratago joan daitezke elektroi korrelazioa gehituz.

Historian zehar post-HF metodo ezberdinak garatu dira eta honako biak ezagunak: (i) Konfigurazio Elkarrekintza, osoa eta moztua, eta (ii) Perturbazio Teoria. Lan honetan bigarren metodoa izan da erabili dena, beraz ondorengo azpiatalean hau azalduko da.

8.2.3.2 Perturbazio Teoria

Arestian aipatu bezala HF metodoak hainbat arazo pairatzen ditu propietate kimikoak erreproduzitzerako garaian eta hortaz elektroi korrelazioaren terminoa, 8.23, beharrezkoa da. Arazo hori aurre egiteko erabiltzen den teoretiko bat Møller-Plesset Perturbazio Teoria (MP) da. Metodo hau Rayleigh-Schrödinger Perturbatio Teorian [58] oinarritua dago. Hildo honetan, batek esan dezake metodo perturbazionalek Hamiltondarra, \hat{H} , perturbaziorik gabeko Hamiltondarraren, \hat{H}_0 , eta perturbazio operadorearen, \hat{V} , batuketa dela,

$$\hat{H} = \hat{H}^{(0)} + \lambda \hat{V} \quad (8.24)$$

non λ perturbazioa kontrolatzen duen parametroa den. Schrödinger ekuazioaren soluzioak degeneratu gabeko eta perturbaziorik gabeko kasuan honela definitzen dira,

$$\hat{H}^{(0)}|\Psi_i^{(0)}\rangle = E_i^{(0)}|\Psi_i^{(0)}\rangle \quad (8.25)$$

$$\hat{H}|\Psi_i\rangle = E_i|\Psi_i\rangle \quad (8.26)$$

i egoera elektronikoa adierazten duen azpiindiezea izanik. 8.24 hartuz eta 8.26 Taylor-en hedapenean garatuz,

$$|\Psi_n\rangle = |\Psi_i^{(0)}\rangle + \lambda|\Psi_i^{(1)}\rangle + \lambda^2|\Psi_i^{(2)}\rangle + \dots \quad (8.27)$$

$$E_n = E_i^{(0)} + \lambda E_i^{(1)} + \lambda^2 E_i^{(2)} + \dots \quad (8.28)$$

Kasu honetan, i hurbilketaren ordena izanik. Deribazioa sinplifikatzeko asmotan, \hat{H}_0 -ren balio propioak normalizatuta daudela onartzen da,

$$\langle \Psi_i^0 | \Psi_i^0 \rangle = 1 \quad (8.29)$$

eta ondorioz honako baldintza inposatzen da,

$$\langle \Psi_i^0 | \Psi_i \rangle = 1 \quad (8.30)$$

2.21 eta 2.22 ekuazioak Schrödinger-en ekuazioan ordeztuz,

$$\begin{aligned} & (\hat{H}^0 + \lambda \hat{V})(|\Psi_i^{(0)}\rangle + \lambda |\Psi_i^{(1)}\rangle + \lambda^2 |\Psi_i^{(2)}\rangle + \dots) = \\ & (E_i^{(0)} + \lambda E_i^{(1)} + \lambda^2 E_i^{(2)} + \dots)(\Psi_i^{(0)} + \lambda \Psi_i^{(1)} + \lambda^2 \Psi_i^{(2)} + \dots) \end{aligned} \quad (8.31)$$

eta berretzaile berdineko λ terminoak identifikatuz,

$$\hat{H}^0 |\Psi_i^{(0)}\rangle = E_i^{(0)} |\Psi_i^{(0)}\rangle \quad (8.32)$$

$$\hat{V} |\Psi_i^{(0)}\rangle + \hat{H}^0 |\Psi_i^{(1)}\rangle = E_i^{(1)} |\Psi_i^{(0)}\rangle + E_i^{(0)} |\Psi_i^{(1)}\rangle \quad (8.33)$$

$$\hat{H} |\Psi_i^{(2)}\rangle + \hat{V} |\Psi_i^{(1)}\rangle = E_i^{(2)} |\Psi_i^{(0)}\rangle + E_i^{(1)} |\Psi_i^{(1)}\rangle + E_i^{(0)} |\Psi_i^{(2)}\rangle \quad (8.34)$$

0., 1.º, 2.º and n. energia ordeneko espresioak lortzeko beharrezkoa da 2.26, 2.27 eta 2.28 ekuazioak $\langle \Psi_n^{(0)} |$ -rekin bidertzea, horrela

$$E_i^{(0)} = \langle \Psi_i^{(0)} | \hat{H}_0 | \Psi_i^{(0)} \rangle \quad (8.35)$$

$$E_i^{(1)} = \langle \Psi_i^{(0)} | \hat{V} | \Psi_i^{(0)} \rangle \quad (8.36)$$

$$E_i^{(2)} = \langle \Psi_i^{(0)} | \hat{V} | \Psi_i^{(1)} \rangle \quad (8.37)$$

MP lehen aipatutako teoriaren kasu berezi bat da. Hau horrela izanda, perturbazio txiki bat, \hat{V} , korrelazio potentzial bezala ezagutua gehitzen da,

$$\hat{V} = \hat{H} - \hat{F} \quad (8.38)$$

$\Psi_0^{(0)}$ uhin-funtzioa \hat{F} -en funtzio propioa denez, dagokion balore propioa, $E_0^{(0)}$, honela definitzen da,

$$E_0^{(0)} = \langle \Psi_0^{(0)} | \hat{F} | \Psi_0^{(0)} \rangle = \sum_a^N \varepsilon_a \quad (8.39)$$

non a okupatutako orbitalei egiten dien erreferentzia. Antzeratu, HF-en uhin-funtziotik eraikitako beste edozein Slaeterren determinantea eta okupatutako orbita-

lak okupatugabekoetatik ordezkutzen badira \hat{F} -ren funtzio propioa da. 2.30 ekuazioa oinarritzat hartuz, froga daiteke lehen ordeneko zuzenketa (MP1) HF-en energian amaitzen duela. Hortik, korrelazio energiaren lehenengo ekarpena, bigarren ordeneko terminotik dator,

$$E_0^{(2)} = \langle \Psi_0^{(0)} | \hat{V} | \Psi_0^{(0)} \rangle = - \sum_{k \neq 0} \frac{|\langle \Psi_0^{(0)} | \hat{V} | \Psi_k^{(1)} \rangle|^2}{E_k^{(0)} - E_0^{(0)}} \quad (8.40)$$

Brillouin-en teoremak [59] dioten bezala, eszitazio bakarreko determinanteak ez dute inongo elkarrekintzarik HF-ren uhin-funtzioarekin. Beraz, eszitazio-bikoitzeko determinanteak dira 2.34 ekuazioari ekarpena egiten diotenak. Spin orbitaletaz hitz egiten denean, MP2 energia honako espresioarekin definitzen da

$$E_0^{(2)} = E_{MP2} = \frac{1}{4} \sum_{occ}^N \sum_{virt}^V \frac{|\langle occ | virt \rangle|^2}{\varepsilon_{occ} - \varepsilon_{virt}} \quad (8.41)$$

non N elektroi kopurua den ta V eszitazio-bikoitzen determinantzeak lortzeko erabili den spin orbital kopurua den.

8.2.4 Dentsitate Funtzio Teoria

Dentsitate Funtzionalaren Teoria da gaur egun hedatuen dagoen teoria egitura elektronikoen kalkulua egiteko. Honen arrazoi nagusia da elektroi dentsitate totala inongo uhin-funtziorik gabe kalkulatu dela. Honen badu bere barne elektroi korrelazioa eta horrela post-HF metodoak baino baliabide konputazional gutxiago behar ditu.

8.2.4.1 Denborarekiko-Independentea den Dentsitate Funtzionalaren Teoria

Hohenberg and Kohn-en [60] 1.go teoreman, degeneratu gabeko oinarri egoera batn propietate elektronikoen determinatzea lortu zuten. Beti ere, dentsitate elektronikoen baliatuz $\rho(\mathbf{r})$. Hori dela eta, oinarritzko egoeraren energia elektronikoa $\rho(\mathbf{r})$ -ren funtzionala da eta honela definitzen da,

$$E_0[\rho] = T[\rho] + E_{ee}[\rho] + V_{ext}[\rho] \quad (8.42)$$

hemen koordinatu elektronikoen (\mathbf{r}) dentsitatearekiko dependentzia alde batera uzten da. $T[\rho]$ energia zinetikoen funtzionala da, $E_{ee}[\rho]$ elektroi-elektroi aldarapena eta

V_{ext} kanpoko potentziala. Azken hau sistema molekularretan elektroi-nukleo arteko erakarpena da, eta ondorioz 8.42 honela idazten da,

$$E_0[\rho] = T[\rho] + E_{ee}[\rho] + E_{en}[\rho] \quad (8.43)$$

non $E_{en}[\rho]$ sistemarekiko dependentzia duen. Bestalde, $T[\rho]$ eta $E_{ee}[\rho]$ -k definizio unibertsalak dituzte. Termino independente hauek Hohenberg-Kohn funtzionalean biltzen dira,

$$F_{HK}[\rho] = T[\rho] + E_{ee}[\rho] \quad (8.44)$$

Nahiz eta 1.go teorema honek ezarri nahikoa dela oinarri egoerako dentsitatea $\rho(\mathbf{r})$ interesezkoak diren propietateak lortzeko, ez da ezer ere ez komentatzen dentsitatea lortzeko zer egin behar den. Puntu honetan, Hohenberg-Kohn-en 2. teoremak hartzen du indarra. Honen arabera, oinarritzko egoeraren dentsitate elektronikoa jakinda posible da egoera horri dagozkion propietate elektroniko guztiak ezagutzea; beti ere funtzional egokia aukeratzen bada. Hauek energiaren funtzionalari printzipio bariasionala aplikatzen diote eta horrela dentsitatea kalkulatu daiteke $E[\rho]$ -ren forma zehatza jakinda.

Kohn-Sham Ekuazioa. Nolanahi ere funtzionalaren forma zehatza ezezaguna denez, Kohn eta Sham-ek [61] interakzio gabeko erreferentzia sistema bat erabiliz hurbilketa bat garatu zuten dentsitate elektronikoa oinarritzko egoeran determinatzeko. Honela, honakoa erakutsi zuten: oinarri egoerako energia elektroniko zehatza, E_0 , N -elektroi dituen molekula batean eta ρ oinarri egoerako dentsitatearekin ondorengo moduan defenitu zitekela,

$$E_0 = -\frac{1}{2} \sum_{i=1}^N \langle \psi_i(1) | \nabla_i^2 | \psi_i(1) \rangle + \int v(r) \rho(1) d\vec{r}_1 + \frac{1}{2} \int \int \frac{\rho(1)\rho(2)}{r_{12}} d\vec{r}_1 d\vec{r}_2 + E_{xc}[\rho] \quad (8.45)$$

non $v(r) = -\sum_{\alpha} \frac{Z_{\alpha}}{r_{1\alpha}}$ nukleoaren presentziagatik sortutako kanpoko potentziala den, θ_i KS orbitalak diren eta $E_{xc}[\rho]$ truke-korrelazio energia den. Eskema honetan, oinarri egoera zehatza ρ KS orbitalak erabiliz eraiki daiteke honakoa jarraituz,

$$\rho = \sum_{i=1}^N |\theta_i|^2 \quad (8.46)$$

eta KS orbitalak KS Fock operadorearen elektroibakarreko funtzio propioak diren,

$$\hat{F}_{KS}(1)\theta_i(1) = \epsilon_i\theta_i(1) \quad (8.47)$$

\hat{F}_{KS} Kohn-Sham operadorea honela definitzen da,

$$\hat{F}_{KS} = -\frac{1}{2}\nabla_1^2 + v(1) + \sum_{j=1}^n \hat{J}_j(1) + V_{xc}(1) \quad (8.48)$$

non \hat{J} Coulomb-en operadorea eta V_{xc} truke-korrelazio potentzialak diren. Korrelazio funtzionala elektroi dentsitatearen menpekoeaenez, KS ekuazioak modu iteratiboan ebatzi behar dira. Hasierako puntua suposatutako dentsitatea da non \hat{F}_{KS} eraikitzen den eta ondoren ekuazio multzo bat ebatzen den. Prozesu hau konbergentzia bat lortu arte errepikatzen da.

Dena den, Kohn-Sham orbitalen zentzu fisikoa ez da guztiz onartzen [62]. Batzuentzat, mota honetako orbitalen esanahiak ahalbidetzen du ρ zehatza (8.45) ekuazioaren bitartez kalkulatzeko. Modu berean, orbital hauek ez dira nahastu behar MO-ren energierekin. Beste batzuentzako, aldiz, KS orbitalen esanahia eta eta HF orbital kanonikoa oso antzekoa da.

Kohn-Sham-en formalismoa elektroi gas uniformearentzeko zehatza den bitartean E_{xc} and v_{ex} ezezagunak dira. Arazo honi aurre egiteko Dentsitate Funtzionalaren Hurbilketak (ingelesez, DFA) bezala ezagunak diren hurbilketak egiten dira. Hauetan lehenengoa Tokiko Dentsitate Hurbilketa (ingelesez, LDA) [65] izenez da ezaguna. Hemen bolumen elementu bakoitza dentsitate lokalarekin $\rho(\vec{r})$ batera elektroi gas homogeneoa dela kontsideratzen da. Dentsitatearen aldaketa ezenez leuna metodo hauetan, zerbait sofistikatuagoa behar da, hala nola, dentsitatearen gradientea ($\nabla\rho(r)$). Hurbilketa hauek Orokortutako Gradientearen Hurbilketa (ingelesez, GGA) bezala ezagutzen dira eta LDA-rekin alderatuz hainbat aplikazio kimiko hobetzen dira [66]. Dentsitatearen Laplaziarra txertatuz, $\nabla^2\rho(r)$, hare hobekuntza gehiago egin daitezke eta hauek meta-GGA izenez ezagutzen dira.

Hori gutxi balitz, HF-en trukaketa zatiaren frakzio batzuk har daitezke Funtzional Hibridoak sortzeko [68]. Hemen, trukaketaren zatia HF-etik dator eta korrelazioarena DFT-tik. Sistemaren ezaugarrien arabera HF trukaketa kopuru desberdina duten funtzionalak aukeratzen dira. Hala ere, funtzional hauek porrot egiten dute absortzio espektro edo Van der Waals-en loturak deskribatzerako garaian. Honi aurre egiteko, iritsiera-luzeko trukea duten funtzionalak erabiltzen dira.

8.2.4.2 Denborarekiko Menpekoea den Dentsitate Funtzionalaren Teoria

Nahiz eta DFT oso garrantzitsua bilakatu da azken urteetan oinarri egoerako GPEak kalkulatzeko teoria honen erabilera oraindik garatzen ari da egoera kitzikatuentzako [71]. DFT-ren azpiegituz baliatuz, kitzikapen elektronikoak Denborarekiko Menpekoea den Dentsitate Funtzionalaren Teoria ingelesez, TDDFT) erabiltzen da [72]–[74]. Denborarekiko dependentziaz hitz egiten denean zera esan nahi da: elektroi denborarekiko dependentzia nukleoaren posizioak finkatuta daudenean.

Runge-Gross Teorema. N-elektroi dituen edozein sistema denborarekiko menpekoea den potentzial bati atxikituta dagoenean, behagarri fisiko guztiak soilik determinatu

daitezke baldin eta dentsitatea eta sistemaren egoera ezagunak badira uneoro [75]. Runge-Gross-en teoremak zihurtatzen duena zera da, sistema molekular baten dentsitateak $\rho(\mathbf{r},t)$ kanpoko potentzial eskalar $\nu(\mathbf{r},t)$ bati erantzuten dionean beti jasango duela atzerapen bat.

Teorema honetan, denborarekiko menpekua den kanpoko potentziala denborarekiko menpekua den dentsitate bati elkartuta dago $\rho(\mathbf{r},t)$. Honek, denborarekiko menpekua den uhin-funtzio totala zehazten du eta bakarra da denborarekiko menpekua den fase faktorea arte $\alpha(t)$,

$$\Psi(t) = e^{-i\alpha(t)}\tilde{\Psi}[\rho](t) \quad (8.49)$$

Denborarekiko-Menpekoak diren Kohn-Sham Ekuazioak. Hohenberg-Kohn-en 2. teoremari erreparatuz ikusi da oinarri egoeraren minimizazio bariazionalak Kohn-Sham orbitaletan amaitzen duela. Bestalde, ez dago printzipio bariazionalik denborarekiko menpekua den energia totalarentzat DFT-ren menpe dagoena. Hala ere, existitzen da oinarritzko egoeraren analogoa den kantitate bat, mekanika kuantiko akzioa, A ,

$$A = \int_{t_0}^{t_1} \left\langle \Psi(t) \left| i \frac{\partial}{\partial t} - \hat{H}t \right| \Psi(t) \right\rangle dt \quad (8.50)$$

hau dentsitatearen terminoetan idatzi daiteke mapeazio bakarra dagoelako dentsitate eta uhin-funtzioaren artean, *e.g.* $A[\rho(\mathbf{r},t)$,

$$A[\rho(\mathbf{r},t)] = \int_{t_0}^{t_1} \left\langle \Psi[\rho](t) \left| i \frac{\partial}{\partial t} - \hat{H}t \right| \Psi[\rho](t) \right\rangle dt \quad (8.51)$$

Denborarekiko menpekua den egitura honetan, dentsitatea izan behar da akzioa geldikor egiten duena,

$$\frac{\partial A[\rho]}{\partial \rho(\mathbf{r},t)} = 0 \quad (8.52)$$

non $A[\rho]$ honela idazten den,

$$A[\rho] = B[\rho] - \int_{t_0}^{t_1} \int \nu(\mathbf{r},t)\rho(\mathbf{r},t)d\mathbf{r}dt \quad (8.53)$$

$B[\rho]$ kanpoko potentzialarekiko independentea da. Potentzial baten existentziaren, $\nu_{eff}(\mathbf{r},t)$, susmopean, Kohn-Sham-em ekuazioak deribatzen dira partikula sistema independente batentzat. $\psi(r,t)$ sistemaren orbitalek interakzionatzen duen sistema errearen karga dentsitatea $\rho(\mathbf{r},t)$ multzokatzen du,

$$\rho(\mathbf{r},t) = \sum_i f_i |\psi_i(\mathbf{r},t)|^2 \quad (8.54)$$

non f_i -k orbitalen okupazio zenbakiari erreferentzia egiten dion. $B[\rho]$ -ren espresiorako $\nu_{eff}(r,t)$ -ren existentzia kontsideratu behar da,

$$B[\rho] = \int_{t_0}^{t_1} \left\langle \Psi[\rho](t) \left| i \frac{\partial}{\partial t} - \hat{H}t \right| \Psi[\rho](t) \right\rangle dt - \frac{1}{2} \int_{t_0}^{t_1} \int \int \frac{\rho(\mathbf{r}_1, t) \rho(\mathbf{r}_2, t)}{|\mathbf{r}_1 - \mathbf{r}_2|} - A_{XC}[\rho] \quad (8.55)$$

$A_{XC}[\rho]$ -k truke-korrelazio funtzionalaren papera jokutzen du eta bere papera DFT-ren truke-korrelazio energiaren analogoa da. Hau horrela izanda, denborarekiko-menpekoa den Kohn-Sham-en ekuazioa honela idatzi daiteke,

$$\left[-\frac{1}{2} \nabla^2 + \nu_{eff}(\mathbf{r}, t) \right] \psi_i(\mathbf{r}, t) = i \frac{\partial}{\partial t} \psi_i(\mathbf{r}, t) \quad (8.56)$$

eta $\nu_{eff}(\mathbf{r}, t)$ -ren definizioa honakoa da,

$$\nu_{eff}(\mathbf{r}, t) = \nu(\mathbf{r}, t) + \int \frac{\rho(\mathbf{r}_1, t)}{|\mathbf{r}_1 - \mathbf{r}'|} d\mathbf{r}' + \nu_{XC}(\mathbf{r}, t) \quad (8.57)$$

Nahiz eta $A_{XC}[\rho]$ ezezaguna izan, bariazio leunak dituen potentzialaren limitean idatzi daiteke,

$$A_{XC} = \int_{t_0}^{t_1} E_{XC}[\rho(t)] dt \quad (8.58)$$

E_{XC} denborarekiko independentea den truke-korrelazio funtzionala izanda. Honi, hurbilketa adiabatikoa deitzen zaio. Denborarekiko lokaza izanik oinarrizkoa bilakatu da TDDFT-n. Hurbilketa adiabatikoa honela definitzen da,

$$\nu_{XC}(\mathbf{r}, t) = \frac{\partial A_{XC}[\rho]}{\partial \rho(\mathbf{r}, t)} \approx \frac{\partial E_{XC}[\rho]}{\partial \rho_t(\mathbf{r})} = \nu_{XC}(\mathbf{r}, t) = \nu_{XC}[\rho(r)_{\rho=\rho(t)}] \quad (8.59)$$

non ν_{XC} DFT-ren truke-korrelazio potentziala den t denbora zehatz batean dentsitate bidez ebaluatua

Erantun Linealaren Teoria. Potentziala ahula den kasuetan, estrategia egokia izan daiteke erantzun lineala erabiltzea TDDFT-n (ingelesez, LR-TDDFT) kitzikapen energiak lortzeko. Honekin, denborarekiko menpekoa den Kohn-Sham ekuazioa lehen ordeneko perturbazio bezala ebatzi daiteke.

Formulazioari erreparatuz, LR-TDDFT-n kitzikapen energia (ω) eta anplitudeak ez-Hermitikoa den balio-propioen ekuazio batetik lortzen dira. Hau ezaguna da baita ere, Casida-ren ekuazioa bezala, [73],

$$\begin{bmatrix} \mathbf{A} & \mathbf{B} \\ \mathbf{B}^* & \mathbf{A}^* \end{bmatrix} \begin{bmatrix} \mathbf{X} \\ \mathbf{Y} \end{bmatrix} = \omega \begin{bmatrix} \mathbf{1} & \mathbf{0} \\ \mathbf{0} & -\mathbf{1} \end{bmatrix} \begin{bmatrix} \mathbf{X} \\ \mathbf{Y} \end{bmatrix} \quad (8.60)$$

non matrizeko elementu bakoitza truke-korrelazio funtzionalaren menpekoa den eta honela definitzen dira,

$$\mathbf{A}_{ia,jb} = \delta_{ij}\delta_{ab}(\varepsilon_a - \varepsilon_i) + (ia|jb) - C_{HF}(ij|ab) + (1 - c_{HF})(ia|f_{xc}|jb) \quad (8.61)$$

$$\mathbf{B}_{ia,jb} = (ia|jb) - c_{HF}(ib|aj) + (1 - c_{HF})(ia|f_{xc}|jb) \quad (8.62)$$

ε orbitalen energia da eta a eta b orbital okupatu eta alegiazkoei egiten dieten erreferentzia, hurrenez hurren. \mathbf{A} matrizearentzako, lehenengo terminoa i eta j -ren arteko energia diferentzia da eta bigarrenak antisimetrikoak diren bi-elektroiren integralari egiten dio erreferentzia. Azken hau, \mathbf{B} -ren lehen terminoaren berdina da.

8.2.4.3 Mugatutako Dentsitate Funtzionalaren Teoria

Mugatutako Dentsitate Funtzionalaren Teoria (ingelesez, C-DFT) oso trena erabilgarria da ez bakarrik dentsitateak kalkulatzeko baizik eta Kohn-Sham-em uhin-funtzioak kalkulatzeko bi egoera diabatiko edo gehiagorako. C-DFT-k zuzenean erakiki ditzate karga eta dentsitate mugak eta neurketa zuzena eman energia berraltolatuz [76].

C-DFT-ren esanahia nahiko aldakorra da erabiltzen den funtzionalaren arabera. C-DFT-ri esker egoera diabatiko elektronikoak lor daitezke baita karga-transferentzia egoera kitzikatuak ere. Guzti hau Kohn-Sham-en ekuazioak erabiliz.

Metodo hau erabiltzerako garaian, kontutan izan behar da zer det mugatu nahi duguna, molekula baten karga edo dentsitatea.

8.2.5 Egoera Elektronikoen Deskonposaketa

Egoera elektronikoen diabatizazioak egoera adiabatikoen transformazioari egiten dio erreferentzia irudikapen berri batean, oinarri diabatikoa. Prozedura honetan, gainazal potentzialaren egoerak eta energia elkartzen dira Hamiltondar elektronikoaren leuntasunagatik eta momentu nuklearra baliogabea delako.

Arestian aipatu bezala, Born-Oppenheimerren hurbilketak sistema molekulararen elektroien eta nukleoaren arteko elkarrekintza banatzen du. Arazoa honako egoeran dator: PES bat baino gehiago energetikoki oso gertu daudenean. Kasu hauetan, egoera elektronikoen elkarrekintza sendoak sortzen dituzte momentu nuklearraren operadorearen eraginez. Egoera honi aurre egiteko, egoera diabatikoak definitu daitezke. Honetarako egoera adiabatikotik diabatikora doan transformazio matrizea eraikitzen da,

$$\phi_k = \sum_{n=1}^N \psi_n T_{nk} \quad (8.63)$$

egoera diabatiko hauek izaera leunako eta mantxoagoa aurkezten dute koordinatu nuklearren aldaketan. Lan honetan bi diabatizazio mota erabili dira: lehena Q-Chem programan ezarritakoa eta bestea Universita di Bolognan garatu dena Prof. Negri-ren taldean. Q-Chem-en ezarrita dauden metodoen artean, bi izan dira hemen erabilitakoak: (i) Edmiston-Ruedenberg (ER) lokalizazioa [84] (ii) Boys lokalizazioa [85], bi prozeduretan egoera diabatikoak adiabatikoen konbinazio lineal gisa eraikitzen dira.

8.2.5.1 Edmiston-Ruedenberg eta Boys Metodoak

Karga edo kitzikapen elektronikoa bat baino gehiago daudenean posible da egoera diabatikoak Edmiston-Ruedenberg eta Boys-en lokalizazio metodoak erabiltzea. Honetarako, egoera diabatikoak $\{|\Xi_I\rangle\}$ egoera adiabatikoen $\{|\Phi_I\rangle\}$ konbinazio lineal gisa eraikitzen dira $N_{state} \times N_{state}$ neurriko errotaizazio matrize orokor batekin,

$$|\Xi_I\rangle = \sum_{J=1}^{N_{states}} |\Phi_J\rangle U_{ji} \quad I = 1 \dots N_{states} \quad (8.64)$$

Orbilatan lokalizazioaren [84] analogian, Boysen diabatizazioak egoera diabatikoen kargen zentroen arteko maximizazio bat egiten du,

$$f_{Boys}(\mathbf{U}) = f_{Boys}(\{|\Xi_I\rangle\}) = \sum_{I,J=1}^{N_{states}} |\langle \Xi_I | \vec{\mu} | \Xi_I \rangle - \langle \Xi_J | \vec{\mu} | \Xi_J \rangle|^2 \quad (8.65)$$

non $\hat{\rho}^{\vec{R}}$ dentsitate operadorea adierazten duen. Bestalde, ER diabatizazioak auto-elkarrekintza energia maximizatzen du,

$$f_{ER}(\mathbf{U}) = f_{ER}(\{|\Xi_I\rangle\}) = \sum_{I=1}^{N_{states}} \int d\vec{R}_1 \int d\vec{R}_2 \frac{\langle \Xi_I | \hat{\rho}(\vec{R}_2) | \Xi_I \rangle \langle \Xi_I | \hat{\rho}(\vec{R}_1) | \Xi_I \rangle}{|\vec{R}_1 - \vec{R}_2|^2} \quad (8.66)$$

$\hat{\rho}^{\vec{R}}$ dentsitate operadorea \vec{R} posizioan izanik,

$$\hat{\rho}(\vec{R}) = \sum_j \delta(\vec{R} - \vec{r}^{(j)}) \quad (8.67)$$

eta $\vec{r}^{(j)}$ -k j . elektroiaren posizioa adierazten duelarik.

Fikziozko kanpoko potentzialari dagokionez hainbat suposizio egiten dira. Boys metodoan, espazioan lineala den eremua erabiltzen da eta ER-n, aldiz, fikziozko kanpo potentzialak linearki erantzuten dio karga dentsitateari.

8.2.5.2 *Hurbilketa Diabatiko Simplea*

Prozedura hau [86] egoera diabatikoak lortzeko helburutan garatu da. Lehenengo pausoa egoera adiabatikoak lortzea da Kimika Kuantikoaz baliatuz, eta ondoren, hainbat konbinazio lineal egin ostean egoera diabatikoak lortzen dira.

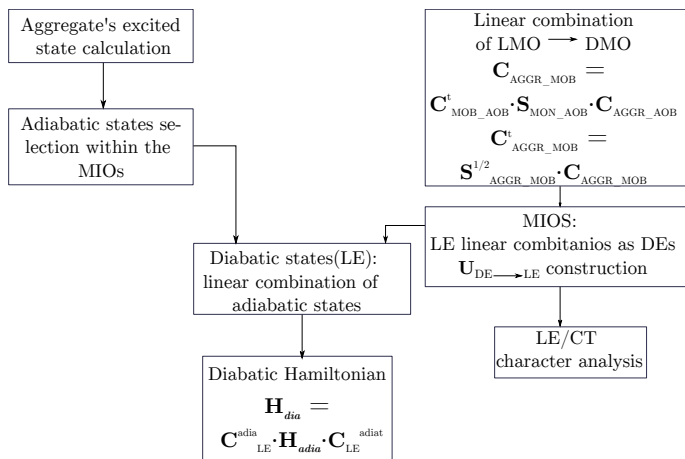


Figure 8.6: Simple schema for the characterization and diabatization

TDDFT-z hitz egitean, kitzikapenaren uhin-funtzioa eszitazio bakarrean oinarritzen dela esan nahi du. Kitzikapenaren izaeraren analisirako eta diabatizaziorako ondorengoak eduki behar dira kontutan,

- Orbitalen Espazio Minimoari (MIOS) tentuz erreparatu behar zaio
- Eszitazio kopurua. n molekula dituen agregatu batek, n^2 izango da aukeratu beharreko kopurua
- Egoera adiabatikoen aukeraketa

– uhin-funtzioak hainbat n^2 kitzikapenen menpekota izan behar du

n^2 -k ere Hamiltondarraren matrizearen neurria izan behar du. Agregatuaren LE oinarri diabatikoak FE (monomero bakoitzan lokalizatuta) eta CT egoerak barne izan behar ditu. Hemen, dimeroaren bi molekulak egon behar dute.

Egoeraren izaeraren analisirako garatu den protokoloan, lehenik eta behin Deslokalizatutako Orbital Molekularrak (ingelesez, DMO) Lokalizatutako Orbital Molekularren (ingelesez, LMO) konbinazio lineal gisa adiarazi behar dira. Horretarako, proiektzio operadorea aplikatu behar da, beste hainbat lanetan egin den bezala [87], [88].

$$\langle \psi_{MON_i} | \langle \psi_{MON_i} | \psi_{AGGR_j} \rangle = C_{i,j}^{AGGR_{MOB}} | \psi_{MON_i} \rangle, \quad (8.68)$$

non $|\psi_{MON_i}\rangle$ monomero isolatuen MO-ak diren orbital atomikoen oinarrian (ingelesez, AOB) eta $|\psi_{AGGR_j}\rangle$ agregatuena diren. Matrize formulaketara salto eginez, $\mathbf{C}_{MON_{AOB}}$ matrize zutabe bektoreak ψ_{MON_i} -rekin eratuta daude. Matrize hau diagonal izango da blokeak eratuz. Diagonal nagusiko blokeek monomero bakoitzaren MO-ren koefizienteak izango ditu AOB-n eta diagonaletik kanpokoko blokek, aldiz, zero izango dira. Zerbati oso antzekoa gertatzen da $|\psi_{AGGR_j}\rangle$ eta berari dagokion matrizearekin.

$\mathbf{C}_{i,j}^{AGGR_{MOB}}$ koefizienteak monomeroaren orbital oinarrian (ingelesez, MOB) DMO-ren konbinazio linealak definitzen ditu LMO-ren terminoetan. Emandako j agregatu orbital batentzat, koefiziente hauek dira $\mathbf{C}_{AGGR_{MOB}}$ matrizearen zutabeak sortzen dituztenak, eta jarraian adierazita dagoen modean lortzen dira,

$$\mathbf{C}_{AGGR_{MOB}} = \mathbf{C}_{MON_{AOB}}^t \cdot \mathbf{S}_{MON_{AOB}} \cdot \mathbf{C}_{AGGR_{AOB}}, \quad (8.69)$$

non $\mathbf{S}_{MON_{AOB}}$ monomeroen gainezartze matrizea den OAO-n eta \mathbf{t} -k iraulia adierazten duen.

Monomeroaren orbitalak ez direnez bi monomero berdinenak, MOB gainezartze matrizea ortogonalizatua izan behar da Löwin-en transformazio simetrikoa [89] erabilita. LOM-ren arteko gainezartze matrizea $\mathbf{S}_{AGGR_{MOB}}$ MO-ak eta agregatuaren gainezartze orbitalen artean kalkulatu da. Azken hauek agregatuaren konfigurazioan idazten direlarik $\mathbf{S}_{AGGR_{AOB}}$,

$$\mathbf{S}_{AGGR_{MOB}} = \mathbf{C}_{MON_{AOB}}^t \cdot \mathbf{S}_{AGGR_{AOB}} \cdot \mathbf{C}_{MOB_{AOB}} \quad (8.70)$$

Löwin-en transformazioa aplikatu ostean, $\mathbf{C}_{AGGR_{MOB}}^L$ matrizea lortzen da,

$$\mathbf{C}_{AGGR_{MOB}}^L = \mathbf{S}_{AGGR_{MOB}}^{-\frac{1}{2}} \cdot \mathbf{C}_{AGGR_{MOB}} \quad (8.71)$$

$\mathbf{C}_{AGGR_{MOB}}^L$ -ren dimentsioa MOBaren dimentsio osoari badagokio ere, okupatutako DMOak okupatutako LMO zehazten dituzte batez ere, non biak MIOSenak diren. Gauza bera gertatzen zaie okupatu gabeko MOei. Beraz, $\mathbf{C}_{AGGR_{MOB}}^L$ -tik ateratako eta OEMIkoak diren azpimultzoak bakarrik izango dira erabilgarriak hurrengo pausoetan.

DOMak MIOSenak diren LMOen konbinazio lineal gisa adierazi ondoren, eszizazio deslokalizatu generikoak (ingelesez, DE) ($i_{occ} \rightarrow j_{empty}$) LMOen arteko LMOen terminoetan zabaldu daitezke. Horrelako hedapenen koefizienteak honela ematen dira

$$U_{k \rightarrow l, i \rightarrow j}^{DE \rightarrow LE} = \text{MIOS}(occ)_{k,i}^{AGGR_{MOB,L}} \cdot \text{MIOS}(unocc)_{l,j}^{AGGR_{MOB,L}} \quad (8.72)$$

$\text{MIOS}(occ)_{k,i}^{AGGR_{MOB,L}}$ eta $\text{MIOS}(unocc)_{l,j}^{AGGR_{MOB,L}}$ agregatuaren orbital okupatuen eta ez okupatuen hedapen-koefiziente ortogonalizatuak dira, hurrenez hurren, MOBn. 8.72 ekuazioaren bidez lortutako elementuak $\mathbf{U}_{DE \rightarrow LE}$ matrize unitario

baterako, zeintzuen zutabeek eszitazio bakoitza deskribatzen duten LE kitzikapenen baitan.

DEak LEn konbinazio lineal gisa deskribatu ondoren, MIOSen barruan, egoera adiabatiko kitzikatuak kalkulatzeko eta hautatzeko unea da. n^2 MIOSetik sortutako estatu azpimultzoak kalkulaturako balio propioen multzotik hautatzen dira, Gram-Schidt ortogonalizatuak[90]. Balio propio hauek erabiltzen dira \mathbf{C}_{DE}^{adia} matrizearen zutabeak osatzeko eta kitzikapen energiak (n^2) matrize diagonalak \mathbf{H}_{adia} osatzen dute.

Egoera adiabatikoak LEn konbinazio lineal gisa adierazteko, komeni da jakitea egoera adiabatiko bakoitzaren CT/FE izaera honako biderketa matrizearen bidez lortzen dela,

$$\mathbf{C}_{LE}^{adia} = \mathbf{U}_{DE \rightarrow LE} \cdot \mathbf{C}_{DE}^{adia} \quad (8.73)$$

Azkenik, Hamiltondarraren irudikapen matrizea lortzeko LE oinarri adiabatikoan \mathbf{H}_{dia} , matrizearen transformazio hau erabiltzen da,

$$\mathbf{H}_{dia} = \mathbf{C}_{LE}^{adia} \cdot \mathbf{H}_{adia} \cdot \mathbf{C}_{LE}^{adia^t} \quad (8.74)$$

8.2.5.3 *Elektroi Bakarraren Trantsio Dentsitate Matrizean oinarritutako Deskonposaketa*

Egoera kitzigatuaren elektronikoaren teoria [91] lortu duen botereari esker, sistema molekular handien gaineko kalkuluak gauzatu daitezke. Horren arrazoia da konputazio ahalmena handitzeaz gain, egitura elektronikoko metodo berrien garapena eman dela [92]–[95]. Gaur egun sistema molekular handietan egoera eszitatuen kalkuluak egin daitezkeenez, kalkulu horien analisiak erronka handia suposatu lezake, sortutako datuen kantitatea dela eta. Horregatik, ahalegin handia egin da metodo berriak garatzen egitura elektronikoko kalkuluak aztertze eta erreproduzitzeko. Metodo horiek [96], [97] bistartzeko teknikak biltzen dituzten bitartean, deskribatzaile kuantitatiboak, kargaren transferentzia (CT) [98]–[100], kitzikapen bikoitzeko karakterea [101], [102], eta nahastea [103] neurtzeko erabili dira.

Zatiketan oinarritutako analisi-eskema bat erabiliz, TheODOREk tresna multzo bat eskaintzen du MOren irudiaz haratago joateko. Horrela, egoera kitzikatuen KTaren karakterizazioa ezaugarritu dezakegu emaile-hartzaile sistemetan [104] edo konplexu metaliko iragankorrei [105] eszitazio egoera baten izaera esleitu dakieke. Lan honetan erabilitako metodoa "Elektroi-zulo korrelazioa barne dituen fragmentuan oinarritutako egoera eszitatuen analisia" da, zeina 8.7 irudian-n irudikatzen den,

Analisi honen ideia nagusia sistemaren zatikatzea da, 8.7 irudian adierazten den bezala. Kasu honetan, sistema 3 zati ezberdinetan banatzen da: 1, 2 eta 3, eta horrela errepresentazioa haien gainean egiten da. Agertzen den lehen agertokia kitzikapen lokalizatu bat da, 8.7 a Irudia. Gainera, karga transferentzia bat lor dezakegu, elektroia zati batetik bestera pasatzen denean, 8.7 b Irudia. 8.7 c Irudian,

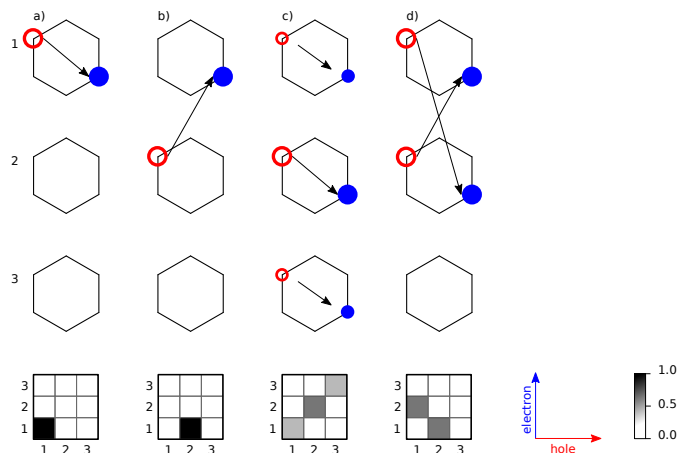


Figure 8.7: Egoera kitzikatuen motak a) tokiko kitzikapena 1.b) kargaren transferentzia 2tik 1era eta 1.c) Frenkel estatu deslokalizatuak eta d) karga-erresonantzia egoeran. Beheko laukietan, analisia irudikatzen da.

2. zatian kokatutako ekarpen nagusi bat da, eta haren atzetik LE motako bi eszitoi pisu gutxiagokoak; Frenkel-en Eszitoi gisa ezagutzen direnak. Azkenik, 8.7d Irudian karga erresonantzia egoera bat erakusten da, hau da, kontrako norabideetan doazen CT egoeren konbinazio lineala.

8.3 DIMERO AROMATIKO TXIKIEN ESZIMERO TRIPLETEAK

8.3.1 Sarrera

Jakina da sistema aromatikoen arteko elkarrekintzek nabarmen alda ditzaketela egoera kitzikatuaren propietateak [106]. Horren adibide nabarmen bat ezximeroen formazioa da. 1996an, eta 2021ean berrikusita, Kimika Puruaren eta Aplikatuaren Nazioarteko Batasunak (ingelesez *IUPAC*) honela definitu zuen eszimero [107] delakoa: elektronikoki kitzikatutako konplexu dimerikoa, oinarri egoeran dagoen monomero batez eta egoera kitzikatu dagoen monomero berdinez eratua. Eszizazioa kentzean, espezie hau segituan desagertzen da oinarritzko egoeran *tz* baita existitzen. Printzipioz, espezie eszimerikoak monomero kitzikatuaren (M^*) izaeraren araberakoa izango da. Hau da, spin singlete edo tripletekoa. Eszimeroaren formakuntza erreazio fotofisiko gisa adieraz daiteke (8.75 ekuazioa) non $^{1,3}M^*$ eta 1M errektiboak diren. Formazio honen garrantzia propietate fotoelektronikoekin lotuta dago π sistema [16] handiak dituzten espezieetan.



Nahiz eta aurreko ikerketak egoera singletean egin, badira beste batzuk non naftaleno dimeroa etorkizun handikoa jotzen duten estatu eszimeriLE/CT akoplamendua dela ekarpen nagusia egiten duena. Gainera, beste sistema batzuetan, hala nola PDI agregatuetan, ikusi da KTren eszitazioek paper garrantzitsua izan dezaketela[4]. Horri jarraituz, sistema aromatiko batzuk diseinatu dira benzenoa, naftalenoa eta antrazeno molekulak erreferentziatzat hartuta.

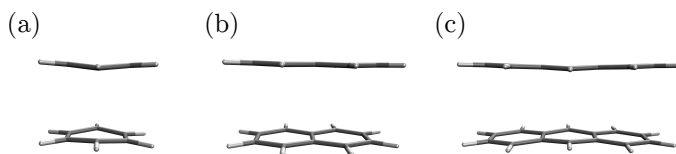


Figure 8.8: Atal honetan aztertutako hidrokarburo aromatikoaren dimero molekularrak: a) bentzenoa ; b) naftalenoa ; c) anthracenoa .

Atal honetan, molekula aromatiko txikien (bentzenoa, naftalenoa eta antrazenoa) energia gutxiko egoera tripleteen azterketari erreparatzen diogu (8.8 Irudia). Bereziki, eszimeri tripleteak sortzea interesatzen zaigu, non monomeroen arteko elkarrekintza handia espero den. Elkarrekintza horrek sistema egonkortzea espero da, eta, beraz, egoera tripletearen energia adiabatikoa baina txikiagoa izango da. Egoera tripletearen izaera ezaugarritzeko, bi gauzetan zentratuko gara nagusiki: (i) desparekatutako bi elektroien banaketa espazialean, eta (ii) tripleteak monomerikoarekiko duen egonkortze energetikoan. Lehenengoa, adibidez spin dentsitatearen irudikapenak determinatua, eszimeri tripletearen formazioaren beharrezko baldintza gisa erabil daiteke eszimerioan bi elektroien desparekatutako bi monomeroen gainean deslokalizatuta beharko lukeelako. Gainera, eszimerioetan bi molekulen arteko elkarrekintza orbital handia dagoenez, monomeroaren T_1 -arekiko egonkortze garrantzitsua espero genezake. Helburu honetarako, molekulen arteko akoplamendu elektronikoak ezaugarrituko ditugu, eszitazio lokalen (LE) eta karga transferentziaren (CT) egoerei dagokienez.

8.3.2 Metodologia

Bentzenoaren, naftalenoaren eta antrazenoaren egitura molekularrak hutsean optimizatu dira MP2 eta DFTren bidez, ω B97X-D [108] irismen luzeko funtzio zuzendua erabiliz cc-pVTZ oinarri-multzoarekin konbinatuta. Bi maila ezberdinetan lortutako geometria molekularrek ez dute desberdintasun esanguratsurik erakutsi.

Singlete eta triplete egoeren trantsizio bertikalen energia baxuenak, konfigurazioaren elkarrekintzaren bigarren mailako zuzenketarekin lortu dira, CIS(D) [109], bai eta TDDFT-rekin. Azken honetan TDA hurbilketa [110] ere erabili da.

Monomeroen kasuan bezala, optimizazio eta kitzikapen bertikaleko energiak DFT bidez egin dira ω B97X-D funtzionala erabiliz. Teoria maila honen arazoetako

bat denbora konputazionala izan da. Hori arintzeko, CC-Pvdz oinarria erabili da dimerren azterketa konputazionalerako, emaitzek aldaketa txikiak baino ez baitituzte cc-pVTZ oinarri handiagoa duten kalkuluekiko. Egitura elektronikoaren deskribapena egiteko Q-Chem programa [111] erabili da.

TDaren barruan konputatutako trantsizio elektronikoen diabatizazioa zehatz-mehatz egin da ER lokalizazio-eskema [84] erabiliz. Energia diabatiko eta akoplamentuak lortzeko Hamiltoniar diabatikoaren matrizearen diagonaleko eta diagonaletik kanpoko elementuak erabili dira, hurrenez hurren. Simetria-arrazoiak direla eta, bentzeno-konformeroaren spin triplete kitzikatuaren diabatizazioa 32 egoera adiabatiko kontuan hartuta egin da, okupatutako bi orbital molekular altuenetatik (HOMO eta HOMO-3) okupatu gabeko bi orbital molekular baxuenetara (LUMO eta LUMO+3) egindako trantsizio elektronikoei dagozkienak. Hala ere, naftalenoaren eta antrazenoaren kormormeroentzat, spin tripleteen diabatizazioa 16 egoera adiabatiko hartuta kalkulatu da. Kasu honetan, HOMO eta HOMO-1 eta LUMO eta LUMO+1ekin ere bat datoz. Egoera diabatikoen informazioa osatzeko, trantsizio-dentsitatearen matrize bakarra aztertu da [91], kitzikapen elektronikoak hobeto ezaugarritzeko elektroi zulo korrelazio-grafikoen bidez.

8.3.3 Monomeroak

Atal honetan hiru molekula aromatik (bentzenoa, naftalenoa eta antrazenoa) aztertu eta karakterizatuko dira, egitura elektronikoari dagokionez, oinarri egoera eta egoera kitzikatu baxuenerako. Egitura elektroniko honen analisiarekin egoera tripletearen ulermenean sakondu nahi da.

8.3.3.1 Egitura Elektronikoa

Lehen aipatutako sistemen egoera tripletearen portaera ondo ulertzeko, garrantzitsua da egitura elektronikoa ezaugarritzea. Analisi honetan sakondu aurretik, aipatu beharra dago bentzenoak bi minimo erakusten dituela geometriaren optimizazioan. Bi minimo hauetan egituraren distortsio bat ikusten da (elongazioa eta konpresioa). Bentzenoaren berezitasuna ez dator soilik erakusten duen simetria handiagatik (D_{6h}). Honetaz bain MOek degenerazio handia erakusten dute. Hau azaldu ahal izateko Jahn-Teller-en distortsioan [113] oinarritu behar gara. Oinarrizko egoeran, bentzenoak energian endekatutako HOMO-1 eta HOMO orbitalak ditu, 8.9 irudian adierazten den bezala. Egoera tripletean, aldiz, orbitalen berrantolaketa bat gertatzen da, α elektroi gehiago baitaude β -1 baino. Honekin MO degenerazioa hautsi eta sistemak D_{6h} simetria galtzen du. Distortsionatutako sistemek D_{2h} -ko simetria erakusten dute sistema elongatu eta konprimatuak. Naftaleno eta antrazeno molekulek, aldiz, ez dute erakusten MO degenerazio indartsu hori beren oinarrizko egoeran eta, beraz, ez dute inolako distorsiorik jasaten egoera tripletean.

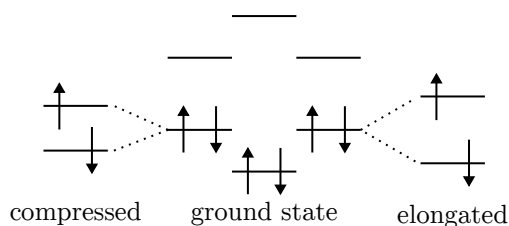
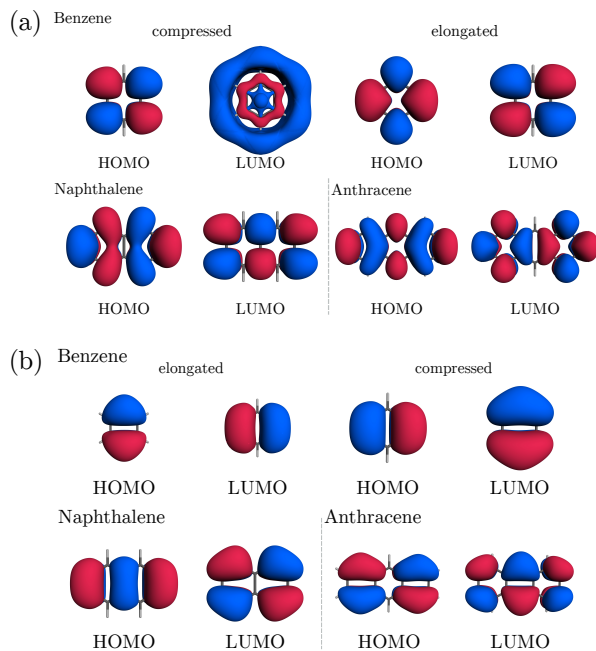


Figure 8.9: Bentzenoak jasaten duen Jahn-Teller distortsioa.

Hiru molekula aromatikoen mugako spin orbitalak (α eta β), egoera tripleterako, oro har, oinarrizko egoeraren antzekoak dira, gehienak deslokalizatutako π -orbitalei dagozkienak (8.10 Irudia).

Figure 8.10: (a) eta (b) sistema bakoitzaren OM α eta β , hurrenez hurren, dira.

Bi elektroien banaketa espaziala deskribatzeko, spin dentsitatearen irudikapenak erabiltzen ditugu (8.11 Irudia). Hiru sistemen biraketa-dentsitatea, molekula guztien gainean deslokalizatua dago. Jahn-Teller distortsioaren ondorioz bentzenoak biraketa-dentsitatearen bi banaketa ezberdin erakusten ditu. Egitura konprimatuak luzetarakoarekiko deslokalizazio handiagoa erakusten du. Naftalenoaren eta antrazenoaren irudikapenean ikus daiteke dentsitatea molekularren gainean deslokalizatuta egon arren, horien kanpoko aldean dentsitate handia dagoela.

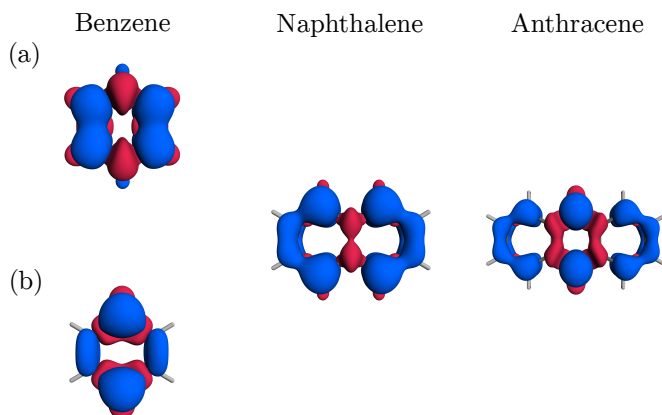


Figure 8.11: Aztertutako monomeroen spin dentsitatea. (a) eta (b) bentzenoaren egoera tripletearen konprimatutako eta elongatutako egiturei dagokie, hurrenez hurren.

8.3.3.2 Franck-Condon Eskualdeko Egoera Kitzikatu Baruenak

Hiru molekula aromatikoen egoera tripletearen analisia osatzeko, kitzikapen elektroniko baxuenak aztertzen ditugu, hau da, T_1 eta S_1 , oinarri egoerako geometrian (8.1 Taula).

Table 8.1: T_1 monomero bakoitzaten energia bertikalak (eV) cc-pVTZ base multzoan kalkulatu. ω B97X-D-ren kasuan orbitaletik orbitalerako konposizioak TDA trantsizioei dagokea. H=HOMO; L=LUMO

metodoa		entzenoa	naftalenoa	antrazenoa
CIS(D)		4.470	3.846	2.553
	Konposizioa	%43 H-L+1	%71 H-L	%78 H-L
ω B97X-D		4.313	3.226	2.309
	Konposizioa	%48 H-L+1	%89 H-L	%91 H-L

Oinarrizko egoeratik egoera triplete baxueneko trantsizio elektronikoak HOMO \rightarrow LUMO trantsizioa inplikatzen du batez ere. Triplete adiabatikoko energien kasuan bezala, kitzikapen bertikaleko energiak (T_1 eta S_1) murrizten dira tamaina molekularren tamainarekin, HOMO-LUMO energia desberdintasunean gertatzen den bezala.

8.3.4 Dimeroak

Helburua egoera eszimerikoa aurkitzea denez, lehenengo pausu garrantzitsua sistemaren egitura ongi ezagutzea da. Egoera berezi hauen ezaugarri nagusia molekula arteko elkarrekintza dago, hau espazio bidez egiten baita eta ez lotura bidez. Egitura posible asko daudenez eszimeriak topatzeko, hainbat egitura eskuz prestatu dira. Horretarako, beti jarraitu den irizpidea izan da koplanarrak diren egiturak eratzea. Hortzan, monomeroetako bat beti distortsionatu da bai ardatz luze eta laburrean, xy planoan eta horretaz gain, sistema eklipsatua ere irudikatu da. Jarraian, ikerketarentzako interesa izan duten egiturak bakarrik aurkeztuko dira, gainontzekoak Appendix F-n eongo dira.

Aurreko atalean ikusi bezala, iritsiera handian zuzendukako ω B97XD funtzionalak eta MP2 metodoak oso emaitza antzekoak ematen dituztela. Ondorioz, dimeroen analisi guztia DFT-ren baitan egin da cc-pVTZ base multzoa erabilita. Dena den, kostu konputazionala gutxitzeko asmoarekin kalkuluak base txikiago bat erabiliz, cc-pVDZ, ere egin dira. Bi oinarrien arteko desberdintasunak ez direnez oso esanguratsuak izan, egoera elektronikoko guztiaz oinarri multzo txikiarekin egin dira.

8.3.4.1 Egonkortasun erlatiboa

Lehenengo urratsa izan da optimizazio bakoitza aztertzea eta ikustea zer konformero mota lortu den. Horrela, ikusi da aztertutako egitura guztiek PESaren hiru minimo ezberdinetan amaitu zutela. Honi esker, hiru taldetan sailka daitezke kriterio bezala molekula arteko distantzia hartuz. 3.4 Taula sistema bakoitzerako lortutako konformero bakoitzari buruzko informazio garrantzitsuena erakusten du. Elkarrekintza eta lotura-energiarako BSSE zuzenketa erabili da, hurrengo nomenklatura orokorra erabiliz,

$$E_{geometry}^{basis}(geometry) \quad (8.76)$$

eta horrela, elkarrekintza eta lotura energiak jarrian dauden ekuazioekin kalkulatu dira,

$$E_{int}^{CP} = E_{AB}^{AB}(AB) - E_{AB}^{AB}(A) - E_{AB}^{AB}(B) \quad (8.77)$$

$$E_b^{CP} = E^{CP}(AB) - E_A^A(A) - E_B^B(B) \quad (8.78)$$

$$E^{CP}(AB) = E_{AB}^{AB}(AB) + \delta_{AB}^{BSSE} \quad (8.79)$$

$$\delta_{AB}^{BSSE} = E_{AB}^A(A) + E_{AB}^B(B) - E_{AB}^{AB}(A) - E_{AB}^{AB}(B) \quad (8.80)$$

non $E_{AB}^{AB}(AB)$ sistemaren energiarekin bat datorren, dimeroaren oinarrian eta geometrian. $E_{AB}^{AB}(A)$ edo $E_{AB}^{AB}(B)$ sistemako monomero bakoitzaren energiari dagokie. eta $E_A^A(A)$ edo $E_B^B(B)$ monomero bakoitzaren energiari dagokie. Egoera tripletearantz, energietako bat monomero singleteari dagokio eta bestea tripleteari.

Table 8.2: Molekula arteko distantzia [d_{inter} (Å)], energia erlatiboak [E_{rel} (kcal/mol)], elkarrekintza energia [E_{int} (kcal/mol)] and lotura energies [E_{bind} (kcal/mol)] for the most representative obtained minima for each of the systems. All computed at ω B97XD/cc-pVTZ level of theory.

Distortsioa	d_{inter}	E_{rel}	E_{int}	E_{bind}
Bentzeno				
eklipsatua	2.733	26.770	-6.722	3.976
luzea	3.536	18.610	-3.920	-4.311
motza	1.588	0.000	-64.834	-22.832
Naftaleno				
eklipsatua	3.134	16.928	-6.920	-0.032
luzea	3.558	9.162	-6.931	-6.855
motza	1.605	0.000	-63.743	-15.782
Antrazeno				
eklipsatua	3.102	19.708	-10.594	-4.448
luzea	3.587	12.707	-10.502	-10.378
motza	1.606	0.000	-74.633	-22.866

Kontuan izanik konformero guztiak egitura koplaneatuak bezala eraiki direla, sistema bakoitzaren energia erlatiboaz hitz egitean, konturatzen gara ardatz motzean distrotsionetutatko egiturak beste bi distortsioak baino energia baxuagoan amaitu dutela optimizatioa. Esaldi hau molekulen arteko distantziari dagokionez ere indartu daiteke. Kasu partikular honetarako, distantzia hain da laburra lotura eraketa gerta daitekeela pentsarazten duen.

Balio horiek egoera singletearenekin alderatuz gero, esan daiteke ez duela axola zein distortsio aukeratzten den, molekulen arteko distantzia ia berdina delako, guztiak 3,4Åtik gorakoak. Gainera, konformero bakoitzaren arteko alde energetikoa ez da tripletean bezain esanguratzua. Bestalde, elkarrekintza eta lotura energietan desberdintasun gehiago aurki litezke. Kasu honetan, monomero bakoitzaren egitura ez da erabat aldatzen eta, beraz, energiak oso antzekoak dira. Informazio hau guztia Appendix F-n aurki daiteke F.1 taulan.

8.3.4.2 *Karbono-Karbono Distantzia Laburra duten Egiturak*

Lehenengo egitura multzoak, karbono-karbono arteko distantziarik laburrenari dagokio. Hiru sistemek komunean duten ezaugarrietako bat da hasierako egitura ardatz laburrenean distrotsionatu dela. PES-aren konbergentziak dimero kobalenteetara eraman gaitu, σ motako loturak eratuz. Emaitza hauekin erlazionatuta, aipatu

azeno hauen dimerizazioa bai termikoki edota argi absortzio bitartez [114] gerta daitekeela.

8.12 Irudiak egoera tripletearen optimizazioaren ostean lortutako benzeno, naftaleno eta antrazenoaren egiturak erakusten ditu bai eta sortu berri den σ loturaren distantzia. Molekula arteko distantzia laburra dela eta, eraztunetako lotura dis-

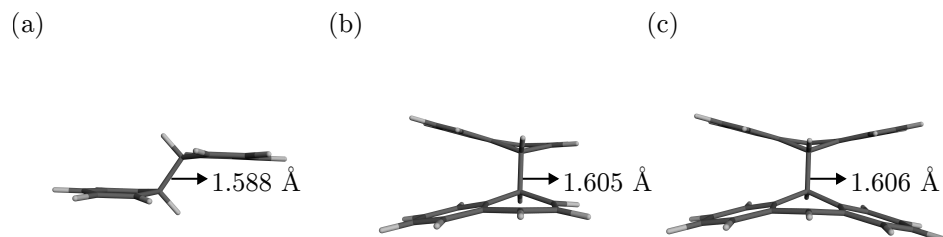


Figure 8.12: Benzeno, naftaleno eta antrazenoarentzako lortu diren egitura kobalenteak ω B97X-D/cc-pVTZ teoria mailan.

tantziak ere aldatu dira. Karbonoa sp^2 hibridizaziotik sp^3 -ra aldatu da, eta lotura distantzietan dagokienez, aldaketa 1.394 Åtik 1.50 Åra.

Aztertzeko interesgarria izan daitekeen beste faktore bat MO eta spin dentsitateak dira. 8.13 irudiak erakusten duen bezela, gauzarik esanguratsuen σ loturaren eraketan dago. Horretaz gain, spin dentsitatearen errepresentazioa oso esanguratsua da egoera tripletearen kokapenaz informazioa ematen baitigu. Nahiz eta dimer horiek interes handikoak izan, adibidez, polimerizazio erradikal induzituaren erreakzioetan [114], [115], ez dira ikerketa honen ardatza, eta ondorioz ez dira gehiago ikertuko.

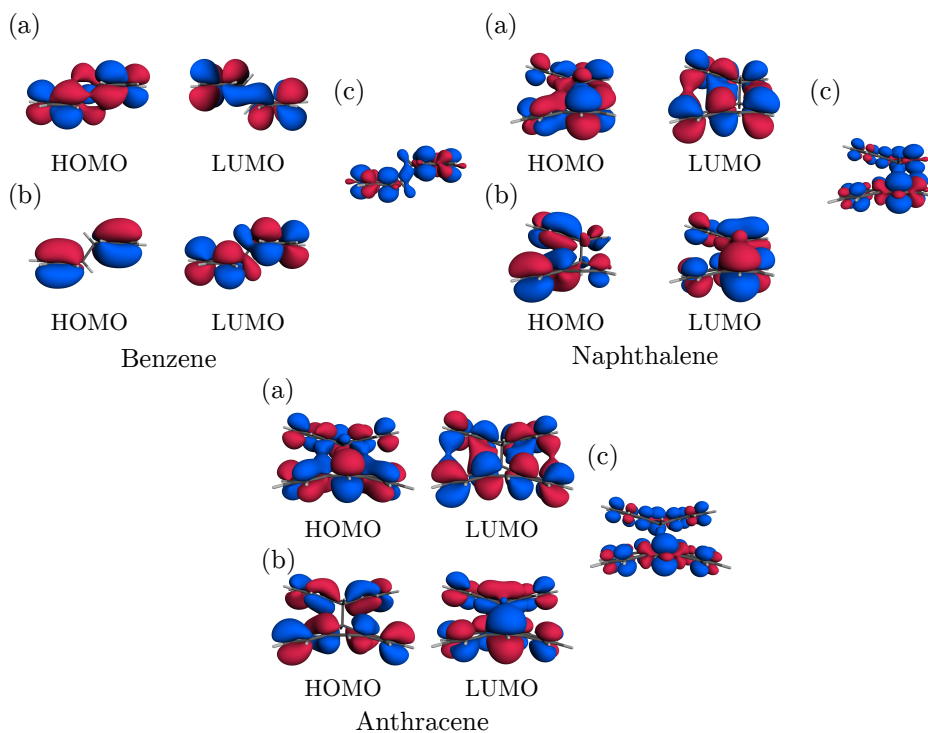


Figure 8.13: OM eta spin dentsitateak benzeno, naftaleno eta antrazenoaren dimero kobalenteentzako, non (a) α orbitalak, (b) β orbitalak eta (c) spin dentsitatea diren ω B97X-D/cc-pVTZ maila teorikoan kalkulaturak

8.3.4.3 π - π Egiturak erakusten duen Karbono-Karbono Distantzia

Lotura eratu duten dimeroez gain, badira lotura kobalenterik erakusten ez duten tokiko beste minimo batzuk (8.14 Irudia). Egitura hauek ardatz luzean egindako distortsioaren bidez lortu dira. Aurreko kasuarekin alderatuz, monomeroak lauak dira, hau da, ez dago sp^3 karbono atomorik. Molekula arteko distantziari dagokionez, ohiko π - π distantziari dagokiola ikus daiteke. Dimero hauetan, egitura molekular indibidualak monomeroen S_0 eta T_1 minimoetatik oso hurbil daude, hurrenez hurren. Horregatik, tripletea lokalizatua duten dimero gisa identifikatzen ditugu. Dimero mota honen simetria orokorra C_1 da (simetria-elementurik gabe), bi monomeroak ez baitira baliokideak.



Figure 8.14: Lokalizatutako tripletea erakusten duten benzeno, naftaleno eta antrazeno dimeroan ω B97X-D/cc-pVTZ maila teoriarik kalkulatuak.

Egin dugun egitura-analisiaren arabera, bi monomeroen arteko baliokidetasunik eza egoera tripletearen lokalizazioarekin erlaziona daiteke. Zehazki, α HOMO eta β LUMO dira lokalizatuen daudenak eta hau ia bat dator T_1 monomeroaren geometriarekin. Ondorioz, egoera triplete honen spin dentsitate oso lokalizatua dago (8.15 Irudia). Egoera eszimerikoak edukitzeko spin dentsitateak molekula osoan egon behar duenez sakabanatuta, sistema multzo hau ez da baliagarria ikerketa sakonagoetarako.

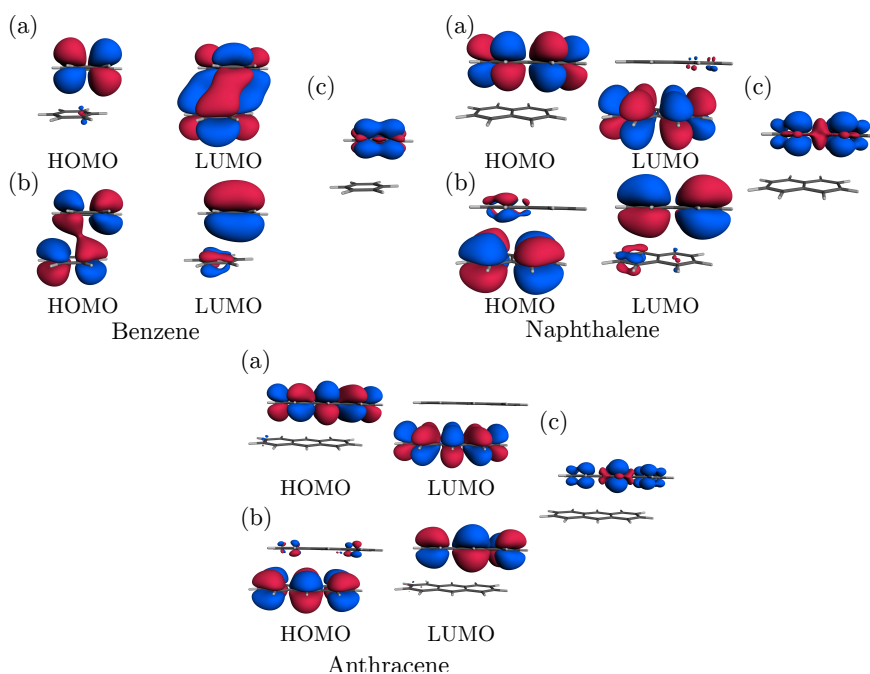


Figure 8.15: OM eta spin dentsitateak benzeno, naftaleno eta antrazenoaren dimero lokalizatuentzako, non (a) α orbitalak, (b) β orbitalak eta (c) spin dentsitatea diren ω B97X-D/cc-pVTZ maila teorikoan kalkulaturak.

8.3.4.4 Tarteko Karbono-Karbono Distantzia duten Egiturak

PES-ean minimoa erakusten duten azken egiturek monomero arteko bitarteko karbono-karbono distantziak dituzten monomeroei dagokie. 8.16 Irudiak eklipsatutako egiturei dagokie, dena den, beste ardatzetan distortsionatutako konformeroekin egitura gehiago lortu dira ere. Egitura horiek guztiak AppendixF -n agertzen dira. Alde batetik, 8.16 Irudiak erakusten duen bezala, monomeroen arteko banaketa nabarmen laburragoa da π - π distantzia tipikoa baino (8.14 Irudia), baina ez dira dimero kobalenteetan bezain laburrak (8.12 Irudia). Distantzia hauek 2.733 Å, 3.134 Å, eta 3.102Å dira, bentzeno, naftaleno eta antrazenoari dagozkienak, hurrenez hurren. Gainera, aipagarria da egitura horietako batzuek monomero ez-planarrak dituztela, bentzenoa. Sistema honek elkarrekintza handiagoa du bi monomeroen artean naftalenoak eta antrazenoak baino. Horregatik, molekulen arteko distantzia txikiagoa da.

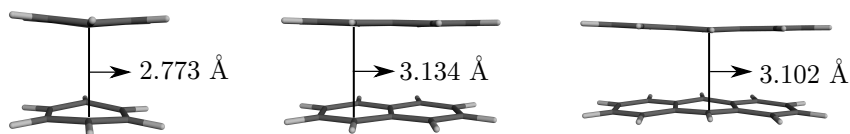


Figure 8.16: Deslokalizatutako tripletea erakusten duten benzeno, naftaleno eta antrazeno dimeroan ω B97X-D/cc-pVTZ maila teoriarik kalkulatuak.

Bitxia bada ere, dimero hauetako bi molekularik baliokideak dira eta, beste triplete dimero moten aldean, simetria handia dute. Ondorioz, triplete deslokalizatutako dimero bezela izendatu ahal ditzakegu. Egitura guztiek konformazio ekipsatua erakusten dute, eta monomeroak planorik gabeak diren arren, guztiek dute D_{2h} simetria globala. Lokalki, bentzeno-monomeroek C_{6v} simetria erakusten dute, eta naftaleno- eta antrazeno-monomeroak, berriz, C_{2v} .

Egoera tripleteko hautagai oparoenak bitarteko C-C distantziak dituzten dimeroak dira. 8.17 Irudiak bentzenoaren, naftalenoaren eta antrazenoaren konformero ekipsatuaren α eta β MOak eta spin dentsitate erabat deslokalizatuak erakusten ditu. Gainera, joera bat ikusten da sistema aromatikoak handitzen den bitartean. Bentzenoak dentsitate handia erakusten du monomero bakoitzaren erdialdean; naftalenoak, berriz, dentsitate handiagoa du monomeroen alde bakoitzean. Antrazenoak, ordea, dentsitate handia erakusten du erdiko eraztunean.

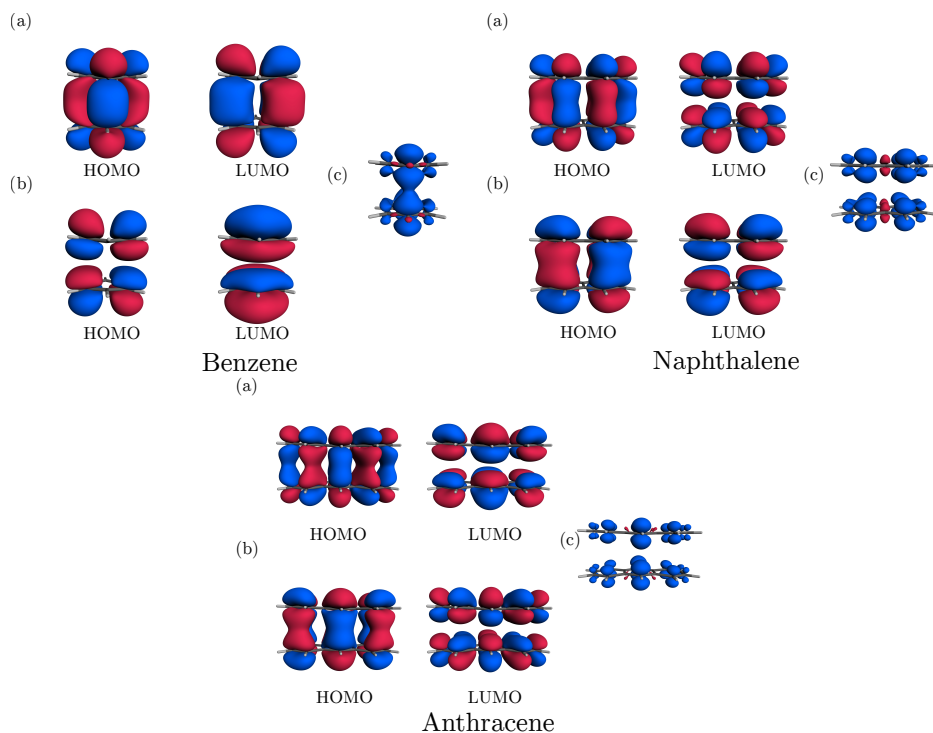


Figure 8.17: OM eta spin dentsitateak benzeno, naftaleno eta antrazenoaren dimero deslokalizatuentzako, non (a) α orbitalak, (b) β orbitalak eta (c) spin dentsitateak diren ω B97X-D/cc-pVTZ maila teorikoan kalkulatuak.

8.3.4.5 Deslokalizatutako Tripleteen Izaera

Estatu elektronikoen esanahi fisikoa aztertu aurretik, garrantzitsua da ikustea CT izaera garrantzizkoa den ala ez. 8.3 Taulak erakusten du LE estatu nagusi dela T_1 egoera adiabatikoa, sistema guztietan % 70etik gorakoa baita beti. Hala ere, CT egoeraren ehunekoa ez da ia 0 eta, beraz, interesgarria izan daiteke analitik aratago joatea eta C_t -ren egoerak garrantzitsua izaten jarraitzen duen ala ez ikustea.

Table 8.3: T_1 egoera adiabatikoa izatera EL eta KT terminoetan adierazita ω B97XD/cc-pVDZ teoria mailan adierazita.

	ω_{LE}	ω_{CT}
benzeno	73	27
naftaleno	87	13
antrazeno	88	12

Behin ikusita T_1 egoera adiabatikoak baduela garrantzitsua izan daiteken CT izatera, egoera hau deskonposatu daiteke eta ikusi ea ondo definitutako LE eta CT egoera diabatikoak lortzen diren, beti ere ER metodoa erabilita, ikus 8.2.5.1. Egoera diabatikoen nondik norakoak ongi ulertu ahal izateko, Hamiltondar diabatikoa eraikitzen da,

$$\begin{pmatrix} E_{LE} & V_{DC} & V_e & V_h \\ V_{DC} & E_{LE} & V_h & V_e \\ V_e & V_h & E_{CT} & V_{CT} \\ V_h & V_e & V_{CT} & E_{CT} \end{pmatrix} \quad (8.81)$$

non E_{LE} eta E_{CT} LE eta CT egoeren energiak diren, hurrenez hurren. V_{DC} eta V_{CT} dira bi LE edo bi CT egoeren arteko akoplamenduak, hurrenez hurren. V_e eta V_h dira elektroien eta zuloen akoplamenduak,

$$V_e = \langle \text{LE}_A | \hat{H} | \text{CT}_{AB} \rangle = \langle \text{LE}_B | \hat{H} | \text{CT}_{BA} \rangle \quad (8.82)$$

$$V_h = \langle \text{LE}_A | \hat{H} | \text{CT}_{BA} \rangle = \langle \text{LE}_B | \hat{H} | \text{CT}_{AB} \rangle \quad (8.83)$$

Analisi horretarako, egoera adiabatiko batzuk hautatu behar dira. Hautaketa hau sistema bakoitzaren MO-ei eta hauek egoera eszitatuei egiten dieten ekarpenaren arabera egiten da. Bentzenoaren, naftalenoaren eta antrazenoaren kasuan, HOMO-1etik LUMO+1era bitarteko MOak hartu dira kontuan. Horren arrazoia da monome-roaren konbinazio linealak direla. Bentzenoaren kasuan, bere degenerazioa dela eta, 32 egoera adiabatiko hautatu dira eta, beraz, hamiltoniar diabatikoa 32x32 matrizea da. Bestalde, naftalenorako eta antrazenerako 16 egoera adiabatiko baino ez dira hautatu, eta 16x16 matrizea dute azkenean.

Sistema bakoitzerako spin-triplet egoera anitzen diabatizazioaren ondorioz, LE eta CT egoera endekatuak sortzen dira, hurrenez hurren. Diabatizazioa egiteko 4 estatu baino gehiago hautatu badira ere, diabatikoen hautaketa honela egin da: (i) energian baxuenak diren LE eta CT egoeren hautaketa, (ii) estatu horietatik, estatu adiabatikoan ekarpen handiena dutenak hautatu. Diabatizazioaren emaitzak 8.4 taulan agertzen dira.

Table 8.4: Energia diabatiko elektronikoa (in eV) eta akoplamenduak (in meV) ER diabatizazio eskema erabilita sistema bakoitzaren konformero eklipsatuentzat (TDA) ω B97X-D/cc-pVDZ teoria mailan kalkulatu.

	$E(^3\text{LE})$	$E(^3\text{CT})$	$\Delta E_{(LE-T_1)}$	$\Delta E_{(CT-LE)}$	V_e	V_h
Benzene	4.120	6.082	1.546	1.982	771	827
Naphthalene	3.621	4.772	1.539	1.158	544	541
Anthracene	2.680	3.641	1.385	0.961	320	335

Bentzenoak honako egoera diabatikoak erakusten ditu: 4.120 eV (LE) eta 6.082 eV (CT). Energia honek energia handia ematen badu ere, LE estatuaren eta T_1 en arteko aldea 1.546 eV-koa da. Gainera, bi diabatikoen arteko energia-aldea 1.982 eV-koa da. Informaziorik interesgarriena elektroien eta zuloen elkarrekintzatik dator. Elektroiarri dagokion akoplamendua 771 meV-koa da eta zuloari dagokiona 827 meV-koa. Balio horiek meV-tan dauden arren, balio handi bezala kontsideratzen dira eta ondorioz etan daiteke LE eta CT egoeren arteko elkarrekintza garrantzitsua dela. Naftalenoan ikus dezakegu LE 6.217 eV-koa dela eta CT 4.772 eV-koa. EL egoera 1.539 eV gorago dago T_1 baino eta diabatikoen arteko aldea 1.158 eV-koa da. Akoplamenduei dagokienez, horiek nabarmen jaitsi dira bentzenoarekiko, 544 meV (V_e) eta 541 meV (V_h), baina, hala ere, balioek bere pisua izaten jarraitzen dute. Beraz, LE eta CT estatuaren arteko elkarrekintzak garrantzitsua izaten jarraitzen du. Azkenik, antrazenoan 2.680 eV-koa da LE egoerara eta 3.641 eV-koa CT. Kasu honetan, T_1 eta LE egoerak energian gertuago daude (1.385 eV aparte). Gauza bera gertatzen da LE eta CT egoera diabatikoen artean (0.961 eV). Nahiz eta akoplamenduak gehiago txikitu kasu honetan, 300 meV inguru, balio honek handia izaten jarraitzen du beraz bi egoera diabatikoen arteko elkarrekintzak garrantzitsua izaten jarraitzen du.

Analisi osoa egin ondoren, esan daiteke bentzeno, naftaleno eta antrazeno konforero eklipsatuek egoera eximerikoa osa dezaketela zenbait arrazoiengatik. Lehenengoak spin dentsitatearekin du zerikusia. Analisi honek molekularen egoera tripletearen kokapenari buruzko informazioa ematen du. Egoera eszimerikoak sistema osoari dagokion bezala, haren deslokalizazioak zera pentsarazten benetan egoera eszimerikoa analizatzen ari garela. Gainera, estatu elektronikoen deskonposizioaren ondoren, ikusi da nahiz eta estatu adiabatikoari egiten zaion ekarpen nagusia EL egoera diabatikoa izan, CT-ren ekarpena ezin daitekela gutxietsi. Hau bi egoera diabatikoen arteko akoplamenduen (V_e eta V_h) balioekin ere baieztatu daiteke. Nahiz eta balio horiek murriztu sistema handitzen den bitartean, altuak izaten jarraitzen dute. Hori da aztertutako sistemak egoera eximeriko bati dagozkiola erakusten duen beste froga bat.

8.3.5 Ondorioak

Ondorio gisa, aipatu, sistema aromatiko txikien egoera excimerikoa aztertu da, LE eta CT egoera diabatikoen eta horien akoplamenduen arabera. Lortutako emaitzek iradokitzen dute LE eta CT-ren arteko elkarrekintzaren ondorioz egoera eximeriko bat egon daitekeela.

Horretarako, spin-dentsitatean jarri da arreta guztia, triplete egoeraren kokapenari buruzko informazioa ematen baitu. Sistemen aukeraketa ziurtatzeko, analisi labur bat egin da monomeroetan. Erronka handienetako bat bentzenorako egitura egokia aukeratzea izan da, bi distortsio ezberdin erakusten dituelako egoera tripletean. Horretarako, honako estrategia honi jarraitu zaio: egituretako zeinek duen spin-dentsitate handiena egiaztatzea. Monomero guztiak aztertu ondoren, ikusi da

hiru molekulek spin-dentsitate deslokalizatuak dituztela, eta, beraz, badirudi aukera onak izan daitezkeela analisi gehiago egiteko.

Konformero desberdinak optimizatu ondoren, hiru egitura mota lortu dira. Lehenengoak lotura kobalentekeo egitura bati egoten dio erreferentzia, lotura eraketaren ondorioz egonkorrenak direnak. Talde honetan karbono-karbono distantzia ez da 1.61 Å baino handiagoa hiru sistemetan. Haien OMaK eta spin-dentsitatea molekularen gainean deslokalizatzen dira. Nahiz eta adostasun horrek ez duen balio analisi gehiago egiteko, zeren egoera eximerikoan monomeroen arteko elkarrekintza espazioaren bidez gertatzen da. Bigarren egitura multzoa ohiko π - π karbono distantziari dagokio, hau da, 3.50-3.60 Å. Konformero horien ezaugarrietako bat OMren lokalizazioa da, baita eta spin-dentsitatearen lokalizazioa. Nahiz eta sistema horiek dispertsio-elkarrekintza erakutsi eta lotura formaziorik ez egon, spin-dentsitatea monomero batean bakarrik dago. Horrek esan nahi du egoera tripleteak monomero horri bakarrik dagokiola eta, beraz, sistema S_0 eta T_1 egituren konbinazio gisa ikus daiteke. Horregatik, egitura multzo hau ez da erabili analisi gehiago egiteko. Azkenik, karbono-karbono bitarteko distantzia duten egiturak aurkitu ditugu. Sistema hauek karbono-karbono distantzia ez da hain laburra, baina ezta luzeegia ere, 2.77 eta 3.11 Å artean mugitzen baita. Gainera, MO eta spin-dentsitateak molekularen gainean deslokalizatzen dira. Horrek esan nahi du tripletea sistema osoari dagokiola, eta, beraz, sistema hauek hutagai egokiak izan daitezke egoera eszimerikoen bilaketari ekiteko.

Bitarteko distantziako egitura horietan egoera eximerikoa eratzen ote den ikusteko, egoera elektroniko kitzikatuen izaera aztertu da. Horretarako, lehen urratsa izan da ikustea ea CT-ren kontribuzioa nahikoa den T_1 egoera adiabatikoan. Zenbakitan, balio hori % 10 baino handiagoa da hiru sistematan, beraz kontribuzio hori nahikoa handia dela kontsideratu daiteke. Horren ondoren, egoera adiabatiko horiek egoera diabatikoetan deskonposatu dira, nolabait ere esanahi fisiko bat lortzeko. Honi esker ikusten da egoera adiabatikoak erakusten duen nahasketa, ondo definitutako egoeratan bereiz daitezke. Hau da, LE eta CT egoerek ez dutela inongo nahasketarik erakusten. LE eta CT-ren energiak kuantifikatzeaz gain, gai izan gara euren arteko elkarrekintzak identifikatzeko. CT-k egoera adiabatikoan duen %-arekin bat etorritik, ikusi da elkarrekintzaren balioa nahiko handia dela. Ondorioz, esan daiteke, hiru sistemen konformero eklipsatuetan egoera eszimerikoak ditugula.

8.4 PDI: MOLEKULA, AGREGATU ETA MODELOAK

8.4.1 Sarrera

Perylene-3,4: 9,10-bis (dikarboximida) edo PDI bezala ezagutzen diren koloratzaile industrialak [116] bezala asko ikertu dira. Gainera, oso erakargarriak izan dira gailu optoelektronikoekin zerikusia duten aplikazioetan duten ahalmenagatik, hala nola,

zelula fotovoltaikoak [8], [117]–[123], argia igortzen duten diodoak [124]–[126], aplikazioak transistoreetan [127], [128] edo kable molekularretan [129], [130]. Aplikazio biokimiko gisa ere erabili izan dira [131], [132] edo singlete fisioaren material gisa [133]–[135]. Gainera, PDIak eraikuntza-bloke gisa erabili dira sistema fotosintetiko artifizialak eraikitzeko. PDI hau eta bere deribatuak (8.18 Irudia) koloratzaileen familia aldakor eta erakargarrietako bat dira, neurri handi batean aplikazio fotofisikoetan erabili direnak [127], [130], [136]–[138]. Zehazki, PDIak optoelektronika organiko-rako hautagai molekular bikainak dira beren propietate ia idealengatik, hala nola xurgatzeko gaitasun handia, π -metaketan elkarrekintza indartsuak, fluoreszentzia handiko errendimendu kuantikoa eta egonkortasun termiko eta fotokimiko bikaina duten egitura zurrunagatik.

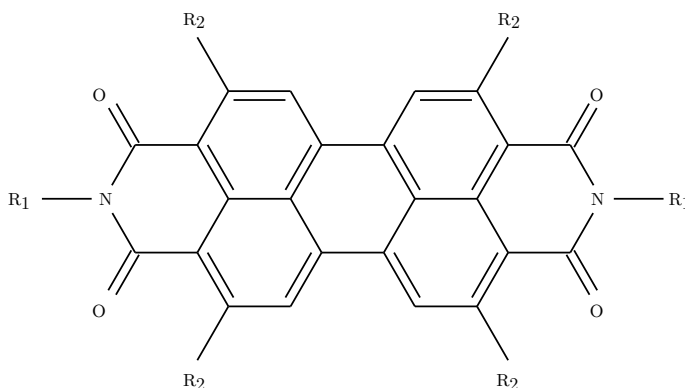


Figure 8.18: Atal honetan aztertutako PDI deribatuak. **1:** bis(*n*-octyl)-2,5,8,11-tetraphenyl-PDI (R_1 : octyl; R_2 : phenyl); **2:** 2,5,8,11-tetraphenyl-PDI (R_1 : H; R_2 : phenyl); **3:** PDI (R_1 : H; R_2 : H).

PDIren egoera singlete baxuenek ikerketa sakona duten bitartean, [143], [149]–[153] egoera tripleteentzako informazioa askoz ere txikiagoa da. Nahiz eta hasiera batean foto-kitzikapenaren bidez egoera tripletea eskuragarria ez izan, azken ikerketek tripleteak identifikatu dituzte dekadentzia prozesuetan produktu PDI dimero [154] eta kristaletan [133]. Konposatu organikoetan, tripleteen espektroak, normalean, optikoki gardenak dira edo, gehienez ere, ahulki aktiboak, eta hainbat abantaila dituzte kitzikatutako singleekin alderatuta. Luzaroago hedatzen dira, eta probabilitate handiagoa dute interfazeetara eta zulo elektronikoen disoziazio-guneetara iristeko. Horrela, errazagoa da horiek manipulatzeko eta egokiak izatea aplikazio optoelektronikoetan [155]–[160].

Atal honetan PDIren egitura elektronikoaren propietateen karakterizazio zehatza egiten du, interes bereziarekin bis (*n*-octyl)-2,5,8,11-tetraphenyl-PDI deribatuan (irudia 8.18). Bestalde, kristalean eta molekula-agregatuetan agertzen den singlete eta tripletearen egitura elektronikoaren zirrikituak argitu nahi ditugu, kimika kuantikoaren hainbat kalkuluren bidez. LE, CT eta akoplamendu elektroniko intermoleku-

larrei dagokienez, egoera eszitzatu baxuenak ezaugarritzea du helburu. Nahiz eta PDI agregatuen eszitzazio singleteen izaera LE eta CT ekarpenak hainbat autorek ikertu, [149], [150], [152] CT egoerek tripletean duten papera ezezaguna da oraindik ere.

Horretaz gain, PDI trimeroaren distortsioa gauza interesgarria izan daieke analisirako. Zehatzago esateko, garrantzitsua izan daiteke egoera tripleteen izaera ulertzea. Horregatik, agregatuak simetrikoki ordenatutako kromoforo baliokidez eratuta daudenean, 8.19 Irudia, LE, Frenker eszitoiak (FE), egoeren simetria egokituko (ingelesez, SA) gainjarpena sortzen da. Honek, LE egoerak nahastuarazten dituen elkarrekintza molekularrak dituelarik. Antzeko zerbait gertatzen da estatu ionikoetan, hau da, karga erresonantzia deslokalizatuetan (ingelesez, CR) [175]–[177]. Kasu honetan, PDI agregatuak $C2h$ talde simetriaren izaera hartzen du bai eta luzetarako desplazamenduan zehar egiten diren molekulen arteko desplazamenduak kontuan hartzen direlarik. Ondorioz, $\pi-\pi^*$ egoera kitzikatu garrantzitsuenak A_g eta B_u errepresentazioare dagokie. Soilik *ungerade* (u) estatuak dipoloak onartzen dituen trantsizioen bidez eskuragarriak direnez, egoeraren simetria erabil daiteke H- eta J-agregazio moduak identifikatzeko.

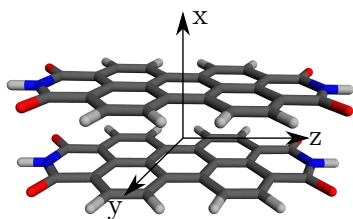


Figure 8.19: Atal honetan erabilitako PDI deribatua. Egoera kitzikatuak eklipsatua den konfigurazioan aztertua izan da eta luzeratako translazio koordinatuan.

Hemen, LE eta CT-ren ekarpenetan jarri da arreta nagusia. Lehenik eta behin, diabatizazio-prozeduraren balidazioa egin da, [86], egoera singlete eta tripleteentzako, eta trantsizio-dentsitatearen matrizearen analisi batekin alderatu da [91]. Ondoren, LE/CT egoeraren modulazioa egin da. Horretarako, translazio koordinatuaren distortsioaren eragina aztertu da egoera simetria baxuenean, (A_g/B_u). Honek erakusten du, distortsioan zehar egoeren aldaketa bar dagoela eta hau H-/J-izaera txandakatuarekin dagoela erlazionatuta. Aurrez singletetarako erakutsi den bezala [86], [167], [171]. Gainera, energia eta izaera kitzikatuak truke-korrelazioko bi funtzionalitatearekin alderatu dira: ω B97X-D eta CAM-B3LYP. Azkenik, erabilitako diabatizazio hurbilketa sinplea ER eta Boys lokalizazio metodoekin alderatu da.

8.4.2 Metodologia

PDI deribatuen egitura molekularrak hutsean optimizatu dira DFT erabiliz, B3LYP (CAM-B3LYP) funtzionalaren bidez eta 6-31G(d) oinarri multzoen bidez. Geometria optimizatuak energia minimo gisa baieztatu dira gainazal energetiko potentzialean, bibrazio harmonikoaren hurbilketaen barruko maiztasun-analisiaren bidez. Egitura guztiek indar positiboko konstanteak erakutsi dituzte.

Maila baxueneko egoera singlete eta tripleteaen kitzikapen bertikaleko energia eta trantsizio-propietateak TDFTarekin (erantzun lineala) lortu dira. Kalkuluak TDArekin eta gabe egin dira, [110] trukatzeko-korrelazio funtzional eta oinarri berarekin. Oinarri multzo handiagoarekin (6-311+G(d)) kalkulatuak kitzikapen energiek osziladore indarrek (C.1 Taula) ezberdintasun txikiak erakusten dituzte. CAM-B3LYP funtzionalaren aukeraketaren arrazoia izan da elektroizulo gainjartze ahulak dituzten trantsizio elektronikoak behar bezala deskribatzeko gaitasunak dituela, hala nola CT eszitazioak.

Duela gutxi, Walter et al.-ek [151] CAM-B3LYP-en egokitasuna zehaztu zuen perilenoizko dimeroen kitzikapen elektronikoetan, ω B97X-D-k [108] perileno bisimidoaren dimeroetan emaitza hobek ematen dituen bitartean. **2** monomeroaren eta dimeroaren eszitazio singlete eta tripleteen karakterizazioan erabili diren CAM-B3LYP, B3LYP, ω B97X eta ω B97X-D truke-korrelazio funtzionalen konparaketa, A eranskinean aurki daiteke. Garrantzitsua da aipatzea, CAM-B3LYP eta ω B97X-D-k antzeko emaitzak ematen dituztela PDI-ren dimeroetan (D.1 eta D.2 Taulak). Aipatu ezean, idatzian agertzen diren kitzikapen-energiak eta trantsizio-propietateak molekula eta oligomeroetarako aztertu dira, adibidez, dimeroak eta trimeroak, **1** kristalean [133], eta hidrogenozko kateak *n*-oktaniloiz ordezkaturik 1.012Å-ko N-H lotura-distantziarekin (PDI **2**).

TDArekin barruan konputatutako trantsizio elektronikoen diabatizazioa ER lokalizazio eskemaren bidez egin da [161]. Energia diabatikoak eta akoplamendu elektronikoak Hamiltondar diabatikoaren matrize diagonaleko eta diagonaletik kanpoko elementu gisa lortu dira, hurrenez hurren. Spin singletaren eta tripleten egoera kitzikatuen diabatizazioa **2**-ko dimerro molekularren lau egoera adiabatiko (batez ere) kontuan hartuta egin da, okupatutako bi orbital molekular altuenetatik (HOMO eta HOMO-1) okupatu gabeko bi orbital molekular baxuenetara (LUMO eta LUMO+1) bitarteko promozio elektronikoei dagozkienak. Tripleten egoera kitzikatuen diabatizazioa **3n** zazpi egoera adiabatikorekin egin da. Egoera adiabatikoen kopurua handitzeak ez du ia aldatzen beheengo singleteen eta hirukien ezaugarriak diabatikoen arabera. Egoera diabatikoaren energia eta akoplamenduak oso antzekoak dira Boys lokalizazio-eskemarekin [162] edo ER eskemarekin kalkulaturik gero (ikus 5.5, 5.6 eta D.5 taulak). KTko egoeren eta lokalizatutako (spin) tripleteen zuzeneko kalkulua PDI dimero eta trimeroetan M-DFT metodoarekin da [76], tokiko karga edo spin-a monomero ezberdinetan murriztuz, hurrenez hurren.

PDI oligomeroen energia eszitatuak eta oszilatzailearen indarrak lortzeko erabilitako parametroak, elkarrekintza klasikoko dipolo-dipol ereduaren bidez kalku-

latu dira, non: $|\mathbf{R}| = 15.95\text{\AA}$, $\theta = 42,5^\circ$ zutabe *barneko* elkarrekintzetarako, eta $|\mathbf{R}| = 4.80\text{\AA}$, $\theta = 47.0^\circ$ eta $|\mathbf{R}| = 5.00\text{\AA}$, $\theta = 44.6^\circ$ zutabe *arteko* dimeroentzako, zelula unitarioaren barruan eta gelaxken artean, hurrenez hurren.

Azkenik, tripletearen izaera analizatu eta karakterizatzeko erabilitako metodoa 8.2.5.2 azpiatalean garatu da. Aurreko azpiatalekin alderatuta, kasu honetan PDI monomeroaren egitura aurreko PDI agregatuen ikerketetan erabili den berbera da, BLYP-D/TZV (P) teoriaren mailan optimizatua [178] eta molekulen arteko distantzia 3.4\AA n finkatua, aurreko lanetan bezala [86], [152]. Kitzikatutako egoeren kalkuluak egin dira konformero eklipsearentzat eta 0.5\AA desplazamenduentzat 8\AA luzetarako translazio koordinatuan zehar.

Kitzikapen energiak DM-DFT-rekin zehaztu dira Tamm-Dancoffen hurbilketa (TDH) [110] erabiliz, CAM-B3LYP [148] eta ω B97X-D [108] funtzionalak eta 6-31G* oinarri multzoa erabiliz. ω B97X-D erabiltzearen arrazoia da CT izaeraren deskribapen fidagarria ematen duela PDIren dimeroetan [151] egoera singletear-entzako. Azkenik, CT karaktereak deskribatu dira HDS-rekin eta trantsizio dentsitate matrizeak analizatze dituen TheoDORRE programa [91] erabiliz.

Atal honetan lehenengo zatian aztertutako egitura elektronikoaren kalkulu guztiak Q-Chem paketearekin egin dira [111], eta bigarren zatikoak Gaussian 16 [179] programarekin.

8.4.3 Molekula

8.4.3.1 Egitura Molekularra

Aztertutako sistemaren ezaugarri fotofisikoak ondo ulertzeko, garrantzitsua da haren egitura elektronikoa ongi ezagutzea. Bereziki, espazio orbital okupatuaren eta bertualaren arteko muga dauden energia-mailen ezaugarriek interes berezia dute, trantsizio elektroniko baxuen izaera kontrolatzen baitu.

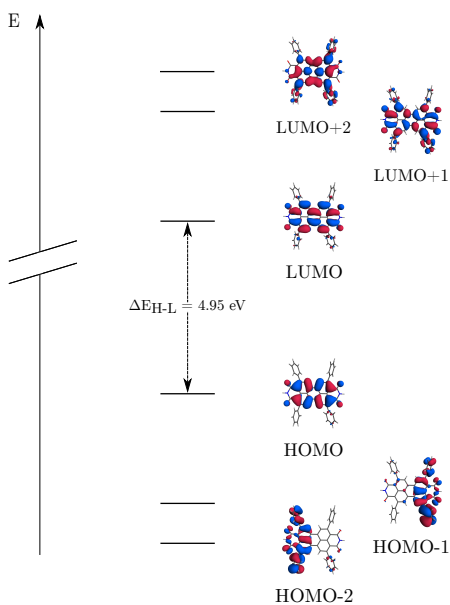


Figure 8.20: PDI kristal molekularren mugako orbital molekularrak CAM-B3LYP/6-31G* maila teorikoan kalkulaturak.

Bi orbital molekular mugakide (**2**), hau da, gehien okupatutako orbital molekularra (HOMO) eta gutxien okupatutako orbital molekularra (LUMO), plano molekular nagusiaren gainean deslokalizatutako π -orbitalei dagozkie, feniloetan elektroi-dentsitate urria dute (8.20 Irudia), eta HOMO eta LUMO-ren π energien eraldaketa txikiarekin, simetria galerarekin erlazionatuta dagoena (8.5 Taula). HOMO-LUMO espazio orbitaletik haratago, energetikoki baxuagoa (altuagoa), okupatua (okupatu gabea), π -orbitalek, PDI bizkarrezurraren eta alboko feniloen orbital molekularren arteko nahasketa gertatzen da.

Table 8.5: DI **2** eta optimizatutako PDI **3** OM energiak (Hartree) CAM-B3LYP/6-31G(d) mailan kalkulaturak.

	HOMO-1	HOMO	LUMO	LUMO+1
PDI 2	-0.281	-0.262	-0.080	-0.023
PDI 3	-0.329	-0.266	-0.093	-0.026

8.4.3.2 *Maila Baxueneko Egoera Kitzikatua*

Oinarrizko egoera zehatz-mehatz aztertu ondoren, PDI molekularren egoera kitzikatua ezaugarritzen dira. Horretarako, TDDFTren bidez kalkulatu dira spin singlerik eta tripleterik baxuenera kitzikatutako egoerak. Kalkulu hauek CAM-B3LYP

truke-korrelazioko funtzioarekin egin dira. 8.6 egoera kitzikatu baxuetarako emaitza konputazionalak ditu: energia kitzikatuak, oszilatzailearen indarra eta ekarpen elektronikoak.

Table 8.6: PDI **2** molekularen energia bertikalak (in eV) and oszilatzailearen indarra (in parenthesis) egoera kitzikatu singlete eta triplete baxuenentzat CAM-B3LYP/6-31G(d) mailan kalkulaturak. Orbitatik orbitarako konposizioak TDA trantsizioei dagokie. H=HOMO; L=LUMO.

Egoera	MDDFT	TDA	Konposizioa
S ₁	3.01(0.720)	3.19(0.986)	% 95 H→L
S ₂	3.42(0.047)	3.47(0.057)	% 75 H-1→L
S ₃	3.58(0.234)	3.61(0.232)	% 72 H-2→L
S ₄	3.88(0.010)	3.91(0.015)	% 57 H-3→L
S ₅	3.94(0.006)	3.97(0.010)	% 41 H-9→L
T ₁	1.46	1.93	% 88 H→L
T ₂	2.67	2.95	% 31 H-2→L,24% H→L+1
T ₃	2.92	3.05	% 32 H-1→L,10% H→L+1
T ₄	3.05	3.14	% 55H-2→L
T ₅	3.11	3.34	% 40 H→L+3

PDI **2**-ren maila energetiko baxueneko trantsizio energetiko bertikalak HOMO → LUMO trantsizioari dagokie (8.6 Taula). S₁erako kitzikapena optikoki aktiboa da eta trantsizio momentu dipolarra plano molekularrean eta ardatz molekular luzean orientatuta. Kalkulatutako trantsizio-energia konputatua (3.01 eV)bat dator TDDFTren beste kalkulu batzuekin, [140], nahiz eta urdinera desplazatuta egon tolueno-soluzioko absortzioarekin alderatuz (2.34 eV) [143]. Hurrengo bi singlete kitzikatuak, hau da, S₂ eta S₃, ~0.3-0.5 eV-tik daude eta batez ere, HOMO-1 eta HOMO-2-tik LUMOrako promozio elektronikoei dagozkie. Tartean dauden orbital okupatuei erreparaturik ikusten da molekula barneko CT badagoela eta alboko feniloetako π-elektroien parte hartze handiarekin. Helburua energia esperimenteral zehatzak irudikatzea ez bada ere, Zimmerman et al. [40] lanaren datu batzuk hartu dira oinarri bezala. Lan honetan, S₁-eko absortzio energia 2.36 eV-koa da eta S₂-rena 2.68 eV-koa. Bestalde, 8.6 taulako emaitza konputazionalak egiaztatzean, bi balio esperimenteral artean egoera bat gehiago dagoela ikus daiteke. Horren arrazoia da S₂ egoera kitzikatuak 0 inguruko indar osziladorea duela, esperimenteral barruan antzematea zailtzen duena.

Egoera tripleterik (T₁) baxuena (HOMO → LUMO) lehenengo egoera singletea baino baxuago dago, ~ 1.25 eV TDA mailan. T₁/S₁ energia-diferentzia handia HOMO/LUMO gainjartze espazial handi batetik dator, eta horren ondorioz, mugako bi orbitalen arteko elkarrekintza integrala handia da. T₁ energia aldetik ondo

bananduta dago gainerako egoera tripleteen artean, T_2 - T_4 egoerek 1 eV baino altuago baitaude energian.

Amaitzeko, interesgarria izan liteke TDA [110]-ren inpaktua aztertzea. Jakina da hurbilketa horrek kostu konputazionala murrizten duela, intentsitate erlatiboak gutxietsiz ditu TDDFT-rekiko. Hala ere, egoera tripleteentzako aukeraketa egokia izan daiteke. Horren arrazoia da TDAk egoeren orden egokia berreskuratuz gain [144], egoera tripletearen egonkortasun arazoa konpontzen duela. Gainera, trantsizio momentuek ez dute asetzen Thomas-Reiche-Kuhn sum araua [145]–[147]. Elektrosistemen interakzioan, arau honek maiztasun kolektiboen zuzeneko kalkulua ahalbidetzen du uhin-luzeraren muga batean. TDA duten energia indibidual konputatuek TDDFT betearen joera bera jarraitzen dute, eta TDAren hutsuneak zertxobait handiagoak dira (0,2-0,3 eV). TDDFT vs. TDA diferentziak nabarmenki handiagoak dira egoera tripleteentzako, bereziki T_1 , $E_{TDA}(T_1) - E_{TDDFT}(T_1) = 0.47$ eV. Garrantzitsua da DM-DFT-ko eta TDA-ko estatuek egitura elektronikoa ia berdindina izatea, kasu honetan TDA-a zentzuzko hurbilketa bat izan litekeela adieraziz, gutxienez PDI sistemetako trantsizio elektronikoen karakterizazio erdi kuantitatiboa egiteko.

8.4.4 Agregatuak

Azpi atal honetan PDI **2** agregatuen egoera kitzikatu singlete eta triplete baxuenak analizatu eta karakterizatuko dira. Horretaz gain, PDI **3**-ren trimeroa erakikiko da eta

8.4.4.1 Zutabe-arteko vs. -barneko elkarrekintzak

Lehenik eta behin, aurretiazko esplorazio bat egin da molekulen arteko elkarrekintzek kristal molekularreko zutabe baten barruan eta alboko zutabeen artean duten magnitude erlatiboa ebaluatzeko. Horretarako, kristalezko egituraren hiru dimero molekular ezberdin hartu dira kontuan, hau da, zutabe barneko bi dimero desberdin, zelula unitarioaren barruan dauden bi molekulek (**D1** dimeroa) eta zelula desberdinen artean (**D2** dimeroa) eratuak, eta espazio-banaketa laburrena duen zutabeko dimeroa. Dimero guztiek dituzte PDI nukleo ia koplaneatuak elkarren gainean pilatutako zutabe barneko dimeroen konformazioan, zutabe arteko dimeroetan bi molekulak ia plano berean etzanda dauden bitartean, alboko fenilozko eraztunez bereizitako diagonalean.

Zutabe barneko eta zutabe arteko sistemen orbital molekularrek profil nahiko desberdinak erakusten dituzte. Mugako lau orbitalak, zutabe arteko dimeroarentzat kalkulatuak, bi monomeroetako batean daude, HOMO/HOMO-1 eta LUMO/LUMO+1 energia-diferentzia txikiekin (8.21 Irudiaren eskuinean). Bestalde, zutabe barneko dimeroaren orbital molekularrak bi molekulen gainean deslokalizatzen dira eta energia banaketak nabarmen handiagoak erakusten dituzte (8.21 Irudiaren

ezkerrean). Emaitza hauek interakzio intermolekular indartsu eta ahuleta bideratzen dute, zutabe barneko eta zutabe arteko dimeroentzat hurrenez hurren.

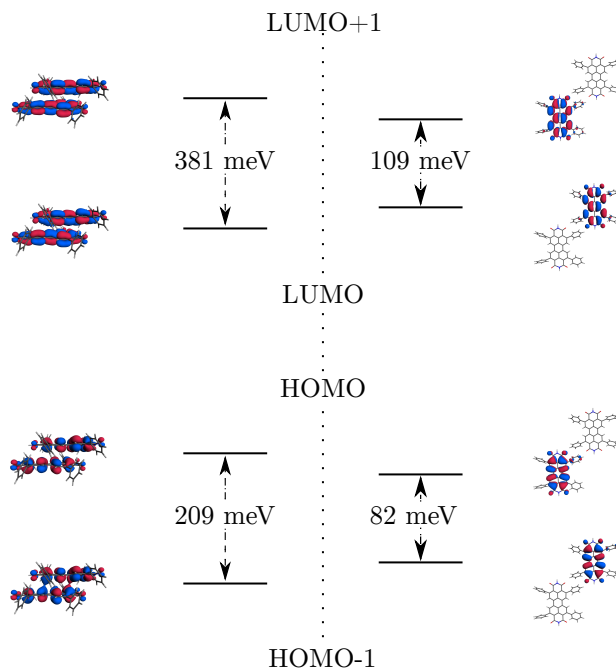


Figure 8.21: OM diagramak zutabe barneko (zelda unitateari dagokion **D1**, ezkerre) eta zutabe arteko (eskubia) TDA, CAM-B3LYP/6-31G(d) teoria mailan kalkulatu. **D2** dimeroaren MOak D.1 Irudian aurki daitezke.

Molekula berdineko dimeroen S_1 eta S_2 -ren arteko energia-aldea monomero bakoitzean lokalizatutako singlete eszitatuen akoplamendu elektronikoko bikoitzaren hurbilketa bezala erabil daiteke. Eszitzazio singlete baxuenak 8.7 Taulan aurkitu daitezke. Kalkulatutako S_1/S_2 energia diferentzia askoz ere handiagoa da zutabe barneko sisteman zutabe artekoan baino. Eta honek esan nahi du, elkarrekintza elektronikoko sendoagoa duela. Azpimarratzekoa da zutabe barkeno TDDFT kitzikapen energia eta oszilatzailearen indarrak bat datozela J-agregatuaren [166] dipolo-dipolo modelo klasikoarekin (8.84 ekuazioa). Tartekatutako dimeroetan kontrobertsia handiagoa dago. Dipolo-dipolo elkarrekintza klasikoak J-agregazioa aurre ikusten du zutabe barneko dimeroentzat, $J_{Coul}^{dd} = -182$ meV (**D1**) eta -212 meV (**D2**)rentzat. Gainera, zutabe barruko bi dimeroetan, egitura elektronikokoaren kalkuluek bi singlete kitzikatuak (S_1 eta S_2) gorrira mgitzen dira monomeroaren (3,19 eV) trantsizio baxuenarekiko.

Table 8.7: Kitzikapen energiak (eV) and oeta oszilatzaile indarrak (parentesi artean) egoera kitzitatu singlete baxuenetara (S_1 and S_2) zutabe barneko (**D1** eta **D2**) eta zutabe arteko dimeroetan TDDFT/TDA CAM-B3LYP/6-31G(d) mailan kalkulata, eta trantsizio monomerikoen dipolo-dipolo elkarrekintza klasikoa dip-dip).

metodoa	S_1	S_2
zutabe barnea D1		
TDA	2.95 (1.009)	3.04 (0.000)
dip-dip	3.01 (1.863)	3.37 (0.000)
zutabe barnea D2		
TDA	3.04 (0.000)	3.12 (1.121)
dip-dip	2.98 (1.844)	3.40 (0.000)
zutabe artea		
TDA	3.17 (2.042)	3.19 (0.021)
dip-dip	3.18 (1.970)	3.20 (0.000)

Emaizta hauek iradokitzen dute pilatutako PDI molekulen arteko akoplamendu eszitonikoak ezin direla eratorri tokiko kitzikapenen zuzeneko akoplamendutik, esate baterako, interakzio-eredu dipolo-dipolo klasikoan,

$$J_{Coul}^{dd} = \frac{|\boldsymbol{\mu}|^2(1 - 3 \cos^2 \theta)}{4\pi\epsilon_0|\mathbf{R}|^3} \quad (8.84)$$

non $\boldsymbol{\mu}$ trantsizio dipolo molekularren momentua den, \mathbf{R} bi trantsizio dipoloak elkartzten dituen distantzia bektorea den, eta θ , $\boldsymbol{\mu}$ eta \mathbf{R} bektoreen arteko angelua. Akoplamendu konputatuek adierazten dute agregazioak eragindako efektuak pilatutako PDI molekula koplanarren akoplamenduak menderatzen dituela, eta zutabe desberdinetako molekulen arteko elkarrekintzak garrantzi txikiagoa duten bitartean. Beraz, zutabe berean pilatutako molekulen klusterrak erabiliko dira ikerketarekin jarraitzeko.

8.4.4.2 *Energetikoki Baxuenak diren Egoera Singlete eta Triplete Kitzikatuak*

PDIren agregazioak egoera kitzikatu elektronikoetan duen eragina sistematikoki aztertzeko, konparazio bat egin da egoera kitzikatu singlete eta triplete baxuenetako kegoeratan tamaina desberdineko klusterrentzat, hau da, metatutako PDI molekula kopuru desberdinekin (8.22 Irudia). Bi egoeretarako kitzikapen energia murriztu egiten da PDI molekula kopuruarekin, eta badirudi konbergentzia batera iristen dela, 5-6 molekula inguru singleterako eta 2-3 molekula T_1 -entzat. S_1 -aren egonko-

rtze energetikoa (311 meV), 6 molekulako klusterraren eta monomeroaren energia diferentzia bezala kalkulatu, T_1 -ena (59 meV) baino askoz handiagoa da. Ez da harriztekoa T_1 eta S_1 kitzikapen energien beherakadarik handiena monomerotik dimero eta trimerora ematea, horrek adierazten baitu ondoz ondoko molekulen elkarrekintzak oso garrantzitsuak direla.

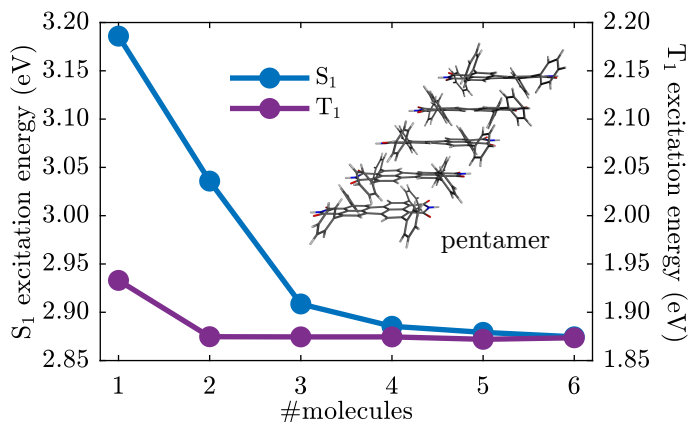


Figure 8.22: Baxuenak diren singlete (urdina, ezkerreko ardatza) eta triplete (morea, eskuineko ardatza) eszitazio energia bertikalak (eV) multzokatutako PDI molekulen funtzio gisa CAM-B3LYP/6-31G(d) eta TDA-n kalkulatuak. Irudian: PDI **2**-ren multzokatutako pentameroa.

Emaitza hau HOMO-LUMO energia tartearren beherakada sistematikoarekin erlaziona daiteke 8.8 taulan agertzen den molekula pilatuen kopuruarekin. Ikus daiteke energia nola gutxitzen den pilatutako PDI molekulen kopurua handitzen den bitartean. Gainera, energiaren beherakada nagusia 1 eta 2 (0.19 eV) eta 2 eta 3 (0.22 eV) molekula metatuen artean gertatzen da PDI kristalean. Pilatutako 4 PDI molekuletatik gora, kalkulatuak energia diferentzia ez da ia aldatzen.

Table 8.8: Energia desberdintasuna (ΔE_{HL}) HOMO eta LUMO orbitalen artean eV-tan. CAM-B3LYP/6-31G* maila teorikoan egindako kalkuluak.

1	2	3	4	5	6
4.95	4.76	4.54	4.54	4.49	4.49

8.4.4.3 Akoplamendu Elektronikoak

PDI agregatuen trantsizio elektronikoak karakterizatzeko eta hurbilketa klasikotik (Kasha-ren Eredua) haratago dagoen elkarrekintza elektronikoen izaera ulertzeko,

kalkulatutako energia adiabatikoen deskonposaketa egiten da trantsizio elektroniko horien izaera egoki definituta geratzeko. Horretarako, ER diabatizazio eskema erabiliko da **D1** eta **D2**-ren energetikoki baxuenak diren singlete eta tripleteak karakterizatzeko LE eta CT terminoetan. Jarraian, LE eta CTko diabatikoen fasea, trantsizio-une dipoloaren simetria translazionalan oinarritutako eredu konbentzionalaren arabera esleitzen da [167], [168]. Egoera tripleteen (ilun) arteko akoplamenduen zeinua singlete singlete balioen arabera esleitzen da.

Egoera diabatikoen arteko akoplamendu elektronikoak interakzio-terminoen izaeraren arabera sailka daitezke, [169], bi LE-ren akoplamendu gisa, edo zuzeneko akoplamendu gisa (V_{DC}), zeina J_{Coul}^{dd} k elkarreragin-distantzia handietarako hurgilketa gisa erabili daiteken; LE eta CT egoeren elkarreragina elektroi (V_e) eta zulo gisa (V_h) (normalean elektroi eto zulo transferentzia integral bezala adierazita); eta bi CT egoeren arteko elkarrekintza (V_{CT}),

$$V_{DC} = \langle LE_A | \hat{H} | LE_B \rangle \quad (8.85)$$

$$V_e = \langle LE_A | \hat{H} | CT_{AB} \rangle = \langle LE_B | \hat{H} | CT_{BA} \rangle \quad (8.86)$$

$$V_h = \langle LE_A | \hat{H} | CT_{BA} \rangle = \langle LE_B | \hat{H} | CT_{AB} \rangle \quad (8.87)$$

$$V_{CT} = \langle CT_{AB} | \hat{H} | CT_{BA} \rangle \quad (8.88)$$

non $LE_A = A^*B$, $LE_B = AB^*$, $CT_{AB} = A^+B^-$, $CT_{BA} = A^-B^+$, eta A eta B dimeroko bi monomeroei dagozkien. Muga perturbatiboan, bi egoera isolatu kitzikatuenen energia simetrikoa (+) eta antisimetrikoa (-), simetria translazionalari dagokionez, EL energiaren batura, bakoitzaren energia Δ_{CT} , eta bi akoplamenduren bidez (V_{DC}) eta LE/CT(J_{CT})[168] adiarazi daiteke,

$$E_{\pm} = E_{LE} + \Delta_{CT} \pm V_{DC} \pm J_{CT} \quad (8.89)$$

$$\Delta_{CT} = -\frac{V_e^2 + V_h^2}{E_{CT} - E_{LE}} \quad (8.90)$$

$$J_{CT} = -\frac{2V_e V_h}{E_{CT} - E_{LE}}. \quad (8.91)$$

Horregatik, V_{DC} , V_e eta V_h eta EL/KT energia diferentziaren magnitude erlatiboak eta zeinuak eszitoi baxuenaren izaera determinatzen dute, hau da, optikoki aktiboa (+) edo iluna (-), azkenean J- edo H-agregazioa eragiten duena. Bestalde, fasean dauden V_e eta V_h ($V_e V_h > 0$), J-agregazioa sustatzen dute (beren zeinu indibidualak alde batera utzita), eta fasez kanpoko akoplamenduek, berriz, H-agregatuak. Agregatuaren propietate fotofisiko globalak LE/LE eta LE/CT interakzioen arteko lehiatik sortzen dira [171]. V_{DC} akoplamendua irismen luzeko elkarrekintzetarako da nagusi, baina kromoforoen arteko distantzia laburretan orbital molekularrak gainjartzen dira eta V_e eta V_h (supertrukea) [168] garrantzitsuak bilakatu daitezke eta LE/LE-ri aurre egin diezaiokie.

Zutabe berneko spin singleteen diabatizazioak endekatutako bi egoera pareetan amaitze da, LE eta CT izaera dutenak, hurrenez hurren. LE energiak 3.16 eV (**D1**) eta 3.14 eV (**D2**), monomeroaren energetik oso gertu daude (8.9 Taula). Gainera, CT egoerak EL baino 0.11-0.13 eV gorago daude energian. Nahiz eta LE/CT energia diferentzia metodoarekiko dependentea izan [151], [152], C-DFT (muga kargan ezarritz) bidez frogatua izan da CT egoera diabatikoa. Horrela, **D1**-en CT egoera 3.33 eV-ra aurki daiteke eta **D2**-ren egoera 3.48 eV-ra.

Table 8.9: Energia elektrokino (eV) and akoplamendu elektroniko diabatikoak (8.85-8.88 ekuazioak, meV-tan) ER diabatizazio eskema erabiliz lortuta beti ere energetikoki baxuenak diren lau singlete eta triplete erabiliz molekula arteko PDI dimeroentzako **D1** (zelda unitatea) and **D2** (zelda artekoa) (TDA) CAM-B3LYP/6-31G(d) maila teorikoa erabilis.

dimer	$E(^1\text{LE})$	$E(^1\text{CT})$	V_{DC}	V_e	V_h	V_{CT}
D1	3.16	3.27	106	-176	-134	-2
D2	3.14	3.27	97	-92	-40	-13
dimer	$E(^3\text{LE})$	$E(^3\text{CT})$	V_{DC}	V_e	V_h	V_{CT}
D1	1.95	3.25	-1	-182	-143	-2
D2	1.94	3.28	1	-123	-54	-3

Bi dimeroetan bi singleteen (lokalen) akoplamendu eszitonikoa positiboa da ($V_{DC} > 0$), eta zertxobait handiagoa **D1** kasuan, trantsizio-une (lokal) dipoloen konfigurazio antiparaleloaren mesedetan. Eraitza hau guztiz kontraesanean dago interakzio dipoloaren hurbilketa puntualarekin, erabat gutxietsi behar baitira PDI agregatuak. Bestalde, V_{DC} balio konputatuak adostasun kuantitatibo psp onean daude Oleson et al. [149]-ek lortutako akoplamendu Coulombikoekin, trantsizio atomikoko kargen dentsitateetatik eratorriak [172], [173].

8.10 taula singletearen eta tripletearen trantsizio elektronikoen deskonposizioa erakusten du, bi zutabe barneko bi dimeroen egoera diabatikoen ekarpeni dagokienez. **D1** dimeroan, supertrukeak zuzeneko akoplamendua gainditzen du, eta energia baxueneko egoera singletea (adiabatikoa) LE eta CT konbinazio simetriko gisa lortzen da. LE/CT nahasketa aipagarria da, trantsizioaren % 50 suposatzen duten CT-ren ekarpenekin. Aitzitik, singlete antisimetrikoa (trantsizio-unea desagertaraziz) ia erabat lortzen da kitzikapen lokal gisa (CT ekarpenak $\sim 4\%$). **D2**-ko bi singlete baxuenen konposizioa gelaxka unitarioaren berdina da ia, baina alderantzizko egoera ordenarekin. Soluzio simetriko eta antisimetrikoen portaera nahiko desberdin hau arrazionalizatu daiteke Frenkel eszitoien (FE, equation 8.92) eta karga erresonantzien (CR, 8.93 ekuazioa) akoplamenduak kontsideratuz. FE simetria bera duen CR egoerarekin bakarrik nahas daiteke (8.95 ekuazioa), eta FE/CR elkarrekintza elektroien eta zuloen akoplamenduen zeinu eta magnitude erlatiboen arabera da (8.94

Table 8.10: Trantsizio energiak (ieV), oszilatzaile indarrak (parentesian), eta kontribuzio diabatikoak ω (in %) ER diabatizazio eskema bidez lortuta energian baxuen dauden bi egoere singlete eta tripleteentzat **D1** and **D2** dimeroetan (TDA) CAM-B3LYP/6-31G(d) maila teorikoan kalkulaturak. $\omega(\text{LE}) = \omega(\text{LE}_A) + \omega(\text{LE}_B)$, $\omega(\text{CT}) = \omega(\text{CT}_{AB}) + \omega(\text{CT}_{BA})$.

egoera	ΔE (f)	$\omega(\text{LE})$	$\omega(\text{CT})$
D1 dimeroa			
S _{1,+}	2.96 (1.009)	50	50
S _{2,-}	3.04 (0.000)	96	4
T _{1,+}	1.87	94	6
T _{2,-}	1.95	100	0
D2 dimeroa			
S _{1,-}	3.04 (0.000)	96	4
S _{2,+}	3.12 (1.123)	52	48
T _{1,+}	1.92	98	2
T _{2,-}	1.94	100	0

ekuazioa). **D1** eta **D2**-n, V_e eta V_h -ek zeinu bera eta antzeko magnitudeak dituzte, elkarreragin indartsuak (simetrikoak) eta ahulak (antimetrikoak) eraginez.

$$|\text{FE}_{\pm}\rangle = \frac{1}{\sqrt{2}}(|\text{LE}_A\rangle \pm |\text{LE}_B\rangle) \quad (8.92)$$

$$|\text{CR}_{\pm}\rangle = \frac{1}{\sqrt{2}}(|\text{CT}_{AB}\rangle \pm |\text{CT}_{BA}\rangle) \quad (8.93)$$

$$\langle \text{FE}_{\pm} | \hat{H} | \text{CR}_{\pm} \rangle = V_e \pm V_h \quad (8.94)$$

$$\langle \text{FE}_{\pm} | \hat{H} | \text{CR}_{\mp} \rangle = 0 \quad (8.95)$$

Nahiz eta V_e eta V_h -ren akoplamenduak indartsuak izan egoera tripletean (8.9), CT terminoak ia ez dira nahasten triplete baxuagoekin, ezta egoera simetrikoetan ere (CT kontribuzioak $\sim 6\%$). Emaitza hau ulertu daiteke supertruketik (J_{CT} , 8.91ekuazioa) datorren energia ebakuazioaren kontribuzio gisa. CT energia ia berdina da spin singleterako eta tripleterako, baina ${}^3E_{LE} \ll {}^1E_{LE}$. Ondorioz, J_{CT} magnitudea txikiagoa da egoera tripletean egoeran singletean baino.

8.4.4.4 *Eszitoi Tripleteak eta Molekula Arteko Distortsioak*

Orain arte xehetasun handiz ezaugarritu dira PDI agregatuen eszitazio baxue-nak. Baina emaitza horiek guztiak hurbilketa estatiko batekin lortu dira, hau da, **1** kristalezko egituratik koordenatu molekular eta oligomerikoak hartuz. Beraz, emaitza

horiek, oro har, agregatu molekularren portaeraren adierazgarri onak izan daitezkeen arren, pilaketa tartekatu moduan zentratzen dira eta ez dute agregazio alternatiborako modurik azaltzen. Gainera, aurrez aurreko pilaketa molekularren kasuan ere, ezin dugu baztertu bertan gerta daitezkeen distortsioak eta honek estatuen arteko energia eta akoplamendu elektronikoetan sor ditzaten aldaketetan. Honek pisu handia izan dezake PDI agregatuen fotofisikan, hainbat ikerketa teorikotan egiaztatu den bezala [150]–[152]. Horregatik, atal honek aztertzen du molekulen arteko distortsioek zer nolako eragina duten egoera kitzikatuaren banaketan eta haien propietateetan. Horretarako, ordezkatu gabeko (D_{2h} simetrikoa) PDI deribatuaeren trimer **3** koplanarra erabili da.

Distortsio bertikala jasaten duen trimeroaren engoera tripletearen energia kalkulak, tripletearen eszitazio energiaren murrizketa dakar 4.5\AA baino txikiagoak diren molekula arteko distantziarako (8.23), batez ere triplet baxuenerako. 4.5\AA baino handiagoak diren banantzeetarako, energia bertikala konbergentzia batera iristen dela ikus daiteke. Konbergentzia hau monomeroaren T_1 -tik gertu dago, beraz, 4.5\AA -tik aurrera monomero independente bezala jokatzeko du monomero bakoitzak.

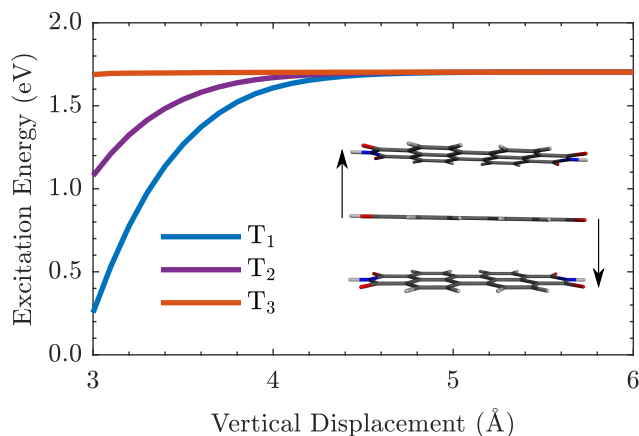


Figure 8.23: T_1 - T_3 egoeren energia kitzikatu bertikalak (eV) z ardatzean (bertikala) distortsionatutako PDI **3** trimero eklipsatu batentzat.

Translazio desplazamenduek tripletearen energian ere eragiten dute, erabatekoa edo partziala den konformazio eklipsatu eta alternatuekin, S_0/T_1 energia diferentzia murriztuz eta handituz (8.24). Distortsioa konfigurazio eklipsatuan dagoenean, T_1 energia gutxitu egiten da, eta energia handitu egiten da distortsioa forma alternatuan dagoenean. Trimeroak behar adina distortsio jasan duenean, energiaren konbergentzia ikusten da.

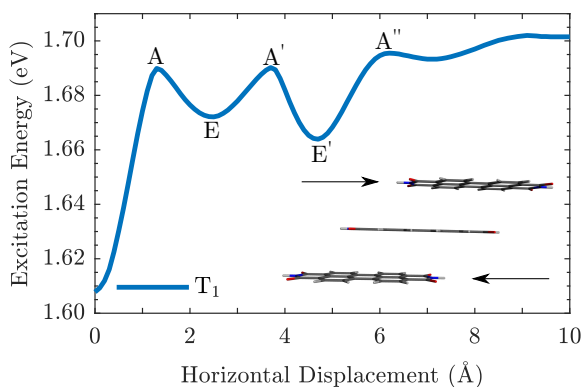


Figure 8.24: T_1 -erako eszitazio energia bertikalak distortsio horizontalean (antiparaleloa) PDI **3** trimeroarentzat 4 Å-ko distantziarekin. A and E etiketek konfigurazio eklipsatu eta alternatuei egiten diete erreferentzia zeinetan $E = 0.0$ Å, $A = 1.3$ Å, $E' = 2.5$ Å, $A' = 3.7$ Å, $E'' = 4.7$ Å and $A'' = 6.2$ Å displacements.

8.4.5 Modeloa

Azpi atal honetan PDI **3**-ren dimeroaren egoera tripletea analizatuko da luzetaka egindako distortsioan (ardatz longitudinalean). Horrela, egoera adiabaticoak, hauen izaera, egoera adiabaticoak eta hauen akoplamendu garrantzitsuetak analizatuko dira.

8.4.5.1 Egoera Adiabatico Kitzikatuak

Egoera tripleteen izaera hobeto ulertzeko asmotan, garrantzitsua izan daiteke egoera singletearen analisisa (8.25 Irudia). Kasu honetan ikusten da, B_u egoera adiabaticoan elkar gurutzatzen ez diren arren, egoera diabatikoak elkartzen direla, eta hau bi egoeren arteko akoplamentu sendoari dagokio.

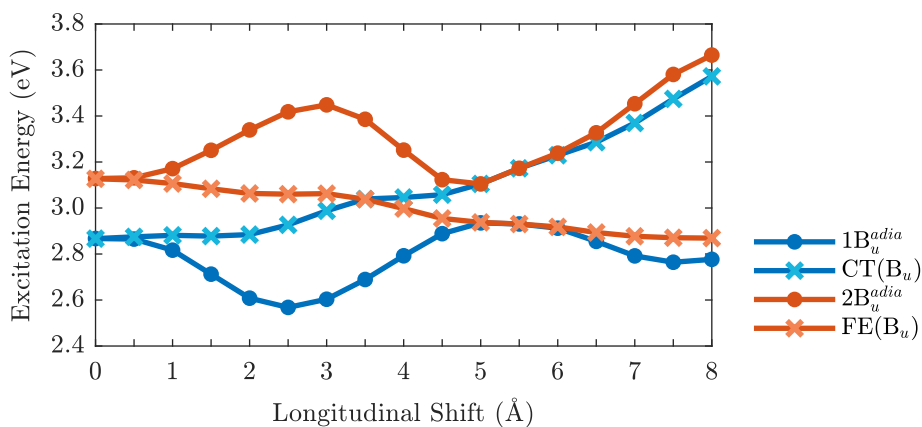


Figure 8.25: Kitzikapen energia profilak (TDA- ω B97XD/6-31G(d)) B_u egoera singlete kitzikatu adiabatikoa (puntuak) eta B_u FE eta KT egoerak (ixa). Elkarrekin zuzen handientzat, egoera adiabatikoa eta diabatikoa elkar eragiten dira.

Egoera tripleteentzako, egoera kitzikatuen analisia TDA mailan egin da, TDDFT osoak erantzun linealaren de-kitzikapen guztiak baititu. Horrela, distortsio horizontaleko energia profinak analizatu dira, 8.26 Irudian ikusten den bezala. Hemen, estatuen oszilazioa ikus daiteke eta honek gidatutako egoera arteko aldaketa.

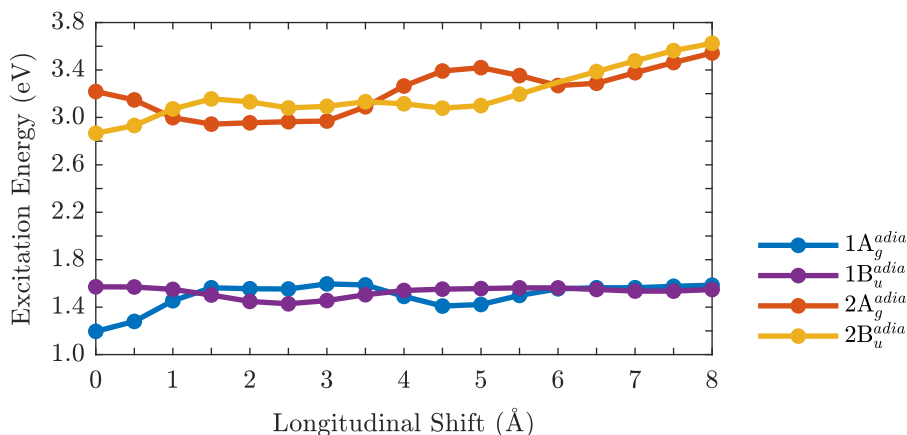


Figure 8.26: PDI dimeroarentzako kalkulaturako energia kitzikatu adiabatikoen profilak TDA- ω B97X-D/6-31G* teoria mailan kalkulaturak

Nahiz eta energia diferentzia handia izan energetikoki baxuenak eta altuagoak diren egoera kitzikatuen artean, esan daiteke egoera singletean ematen den eredu jarraitzen duela.

CT izaerari erreparatuz (8.27) bi ideia nagusi ondorioztatu daitezke. Lehen da, energetikoki baxuenak diren egoerak LE izaera purua dutela. Eta bigarrenak

adierazten digu, energian altuagoak diren egoeren izaera CT puru bati dagokiola. Ideia hau bat dator beste lan batzuekin, [4].

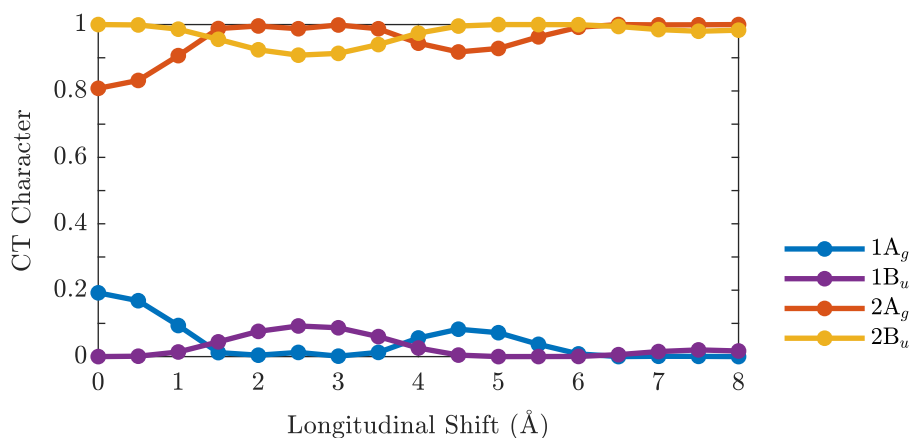


Figure 8.27: Egoera adiabatikoen CT izaera.

CT-ren izaera analizatzeko beste modu bat elektroizulo korrelazio irudia errepresentatzea izan daiteke TheoDORRE programa erabiliz [91]. Honi esker, modu bisual batean egoera kitzikatuen izaera analizatu daiteke. Analisia ulertzeko, aipatu karratuaren diagonal nagusiak baldin badaude koloreztatuta CT egoerari egiten diola erreferentzia. Eta alderantziz, diagonaletik kanpo dauden karratuak baldin badaude koloreztatuta egoera kitzikatuen izaera LE izango da.

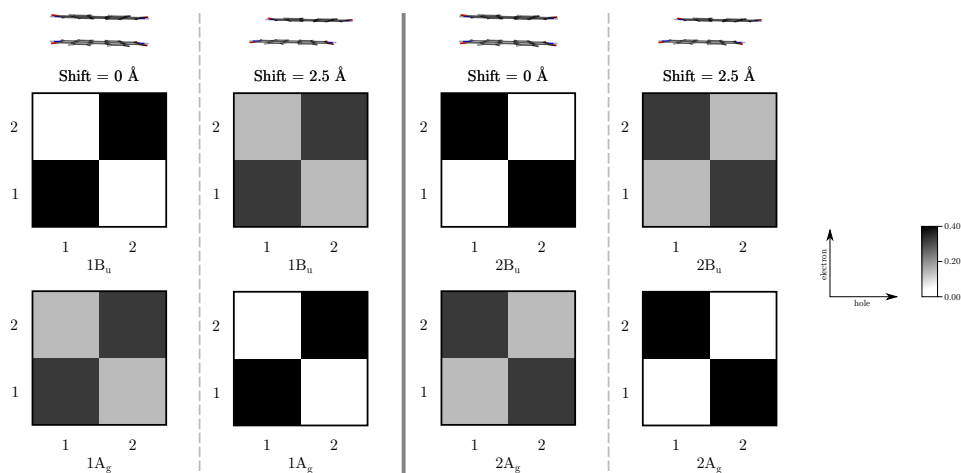


Figure 8.28: Elektroi-zulo korrelazio grafikoa egoera kitzikatu tripleterako PDI dimeroaren bi konformeroentzat: eklipsatua 0.00 Å eta distrotsionatua, 2.5 Å TDA- ω B97XD/6-31G(d) teoria mailan kalkulatu.

Irudikapen honek 8.27 Irudiaren emaitzak nabarmentzen ditu. Egitura eklipsatuari erreparatuz gero, argi ikusten da $1B_u$ eta $2B_u$ EL eta KT estatu puruak direla, hurrenez hurren, elektroi-zulo errepresentazio grafikoak baieztatzen duen bezela. $1A_g$ eta $2A_g$ egoerak, berriz, batez ere LE eta CT dira, estatu-nahasketa apur batekin, gris argiz irudikatuta. 2.5Å luzetarako desplazamenduak eredu berdina jarrai dezake, baina desberdintasun batzuekin. Kasu honetan, LE eta CT egoera puruak $1B_u$ eta $2B_u$ estatuak dira, hurrenez hurren. Eta B_u estatuak, berriz, nahasketa txikia erakusten dute.

TheoDOREn elektroi-zulo korrelazio grafikez gain, egoera kitzikatuaren CT karakterea jakiteko aukera ere ematen du (8.29 Irudia). Bi metodoetarako akordio ona ikusten da egoera baxuenetan. Altuagoetan, berriz, akordio hori hautsi egiten da. Horren arrazoa da molekulen arteko konfigurazio batzuen kasuan, aukeratu-tako $\pi - \pi^*$ estatu gehiagorekin nahasten direla, egoera kitzikatu bakarrarentzako. Diabatizazio-prozedurak ondo definitutako CT izaera ematen du, aukeratu-tako $\pi - \pi^*$ estatuak ez direlako proiektatzen espazio osoan eta, gainera, birnormalizatu egiten direlako. TheoDORek, aldiz, aukeratu-tako estatuen CT izaera ematen du $\pi - \pi^*$ estatu konputatuen espazio osoan; horregatik ez datoz bat bi emaitzak egoera kitzikatu altuagoetan.

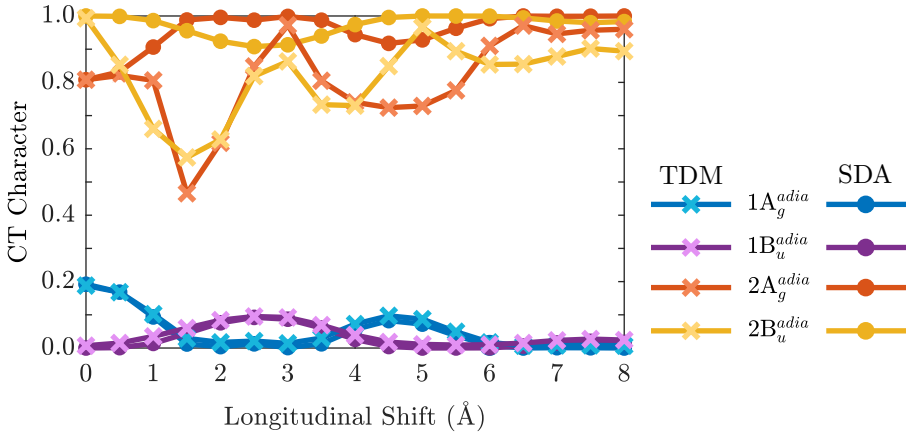


Figure 8.29: CT izaeraren konparaketa diabatizazio prozedurarekin (puntuak) eta trantsizio dentsitate matrizearekin (ixa)[91] aukatutako egoera kitzikatu tripleteentzat.

8.4.5.2 *LE/CT Elkarrekintzak*

Egoera orden aldaketa erraz arrazionalizatzen da LE eta CT estatuen arteko elkar-reraginen joera gorabeheratsuen ondorioz. Interakzio hauek, [4], [86], [152], [169], D_e eta D_h transferentzia integralen konbinazioek ematen dituzte (8.30 Irudia). Hemen argi ikusten da LE/CT elkarrekintzaren gorabehera. Honek A_g eta B_u simetriari deskribatutako egoerarik baxuenen arteko aldaketa zehazten du. Zehatzago esateko, hau $2-3\text{\AA}$ tartean gertatzen da, non LE eta CT arteko elkarrekintza ia hutsala den A_g simetriarentzat. Oszilazio honek 8.26 irudiaren konmutazioa ulertzen ere laguntzen du. Izan ere, EL eta KTren arteko elkarrekintza B_u -ko maximoan dagoenean, $1B_u$ egoera $1A_g$ -ren azpira bidaltzen du.

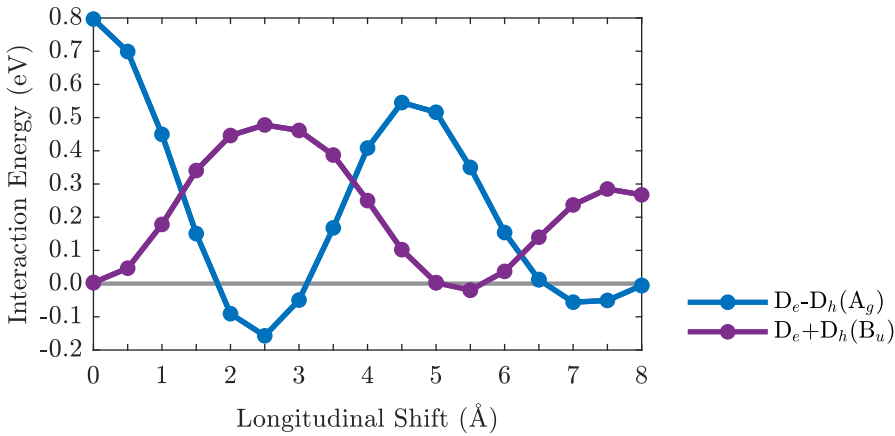


Figure 8.30: $D_e \pm D_h$ terminoen modulatioa translazio ardatz longitudinalean KT/EL elkarrekintzetarako.

8.4.5.3 Simetrizatutako Egoera Diabatikoak

Sistema berezi honetarako simetriarekiko moldaturiko Hamiltondarra erabil daiteke, sistemaren simetria handia dela eta. Kasu honetan, simetria bakoitza, A_g eta B_u , bi grafikotan tratatu da, egoera hobeto aztertzeko.

A_g simetriarako, egoera singlete (Appendix E) eta tripletearen (8.31) arteko alde nagusia 1.go eta 2. egoeretan dago. Gauza jakina da, [4] estatu singleteen kasuan, diabatikoen arteko elkarrekintza handiagoa dela egoera tripleteena baino. Hala ere, LE/CT nahaste baxu hau nahikoa den tripleteen egoera kitzikatuen energiak modulatu eta A_g eta B_u estatuen artean konmutazio bat izateko.

A_g simetriei dagokienez, ikus daiteke translazio txikietarako, 0.0\AA - 1.5\AA , adiabatikoen eta diabatiko simetrikoaren artean aldentze bat dagoela, baina ez da horrela gertatzen B_u simetrian. Honek lotura zuzena du 8.30 irudiarekin. $D_e - D_h$ kurba maximoan dagoenean, energia energia adiabatikoa eta simetrizatutako diabatikoa hurruntzen dira. Puntu honetan, $D_e + D_h$ minimoa da, beraz, energia adiabatikoa eta diabatiko simetrizatuak batu egiten dira. Aldaketa sorta honetan, B_u simetriari dagokion disoziazioa txikiagoa da eta hau elkarrekintzaren balio energetiko txikiagoarekin justifika liteke; 80 meV A_g simetriarako eta 50 meV B_u simetriarako.

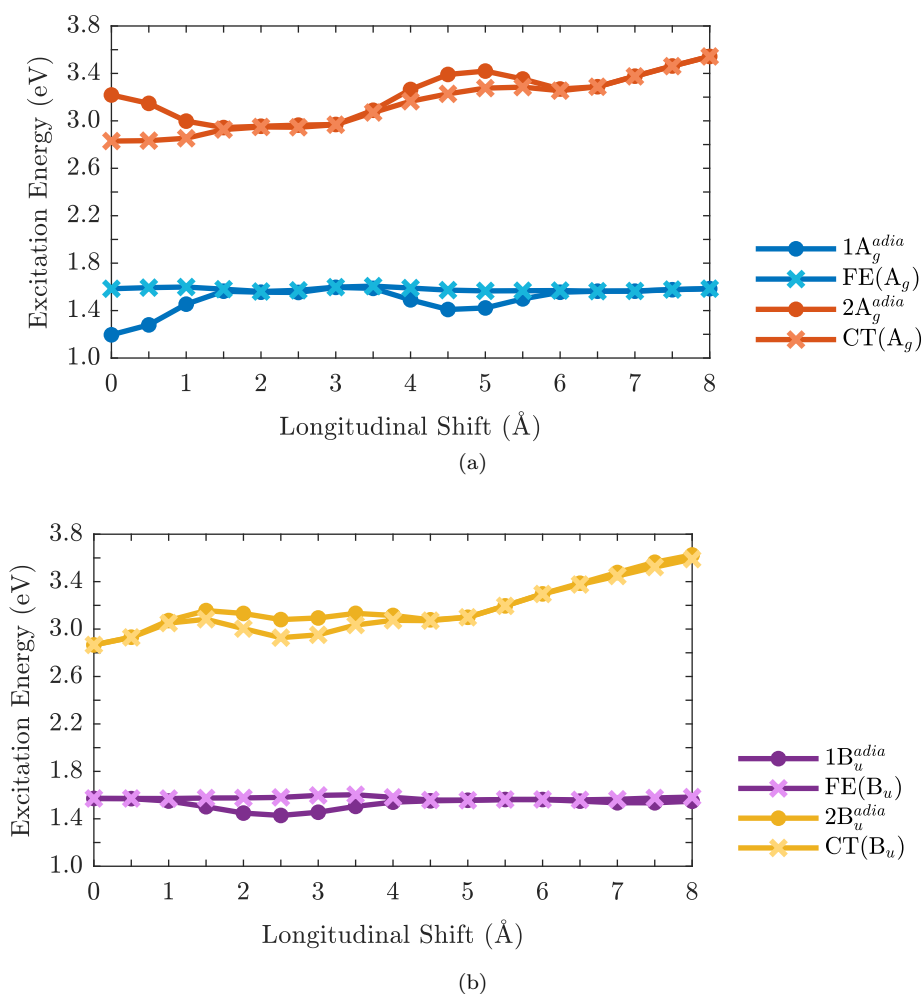


Figure 8.31: Energia adiabatiko (puntuak) eta simetrizatutako diabatikoa (ixa) (a) A_g simetria eta (b) B_u simetriarako TDA- ω B97X-D/6-31G* maila teorikoan kalkulatuak.

8.4.5.4 *Metodoen Konparaketa*

Atal honetan erabili den metodoa egoera diabatikoak kalkulatzeko HDS izan da, eta hemen oso garrantzitsua da OEMI-ren aukeraketa zuzena. Dena dela, posible da espazio guztia hartzea kontutan eta ER edo Boys diabatizazio eskemekin kalkulatzeko egoera diabatikoak. Hiru metodo hauen konparaketa 8.32 irudian agertzen da. Analisia bi konformerotan oinarritu da: eklipsatuan, 0.0 Å eta 2.5 Å-ra distortsionatuta.

1: Simple Diabatization Approach; 2: ER Method; 3: Boys Method

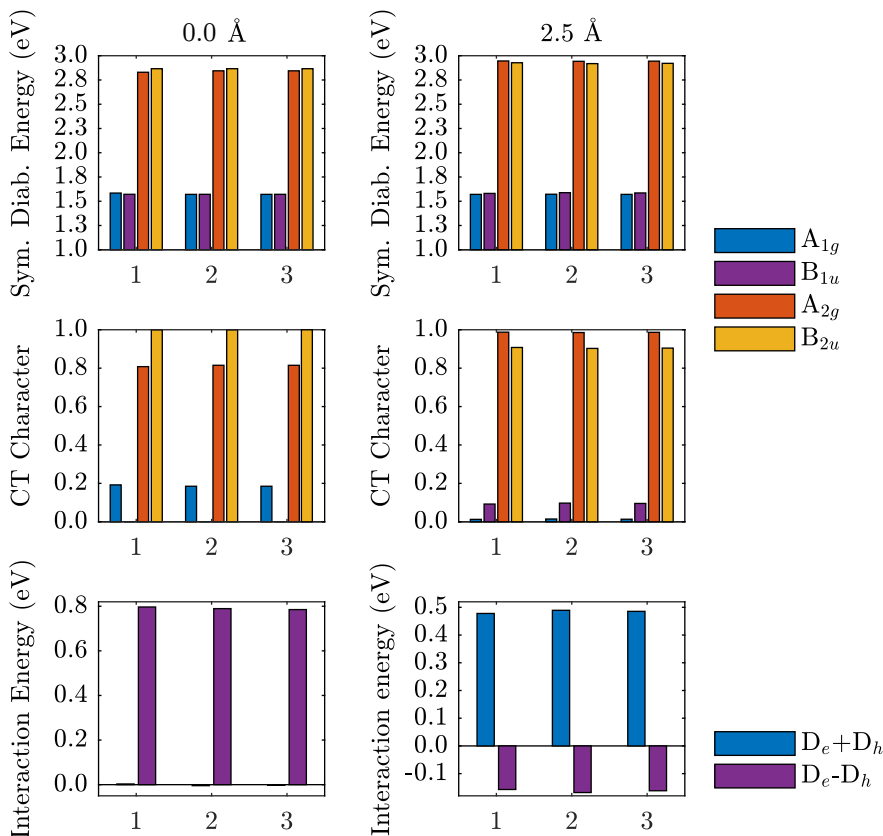


Figure 8.32: Energia diabatiko simetrikoaren (goian), CT izaeraren (erdian) eta elkarrekintza energiearen (behean) konparaketa hiru diabatizazio prozedura desberdinetarako. (i) MIOS zehatz batzentako, (ii) ER eskema eta (iii) Boys eskema (TDA)- ω B97X-D/6-31G* maila teorikoan kalkulaturak.

Ondorio gisa, aipatu hiru metodoek emaitza ia berdinak ematen dituztela. Analizatutako sistemaren egoera eszitatutak oso ongi deskribatzen direla HOMO-1, HOMO, LUMO eta LUMO+1 orbitalekin, egoera diabatikoak kalkulatzeko garatutako prozedura berriak ederki deskriba ditzake egoera diabatikoak.

8.4.6 Ondorioak

Amaitzeko, PDI molekularen egoera elektronikoko baxuak ezaugarritu dira. Lortutako emaitza konputazionalak PDIaren propietate fotofisiko eta intermolekulen arteko elkarrekintzetatik eratortzen diren efektuak arrazionalizatzen dituzte.

PDI deribatuak **1** dituen alboko lau fenilo-eraztunek PDI erdigunearen planarizazioa galtzea eragiten dute (txikia); Fermi mailaren inguruko partikula bakar-reko energiak pixka bat afinatuz, nahiz eta HOMO eta LUMO ia PDI nukleoan bakarrik badauden lokalizatuta. Nitrogeno atomoetako alkil katearen ordezkape-nak ia ez du eraginik balentzia elektroiaren propietateetan. Bestalde, R_1 eta R_2 ordezkape-nak garrantzi handia dute PDI molekulen agregazioan, alboetako elkar-reraginak asko mugatuz. Efektu hori argi eta garbi agertzen da **1** kristal-egituran, ongi bereizitako zutabe molekularretan antolatuta, zutabe barruko elkar-reragin elektronikoen indartsuekin eta zutabe arteko kontaktu ahulekin. Ezaugarri horrek ahalbidetzen du aurreikustea $\pi - \pi$ interakzioak nagusi direla **1**-ren propietate elektronikoen, kristalean eta, oro har, agregatu molekularretan.

Singlete eta triplete egoerarik baxuenetarako trantsizio elektronikoen HOMO \rightarrow LUMO elektroien bakarraren promozioei dagozkien, non alboko fenilo-eraztunek ez duten ekarpenik egiten. Egoera kitzikatu singlete baxuena asko egonkortzen da agregazioan. Efektu hori ezin da bakarrik azaldu singlete lokalizatuen eszitazio akoplamenduengatik, honi orbital molekularren gainjartzea, EL eta KT egoera diabatikoen arteko energia baxua eta LE/LE, LE/CT akoplamendu indartsuen lehia gehitu behar zaizkio. CT terminoen nahasketa nabarmena da dimero molekularretan kitzikatutako egoerarik baxueneko trantsizioan (trantsizioaren % 50 arte), honek baliogabe uzten du ikuspegi perturbatiboen erabilera tetraphenilozko PDI agregatuetan eta orokorren π -pilatutako PDI molekuletan.

$\pi - \pi$ elkarrekintzen bidezko egoera tripletearen erlaxazioa askoz ere leunagoa da egoera singletean baino. PDIn agregatu molekularrek elektroien-zulo bikote oso mugatuak erakusten dituzte egoera tripletean, eta, ondorioz, desparekatutako bi elektroien molekula bakar batean lokalizatzen dira. CT-en konfigurazioen eragina askoz ere ahulagoa da egoera tripletean. Bitxia bada ere, tripletean supertrukeko elkarrekintza singletean bezain indartsua da, baina ${}^3\text{LE}$ eta ${}^3\text{CT}$ ren arteko energia diferentzia handiak zaildu egiten du bere papera. Ondorio hau bereziki garrantzitsua da egoera tripletean CT izaera sendoa duten dimero molekularren, oligomeroen edo agregatuen diseinuan.

Tripletearen LE izaera sendoa neurri bateraino erlaxatu daiteke molekulen arteko $\pi - \pi$ elkarrekintzak handitzeko gai diren distorsio molekularren bidez, eta karga banatzeko energia egonkortuz. Horretarako, molekula arteko desplazamenduari erreparatu zaio.

Nahiz eta egoera tripleteak, egoera ilunak izan, singletean ematen den KT bidezko J-agregazio mekanismoaren antzeko izaera ikusi da desplazamendu longitudinal txikietan. Gainera, ikusi da nahiz eta irismen handiko bi funtzional desberdin erabili, LE/CT elkarrekintzen modulazioak bere horretan jarraitzen duela. Honen arrazoi nagusia da, LE eta CT egoeren arteko energia desberdintasuna nahikoa handia dela. Amaitzeko, diabatizazioa bi metodo desberdin erabilita egin da. Honen ondorio nagusia izan da, bi metodoek energia eta akoplamendu oso antzekoak ematen dituztela sistema honetarako behintzat. Hau da, aukeratutako MIOSe a gokia izan delako.

8.5 ONDORIO NAGUSIAK

Tesi honetan, sistema aromatikoaren egoera eszizatu tripletea aztertu da. Horretarako, lan idatzi hau bi bloke nagusitan banatu da. Lehenengoak egoera tripletearen oinarriko analisia egiten du eredu aromatikoaren sistema batzuetan; hala nola, bentzenoaren, naftalenoaren eta antrazenoaren konformero dimeriko desberdinetan. Sistema horietan egoera eszimerikorik ba ote dagoen ikustea izan da helburua. Eta lanaren PDI molekulari eta bere deribatuei dagokie. Honek xehetasunez aztertzen eta ezaugarritzen duitu PDI molekula eta honen deribatu jakin bat, PDI **2** bezala deitua izan dena.

Egoera kitzikatuak karakterizatzeko ikuspegi desberdinak daude eta lan honetan erabili dena egoera elektronikoaren deskonposizioa izan da. Horretarako, garrantzitsua da aztertutako monomeroa ondo ezagutzeko, dimeroen portaerari buruzko informazio garrantzitsua ematen duelako. Monomeroen analisiaren ondoren, dimeroetan barneratu eta bakoitzaren egoera ezaugarritzen saiatzen gara LE eta KT terminoetan.

Lehenengo zatian dimero aromatikoak aztertzen saiatu gara, batez ere, hauek izan dezaketen egoera eszimerikoan. Horretarako, lehenengo urratsa izan da egoera tripletearen portaera ulertzea dagozkien monomeroetan. Atal honetako alderdirik garrantzitsuen spin-dentsitatea aztertzea izan da. Horren arrazoia da bere deslokalizazioak berresten duela egoera tripletea molekularen gainean deslokalizatuta dagoela eta horrela gauza bera gerta daitekeela konformeroetan.

Egoera eszimerikoa aurkitzeko, konformero talde bat diseinatu da monomeroetako bat ardatz luze eta motzean distortsionatuz, baita konformero eklipsatua kontuan hartuz ere. Distortsio horiek guztiek minimo bat erakutsi dute PGEN, eta hiru egitura nagusi lortu dira sistema bakoitzarentzat: (i) dimero kobalenteak, (ii) triplete lokalizatua duten sistemak eta (iii) tripletea molekula osoan deslokalizatuta duten sistemak. Lehenengoak lotura formazio bat erakusten du OM eta spin dentsitate deslokalizatuekin. Bigarrenak eohikoa den π - π karbono-karbono distantzia eta MO eta spin dentsitate lokalizatuak erakusten ditu. Azken multzoak monomeroen arteko karbono-karbono bitarteko distantziari dagokie. Hauek ez dute inolako lotura formakuntzarik erakusten. Horretaz gain, MO eta spin dentsitateak lokalizatuak dituzte. Egoera eszimeriko baten aurrean egoteko, bi baldintza nagusi bete behar dira: (i) monomeroen arteko elkarrekintzak espazio bidezkoa izan behar du, hau da, inolako loturarik sortu gabe, eta (ii) egoera tripleteak sistema osoarena izan behar du, hau da, spin dentsitateak sistema osoan egon behar du deslokalizatua. Horregatik, bitarteko karbono-karbono distantziarekin bat datozenak dira ikerketarekin jarraitzeko hautagairik onenak.

Spin-aren deslokalizazioaz gain, garrantzitsua da kitzikatutako egoera tripletearen analisia ere. T_1 egoera adiabatikoaren osaerari dagokionez, ikusi da CTren parte-hartzea ez dela hutsala, sistema guztietan bere pisua % 10etik gorakoa baita. Emaitza bera lortu da kualitatiboki eta kuantitatiboki.

Elektroi baten dentsitatearen matrizearen deskonposizioaren grafikazioan ikusi dugu T_1 -ak erakusten duen nahasketa, LE eta CT egoeretan ondo definituta deskon-

posatu daitekeela. Gainera, ikusi ahal izan dugu zeintzuk diren estatu diabatiko bakoitzean parte hartzen duten atomoen taldeak. Estatu diabatizazioari esker, LE eta CT estatuak energia batekin kuantifikatu dira. Ikusi dugu estatu diabatikoak hurbiltzen doazela sistemak handitzen diren bitartean. Gainera, beste alderdi garrantzitsu bat LE eta CT estatu arteko elkarrekintza aztertzea izan da. Nahiz eta propietate hori meV-tan eman, ikusi dugu balio horiek altuak direla oraindik, eta hori bat dator CT-ren egoera adiabatikoan zuen pisuarekin. Baieztapen hauek direla medio, esan daiteke bentzeno, naftaleno eta antrazeno molekulen konformero eklipsatuek egoera triplete eszimerikoa aurkezten dutela.

Bigarren zatia PDI molekulari eta bere deribatuei dagokie. Molekularen kasuan ikusi dugu egitura elektronikoaren analisisian MO adierazgarriek barneko CT bat erakusten dutela. Horren arrazoia da HOMO-2 eta HOMO-1 MO molekularen gune batean lokalizatuta daudela, eta HOMO, LUMO+1 eta LUMO+2 molekula osoan deslokalizatuta daudela. Kitzikatutako egoera elektronikoak DFT funtzional desberdinekin kalkulatu dira. Kasu honetan, B3LYP baztertu egin da CT estatuaren energia gutxiesten duelako. Horregatik egin da azterketa gehiago CAM-B3LYP-rekin.

Agregatuaren kasuan, lehenik eta behin trantsizio egoereren singlete eta triplete baxuenak karakterizatzea izan da. Karakterizazio honek adierazi du HOMO \rightarrow LUMO trantsizioa dela pisu handiena duena. Bestalde, bai singletea baita tripletea ere egonkortu egiten dira, PDI agregatuak 6 unitate hartzen dituenenak. Singlete lokalizatuen akoplamendu eszitonikoaz gain, egonkortzea MO-ren gainjartzearekin, LE eta CT egoeren arteko alde energetiko txikiarekin eta LE/LE eta LE/CT akoplamendu indartsuekin ere azal daiteke. Egoera tripletearen erlaxazioaren kasuan π - π interakzioak ez dira egoera singletean bezain indartsuak. Elektroi-zulo pareak oso mugatuta daude eta beraz, CT-ren inpaktua ahulagoa da.

Dena den, elkarrekintzat handitzeko asmoz, distortsio molekularrak gai dira π - π elkarrekintza intermolekularrak handitzeko eta karga energia banaketa egonkortzeko. Hau PDIn hirugarren zatiari dagokigo, hau da, PDI **3**-z osatuta dagoen modelo dimerikoari. Emaitzarik harrigarrietako bat da, nahiz eta tripleteak egoera ilunak izan, CT-ren bitarteko J-agregazio mekanismoa antzeman daiteke.

Beste gauza bat ere aipatu behar da: estatu adiabatikoak deskonposatzeko erabiltzen den metodoa, LE eta CT egoerei dagokienez. Orain arte, deskonposizioa ER metodoaren bidez egiten izan da, baina hemen SDA erabili da. Azken metodo honetan MOISen (Espazio Orbital Minimoa) oinarritzen bada ere, lan honen azken atalak erakusten du bi metodoek balio ia berdinak ematen dituztela sistema honetarako gutxienez.

Oro har, ikusi dugu egoera tripleteek zeregin garrantzitsua izan dezaketela optoelektronikaren arloan etorkizun handiko molekula organiko ezberdinen propietateetan. Kasu horietan, aztertutako sistemek elkarrekintza ona erakusten dute LE eta CT egoeren artean, zeinak etorkizun handiko aplikazioak izan ditzaketen, nahiz eta prozesurik ohikoenak aztertu ez diren, hala nola, Singlete Fisioa (SF) edo TTermikoki Aktibatutako Fluoreszentzia Atzeratua (TADF). Gainera, ikusi dugu sistema guztietan egoera tripletea aztertzeko erabiltzen diren tresnak nahikoak

dira egoera tripletearen informazioa lortzeko. Horregatik, analisi honek erakutsi du CTren izaera oso garrantzitsua dela sistema desberdinen egoera tripletean.

Appendix A

DENSITY FUNCTIONAL APPROXIMATION

Even if the Kohn-Sham formalism is exact, E_{xc} and V_{xc} are unknown except for the electron gas. Because of this some approximations have to be done.

A.1 LOCAL DENSITY APPROXIMATION (LDA)

The first of these approximations is called Local Density Approximation [65]. Here, each volume element with a local density $\rho(\vec{r})$ is considered to be a homogeneous electron gas. In the case where the density variation is slow, the approximation would be accurate and would have the following form,

$$E_{xc}^{LDA}[\rho] = \int \rho(\vec{r})\varepsilon_{xc}(\rho)d\vec{r} \quad (\text{A.1})$$

where $\varepsilon_{xc}(\rho)$ is sum of the exchange and correlation energy per electron in a homogeneous electron gas with electron density ρ . In the case of open-shell systemsthe Local Spin Density Approximation is used where ρ is replaced by ρ^α and ρ^β , for electrons with different spins.

A.2 GENERALIZED GRADIENT APPROXIMATION (GGA)

As ρ is not homogeneous, LDA has been improved using more sophisticated methods. To take into account the inhomogeneous character of ρ , its variation with respect to the distance is introduced as a gradient,

$$E_{xc}^{GGA}[\rho] = \int f(\rho, \nabla\rho) dr \quad (\text{A.2})$$

These type of methods known as generalized gradient approximations (GGA) have become important to study molecules because it enables to consider a inhomogeneous electron density. In general, E_{xc}^{GGA} is divided into the exchange and correlation contributions,

$$E_{xc}^{GGA} = E_x^{GGA} + E_c^{GGA} \quad (\text{A.3})$$

In some exchange functionals the the expression of E_{xc}^{GGA} is the following,

$$E_x^{GGA} = E_x^{LDA} + E_x^{LSDA} = E_x^{LDA} + \int f(s)\rho^{\frac{4}{3}} dr \quad (\text{A.4})$$

where $f(s)$ si a function of the reduced density gradient: $s = \frac{|\nabla\rho|}{\rho^{\frac{4}{3}}}$. With this, the adimensional parameter s takes into account the inhomogeneous character of ρ .

A.3 META-GENERALIZED GRADIENT APPROXIMATION (MGGA)

With the aim to improve the previously explained GGA methods, the Laplacian of the density , $\nabla^2\rho(r)$, and/or the local kinetic energy density are introduced,

$$\tau(r) = \frac{1}{2} \sum_{i=1}^{N_{occ}} |\nabla\theta_i(r)|^2 \quad (\text{A.5})$$

where θ_i are the Kohn-Sham orbitals. These functionals are known as meta-GGA (mGGA) and follow the next expression,

$$E_{xc}^{mGGA}[\rho] = \int f(\rho, \nabla\rho, \nabla^2\rho) dr \quad (\text{A.6})$$

A.4 HYBRID FUNCTIONALS

To have a correct description of the molecular system the exchange energy is fundamental, and so the hybrid functionals might be a good choice because they are based on the combination of the Hartree-Fock exchange and DFT correlation. In this type of functionals, the two limiting systems, the non-interacting (Kohn-Sham) and the real one, are connected by a coupling parameter λ operating on the electron interaction as,

$$\hat{H}^\lambda = \sum_{i=1}^N -\frac{1}{2}\nabla_i^2 + \sum_{i=1}^N \hat{v}_s^\lambda(i) + \sum_{i=1}^N \sum_{j>i}^N \frac{\lambda}{r_i - r_j} \quad (\text{A.7})$$

where, the non-interacting system has a value of $\lambda=0$ and the real system $\lambda=1$. For intermediate values of λ , the effective external potential \hat{v}_s^λ changes in order to keep the density always as the real density of the system, being $\rho(r)$ independent from λ .

Appendix B

LONG-RANGE CORRECTED DENSITY FUNCTIONAL THEORY

Even if the representation of exchange-correlation functionals has been done using local quantities at a reference point, such as, electron density or gradient density, it has been seen that these functionals overestimate the local contributions and underestimate the non-local ones, *i.e.* van der Waals interactions or charge-transfer processes. One of the most significant non-local contribution might be the long-range electron-electron exchange correlation due to the impossibility to represent the interaction as a functional of a one-electron quantity [182], [183].

In such functionals the long-range HF exchange [184], [185] is smoothly included. This seems to be successful to calculate CT states in different systems. The Hamiltonian's Coulomb operator is divided in two different components: short-range and long-range. These are obtained through the error function,

$$\frac{1}{r_{12}} = \frac{1 - \text{erf}(\omega r_{12})}{r_{12}} + \frac{\text{erf}(\omega r_{12})}{r_{12}} \quad (\text{B.1})$$

where $\frac{1}{r_{12}}$ corresponds to the long-range component and $\frac{1 - \text{erf}(\omega r_{12})}{r_{12}}$ corresponds to the short-range component. When $r_{12} \approx \frac{1}{\omega}$ this short-range component decays to zero. On the other hand, the ω parameter determines the proportion for each of the components and depends on r_{12} . This last parameter is determined either empirically or by physical arguments [108].

Appendix C

PDI MOLECULE

Table C.1: Vertical excitation energies (in eV) and oscillator strengths (in parenthesis) to the lowest singlet and triplet excited states computed at CAM-B3LYP/6-311+G(d) level for the PDI **2**. Orbital-to-orbital composition correspond to TDA transitions. H=HOMO; L=LUMO.

State	TDDFT	TDA	Composition
S ₁	2.94(0.699)	3.11(0.945)	94 % H→L
S ₂	3.37(0.043)	3.42(0.054)	75 % H-1→L
S ₃	3.54(0.279)	3.57(0.285)	72 % H-2→L
S ₄	3.85(0.012)	3.88(0.016)	69 % H-3→L
S ₅	3.94(0.004)	3.96(0.006)	44 % H-9→L
T ₁	1.47	1.92	88% H→L
T ₂	2.66	2.92	41% H-1→L,18% H→L+1
T ₃	2.88	3.01	21% H-1→L,16% H→L+1
T ₄	3.00	3.09	53% H-2→L
T ₅	3.08	3.30	75% H-1→L

Appendix D

PDI AGGREGATE

D.1 *INTRA*- AND *INTER*-COLUMN PDI DIMERS

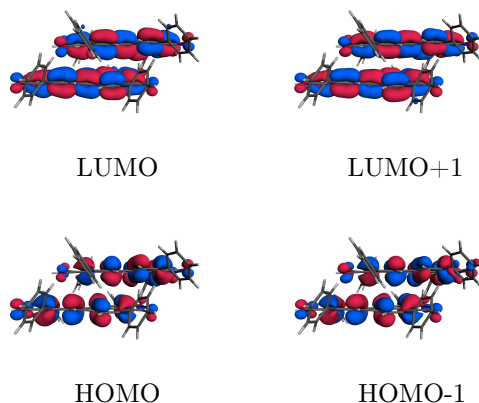


Figure D.1: Molecular orbital diagram of **D2** computed at the TDA, CAM-B3LYP/6-31G(d) level.

Table D.1 shows low-lying singlet and triplet excited state energies and oscillator strengths for the *intra* and *inter* column dimers of PDI from the crystal structure of **1**. Excited state distribution in the *inter*-dimer, near degeneracy between pairs of states, indicates weak coupling. Energy splitting between low-lying states is much larger for the *intra*-dimer.

Table D.1: Excitation energies (in eV) and oscillator strengths (f) to the lowest singlet and triplet excited states of *inter*-column and *intra*- (**D2**) dimers computed at the TDA, CAM-B3LYP/6-31G(d) level.

state	<i>inter</i>		<i>intra</i>	
	ΔE	f	ΔE	f
S ₁	3.17	2.042	3.04	0.0000
S ₂	3.19	0.021	3.12	1.1228
S ₃	3.38	0.116	3.29	0.0000
S ₄	3.47	0.056	3.38	0.5012
S ₅	3.60	0.421	3.42	0.0000
S ₆	3.61	0.035	3.43	0.2152
T ₁	1.93	-	1.92	-
T ₂	1.94	-	1.94	-
T ₃	2.89	-	2.94	-
T ₄	2.94	-	2.94	-
T ₅	3.04	-	2.96	-
T ₆	3.04	-	2.97	-

Table D.2: Excitation energies (in eV) and oscillator strengths (f) to the lowest singlet and triplet excited states of *inter*-column and *intra*- (**D2**) dimers computed at the TDA, ω B97X-D/6-31G(d) level.

state	<i>inter</i>		<i>intra</i>	
	ΔE	f	ΔE	f
S ₁	3.21	2.049	3.08	0.000
S ₂	3.23	0.017	3.19	1.442
S ₃	3.48	0.119	3.47	0.000
S ₄	3.55	0.057	3.49	0.218
S ₅	3.68	0.487	3.53	0.000
S ₆	3.69	0.002	3.57	0.188
T ₁	1.99	-	1.98	-
T ₂	1.99	-	1.99	-
T ₃	2.96	-	2.99	-
T ₄	3.00	-	3.00	-
T ₅	3.09	-	3.03	-
T ₆	3.10	-	3.04	-

D.2 PDI PENTAMER

Table D.3: Vertical excitation energies (in eV) and oscillator strengths (in parenthesis) to the lowest singlet and triplet excited states computed at B3LYP/6-31G(d) level for the PDI pentamer. Orbital-to-orbital composition correspond to TDA transitions. H=HOMO; L=LUMO

State	TDDFT	TDA	Composition
S ₁	2.13(0.356)	2.13(0.362)	90% H→L
S ₂	2.16(0.002)	2.16(0.002)	79% H-1→L
S ₃	2.21(0.020)	2.20(0.021)	43% H-2→L
S ₄	2.22(0.000)	2.22(0.001)	36% H→L+1
S ₅	2.26(0.216)	2.27(0.222)	57% H-1→L+1
T ₁	1.50	2.06	53% H→L
T ₂	1.51	3.08	40% H-1→L
T ₃	1.56	3.26	36% H-2→L+2
T ₄	1.61	3.35	26% H-3→L
T ₅	1.64	3.46	27% H-4→L

Table D.4: Vertical excitation energies (in eV) and oscillator strengths (in parenthesis) to the lowest singlet and triplet excited states computed at wB97X/6-31G(d) level for the PDI pentamer. Orbital-to-orbital composition correspond to TDA transitions. H=HOMO; L=LUMO

State	TDDFT	TDA	Comp.
S ₁	3.17(0.010)	3.17(0.010)	26% H-1→L
S ₂	3.20(0.227)	3.20(0.228)	13% H-4→L
S ₃	3.26(0.925)	3.26(0.927)	30% H→L
S ₄	3.27(1.005)	3.27(1.028)	19% H-1→L+1
S ₅	3.35(1.279)	3.35(1.300)	42% H-2→L+2
T ₁	1.39	2.01	30% H→L
T ₂	1.40	2.01	25% H-1→L
T ₃	1.44	2.06	40% H-2→L+2
T ₄	1.46	2.07	20% H-3→L
T ₅	1.48	2.08	21% H-4→L

D.3 DIABATIC STATES OF PDI DIMERS

Table D.5: Transition energies (in eV), oscillator strengths (in parenthesis), and diabatic contributions ω (in %) obtained through the ER diabatization for four excited singlet and triplet states of **D1** and **D2** dimers computed at the (TDA) CAM-B3LYP/6-31G(d) level. Diabatic states correspond to the ones mainly obtained as H,H-1 \rightarrow L,L+1 electronic promotions. $LE_A = A^*B$, $LE_B = AB^*$, $CT_{AB} = A^+B^-$, $CT_{BA} = A^-B^+$.

state	ΔE (f)	$\omega(LE_A)$	$\omega(LE_B)$	$\omega(CT_{AB})$	$\omega(CT_{BA})$
D1 dimer					
S _{1,+}	2.96 (1.009)	25	25	25	25
S _{2,-}	3.04 (0.000)	48	48	2	2
S _{3,-}	3.27 (0.000)	2	2	48	48
S _{8,+}	3.58 (0.645)	25	25	25	25
T _{1,+}	1.87	47	47	3	3
T _{2,-}	1.95	50	50	0	0
T _{9,-}	3.26	0	0	50	50
T _{11,+}	3.33	3	3	47	47
D2 dimer					
S _{1,-}	3.04 (0.000)	48	48	2	2
S _{2,+}	3.12 (1.123)	26	26	24	24
S _{3,-}	3.29 (0.000)	2	2	48	48
S _{4,+}	3.38 (0.502)	24	24	26	26
T _{1,-}	1.92	49	49	1	1
T _{2,+}	1.94	50	50	0	0
T _{9,-}	3.29	0	0	50	50
T _{12,+}	3.35	1	1	49	49

Table D.6: Diabatic electronic energies (in eV) and electronic couplings obtained through the Boys diabatization of the four lowest excited singlets and triplet states of the PDI *intra*-dimers **D1** (unit cell) computed at the (TDA) CAM-B3LYP/6-31G(d) level.

dimer	$E(^1\text{LE})$	$E(^1\text{CT})$	V_{DC}	V_e	V_h	V_{CT}
D1	3.16	3.27	105	-176	-134	-3
dimer	$E(^3\text{LE})$	$E(^3\text{CT})$	V_{DC}	V_e	V_h	V_{CT}
D1	1.95	3.25	0	-183	-145	-3

Table D.7: Transition energies (in eV), oscillator strengths (in parenthesis), and diabatic contributions ω (in %) obtained through the Boys diabatization for four excited singlet and triplet states of **D1** dimer computed at the (TDA) CAM-B3LYP/6-31G(d) level. Diabatic states correspond to the ones mainly obtained as H_iH_j-1→L_iL_j+1 electronic promotions. $\text{LE}_A = \text{A}^*\text{B}$, $\text{LE}_B = \text{AB}^*$, $\text{CT}_{AB} = \text{A}^+\text{B}^-$, $\text{CT}_{BA} = \text{A}^-\text{B}^+$.

state	ΔE (f)	$\omega(\text{LE}_A)$	$\omega(\text{LE}_B)$	$\omega(\text{CT}_{AB})$	$\omega(\text{CT}_{BA})$
S _{1,+}	2.96 (1.009)	25	25	25	25
S _{2,-}	3.04 (0.000)	48	48	2	2
S _{3,-}	3.27 (0.000)	2	2	48	48
S _{8,+}	3.58 (0.645)	25	25	25	25
T _{1,+}	1.87	47	47	3	3
T _{2,-}	1.95	50	50	0	0
T _{9,-}	3.26	0	0	50	50
T _{11,+}	3.33	3	3	47	47

D.4 TRIPLET EXCITONS ALONG INTERMOLECULAR DISTORTIONS

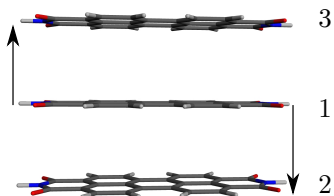


Figure D.2: Molecular trimer of PDI **3**. Numbers indicate molecular labelling in Tables D.8-D.17.

Table D.8: Diabatic electronic energies (in eV) and electronic couplings (in meV) obtained through the ER diabatization of the seven lowest excited triplet states of the eclipsed trimer along the vertical distortion (3.7 Å) computed at the (TDA) CAM-B3LYP/6-31G(d) level. $LE_1 = 1^*23$, $LE_2 = 12^*3$, $LE_3 = 123^*$, $CT_{12} = 1^+2^-3$, $CT_{13} = 1^+23^-$, $CT_{21} = 1^-2^+3$, $CT_{31} = 1^-23^+$.

H_{diab}	3LE_1	3LE_3	3LE_2	${}^3CT_{31}$	${}^3CT_{21}$	${}^3CT_{12}$	${}^3CT_{13}$
3LE_1	1.69	6	6	-219	219	230	-230
3LE_3	6	1.70	-3	239	7	10	231
3LE_2	6	-3	1.70	-7	-239	-231	-10
${}^3CT_{31}$	-219	239	-7	2.87	10	84	-7
${}^3CT_{21}$	219	7	-239	10	2.87	-7	84
${}^3CT_{12}$	230	10	-231	84	-7	2.95	0
${}^3CT_{13}$	-230	231	-10	-7	84	0	2.95

Table D.9: Diabatic electronic energies (in eV) and electronic couplings (in meV) obtained through the ER diabatization of the seven lowest excited triplet states of the eclipsed trimer along the vertical distortion (4.0 Å) computed at the (TDA) CAM-B3LYP/6-31G(d) level. $LE_1 = 1^*23$, $LE_2 = 12^*3$, $LE_3 = 123^*$, $CT_{12} = 1^+2^-3$, $CT_{13} = 1^+23^-$, $CT_{21} = 1^-2^+3$, $CT_{31} = 1^-23^+$.

H_{diab}	3LE_1	3LE_3	3LE_2	${}^3CT_{31}$	${}^3CT_{21}$	${}^3CT_{12}$	${}^3CT_{13}$
3LE_1	1.70	1	1	139	139	-148	-148
3LE_3	1	1.70	0	-151	2	-3	142
3LE_2	1	0	1.70	2	-151	142	-3
${}^3CT_{31}$	139	-151	2	3.00	-3	35	2
${}^3CT_{21}$	139	2	-151	-3	3.00	2	35
${}^3CT_{12}$	-148	-3	142	35	2	3.08	0
${}^3CT_{13}$	-148	142	-3	2	35	0	3.08

Table D.10: Diabatic electronic energies (in eV) and electronic couplings (in meV) obtained through the ER diabatization of the seven lowest excited triplet states of the eclipsed trimer along the vertical distortion (4.2 Å) computed at the (TDA) CAM-B3LYP/6-31G(d) level. $LE_1 = 1^*23$, $LE_2 = 12^*3$, $LE_3 = 123^*$, $CT_{12} = 1^+2^-3$, $CT_{13} = 1^+23^-$, $CT_{21} = 1^-2^+3$, $CT_{31} = 1^-23^+$.

H_{diab}	3LE_1	3LE_3	3LE_2	${}^3CT_{31}$	${}^3CT_{21}$	${}^3CT_{12}$	${}^3CT_{13}$
3LE_1	1.70	0	0	101	101	109	109
3LE_3	0	1.70	0	1	-110	-102	1
3LE_2	0	0	1.70	-110	1	1	-102
${}^3CT_{31}$	101	1	-110	3.06	-1	-19	-1
${}^3CT_{21}$	101	-110	1	-1	3.06	-1	-19
${}^3CT_{12}$	109	-102	1	-19	-1	3.15	0
${}^3CT_{13}$	109	1	-102	-1	-19	0	3.15

Table D.11: Diabatic electronic energies (in eV) and electronic couplings (in meV) obtained through the ER diabatization of the seven lowest excited triplet states of the eclipsed trimer along the vertical distortion (4.8 Å) computed at the (TDA) CAM-B3LYP/6-31G(d) level. $LE_1 = 1^*23$, $LE_2 = 12^*3$, $LE_3 = 123^*$, $CT_{12} = 1^+2^-3$, $CT_{13} = 1^+23^-$, $CT_{21} = 1^-2^+3$, $CT_{31} = 1^-23^+$.

H_{diab}	3LE_2	3LE_3	3LE_1	${}^3CT_{31}$	${}^3CT_{21}$	${}^3CT_{12}$	${}^3CT_{13}$
3LE_2	1.70	0	0	0	-38	34	0
3LE_3	0	1.70	0	-38	0	0	34
3LE_1	0	0	1.70	34	34	-38	-38
${}^3CT_{31}$	0	-38	34	3.21	0	2	0
${}^3CT_{21}$	-38	0	34	0	3.21	0	2
${}^3CT_{12}$	34	0	-38	2	0	3.30	0
${}^3CT_{13}$	0	34	-38	0	2	0	3.30

Table D.12: Diabatic electronic energies (in eV) and electronic couplings (in meV) obtained through the ER diabatization of the seven lowest excited triplet states of the eclipsed trimer along the vertical distortion (5.3 Å) computed at the (TDA) CAM-B3LYP/6-31G(d) level. $LE_1 = 1^*23$, $LE_2 = 12^*3$, $LE_3 = 123^*$, $CT_{12} = 1^+2^-3$, $CT_{13} = 1^+23^-$, $CT_{21} = 1^-2^+3$, $CT_{31} = 1^-23^+$.

H_{diab}	3LE_3	3LE_2	3LE_1	${}^3CT_{31}$	${}^3CT_{21}$	${}^3CT_{12}$	${}^3CT_{13}$
3LE_3	1.70	0	0	-13	0	0	-12
3LE_2	0	1.70	0	0	-13	12	0
3LE_1	0	0	1.70	12	12	-13	13
${}^3CT_{31}$	-13	0	12	3.30	0	0	0
${}^3CT_{21}$	0	-13	12	0	3.30	0	0
${}^3CT_{12}$	0	12	-13	0	0	3.39	0
${}^3CT_{13}$	-12	0	13	0	0	0	3.39

Table D.13: Transition energies (in eV), oscillator strengths (in parenthesis), and diabatic contributions ω (in %) obtained through the ER diabatization for the lowest seven excited triplet states of the eclipsed trimer along the vertical distortion computed at the (TDA) CAM-B3LYP/6-31G(d) level. 3.7 Å displacement.

	T _{1,+}	T _{2,-}	T _{3,+}	T _{4,+}	T _{5,+}	T _{6,-}	T _{7,-}
ΔE (f)	1.46 (-)	1.61 (-)	1.70 (-)	2.83 (-)	2.97 (-)	3.07 (-)	3.09 (-)
$\omega(\text{LE}_1)$	57	0	33	0	3	6	0
$\omega(\text{LE}_3)$	14	47	33	0	1	2	3
$\omega(\text{LE}_2)$	14	47	34	0	1	2	3
$\omega(\text{CT}_{31})$	5	2	0	31	45	2	17
$\omega(\text{CT}_{21})$	4	2	0	31	45	2	17
$\omega(\text{CT}_{12})$	3	1	0	19	3	43	30
$\omega(\text{CT}_{13})$	3	1	0	19	2	43	30

Table D.14: Transition energies (in eV), oscillator strengths (in parenthesis), and diabatic contributions ω (in %) obtained through the ER diabatization for the lowest seven excited triplet states of the eclipsed trimer along the vertical distortion computed at the (TDA) CAM-B3LYP/6-31G(d) level. 4.0 Å displacement.

	T _{1,+}	T _{2,-}	T _{3,+}	T _{4,+}	T _{5,+}	T _{6,-}	T _{7,-}
ΔE (f)	1.61 (-)	1.67 (-)	1.70 (-)	3.00 (-)	3.04 (-)	3.12 (-)	3.13 (-)
$\omega(\text{LE}_1)$	63	0	32	0	2	0	2
$\omega(\text{LE}_3)$	15	49	34	0	0	1	1
$\omega(\text{LE}_2)$	15	49	34	0	0	1	1
$\omega(\text{CT}_{31})$	3	1	0	40	49	9	0
$\omega(\text{CT}_{21})$	2	1	0	40	49	9	0
$\omega(\text{CT}_{12})$	1	0	0	10	0	40	48
$\omega(\text{CT}_{13})$	1	0	0	10	0	40	48

Table D.15: Transition energies (in eV), oscillator strengths (in parenthesis), and diabatic contributions ω (in %) obtained through the ER diabatization for the lowest seven excited triplet states of the eclipsed trimer along the vertical distortion computed at the (TDA) CAM-B3LYP/6-31G(d) level. 4.2 Å displacement.

	T _{1,+}	T _{2,-}	T _{3,+}	T _{4,+}	T _{5,+}	T _{6,-}	T _{7,-}
ΔE (f)	1.65 (-)	1.69 (-)	1.70 (-)	3.06 (-)	3.08 (-)	3.16 (-)	3.17 (-)
$\omega(\text{LE}_1)$	65	0	32	0	2	0	2
$\omega(\text{LE}_3)$	16	49	34	0	0	0	0
$\omega(\text{LE}_2)$	16	49	34	0	0	0	0
$\omega(\text{CT}_{31})$	1	1	0	46	49	4	0
$\omega(\text{CT}_{21})$	1	1	0	46	49	4	0
$\omega(\text{CT}_{12})$	1	0	0	4	0	46	49
$\omega(\text{CT}_{13})$	1	0	0	4	0	46	49

Table D.16: Transition energies (in eV), oscillator strengths (in parenthesis), and diabatic contributions ω (in %) obtained through the ER diabatization for the lowest seven excited triplet states of the eclipsed trimer along the vertical distortion computed at the (TDA) CAM-B3LYP/6-31G(d) level. 4.8Å displacement.

	T _{1,+}	T _{2,-}	T _{3,+}	T _{4,+}	T _{5,+}	T _{6,-}	T _{7,-}
ΔE (f)	1.70 (-)	1.70 (-)	1.70 (-)	3.21 (-)	3.21 (-)	3.30 (-)	3.30 (-)
$\omega(\text{LE}_1)$	17	50	33	0	0	0	0
$\omega(\text{LE}_3)$	17	50	33	0	0	0	0
$\omega(\text{LE}_2)$	66	0	34	0	0	0	0
$\omega(\text{CT}_{31})$	0	0	0	50	50	0	0
$\omega(\text{CT}_{21})$	0	0	0	50	50	0	0
$\omega(\text{CT}_{12})$	0	0	0	0	0	50	50
$\omega(\text{CT}_{13})$	0	0	0	0	0	50	50

Table D.17: Transition energies (in eV), oscillator strengths (in parenthesis), and diabatic contributions ω (in %) obtained through the ER diabatization for the lowest seven excited triplet states of the eclipsed trimer along the vertical distortion computed at the (TDA) CAM-B3LYP/6-31G(d) level. 5.3Å displacement.

	T _{1,+}	T _{2,-}	T _{3,+}	T _{4,+}	T _{5,+}	T _{6,-}	T _{7,-}
ΔE (f)	1.70 (-)	1.70 (-)	1.70 (-)	3.30 (-)	3.30 (-)	3.30 (-)	3.30 (-)
$\omega(\text{LE}_1)$	28	0	22	0	0	0	0
$\omega(\text{LE}_3)$	28	50	22	0	0	0	0
$\omega(\text{LE}_2)$	44	50	56	0	0	0	0
$\omega(\text{CT}_{31})$	0	0	0	51	49	0	0
$\omega(\text{CT}_{21})$	0	0	0	49	51	0	0
$\omega(\text{CT}_{12})$	0	0	0	0	0	53	47
$\omega(\text{CT}_{13})$	0	0	0	0	0	47	53

Appendix E

SINGLET EXCITON STATE RESULTS FOR THE DIABATIC PROCEDURE

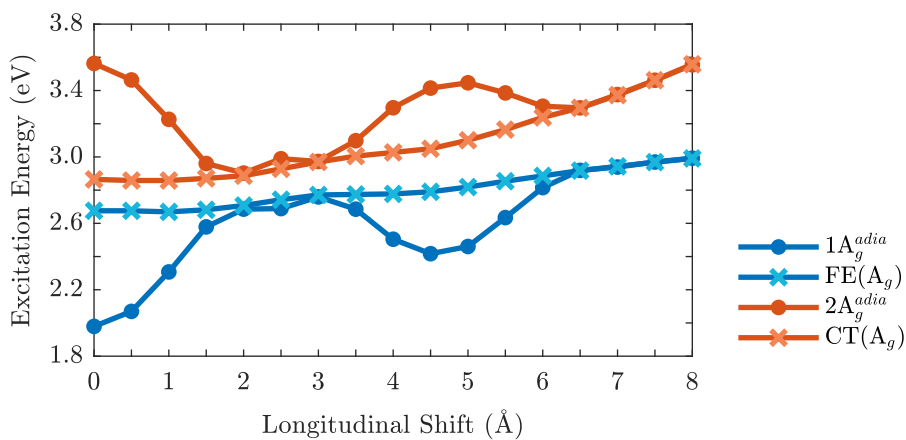


Figure E.1: Energy profile (TDA- ω B97XD/6-31G(d)) of (dot) A_g adiabatic states and (cross) A_g LE and CT states for the PDI dimer along the longitudinal translation coordinate.

Appendix F

SMALL AROMATIC EXCIMERS

F.1 MONOMER MOLECULAR STRUCTURE

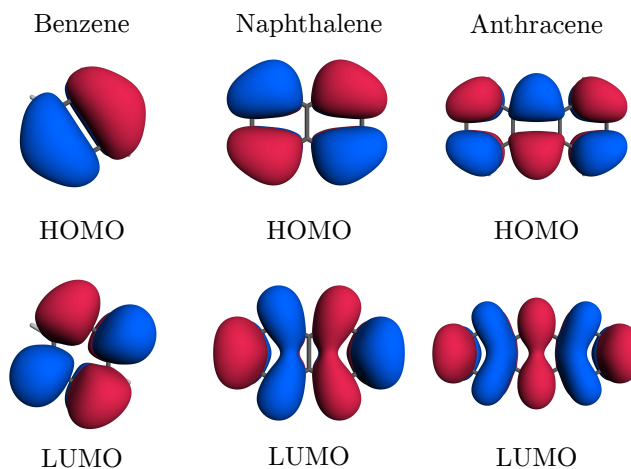


Figure F.1: MOs of the aromatic monomer systems.

F.2 AROMATIC DIMERS

F.2.1 Relative Energies

Table F.1: Intermolecular distances [d_{inter} (Å)], relative energies [E_{rel} (kcal/mol)], interaction energies [E_{int} (kcal/mol)] and binding energies [E_{bind} (kcal/mol)] for the most representative obtained minima for each of the systems. All computed at ω B97XD/cc-pVTZ level of theory.

Distortion	d_{inter}	E_{rel}	E_{int}	E_{bind}
Benzene				
eclipsed	3.843	1.335	-1.963	-1.963
long	3.540	0.000	-3.119	-3.106
short	3.513	0.034	-3.128	-3.139
Naphthalene				
eclipsed	3.722	2.247	-4.778	-4.778
long	3.543	0.344	-6.687	-6.632
short	3.436	0.000	-7.160	-6.862
Anthracene				
eclipsed	3.699	2.976	-7.724	-7.724
long	3.589	0.522	-10.178	-10.162
short	3.419	0.000	-11.417	-11.595

F.2.2 Intermediate Carbon-Carbon Distance

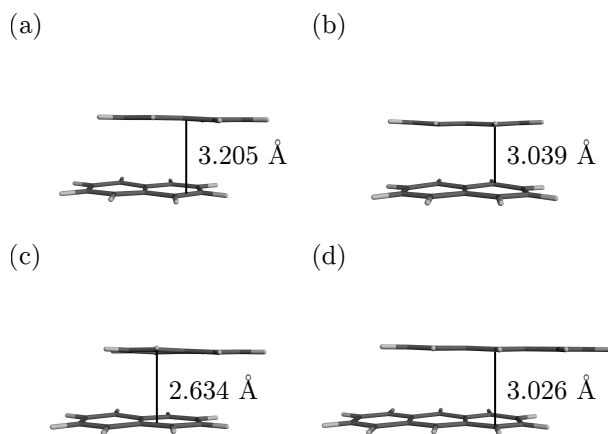


Figure F.2: Structures corresponding to different intermediate carbon-carbon distance. (a) naphthalene distorted in the long axis, (b) naphthalene distorted in the short axis; (c) naphthalene distorted in the xy plane, (d) anthracene distorted in the long axis.

BIBLIOGRAPHY

- [1] Y. Dai, **Zubiria-Ulacia, Maria**, D. Casanova, and F. Negri, “Impact of Charge-Resonance Excitations on CT-Mediated J-Type Aggregation in Singlet and Triplet Exciton States of Perylene Di-Imide Aggregates: A TDDFT Investigation,” *Computation*, vol. 10, no. 2, p. 18, 2022.
- [2] S. Medina Rivero, J. Urieta-Mora, A. Molina-Ontoria, *et al.*, “A Trapezoidal Octacyanoquinoid Acceptor Forms Solution and Surface Products by Antiparallel Shape Fitting with Conformational Dipole Momentum Switch,” *Angewandte Chemie International Edition*, vol. 60, no. 33, pp. 17 887–17 892, 2021.
- [3] V. Kachwal, A. Srivastava, S. Thakar, *et al.*, “Engineering a light-driven cyanine based molecular rotor to enhance the sensitivity towards a viscous medium,” *Materials Advances*, vol. 2, no. 14, pp. 4804–4813, 2021.
- [4] **Zubiria-Ulacia, Maria**, J. M. Matxain, and D. Casanova, “The role of CT excitations in PDI aggregates,” *Physical Chemistry Chemical Physics*, vol. 22, no. 28, pp. 15 908–15 918, 2020.
- [5] D. López-Carballeira, D. **Zubiria, Maria** and Casanova, and F. Ruipérez, “Improvement of the electrochemical and singlet fission properties of anthraquinones by modification of the diradical character,” *Physical Chemistry Chemical Physics*, vol. 21, no. 15, pp. 7941–7952, 2019.
- [6] T. F. Schulze and T. W. Schmidt, “Photochemical upconversion: Present status and prospects for its application to solar energy conversion,” *Energy and Environmental Science*, vol. 8, no. 1, pp. 103–125, 2015. arXiv: [\barataMaterialsandTechniquesofpolychromewoodensculpture](#).
- [7] B. Parida, S. Iniyar, and R. Goic, “A review of solar photovoltaic technologies,” *Renewable and Sustainable Energy Reviews*, vol. 15, no. 3, pp. 1625–1636, 2011. arXiv: [1303.4604](#).
- [8] E. Kozma and M. Catellani, “Perylene diimides based materials for organic solar cells,” *Dyes and Pigments*, vol. 98, no. 1, pp. 160–179, 2013.
- [9] S. R. Forrest and M. E. Thompson, “Introduction: Organic electronics and optoelectronics,” *Chemical Reviews*, vol. 107, no. 4, pp. 923–925, 2007.
- [10] C. W. Tang and S. A. Vanslyke, “Organic electroluminescent diodes,” *Applied Physics Letters*, vol. 51, no. 12, pp. 913–915, 1987.
- [11] O. Ostroverkhova, “Organic Optoelectronic Materials: Mechanisms and Applications,” *Chemical Reviews*, vol. 116, no. 22, pp. 13 279–13 412, 2016.

- [12] F. Wudl, N. Sariciftci, L. Smilowitz, and A. Heeger, "Photoinduced Electron Transfer from a Conducting Polymer to Buckminsterfullerene," *Science*, vol. 258, no. 5087, pp. 1474–1476, 1992.
- [13] A. M. Bagher, "Introduction to {Organic} {Solar} {Cells}," *Sustainable Energy, Sustainable Energy*, vol. 2, no. 3, pp. 85–90, 2014.
- [14] D. Kim, "A Theoretical Study of the Formation of Benzene Excimer: Effects of Geometry Relaxation and Spin-state Dependence," *Bulletin of the Korean Chemical Society*, vol. 35, no. 9, pp. 2738–2742, 2014.
- [15] A. Diaz-Andres and D. Casanova, "Benzene Excimer and Excited Multimers: Electronic Character, Interaction Nature, and Aromaticity," *The Journal of Physical Chemistry Letters*, vol. 12, no. 31, pp. 7400–7408, 2021.
- [16] M. Pabst, B. Lunkenheimer, and A. Köhn, "The triplet excimer of naphthalene: A model system for triplet-triplet interactions and its spectral properties," *Journal of Physical Chemistry C*, vol. 115, no. 16, pp. 8335–8344, 2011.
- [17] J. Quenneville and T. C. Germann, "A quantum chemistry study of diels–alder dimerizations in benzene and anthracene," *The Journal of Chemical Physics*, vol. 131, no. 2, p. 024 313, 2009.
- [18] B. Zhang, H. Soleimanejad, D. J. Jones, *et al.*, "Highly Fluorescent Molecularly Insulated Perylene Diimides: Effect of Concentration on Photophysical Properties," *Chemistry of Materials*, vol. 29, no. 19, pp. 8395–8403, 2017.
- [19] Q. Fan, K. Cheng, Z. Yang, *et al.*, "Perylene-diimide-based nanoparticles as highly efficient photoacoustic agents for deep brain tumor imaging in living mice," *Advanced Materials*, vol. 27, no. 5, pp. 843–847, 2015.
- [20] S. L. Li, D. G. Truhlar, M. W. Schmidt, and M. S. Gordon, "Model space diabaticization for quantum photochemistry," *Journal of Chemical Physics*, vol. 142, no. 6, 2015.
- [21] A. A. Rachford, S. Goeb, and F. N. Castellano, "Accessing the Triplet Excited State in Perylenediimides," *Journal of the American Chemical Society*, vol. 130, no. 9, pp. 2766–2767, 2008.
- [22] M. Mayländer, O. Nolden, M. Franz, *et al.*, "Accessing the triplet state of perylenediimide by radical-enhanced intersystem crossing," *Chemical Science*, vol. 13, no. 22, pp. 6732–6743, 2022.
- [23] W. T. Godbey, "Fluorescence," in *Biotechnology and its Applications*, Elsevier, 2022, pp. 187–201.
- [24] D. S. McClure, "Triplet-singlet transitions in organic molecules. lifetime measurements of the triplet state," *The Journal of Chemical Physics*, vol. 17, no. 10, pp. 905–913, 1949.
- [25] A. Köhler and H. Bässler, "Triplet states in organic semiconductors," *Materials Science and Engineering: R: Reports*, vol. 66, no. 4–6, pp. 71–109, 2009.

- [26] M. A. Fox, "Excited States in Photochemistry of Organic Molecules Edited by Martin Klessinger (University of Munster) and Josef Michl (University of Colorado). VCH: New York. 1995. xxiv + 537 pp. \$89.95. ISBN 1-56081-588-4.," *Journal of the American Chemical Society*, vol. 118, no. 7, pp. 1815–1816, 1996.
- [27] R. Peeling, "WHO programme on the evaluation of diagnostic tests.," *Bulletin of the World Health Organization.*, vol. 84, no. 8, p. 594, 2006.
- [28] S. Mai, P. Marquetand, and L. González, "A general method to describe intersystem crossing dynamics in trajectory surface hopping," *International Journal of Quantum Chemistry*, vol. 115, no. 18, pp. 1215–1231, 2015. arXiv: 1703.09456.
- [29] P. Alam, I. R. Laskar, C. Climent, *et al.*, "Microwave-assisted facile and expeditive syntheses of phosphorescent cyclometallated iridium(III) complexes," *Polyhedron*, vol. 53, pp. 286–294, 2013.
- [30] P. Alam, G. Kaur, C. Climent, *et al.*, "New 'aggregation induced emission (AIE)' active cyclometalated iridium(iii) based phosphorescent sensors: High sensitivity for mercury(ii) ions," *Dalton Transactions*, vol. 43, no. 43, pp. 16 431–16 440, 2014.
- [31] P. Alam, C. Climent, G. Kaur, *et al.*, "Exploring the Origin of Aggregation Induced Emission Activity and Crystallization Induced Emission in Organometallic Iridium(III) Cationic Complexes: Influence of Counterions," *Crystal Growth and Design*, vol. 16, no. 10, pp. 5738–5752, 2016.
- [32] P. Alam, S. Dash, C. Climent, *et al.*, "'Aggregation induced emission' active iridium(III) complexes with applications in mitochondrial staining," *RSC Advances*, vol. 7, no. 10, pp. 5642–5648, 2017.
- [33] C. Climent, P. Alam, S. S. Pasha, *et al.*, "Dual emission and multi-stimuli-response in iridium(III) complexes with aggregation-induced enhanced emission: Applications for quantitative CO₂ detection," *Journal of Materials Chemistry C*, vol. 5, no. 31, pp. 7784–7798, 2017.
- [34] S. Millicent B and M. Josef, "Singlet fission," *Chemical reviews*, vol. 110, no. 11, pp. 6891–936, 2010.
- [35] D. Casanova, "Theoretical Modeling of Singlet Fission," *Chemical Reviews*, vol. 118, no. 15, pp. 7164–7207, 2018.
- [36] M. B. Smith and J. Michl, "Recent Advances in Singlet Fission," *Annual Review of Physical Chemistry*, vol. 64, no. 1, pp. 361–386, 2013.
- [37] J. Singh, "The theory of fission of a singlet frenkel exciton into two localised triplet excitations," *Journal of Physics and Chemistry of Solids - J PHYS CHEM SOLIDS*, vol. 39, pp. 1207–1209, 1978.

- [38] M. C. Hanna and A. J. Nozik, "Solar conversion efficiency of photovoltaic and photoelectrolysis cells with carrier multiplication absorbers," *Journal of Applied Physics*, vol. 100, no. 7, 2006.
- [39] J. Lee, P. Jadhav, P. D. Reusswig, *et al.*, "Singlet exciton fission photovoltaics," *Accounts of Chemical Research*, vol. 46, no. 6, pp. 1300–1311, 2013.
- [40] P. M. Zimmerman, F. Bell, D. Casanova, and M. Head-Gordon, "Mechanism for singlet fission in pentacene and tetracene: From single exciton to two triplets," *Journal of the American Chemical Society*, vol. 133, no. 49, pp. 19 944–19 952, 2011.
- [41] D. Casanova, "Bright Fission: Singlet Fission into a Pair of Emitting States," *Journal of Chemical Theory and Computation*, vol. 11, no. 6, pp. 2642–2650, 2015.
- [42] G. Baryshnikov, B. Minaev, and H. Ågren, "Theory and Calculation of the Phosphorescence Phenomenon," *Chemical Reviews*, vol. 117, no. 9, pp. 6500–6537, 2017.
- [43] B. Minaev, G. Baryshnikov, and H. Agren, "Principles of phosphorescent organic light emitting devices," *Physical Chemistry Chemical Physics*, vol. 16, no. 5, pp. 1719–1758, 2014.
- [44] F. McCapra, "The chemiluminescence of organic compounds," *Quarterly Reviews, Chemical Society*, vol. 20, no. 4, pp. 485–510, 1966.
- [45] H. Uoyama, K. Goushi, K. Shizu, H. Nomura, and C. Adachi, "Highly efficient organic light-emitting diodes from delayed fluorescence," *Nature*, vol. 492, no. 7428, pp. 234–238, 2012. arXiv: arXiv:1011.1669v3.
- [46] Q. Zhang, B. Li, S. Huang, H. Nomura, H. Tanaka, and C. Adachi, "Efficient blue organic light-emitting diodes employing thermally activated delayed fluorescence," *Nature Photonics*, vol. 8, no. 4, pp. 326–332, 2014. arXiv: arXiv:1011.1669v3.
- [47] S. Y. Lee, T. Yasuda, Y. S. Yang, Q. Zhang, and C. Adachi, "Luminous butterflies: Efficient exciton harvesting by benzophenone derivatives for full-color delayed fluorescence OLEDs," *Angewandte Chemie - International Edition*, vol. 53, no. 25, pp. 6402–6406, 2014.
- [48] Z. Yang, Z. Mao, Z. Xie, *et al.*, "Recent advances in organic thermally activated delayed fluorescence materials," *Chemical Society Reviews*, vol. 46, no. 3, pp. 915–1016, 2017.
- [49] C. A. Parker and C. G. Hatchard, "Triplet-singlet emission in fluid solutions. Phosphorescence of eosin," *Transactions of the Faraday Society*, vol. 57, pp. 1894–1904, 1961. arXiv: arXiv:1011.1669v3.
- [50] C. A. Parker, "Sensitized P-Type Delayed Fluorescence," *Proceedings of the Royal Society of London Series a-Mathematical and Physical Sciences*, vol. 276, no. 1364, pp. 125–+, 1963.

- [51] Y. Y. Cheng, B. Fückel, T. Khoury, *et al.*, “Kinetic analysis of photochemical upconversion by triplet-triplet annihilation: Beyond any spin statistical limit,” *Journal of Physical Chemistry Letters*, vol. 1, no. 12, pp. 1795–1799, 2010. arXiv: jz100566u [10.1021].
- [52] E. Schrodinger, “Quantisierung als Eigmwertproblem,” *Annalen der Physik*, vol. 13, pp. 438–490, 1926.
- [53] D. P. A. M., “On the Theory of Quantum Mechanics,” *Proceedings of the Royal Society of London. Series A, Containing Papers of a Mathematical and Physical Character*, vol. 112, no. 762, pp. 661–677, 1926.
- [54] W. Heisenberg, “Über quantentheoretische Umdeutung kinematischer und mechanischer Beziehungen.,” *Zeitschrift für Physik*, vol. 33, no. 1, pp. 879–893, 1925.
- [55] E. Schrödinger, “Der Energieimpulssatz der Materiewellen,” *Annalen der Physik*, vol. 387, no. 2, pp. 265–272, 1927.
- [56] M. Born and R. Oppenheimer, “Zur Quantentheorie der Molekeln,” *Annalen der Physik*, vol. 389, no. 20, pp. 457–484, 1927.
- [57] M. Chr and P. M.S., “Note on an Approximation Treatment for Many-Electron Systems,” *Physical Review*, vol. 46, no. 1, 618-622, 1934.
- [58] A. Szabo and N. S. Ostlund, *Modern quantum chemistry: introduction to advanced electronic structure theory*, 1989.
- [59] B. N. Plakhutin, “Brillouin’s theorem in the Hartree–Fock method: Eliminating the limitation of the theorem for excitations in the open shell,” *The Journal of Chemical Physics*, vol. 153, no. 22, p. 224110, 2020.
- [60] P. Hohenberg and W. Kohn, “Inhomogeneous Electron Gas,” *Physical Review*, vol. 136, no. 3B, B864–B871, 1964. arXiv: 1108.5632.
- [61] W Kohn and L. J. Sham, “Self-Consistent Equations Including Exchange and Correlation Effects,” *Physical Review*, vol. 140, no. 4A, A1133–A1138, 1965.
- [62] R. Stowasser and R. Hoffmann, “What Do the Kohn-Sham Orbitals and Eigenvalues Mean?” *Journal of the American Chemical Society*, vol. 121, no. 14, pp. 3414–3420, 1999.
- [63] O. Gunnarsson, B. I. Lundqvist, and J. W. Wilkins, “Contribution to the cohesive energy of simple metals: Spin-dependent effect,” *Physical Review B*, vol. 10, no. 4, pp. 1319–1327, 1974.
- [64] T. Kar, J. G. Ángyán, and A. B. Sannigrahi, “Comparison of ab Initio Hartree-Fock and Kohn-Sham Orbitals in the Calculation of Atomic Charge, Bond Index, and Valence,” *The Journal of Physical Chemistry A*, vol. 104, no. 44, pp. 9953–9963, 2000.

- [65] M. Hofmann and H. F. Schaefer, “Computational chemistry,” in *Encyclopedia of Physical Science and Technology (Third Edition)*, R. A. Meyers, Ed., Third Edition, New York: Academic Press, 2003, pp. 487–506.
- [66] X. Hua, X. Chen, and W. A. Goddard, “Generalized generalized gradient approximation: An improved density-functional theory for accurate orbital eigenvalues,” *Physical Review B*, vol. 55, no. 24, pp. 16 103–16 109, 1997.
- [67] J. Tao, J. P. Perdew, A. Ruzsinszky, G. E. Scuseria, G. I. Csonka, and V. N. Staroverov, “Meta-generalized gradient approximation: Non-empirical construction and performance of a density functional,” *Philosophical Magazine*, vol. 87, no. 7, pp. 1071–1084, 2007.
- [68] J. Jaramillo, G. E. Scuseria, and M. Ernzerhof, “Local hybrid functionals,” *The Journal of Chemical Physics*, vol. 118, no. 3, pp. 1068–1073, 2003.
- [69] T. Tsuneda and K. Hirao, “Long-range correction for density functional theory,” *Wiley Interdisciplinary Reviews: Computational Molecular Science*, vol. 4, no. 4, pp. 375–390, 2014.
- [70] S. Grimme, “Density functional theory with London dispersion corrections,” *WIREs Computational Molecular Science*, vol. 1, no. 2, pp. 211–228, 2011.
- [71] B. G. Levine, C. Ko, J. Quenneville, and T. J. Martínez, “Conical intersections and double excitations in time-dependent density functional theory,” *Molecular Physics*, vol. 104, no. 5-7, pp. 1039–1051, 2006.
- [72] E. Gross and W. Kohn, “Time-dependent density-functional theory,” in *Density Functional Theory of Many-Fermion Systems*, ser. Advances in Quantum Chemistry, P.-O. Löwdin, Ed., vol. 21, Academic Press, 1990, pp. 255–291.
- [73] M. Casida, *Recent Advances in Density Functional Methods*. WORLD SCIENTIFIC, 1995. eprint: <https://www.worldscientific.com/doi/pdf/10.1142/2914>.
- [74] —, *Recent Developments and Applications of Modern Density Functional Theory, Theoretical and Computational Chemistry*. Elsevier, 1996.
- [75] T. R. Cundari and W. J. Stevens, “Effective core potential methods for the lanthanides,” *The Journal of Chemical Physics*, vol. 98, no. 7, pp. 5555–5565, 1993.
- [76] Q. Wu and T. Van Voorhis, “Constrained Density Functional Theory and Its Application in Long-Range Electron Transfer,” *Journal of Chemical Theory and Computation*, vol. 2, no. 3, pp. 765–774, 2006.
- [77] D. R. Yarkony, “Current Issues in Nonadiabatic Chemistry †,” *The Journal of Physical Chemistry*, vol. 100, no. 48, pp. 18 612–18 628, 1996.

- [78] B. H. Lengsfeld and D. R. Yarkony, "On the evaluation of nonadiabatic coupling matrix elements for MCSCF/CI wave functions using analytic derivative methods. III. Second derivative terms," *The Journal of Chemical Physics*, vol. 84, no. 1, pp. 348–353, 1986.
- [79] M. H. Alexander, D. E. Manolopoulos, and H.-J. Werner, "An investigation of the F+H₂ reaction based on a full ab initio description of the open-shell character of the F(2P) atom," *The Journal of Chemical Physics*, vol. 113, no. 24, pp. 11 084–11 100, 2000.
- [80] C. A. Mead and D. G. Truhlar, "Conditions for the definition of a strictly diabatic electronic basis for molecular systems," *The Journal of Chemical Physics*, vol. 77, no. 12, pp. 6090–6098, 1982.
- [81] F. T. Smith, "Diabatic and adiabatic representations for atomic collision problems," *Phys. Rev.*, vol. 179, pp. 111–123, 1 1969.
- [82] L. F. Errea, A. Macías, L. Méndez, *et al.*, "Properties and removal of singular couplings at conical intersections," *Phys. Rev. A*, vol. 63, p. 062 713, 6 2001.
- [83] B. K. Kendrick, C. Alden Mead, and D. G. Truhlar, "Properties of nonadiabatic couplings and the generalized born–oppenheimer approximation," *Chemical Physics*, vol. 277, no. 1, pp. 31–41, 2002.
- [84] C. Edmiston and K. Ruedenberg, "Localized Atomic and Molecular Orbitals," *Reviews of Modern Physics*, vol. 35, no. 3, pp. 457–464, 1963.
- [85] S. F. Boys, "Construction of some molecular orbitals to be approximately invariant for changes from one molecule to another," *Reviews of Modern Physics*, vol. 32, no. 2, pp. 296–299, 1960.
- [86] S. Canola, G. Bagnara, Y. Dai, G. Ricci, A. Calzolari, and F. Negri, "Addressing the Frenkel and charge transfer character of exciton states with a model Hamiltonian based on dimer calculations: Application to large aggregates of perylene bisimide," *The Journal of Chemical Physics*, vol. 154, no. 12, p. 124 101, 2021.
- [87] J. E. Norton and J.-L. Brédas, "Theoretical characterization of titanyl phthalocyanine as a p-type organic semiconductor: Short intermolecular π - π interactions yield large electronic couplings and hole transport bandwidths," *The Journal of Chemical Physics*, vol. 128, no. 3, p. 034 701, 2008.
- [88] D. Kim, "A Theoretical Analysis of the Excited State of Oligoacene Aggregates: Local Excitation vs. Charge-Transfer Transition," *Bulletin of the Korean Chemical Society*, vol. 36, no. 9, pp. 2284–2289, 2015.
- [89] P. Löwdin, "On the non-orthogonality problem connected with the use of atomic wave functions in the theory of molecules and crystals," *The Journal of Chemical Physics*, vol. 18, no. 3, pp. 365–375, 1950.
- [90] A. Björck, "Numerics of gram-schmidt orthogonalization," *Linear Algebra and its Applications*, vol. 197-198, pp. 297–316, 1994.

- [91] F. Plasser, “TheoDORE: A toolbox for a detailed and automated analysis of electronic excited state computations,” *The Journal of Chemical Physics*, vol. 152, no. 8, p. 084108, 2020.
- [92] A. V. Titov, I. S. Ufimtsev, N. Luehr, and T. J. Martinez, “Generating Efficient Quantum Chemistry Codes for Novel Architectures,” *Journal of Chemical Theory and Computation*, vol. 9, no. 1, pp. 213–221, 2013.
- [93] M. Vacher, I. Fdez. Galván, B.-W. Ding, *et al.*, “Chemi- and Bioluminescence of Cyclic Peroxides,” *Chemical Reviews*, vol. 118, no. 15, pp. 6927–6974, 2018.
- [94] S. Ghosh, P. Verma, C. J. Cramer, L. Gagliardi, and D. G. Truhlar, “Combining Wave Function Methods with Density Functional Theory for Excited States,” *Chemical Reviews*, vol. 118, no. 15, pp. 7249–7292, 2018.
- [95] H. Lischka, D. Nachtigallova, A. J. A. Aquino, *et al.*, “Multireference Approaches for Excited States of Molecules,” *Chemical Reviews*, vol. 118, no. 15, pp. 7293–7361, 2018.
- [96] F. Plasser, M. Wormit, and A. Dreuw, “New tools for the systematic analysis and visualization of electronic excitations. I. Formalism,” *The Journal of Chemical Physics*, vol. 141, no. 2, p. 024106, 2014.
- [97] R. L. Martin, “Natural transition orbitals,” *The Journal of Chemical Physics*, vol. 118, no. 11, pp. 4775–4777, 2003.
- [98] M. J. G. Peach, P. Benfield, T. Helgaker, and D. J. Tozer, “Excitation energies in density functional theory: An evaluation and a diagnostic test,” *The Journal of Chemical Physics*, vol. 128, no. 4, p. 044118, 2008.
- [99] S. A. B appler, F. Plasser, M. Wormit, and A. Dreuw, “Exciton analysis of many-body wave functions: Bridging the gap between the quasiparticle and molecular orbital pictures,” *Physical Review A*, vol. 90, no. 5, p. 052521, 2014.
- [100] E. Ronca, C. Angeli, L. Belpassi, F. De Angelis, F. Tarantelli, and M. Pastore, “Density Relaxation in Time-Dependent Density Functional Theory: Combining Relaxed Density Natural Orbitals and Multireference Perturbation Theories for an Improved Description of Excited States,” *Journal of Chemical Theory and Computation*, vol. 10, no. 9, pp. 4014–4024, 2014.
- [101] J. Coe and M. Paterson, “Characterising a configuration interaction excited state using natural transition geminals,” *Molecular Physics*, vol. 112, no. 5-6, pp. 733–739, 2014.
- [102] G. M. J. Barca, A. T. B. Gilbert, and P. M. W. Gill, “Excitation Number: Characterizing Multiply Excited States,” *Journal of Chemical Theory and Computation*, vol. 14, no. 1, pp. 9–13, 2018.
- [103] F. Plasser, “Entanglement entropy of electronic excitations,” *The Journal of Chemical Physics*, vol. 144, no. 19, p. 194107, 2016.

- [104] F. Glöckhofer, A. Rosspeintner, P. Pasitsuparoad, *et al.*, “Effect of symmetric and asymmetric substitution on the optoelectronic properties of 9,10-dicyanoanthracene,” *Molecular Systems Design & Engineering*, vol. 4, no. 4, pp. 951–961, 2019.
- [105] F. Plasser and A. Dreuw, “High-Level Ab Initio Computations of the Absorption Spectra of Organic Iridium Complexes,” *The Journal of Physical Chemistry A*, vol. 119, no. 6, pp. 1023–1036, 2015.
- [106] A. L. L. East and E. C. Lim, “Naphthalene dimer: Electronic states, excimers, and triplet decay,” *The Journal of Chemical Physics*, vol. 113, no. 20, pp. 8981–8994, 2000.
- [107] J. W. Verhoeven, “Glossary of terms used in photochemistry (iupac recommendations 1996),” *Pure and Applied Chemistry*, vol. 68, no. 12, pp. 2223–2286, 1996.
- [108] J.-D. Chai and M. Head-Gordon, “Long-range corrected hybrid density functionals with damped atom–atom dispersion corrections,” *Physical Chemistry Chemical Physics*, vol. 10, no. 44, pp. 6615–6620, 2008.
- [109] M. Head-Gordon, R. J. Rico, M. Oumi, and T. J. Lee, “A doubles correction to electronic excited states from configuration interaction in the space of single substitutions,” *Chemical Physics Letters*, vol. 219, no. 1, pp. 21–29, 1994.
- [110] S. Hirata and M. Head-Gordon, “Time-dependent density functional theory within the Tamm–Dancoff approximation,” *Chemical Physics Letters*, vol. 314, no. 3, pp. 291–299, 1999.
- [111] Y. Shao, Z. Gan, E. Epifanovsky, *et al.*, “Advances in molecular quantum chemistry contained in the q-chem 4 program package,” *Molecular Physics*, vol. 113, no. 2, pp. 184–215, 2015.
- [112] M. Kołaski, C. R. Arunkumar, and K. S. Kim, “Aromatic Excimers: Ab Initio and TD-DFT Study,” *Journal of Chemical Theory and Computation*, vol. 9, no. 1, pp. 847–856, 2013.
- [113] H. A. J. Teller and E., “Stability of polyatomic molecules in degenerate electronic states - I—Orbital degeneracy,” *Proceedings of the Royal Society of London. Series A - Mathematical and Physical Sciences*, vol. 161, no. 905, pp. 220–235, 1937.
- [114] S. S. Zade, N. Zamoshchik, A. R. Reddy, G. Fridman-Marueli, D. Sheberla, and M. Bendikov, “Products and Mechanism of Acene Dimerization. A Computational Study,” *Journal of the American Chemical Society*, vol. 133, no. 28, pp. 10 803–10 816, 2011.
- [115] F. S. Gentile, F. Picca, G. De Falco, *et al.*, “Soot inception: A DFT study of σ and π dimerization of resonantly stabilized aromatic radicals,” *Fuel*, vol. 279, p. 118 491, 2020.

- [116] C. Huang, S. Barlow, and S. R. Marder, "Perylene-3,4,9,10-tetracarboxylic acid diimides: Synthesis, physical properties, and use in organic electronics," *The Journal of Organic Chemistry*, vol. 76, no. 8, pp. 2386–2407, 2011.
- [117] J. Li, F. Dierschke, J. Wu, A. C. Grimsdale, and K. Müllen, "Poly(2,7-carbazole) and perylene tetracarboxydiimide: A promising donor/acceptor pair for polymer solar cells," *J. Mater. Chem.*, vol. 16, pp. 96–100, 2006.
- [118] H. Dinçalp, Z. Aşkar, C. Zafer, and S. İçli, "Effect of side chain substituents on the electron injection abilities of unsymmetrical perylene diimide dyes," *Dyes and Pigments*, vol. 91, no. 2, pp. 182–191, 2011.
- [119] C. Ramanan, A. L. Smeigh, J. E. Anthony, T. J. Marks, and M. R. Wasielewski, "Competition between Singlet Fission and Charge Separation in Solution-Processed Blend Films of 6,13-Bis(triisopropylsilylethynyl)pentacene with Sterically-Encumbered Perylene-3,4:9,10-bis(dicarboximide)s," *Journal of the American Chemical Society*, vol. 134, no. 1, pp. 386–397, 2012.
- [120] Y. Shibano, T. Umeyama, Y. Matano, and H. Imahori, "Electron-Donating Perylene Tetracarboxylic Acids for Dye-Sensitized Solar Cells," *Organic Letters*, vol. 9, no. 10, pp. 1971–1974, 2007.
- [121] H. Tian, P.-H. Liu, W. Zhu, E. Gao, D.-J. Wu, and S. Cai, "Synthesis of novel multi-chromophoric soluble perylene derivatives and their photosensitizing properties with wide spectral response for SnO₂ nanoporous electrode," *Journal of Materials Chemistry*, vol. 10, no. 12, pp. 2708–2715, 2000.
- [122] "Synthesis of annulated thiophene perylene bisimide analogues: their applications to bulk heterojunction organic solar cells," *Chemical Communications*, vol. 47, no. 19, pp. 5509–5511, 2011.
- [123] C. Huang, S. Barlow, and S. R. Marder, "Perylene-3,4,9,10-tetracarboxylic acid diimides: Synthesis, physical properties, and use in organic electronics," *Journal of Organic Chemistry*, vol. 76, no. 8, pp. 2386–2407, 2011.
- [124] B. Ventura, H. Langhals, B. Böck, and L. Flamigni, "Phosphorescent perylene imides," *Chemical Communications*, vol. 48, no. 35, p. 4226, 2012.
- [125] M MATSUI, M WANG, K FUNABIKI, Y HAYAKAWA, and T KITAGUCHI, "Properties of novel perylene-3,4:9,10-tetracarboxydiimide-centred dendrimers and their application as emitters in organic electroluminescence devices," *Dyes and Pigments*, vol. 74, no. 1, pp. 169–175, 2007.
- [126] E. Lucenti, C. Botta, E. Cariati, *et al.*, "New organic–inorganic hybrid materials based on perylene diimide–polyhedral oligomeric silsesquioxane dyes with reduced quenching of the emission in the solid state," *Dyes and Pigments*, vol. 96, no. 3, pp. 748–755, 2013.

- [127] B. A. Jones, A. Facchetti, M. R. Wasielewski, and T. J. Marks, "Tuning Orbital Energetics in Arylene Diimide Semiconductors. Materials Design for Ambient Stability of n-Type Charge Transport," *Journal of the American Chemical Society*, vol. 129, no. 49, pp. 15 259–15 278, 2007.
- [128] F. Würthner and M. Stolte, "Naphthalene and perylene diimides for organic transistors," *Chemical Communications*, vol. 47, no. 18, p. 5109, 2011.
- [129] E. A. Weiss, M. J. Ahrens, L. E. Sinks, A. V. Gusev, M. A. Ratner, and M. R. Wasielewski, "Making a Molecular Wire: Charge and Spin Transport through para-Phenylene Oligomers," *Journal of the American Chemical Society*, vol. 126, no. 17, pp. 5577–5584, 2004.
- [130] T. M. Wilson, M. J. Tauber, and M. R. Wasielewski, "Toward an n-Type Molecular Wire: Electron Hopping within Linearly Linked Perylenediimide Oligomers," *Journal of the American Chemical Society*, vol. 131, no. 25, pp. 8952–8957, 2009.
- [131] F. J. Céspedes-Guirao, A. B. Ropero, E. Font-Sanchis, Á. Nadal, F. Fernández-Lázaro, and Á. Sastre-Santos, "A water-soluble perylene dye functionalised with a 17 β -estradiol: A new fluorescent tool for steroid hormones," *Chemical Communications*, vol. 47, no. 29, pp. 8307–8309, 2011.
- [132] Y. Zhao, X. Zhang, D. Li, *et al.*, "Water-soluble 3,4:9,10-perylene tetracarboxylic ammonium as a high-performance fluorochrome for living cells staining," *Luminescence*, vol. 24, no. 3, pp. 140–143, 2009.
- [133] S. W. Eaton, L. E. Shoer, S. D. Karlen, *et al.*, "Singlet exciton fission in polycrystalline thin films of a slip-stacked perylenediimide," *Journal of the American Chemical Society*, vol. 135, no. 39, pp. 14 701–14 712, 2013.
- [134] A. K. Le, J. A. Bender, and S. T. Roberts, "Slow Singlet Fission Observed in a Polycrystalline Perylenediimide Thin Film," *Journal of Physical Chemistry Letters*, vol. 7, no. 23, pp. 4922–4928, 2016.
- [135] A. K. Le, J. A. Bender, D. H. Arias, D. E. Cotton, J. C. Johnson, and S. T. Roberts, "Singlet Fission Involves an Interplay between Energetic Driving Force and Electronic Coupling in Perylenediimide Films," *Journal of the American Chemical Society*, vol. 140, no. 2, pp. 814–826, 2018.
- [136] X. Zhan, A. Facchetti, S. Barlow, *et al.*, "Rylene and Related Diimides for Organic Electronics," *Advanced Materials*, vol. 23, no. 2, pp. 268–284, 2011.
- [137] F. Würthner, C. R. Saha-Möller, B. Fimmel, S. Ogi, P. Leowanawat, and D. Schmidt, "Perylene Bisimide Dye Assemblies as Archetype Functional Supramolecular Materials," *Chemical Reviews*, vol. 116, no. 3, pp. 962–1052, 2016.
- [138] F. Würthner, "Perylene bisimide dyes as versatile building blocks for functional supramolecular architectures," *Chemical Communications*, no. 14, pp. 1564–1579, 2004.

- [139] T. Yanai, D. P. Tew, and N. C. Handy, "A new hybrid exchange–correlation functional using the Coulomb-attenuating method (CAM-B3LYP)," *Chemical Physics Letters*, vol. 393, no. 1-3, pp. 51–57, 2004.
- [140] M. H. Farag and A. I. Krylov, "Singlet Fission in Perylenediimide Dimers," *Journal of Physical Chemistry C*, vol. 122, no. 45, pp. 25 753–25 763, 2018.
- [141] F. H. Allen, D. G. Watson, L. Brammer, A. G. Orpen, and R Taylor, "Typical interatomic distances: organic compounds," in *International Tables for Crystallography Volume C: Mathematical, physical and chemical tables*, E Prince, Ed., Dordrecht: Springer Netherlands, 2004, pp. 790–811.
- [142] H. Bu, H. Zheng, H. Zhou, *et al.*, "The role of sp² and sp³ hybridized bonds on the structural, mechanical, and electronic properties in a hard BN framework," *RSC Advances*, vol. 9, no. 5, pp. 2657–2665, 2019.
- [143] A. Schubert, V. Settels, W. Liu, *et al.*, "Ultrafast exciton self-trapping upon geometry deformation in perylene-based molecular aggregates," *Journal of Physical Chemistry Letters*, vol. 4, no. 5, pp. 792–796, 2013.
- [144] M. J. G. Peach, M. J. Williamson, and D. J. Tozer, "Influence of Triplet Instabilities in TDDFT," *Journal of Chemical Theory and Computation*, vol. 7, no. 11, pp. 3578–3585, 2011.
- [145] W. Kuhn, "Über die Gesamtstärke der von einem Zustande ausgehenden Absorptionslinien," *Zeitschrift für Physik*, vol. 33, no. 1, pp. 408–412, 1925.
- [146] F. Reiche and W. Thomas, "Über die Zahl der Dispersionselektronen, die einem stationären Zustand zugeordnet sind," *Zeitschrift für Physik*, vol. 34, no. 1, pp. 510–525, 1925.
- [147] W. Thomas, "Über die Zahl der Dispersionselektronen, die einem stationären Zustande zugeordnet sind. (Vorläufige Mitteilung)," *Die Naturwissenschaften*, vol. 13, no. 28, pp. 627–627, 1925.
- [148] T. Yanai, D. P. Tew, and N. C. Handy, "A new hybrid exchange–correlation functional using the Coulomb-attenuating method (CAM-B3LYP)," *Chemical Physics Letters*, vol. 393, no. 1-3, pp. 51–57, 2004.
- [149] A. Oleson, T. Zhu, I. S. Dunn, *et al.*, "Perylene Diimide-Based H_j- and hJ-Aggregates: The Prospect of Exciton Band Shape Engineering in Organic Materials," *Journal of Physical Chemistry C*, vol. 123, no. 33, pp. 20 567–20 578, 2019.
- [150] V. Settels, W. Liu, J. Pflaum, R. F. Fink, and B. Engels, "Comparison of the electronic structure of different perylene-based dye-aggregates," *Journal of Computational Chemistry*, vol. 33, no. 18, pp. 1544–1553, 2012.

- [151] C. Walter, V. Krämer, and B. Engels, “On the applicability of time-dependent density functional theory (TDDFT) and semiempirical methods to the computation of excited-state potential energy surfaces of perylene-based dye-aggregates,” *International Journal of Quantum Chemistry*, vol. 117, no. 6, e25337, 2017.
- [152] W. Liu, S. Canola, A. Köhn, B. Engels, F. Negri, and R. F. Fink, “A model hamiltonian tuned toward high level ab initio calculations to describe the character of excitonic states in perylenebisimide aggregates,” *Journal of Computational Chemistry*, vol. 39, no. 24, pp. 1979–1989, 2018.
- [153] V. Settels, A. Schubert, M. Tafipolski, *et al.*, “Identification of ultrafast relaxation processes as a major reason for inefficient exciton diffusion in perylene-based organic semiconductors,” *Journal of the American Chemical Society*, vol. 136, no. 26, pp. 9327–9337, 2014.
- [154] K. M. Lefler, K. E. Brown, W. A. Salamant, S. M. Dyar, K. E. Knowles, and M. R. Wasielewski, “Triplet state formation in photoexcited slip-stacked perylene-3,4:9,10- bis(dicarboximide) dimers on a xanthene scaffold,” *Journal of Physical Chemistry A*, vol. 117, no. 40, pp. 10 333–10 345, 2013.
- [155] W.-Y. Wong, “Metallopolyyne Polymers as New Functional Materials for Photovoltaic and Solar Cell Applications,” *Macromolecular Chemical and Physics*, vol. 209, no. 1, pp. 14–24, 2008.
- [156] A. Köhler, H. Wittmann, R. Friend, M. Khan, and J. Lewis, “The photovoltaic effect in a platinum poly-yne,” *Synthetic Metals*, vol. 67, no. 1-3, pp. 245–249, 1994.
- [157] F. Guo, Y.-G. Kim, J. R. Reynolds, and K. S. Schanze, “Platinum–acetylide polymer based solar cells: involvement of the triplet state for energy conversion,” *Chemical Communications*, no. 17, pp. 1887–1889, 2006.
- [158] Y. Shao and Y. Yang, “Efficient Organic Heterojunction Photovoltaic Cells Based on Triplet Materials,” *Advanced Materials*, vol. 17, no. 23, pp. 2841–2844, 2005.
- [159] A. Köhler, H. Wittmann, R. Friend, M. Khan, and J. Lewis, “Enhanced photocurrent response in photocells made with platinum-poly-yne/C60 blends by photoinduced electron transfer,” *Synthetic Metals*, vol. 77, no. 1-3, pp. 147–150, 1996.
- [160] M. Arif, K. Yang, L. Li, *et al.*, “Harvesting triplet excitons for application in polymer solar cells,” *Applied Physics Letter*, vol. 94, no. 6, p. 063 307, 2009.
- [161] J. E. Subotnik, R. J. Cave, R. P. Steele, and N. Shenvi, “The initial and final states of electron and energy transfer processes: Diabatization as motivated by system-solvent interactions,” *The Journal of Chemical Physics*, vol. 130, no. 23, p. 234 102, 2009.

- [162] J. E. Subotnik, S. Yeganeh, R. J. Cave, and M. A. Ratner, "Constructing diabatic states from adiabatic states: Extending generalized Mulliken–Hush to multiple charge centers with Boys localization," *The Journal of Chemical Physics*, vol. 129, no. 24, p. 244 101, 2008.
- [163] C. Janiak, "A critical account on π – π stacking in metal complexes with aromatic nitrogen-containing ligands †," *Journal of the Chemical Society, Dalton Transactions*, no. 21, pp. 3885–3896, 2000.
- [164] C. Zhang, "Shape and size effects in π – π interactions: Face-to-face dimers," *Journal of Computational Chemistry*, vol. 32, no. 1, pp. 152–160, 2011.
- [165] J. Zhang, F. Bai, Y. Li, *et al.*, "Intramolecular π -stacked perylene-diimide acceptors for non-fullerene organic solar cells," *Journal of Materials Chemistry A*, vol. 7, no. 14, pp. 8136–8143, 2019.
- [166] M. Kasha, "Energy Transfer Mechanisms and the Molecular Exciton Model for Molecular Aggregates," *Radiation Research Society*, vol. 20, no. 1, p. 55, 1963.
- [167] N. J. Hestand and F. C. Spano, "Expanded Theory of H- and J-Molecular Aggregates: The Effects of Vibronic Coupling and Intermolecular Charge Transfer," *Chemical Reviews*, vol. 118, no. 15, pp. 7069–7163, 2018.
- [168] H. Yamagata, C. M. Pochas, and F. C. Spano, "Designing J- and H-Aggregates through Wave Function Overlap Engineering: Applications to Poly(3-hexylthio phene)," *Journal of Physical Chemistry B*, vol. 116, no. 49, pp. 14 494–14 503, 2012.
- [169] A. Carreras, O. Uranga-Barandiaran, F. Castet, and D. Casanova, "Photophysics of Molecular Aggregates from Excited State Diabatization," *Journal of Chemical Theory and Computation*, vol. 15, no. 4, pp. 2320–2330, 2019.
- [170] R. D. Harcourt, K. P. Ghiggino, G. D. Scholes, and S. Speiser, "On the origin of matrix elements for electronic excitation (energy) transfer," *Journal of Chemical Physics*, vol. 105, no. 5, pp. 1897–1901, 1996.
- [171] N. J. Hestand and F. C. Spano, "Molecular Aggregate Photophysics beyond the Kasha Model: Novel Design Principles for Organic Materials," *Accounts of Chemical Research*, vol. 50, no. 2, pp. 341–350, 2017.
- [172] J. C. Chang, "Monopole effects on electronic excitation interactions between large molecules. I. Application to energy transfer in chlorophylls," *Journal of Chemical Physics*, vol. 67, no. 9, p. 3901, 1999.
- [173] D. Beljonne, G. Pourtois, C. Silva, *et al.*, "Interchain vs. intrachain energy transfer in acceptor-capped conjugated polymers," *PANAS*, vol. 99, no. 17, pp. 10 982–10 987, 2002.

- [174] E. F. Valeev, V. Coropceanu, D. A. da Silva Filho, S. Salman, and J.-L. Brédas, “Effect of Electronic Polarization on Charge-Transport Parameters in Molecular Organic Semiconductors,” *Journal of the American Chemical Society*, vol. 128, no. 30, pp. 9882–9886, 2006.
- [175] C. J. Bardeen, “The Structure and Dynamics of Molecular Excitons,” *Annual Review of Physical Chemistry*, vol. 65, no. 1, pp. 127–148, 2014.
- [176] F. Plasser and H. Lischka, “Analysis of Excitonic and Charge Transfer Interactions from Quantum Chemical Calculations,” *Journal of Chemical Theory and Computation*, vol. 8, no. 8, pp. 2777–2789, 2012.
- [177] D. Casanova and A. I. Krylov, “Quantifying local exciton, charge resonance, and multiexciton character in correlated wave functions of multichromophoric systems,” *The Journal of Chemical Physics*, vol. 144, no. 1, p. 014 102, 2016.
- [178] R. F. Fink, J. Seibt, V. Engel, *et al.*, “Exciton Trapping in π -Conjugated Materials: A Quantum-Chemistry-Based Protocol Applied to Perylene Bisimide Dye Aggregates,” *Journal of the American Chemical Society*, vol. 130, no. 39, pp. 12 858–12 859, 2008.
- [179] M. J. Frisch, G. W. Trucks, H. B. Schlegel, *et al.*, *Gaussian~16 Revision C.01*, Gaussian Inc. Wallingford CT, 2016.
- [180] L. A. Galán, J. M. Andrés Castán, C. Dalinot, *et al.*, “Exploring the Concept of Dimerization-Induced Intersystem Crossing: At the Origins of Spin–Orbit Coupling Selection Rules,” *The Journal of Physical Chemistry B*, vol. 125, no. 30, pp. 8572–8580, 2021.
- [181] W. Liu, V. Settels, P. H. Harbach, A. Dreuw, R. F. Fink, and B. Engels, “Assessment of TD-DFT- and TD-HF-based approaches for the prediction of exciton coupling parameters, potential energy curves, and electronic characters of electronically excited aggregates,” *Journal of Computational Chemistry*, vol. 32, no. 9, pp. 1971–1981, 2011.
- [182] H. Iikura, T. Tsuneda, T. Yanai, and K. Hirao, “A long-range correction scheme for generalized-gradient-approximation exchange functionals,” *The Journal of Chemical Physics*, vol. 115, no. 8, pp. 3540–3544, 2001.
- [183] T. M. Henderson, B. G. Janesko, and G. E. Scuseria, “Generalized gradient approximation model exchange holes for range-separated hybrids,” *The Journal of Chemical Physics*, vol. 128, no. 19, p. 194 105, 2008.
- [184] D. Casanova, F. P. Rotzinger, and M. Grätzel, “Computational Study of Promising Organic Dyes for High-Performance Sensitized Solar Cells,” *Journal of Chemical Theory and Computation*, vol. 6, no. 4, pp. 1219–1227, 2010.
- [185] D. Casanova, “The Role of the π Linker in Donor- π -Acceptor Organic Dyes for High-Performance Sensitized Solar Cells,” *ChemPhysChem*, vol. 12, no. 16, pp. 2979–2988, 2011.

